A study of the selective pressures on inherited mitochondrial DNA mutations in mitotic cell populations

Tianhong Su

MBBS, MRes

This thesis is submitted for the degree of Doctor of Philosophy at Newcastle University

Wellcome Centre for Mitochondrial Research

Institute of Neuroscience

October 2018

天道酬勤

Heaven rewards the diligent.

For my beloved grandmother who is forever in my thoughts.

Author's Declaration

This thesis is submitted for the degree of Doctor of Philosophy at Newcastle University. The research was conducted in the Wellcome Trust Centre for Mitochondrial Research, Institute of Neuroscience, Newcastle University under the supervision of Prof Sir Doug Turnbull and Dr Laura Greaves, and is my own work unless stated otherwise.

I certify that none of the material presented here in this thesis has previously been submitted by me for a degree or qualification at this or any other university.

Abstract

Mitochondrial DNA (mtDNA) mutations accumulate somatically with age in normal individuals causing defects in oxidative phosphorylation (OXPHOS), with no selective pressures promoting their accumulation or removal. mtDNA mutations are also inherited through the germline causing mtDNA disease. In contrast to somatic mutations, they are lost in blood over time, suggesting selective pressure against them. This project aims to further investigate the selective loss of inherited mtDNA point mutations in mitotic tissues, using gastrointestinal epithelium as a model.

I have determined the mtDNA mutation load and OXPHOS protein levels in various gastrointestinal segments of patients with the inherited m.3243A>G and m.8344A>G mtDNA mutations. The data shows selective loss of these mutations in the mitotic epithelium, but not the post-mitotic smooth muscle and suggests that the selection occurs in the gastrointestinal stem cells.

I have further characterised a mouse model of mitochondrial disease carrying the inherited m.5024C>T mutation and have used them to study potential mechanisms of selective mtDNA mutation loss. These mice show: (1) loss of the m.5024C>T in the mitotic spleen and gastrointestinal epithelium with age but not in the post-mitotic tissues; (2) the rate of mutation loss is related to the rate of epithelial cell turnover; (3) the mutation loss in the intestinal epithelium is consistent with maintained levels of OXPHOS proteins with age, in contrast to the accumulation of cells with OXPHOS defects in aged wild-type mice; (4) significantly upregulated mitochondrial proliferation in the intestinal epithelium.

These key findings highlight differences in the selective pressures on inherited and somatic mtDNA mutations in mitotic tissue, and the contrasting tissue-specific dynamics of inherited mtDNA mutations in mitotic and post-mitotic tissues. These findings are important to further the understanding of phenotype development, progression and potential treatment of mtDNA disease, and the effect of mtDNA mutations on ageing stem cell biology.

Acknowledgements

I would like to sincerely thank my supervisors Professor Sir Doug Turnbull and Dr Laura Greaves for supporting me in many aspects during my PhD. They have given me valuable advice for research ideas and academic writing. They also inspired me when experiments were unsuccessful.

I must thank my collaborators, Professor Robert Taylor (Wellcome Centre for Mitochondrial Research), and Dr Sorena Afshar (Human Nutrition Research Centre, Institute of Cellular Medicine, Newcastle University, Campus for Aging and Vitality) for providing precious patients' samples for this research and Dr James Stewart and Professor Nils-Göran Larsson (Max Planck Institute for Biology of Ageing, Cologne, Germany) for breeding the $tRNA^{Ala}$ mice and providing all the mouse tissue used in this study. None of this work could be completed without these specimens provided by the collaborators.

I would also like to thank Dr John Grady and Dr Alasdair Blain for the help with the statistical analysis. A great deal of immunofluorescence data was processed through a script that Dr John Grady wrote. Dr Alasdair Blain has offered massive help for modelling analysis. I must express my gratitude to Dr Alex Laude and Dr Rolando Berlinguer Palmini who trained me in the use of imaging facilities and helped me with a huge amount of image analysis at the Bioimaging Facility. In particular, Dr Alex Laude has answered myriads of my questions about imaging techniques with great patience.

Next, I would like to thank many people in the lab who have helped me with lab work and thesis writing. Anna Smith did a large amount of tissue sectioning for this work. She, Dr Craig Stamp, Gavin Falkous and Dr Lyndsey Craven have taught me essential experimental techniques. Finally, I would like to thank Jordan Marley, Dr Ashwin Sachdeva, Dr Catherine Hossain and Chun Chen who are my co-workers and also my friends in the lab for supporting me in all aspects during my PhD. I would also like to thank Dr Amy Reeve, Dr Lyndsey Craven and Dr Amy Vincent for helping me with the thesis writing.

Table of Contents

Table of Figures

List of Tables

Publications

- **Su, Tianhong**, Lawless, Conor, Bernardino Gomes, Tiago M., Stewart, James B., Smith, Anna L.M., Baines, Holly L., Blain, Alasdair P., Vincent, Amy E., Larsson, Nils-Göran, Turnbull, Doug M., and Greaves, Laura C.. Selection against a germline mitochondrial tRNA mutation maintains mitochondrial function against ageing in mitotic cell populations. *Submitted*.
- **Su, Tianhong**, Grady, John P., Afshar, Sorena, McDonald, Stuart A. C., Taylor, Robert W., Turnbull, Doug M., & Greaves, Laura C. (2018). Inherited pathogenic mitochondrial DNA mutations and gastrointestinal stem cell populations. *The Journal of Pathology*, 246(4), 427-432.
- **Su, Tianhong**, Turnbull, Doug, & Greaves, Laura. (2018). Roles of Mitochondrial DNA Mutations in Stem Cell Ageing. *Genes, 9*(4), 182.

Abbreviations

ADP	Adenosine diphosphate
AMP	Adenosine monophosphate
ANT	Adenine nucleotide translocator
ATP	Adenosine Triphosphate
Ca^{2+}	Calcium
CI	Complex I
CldU	5-Chloro-2-deoxyuridine
CIV	Complex IV
CM	Cristae membrane
CoA	Coenzyme A
COX	Cytochrome c oxidase
CPEO	Chronic Progressive External Opthalmoplegia
Dels	Deletions
dH_2O	Distilled water
dNTP	Deoxynucleotide
DAB	Diaminobenzidine
DNA	Deoxyribonucleic acid
D-loop	Displacemnet loop
DRP	Dynamin-related proteins
EDTA	Ethylenediaminetetraacetic acid
EGFP	Enhanced green fluorescent protein
ETC	Electron transport chain
EtOH	Ethanol
FACS	Fluorescence-activated cell sorting

FADH2	Flavin adenine dinucleotide
Fe-S	Iron-sulphur
GI	Gastrointestinal
GTP	Guanosine triphosphate
H^+	Proton
H_2O	Water
HCl	Hydrochloric acid
H strand	Heavy strand
HSP	Heavy strand promoter
IBM	Inner boundary membrane
IdU	5-Iodo-2-deoxyuridine
IF	Immunofluorescence
IMM	Inner mitochondrial membrane
Ins	Insertions
Kb	Kilobase
KSS	Kearn-Sayre Syndrome
LHON	Leber's hereditary optic neuropathy
Leu	Leucine
L strand	Light strand
LSP	Light strand promoter
Lys	Lysine
M	Molar
mRNA	Messenger ribonucleic acid
mtDNA	Mitochondrial DNA
MELAS	Mitochondrial encephalopathy, lactic acidosis and stroke-like episodes
MERRF	Myoclonic epilepsy with ragged red fibres

MIDD	Maternally inherited diabetes and deafness
MIM	Mitochondrial import complex
ml	millilitre
mM	millimolar
MM	Mitochondrial mass
mTERF	Mitochondrial termination factors
mtSSB	Mitochondrial single stranded DNA binding protein
NADH	Nicotinamide adenine dinucleotide
NGS	Next generation sequencing
NBT	Nitro blue tetrazolium
O_H	Origin of heavy strand replication
O_L	Origin of light strand replication
OMM	Outer mitochondrial membrane
OPA1	Optic Atrophy 1
OXPHOS	Oxidative phosphorylation
PBS	Phosphate buffered saline
PCR	Polymerase chain reaction
PEN	Polyethylenenaphthalate
PEO	Progressive external opthalmoplegia
PGC1-α	Peroxisome proliferator-activated receptor gamma, coactivator 1 alpha
POLMRT	Mitochondrial ribonucleic acid polymerase
PolγA	Catalytic subunit of polymerase gamma
PolγB	Accessory subunit of polymerase gamma
$PolgA^{+/mut}$	Heterozygous polymerase gamma mutator mouse
$PolgA^{mut/mut}$	Homozygous polymerase gamma mutator mouse
POLG/Polγ	Mitochondrial polymerase gamma

PPARγ	Peroxisome proliferator-activated receptor γ
PMS	Phenazine methosulphate
Q	Ubiquinone
RC	Respiratory chain
RITOLS	Ribonucleotide incorporation throughout the lagging strand
RNA	Ribonucleic acid
ROS	Reactive Oxygen species
RRF	Ragged Red Fibre
RNA	Ribonucleic acid
rRNA	Ribosomal ribonucleic acid
SAM	Sorting and assembly machinery
SD	Standard deviation
SDH	Succinate dehyrdogenase
SI	Small intestine
SEM	Standard error of the mean
SKM	Skeletal muscle
SM	Smooth muscle
SS	Single stranded
TBS	Tris buffered saline
TBST	Tris buffered saline with Tween
TCA	Tricarboxylic acid cycle
TERM	Mitochondrial elongation factor
TFAM	Mitochondrial transcription factor A
TFB1M	Mitochondrial transcription factor B1
TFB2M	Mitochondrial transcription factor B2
TIM	Translocase of the inner membrane

TOM	Translocase of the outer membrane
tRNA	Transfer ribonucleic acid
TWINKLE	Twinkle helicase
VDAC	Voltage dependent anion channel
WT	Wild-type
W/V	Weight/volume
μm	micromolar
μl	microliter

Chapter 1 Introduction

1.1 Mitochondria

Mitochondria are dynamic organelles located in the cytoplasm of all mammalian eukaryotes. Their primary function is to supply cellular activities with energy in the form of adenosine triphosphates (ATP) through oxidative phosphorylation (OXPHOS) (Hatefi, 1985). Mitochondria also contribute to many other processes, such as generation of reactive oxygen species (ROS) (Sena and Chandel, 2012), calcium management (Raffaello *et al.*, 2016), iron-sulphur (Fe-S) cluster biogenesis (Stehling and Lill, 2013) and apoptosis (Wang and Youle, 2009), which makes mitochondria essential to cellular function and metabolism.

1.1.1 Origin and evolution

Two theories have been proposed to account for the origin and evolution of mitochondria. The earlier "serial hypothesis" describes that endosymbiosis is comprised of two events: the formation of the nucleus in Archaebacteria and the subsequent endocytosis of Eubacteria (proto-mitochondria) (Margulis, 1971). The alternative theory, "hydrogen hypothesis", describes a simultaneous formation of nucleus and mitochondrion through the integration of hydrogen-producing Eubacteria and hydrogen-dependent Archaebacteria (Martin and Müller, 1998). Both of the hypotheses agree that endosymbiosis occurs and the majority of the Eubacterial genes were transported to the host nucleus, which establishes a steady symbiotic relationship between them.

1.1.2 Structure

The first electron micrograph showed oval mitochondria with 1 – 2 μm in length and 0.5 – 1 μm in diameter (Palade, 1952). However, the shape of mitochondria is changeable, from the elongated rod to oval. The size and number of mitochondria are also cell-specific and dynamic, largely depending on the metabolic requirement of the cell (Scarpulla, 2011; Chan, 2012). Mitochondria have a double-membrane structure, comprising an outer and inner membrane with the intermembrane space in between (Figure 1.1). The outer mitochondrial membrane (OMM) separates mitochondria from the cytosol, whereas the inner mitochondrial membrane (IMM) invaginates inwards to form cristae and enclose the matrix (Figure 1.1)(Palade, 1952).

The OMM is a phospholipid bilayer, resembling a normal cell membrane. It is punctuated with numerous voltage-dependent anion channels (VDAC, a.k.a. porin), which permits the shuttling of small molecules up to 10 kDa (Bayrhuber *et al.*, 2008; Shoshan-Barmatz *et al.*, 2010). The IMM is a protein-rich lipid bilayer, containing ~75% proteins and ~25% lipidic constituents, in particular, cardiolipin (Fleischer *et al.*, 1961; Ardail *et al.*, 1990). This structure ensures electrochemical insulation that is crucial for OXPHOS and endows the IMM impermeability to polar molecules but not O_2, CO_2, H_2O and NH_3. Two components: the inner boundary membrane (IBM) and the cristae membrane (CM) form the IMM through the connections at cristae junctions (Frey and Mannella, 2000). The IBM is intimately interacted with the OMM and is enriched in proteins involved in mitochondrial fusion and import of nuclear-encoded proteins (Vogel *et al.*, 2006). The CM is densely folded, providing multi-subunit OXPHOS complexes with an extensive anchoring surface. The CM is also enriched in proteins associated with the transport of mitochondrial translation products and Fe-S cluster biogenesis (Vogel *et al.*, 2006).

The majority of mitochondrial proteins are nuclear encoded and are required to be imported into mitochondria to function. Most of these proteins are synthesised as a pre-protein with an N-terminal presequence, which are recognised and imported by the translocase of the outer membrane (TOM) and the presequence translocase of the inner membrane (TIM23) into the matrix to be further cleaved and processed (Wiedemann and Pfanner, 2017). Other machinery, such as the sorting and assembly machinery (SAM), mitochondrial import complex (MIM) at the OMM and the carrier translocase of the inner membrane (TIM22) at the IMM allow the import of peptides without any cleavable presequence (Wiedemann and Pfanner, 2017). In addition, the IMM contains abundant transporters termed adenine nucleotide translocator (ANT), for the exchange of ATP, ADP and ions between the matrix and the intermembrane space (Pfaff and Klingenberg, 1968).

The mitochondrial matrix encompasses multiple copies of mitochondrial DNA (mtDNA) packed in associated proteins to form nucleoids and transcription and translation machinery for the expression of mtDNA (Bonekamp and Larsson, 2018). It is also the site of Fe-S cluster biogenesis and important intermediary metabolism for OXPHOS, such as the TCA cycle and fatty-acid β-oxidation (Llopis *et al.*, 1998).

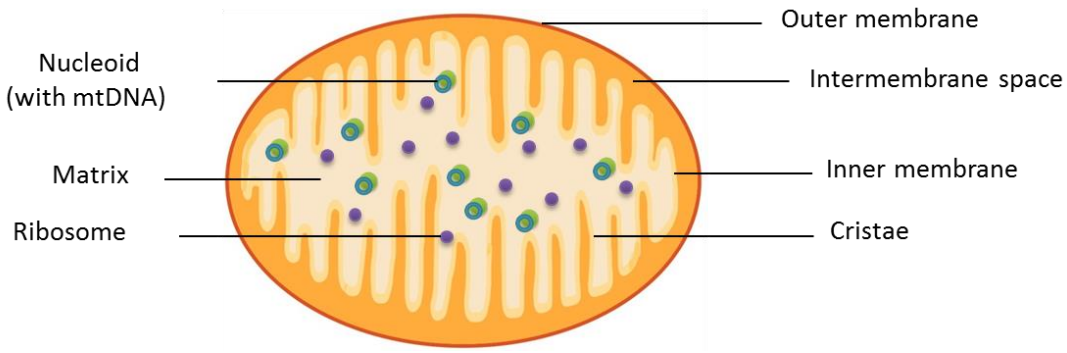

Figure 1.1 Microstructure of a mitochondrion. The mitochondrion is a double-membrane organelle containing 2-10 copies of mtDNA combined with proteins as nucleoids in the matrix. Respiratory chain complexes that are responsible for producing abundant energy via respiratory chain complexes at the inner mitochondrial membrane.

1.2 Mitochondrial Function

1.2.1 ATP synthesis

To maintain normal cellular functions, eukaryotic cells consume energy by hydrolysing ATP produced by aerobic and anaerobic cellular respiration. Mitochondria play an essential role in aerobic respiration to produce the majority of ATP for cellular activities. Resources such as monosaccharides, fatty acids and amino acids can all be utilised to generate ATP, in which glucose, a type of monosaccharide, is preferable (Smeitink *et al.*, 2001; Koopman *et al.*, 2012; Koopman *et al.*, 2013). ATP generation through aerobic respiration takes place in the cytosol where glucose is catalysed by a series of enzymes to produce pyruvate and reduced nicotinamide adenine dinucleotides (NADH), a crucial electron carrier (Koopman *et al.*, 2013). If the environment is oxygen-deficient, pyruvate tends to undergo anaerobic respiration catalysed by lactate dehydrogenase (LDH) to generate a small number of ATP molecules and lactic acid as a metabolite in the cytosol (Koopman *et al.*, 2013). This process is fundamental for providing energy for cells that do not contain mitochondria (e.g. erythrocytes) or for skeletal muscle fibres for sudden intense activities (Koopman *et al.*, 2013). In an oxygen-sufficient environment, pyruvate will be transferred into the mitochondrial matrix, and by virtue of pyruvate dehydrogenase (PDH), it will be converted to equimolar NADH and acetyl coenzyme A (CoA) through pyruvate decarboxylation (Koopman *et al.*, 2013). Acetyl CoA serves as the major substrate for the tricarboxylic acid (TCA) cycle (a.k.a. citric acid cycle or Krebs cycle) in the mitochondrial matrix, where NADH and another electron carrier, reduced flavin adenine dinucleotide ($FADH_2$) are yielded. NADH and $FADH_2$ are subsequently

transported to the IMM for OXPHOS, the end stage of aerobic respiration (Figure 1.2) (DiMauro and Schon, 2003).

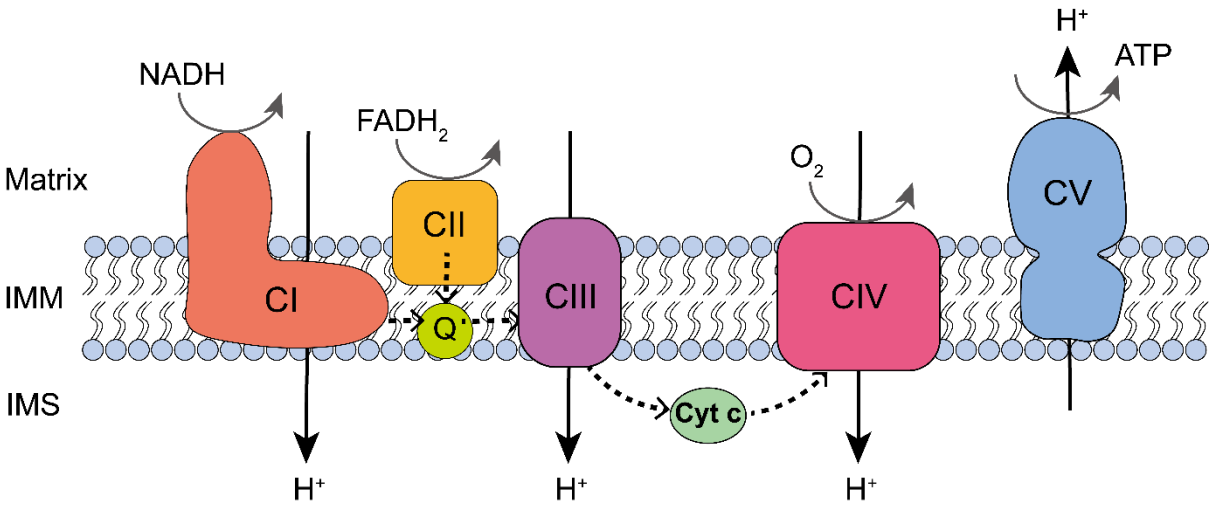

Figure 1.2 The OXPHOS system. The respiratory chain complex I (CI) and complex II (CII) obtain electrons from NADH and FADH2 respectively and transport them to complex III (CIII) through ubiquinone (Q). Electrons are further transferred via cytochrome *c* (Cyt *c*) to complex IV (CIV) and employed to reduce oxygen to water. H^+ are pumped into the intermembrane space (IMS) at the sites of CI, CIII and CIV, the reflux of which are employed by complex V (CV) to synthesise ATP. IMM, inner mitochondrial membrane. Dotted arrows indicate the transport route of electrons.

1.2.1.1 OXPHOS system and respiratory chain complexes

OXPHOS is conducted through five respiratory chain (RC) complexes: complex I, II, III and IV (CI, CII, CIII and CIV) together as the electron transport chain (ETC) and the ATP synthase (CV) (Hatefi, 1985). In brief, the electron carriers, NADH and FADH2, donate electrons to RC complex I and II, which are transported through the ETC (Hatefi, 1985). In the course of this process, protons (H^+) are pumped from the mitochondrial matrix to the intermembrane space at CI, CII and CIV to establish an electrochemical gradient, which is subsequently employed by CV to generate ATP (Figure 1.2) (Hatefi, 1985).

The RC complexes except CII have a transmembrane architecture with multiple subunits encoded by both nuclear and mitochondrial DNA (Brière *et al.*, 2005; Koopman *et al.*, 2013). The L-shaped CI (a.k.a. NADH: ubiquinone oxidoreductase) is the largest RC complex with 45 subunits: seven encoded by mtDNA and 38 encoded by nuclear DNA (nDNA). Its lipophilic arm is embedded in the OMM whereas the hydrophilic arm projects to the mitochondrial matrix (Clason *et al.*, 2010). CII (a.k.a. succinate: ubiquinone oxidoreductase)

is comprised of four subunits: two of them (SDHA and SDHB) protrude into the matrix with the base (SDHC and SDHD) anchoring to the OMM. It is entirely encoded by nDNA and is also involved in the TCA cycle as succinate dehydrogenase to convert succinate to fumarate (Brière *et al.*, 2005). CIII (a.k.a. ubiquinol: cytochrome *c* oxidoreductase) comprises 11 subunits, of which one (cytochrome *b*) is encoded by mtDNA. The terminal of the ETC is CIV (a.k.a. cytochrome *c* oxidase) that incorporates 13 subunits, of which three are mtDNA-encoded (MT-CO1, MT-COII and MT-COIII; also referred to as COX1, COX2 and COX3). ATP is produced at CV (a.k.a. F_0F_1 ATP synthase) that is composed of two rotary motors: the F_0 domain spanning the IMM and the F_1 domain projecting to the matrix. It comprises 19 subunits, and two of them in the F_0 domain (ATP6 and ATP8) are encoded by mtDNA. Information of the subunits in each RC complex is summarised in Table 1.1.

Respiratory chain complexes	**Total number of subunits**	**Number of mtDNA-encoded subunits**	**Subunit-encoding genes in mtDNA**
Complex I	45	7	ND1, ND2, ND3, ND4, ND4D, ND5 and ND6
Complex II	4	0	N/A
Complex III	11	1	Cytochrome *b*
Complex IV	13	3	COXI, COXII and COXIII
Complex V	19	2	ATP6 and ATP8

Table 1.1 A summary of mtDNA-encoded subunits in each respiratory chain complex.

During OXPHOS, CI and CII receive the electrons from NADH and $FADH_2$ respectively and transport them to ubiquinone (a.k.a. coenzyme Q_{10}; CoQ_{10}) (Figure 1.2). In parallel, CI pumps four protons to the intermembrane space. Ubiquinone is ultimately reduced to ubiquinol, both of which are lipophilic and can travel freely in the IMM. Electrons from ubiquinol are sequentially transferred by CIII to CIV via cytochrome *c* (Figure 1.2). Concurrently, CIII pumps four protons into the intermembrane space through continuous processing of two ubiquinol molecules (Hayashi and Stuchebrukhov, 2010). Cytochrome *c* is a nuclear-encoded haemoprotein, which also plays an important role in the mitochondria-dependent intrinsic pathway of apoptosis (Hüttemann *et al.*, 2011). Electrons carried by cytochrome *c* ultimately reach CIV, the final acceptor that reduces oxygen to water, which engenders translocation of

four protons into the intermembrane space (Figure 1.2). Protons pumped at CI, CIII and CIV build up an H^+ electrochemical gradient across the IMM (Figure 1.2). The backflow of protons through CV drives the rotation of its two sectors to phosphorylate ADP to ATP (Figure 1.2) (Okuno *et al.*, 2011; Koopman *et al.*, 2012). OXPHOS can generate approximately 30 ATP molecules in an ideal oxygen-sufficient environment with the consumption of one glucose molecule, making it the most efficient machinery to produce energy in eukaryotes (Rich, 2003). However, its efficiency never reaches 100% due to the leakage of protons and electrons (Brand, 1990; Jastroch *et al.*, 2010).

OXPHOS defects are common in patients with mitochondrial disease, which can occur in a single RC complex or in multiple complexes. Isolated CI defect is the most frequent type of isolated defects, followed by those in CIV and CV, whereas isolated CII defect is extremely rare (Mayr *et al.*, 2015; Alston *et al.*, 2017). Compared with isolated deficiency, combined defects in multiple RC complexes is more common in mitochondrial disease, which is predominantly caused by mutations in nuclear genes that encode proteins associated with mtDNA maintenance and mitochondrial protein synthesis (Mayr *et al.*, 2015). Combined defects are also seen in patients with mutations in mt-tRNA genes (Rocha *et al.*, 2015).

1.2.1.2 Respiratory chain supercomplexes

RC complexes not only exist as single entities but also link each other to form supercomplexes (Dudkina *et al.*, 2010), which was revealed by means of blue native polyacrylamide gel electrophoresis (BN-PAGE) and electron microscopy (Schägger and Pfeiffer, 2000; Schäfer *et al.*, 2006). In mammalian cells, CI associates with CIII, but more frequently, it integrates with CIII and CIV together to form supercomplexes termed "respirasome" (Winge, 2012). This structure is functional; it is able to complete the ETC in the presence of ubiquinone and cytochrome *c* (Acín-Pérez *et al.*, 2004). Assembly of respirasomes is organised. An intermediate of CI is initially created as a scaffold for subsequent aggregation of CIII and IV, which incorporates the catalytic subunit of CI for the final activation of respirasomes (Moreno-Lastres *et al.*, 2012). Lack of any component complex would fail the formation of supercomplexes (Acín-Pérez *et al.*, 2004). Functional respirasomes require intact complex constitutes. Specific mutations in an individual complex can cause secondary defects in other components of the supercomplex (Acín-Pérez *et al.*, 2004; Winge, 2012). The formation of supercomplexes is suggested to be advantageous, as it can probably enhance OXPHOS efficiency by facilitating electron carriers to targeted

enzymes and reducing the leak of protons and electrons (Schägger and Pfeiffer, 2000; Lenaz and Genova, 2009). The interactions between RC complexes have a profound implication for understanding mitochondrial dysfunction, in particular, combined OXPHOS defects, in mitochondrial disease and ageing.

1.2.2 Iron-sulphur cluster biogenesis

Mitochondria are the main site of haem and Fe-S cluster biogenesis and are essential for iron metabolism (Wang and Pantopoulos, 2011). Cellular iron is imported into the mitochondrial matrix by mitoferrin located at the IMM for multi-stage Fe-S cluster production (Paradkar *et al.*, 2009). Early synthesis machinery includes mitochondrial protein Isu1 (also Isu2 in yeast) as a scaffold with sulphide donated by the cysteine desulfurase complex. It is then delivered to Grx5 by virtue of chaperone proteins and can be received by specific mitochondrial apoproteins or assembled into polypeptide chains to form Fe/S proteins with the aid of Fe-S cluster targeting factors (e.g. Nfu1) (Stehling and Lill, 2013; Braymer and Lill, 2017). Fe-S clusters primarily contribute to OXPHOS, in which they facilitate electron transport and catalytic enzyme reactions in the ETC. They are also involved in the regulation and maintenance of iron homeostasis in mitochondria (Schultz and Chan, 2001).

1.2.3 Calcium homeostasis

Mitochondria are important for regulating intracellular calcium ion (Ca^{2+}) concentrations, where the mitochondrial membrane potential established by the ETC could drive the accumulation of Ca^{2+} in the mitochondrial matrix (Rizzuto *et al.*, 2012). Ca^{2+} crosses the OMM through VDAC and is imported into the matrix by the mitochondrial calcium uniporters (Kirichok *et al.*, 2004). The outflow of Ca^{2+} is facilitated by Na^{+}/$Ca2^{+}$ exchangers (Palty *et al.*, 2010). Ca^{2+} is an important signalling molecule mediating cellular communication (Hofer *et al.*, 2000), apoptosis (Orrenius *et al.*, 2003) and ATP production (Tarasov *et al.*, 2012) and plays a critical role in a number of physiological activities, such as the regulation of muscle contraction, synaptic transmission of signals as well as development of neuronal polarity and axonogenesis (Mattson and Partin, 1999; Abramov and Duchen, 2010; Gehlert *et al.*, 2015). The key role that mitochondria play in the regulation of Ca^{2+} homeostasis further expands their influence on a variety of cellular functions.

1.2.4 Generation of reactive oxygen species

Reactive oxygen species (ROS) are a collective name of superoxide radical anions (O_2^-), hydroxyl radicals (-OH) and hydrogen peroxide (H_2O_2), which derive from incomplete reduction of oxygen (Hämäläinen, 2016; Tan and Suda, 2017). The commonly believed major form of ROS, H_2O_2 that easily diffuse across membranes, is transformed from O_2^- by superoxide dismutase (SODs) (Dikalov and Harrison, 2012; Sena and Chandel, 2012). Although ROS are produced at multiple sites, it is generated mainly at mitochondrial ETC, in particular, CI and CIII, where CIII but not CI can produce ROS into the intermembrane space (Sena and Chandel, 2012). ROS are involved in a variety of signalling pathways regulating activation of immune cells, autophagy, senescence and apoptosis (Valko *et al.*, 2007; Sena and Chandel, 2012). ROS are also crucial for the maintenance of stem cell homeostasis and play a role in manipulating cell proliferation and differentiation (Hämäläinen, 2016; Tan and Suda, 2017). However, an excessive amount of ROS beyond the load of antioxidant systems can be detrimental. They cause cellular oxidative stress and damage biomolecules, such as DNA, proteins and lipids, which is believed to contribute to ageing (Forkink *et al.*, 2010; Chen *et al.*, 2017).

1.2.5 Apoptosis

Apoptosis is a delicate programmed process of cell death, which is essential for the maintenance of tissue homeostasis (Pellettieri and Alvarado, 2007). In mammalian cells, apoptosis is conducted through two pathways: mitochondria-independent extrinsic pathway and mitochondria-dependent intrinsic pathway, which display crosstalk and both lead to activation of executioner caspases, caspase 3 and caspase 7 to complete the death programme (Wang and Youle, 2009; Tait and Green, 2010; Lopez and Tait, 2015). In the intrinsic pathway, apoptotic stimuli, e.g. DNA damage, oxidative stress and excessive Ca^{2+}, activate pro-apoptotic BH3-only proteins, which further triggers the activation of pro-apoptotic effector proteins BAX and BAK, causing mitochondrial outer membrane permeabilisation (MOMP)(Cory and Adams, 2002; Pradelli *et al.*, 2010). Anti-apoptotic BCL-2 proteins can bind BH3-only proteins and activated BAX and BAK to antagonise this process (Cory and Adams, 2002; Lopez and Tait, 2015). Once MOMP occurs, it is irreversible and triggers the release of apoptotic proteins cytochrome *c* from the mitochondrial intermembrane space to the cytosol (Lopez and Tait, 2015). Cytochrome *c* then binds apoptotic protease activating factor 1 (APAF1), altering its conformation and causing its oligomerisation to form heptameric apoptosomes (Wang and Youle, 2009; Tait and Green, 2010; Lopez and Tait, 2015).

Subsequently, apoptosomes activate the initiator caspase protein, caspase 9, which cleaves and activates the executioner proteins, caspase 3 and caspase 7. In addition to cytochrome *c*, mitochondria discharge other apoptotic proteins, such as SMAC (a.k.a. DIABLO) and OMI, to facilitate the ultimate activation of the executioners by counteracting the function of the endogenous caspase inhibitor XIAP (Srinivasula *et al.*, 2001; Eckelman *et al.*, 2006; Tait and Green, 2010).

1.3 Mitochondrial dynamics and turnover

1.3.1 Fusion and fission

Mitochondria are dynamic organelles that constantly undergo fusion and fission, endowing them miscellaneous morphology (Chan, 2012). These two processes are also involved in the regulation of various mitochondrial functions, including maintenance of mtDNA stability, respiration, apoptosis, stress handling and quality control (Chan, 2012).

Both fusion and fission are mediated by a group of large guanosine triphosphates (GTPase) that are members of the dynamin family (Youle and Van Der Bliek, 2012). These proteins are highly conserved between different species (Hoppins *et al.*, 2007). Mitochondrial fusion involves the coordinated merging of the OMM and the IMM. In mammals, fusion of the OMM is mediated by transmembrane proteins Mfn1 and Mfn2 at the OMM and fusion of the IMM is regulated by Opa1 (Chen *et al.*, 2003; Cipolat *et al.*, 2004; Chan, 2012; Youle and Van Der Bliek, 2012). Mitochondrial fission in mammals is manipulated by a cytosolic protein Drp1, which needs to be recruited by secondary proteins, e.g. Mid49, Mid51 and Mff, to mitochondria, where it forms spirals to constrict and sever both the OMM and IMM (Smirnova *et al.*, 2001; Losón *et al.*, 2013; van der Bliek *et al.*, 2013).

Fusion and fission are crucial for modulating mitochondrial population and function. Below a specific threshold of mitochondrial stress, fusion benefits the maintenance of mitochondrial function by compensating damaged mitochondria with comparatively healthy mitochondria until they have reached the limit of repair (Nakada *et al.*, 2001; Youle and Van Der Bliek, 2012). Fission increases mitochondrial population and also segregates severely damaged mitochondria, contributing to mitophagy, i.e. selective autophagy of mitochondria, to maintain a healthy mitochondrial network (Youle and Van Der Bliek, 2012). Fusion and fission are also essential for embryonic development and directly affect embryonic survival (Chen *et al.*, 2003). Defects in mitochondrial dynamics are associated with ageing, which mainly manifest in the neurons of cases with neurodegenerative disease (Chen and Chan,

2006; Seo *et al.*, 2010). Furthermore, fusion and fission are involved in the regulation of stem cell homeostasis (Su *et al.*, 2018). Increased fission tends to maintain stem cell self-renewal and potency, whereas fusion counteracts the effect of fission and drives stem cell differentiation (Chen and Chan, 2017).

1.3.2 Mitophagy

Mitophagy is a quality control process that selectively removes dysfunctional mitochondria by autophagy from mitochondrial populations (Kim *et al.*, 2007). Mitochondrial fission is requisite to segregate the impaired portion of mitochondria to facilitate mitophagy (Chan, 2012; Youle and Van Der Bliek, 2012). Mitophagy is mediated primarily through the PINK1/Parkin pathway (Kitada *et al.*, 1998; Valente *et al.*, 2004). In healthy mitochondria, PTEN-induced putative kinase protein 1 (PINK1) is imported to the mitochondrial intermembrane space and cleaved by protease PARL (Meissner *et al.*, 2011). When mitochondria are dysfunctional and uncoupled, the import of PINK1 is blocked, leading to its accumulation at the OMM (Narendra *et al.*, 2008). PINK1 then recruits E3 ubiquitin ligase Parkin from the cytosol, resulting in ubiquitylation of OMM proteins (Narendra *et al.*, 2008). This entails mitochondria to be engulfed by double-membrane vesicles, i.e. autophagosomes, which then fuse with lysosomes for degradation (Youle and Narendra, 2011).

1.3.3 Mitochondrial biogenesis

Mitochondrial biogenesis is a process that aims to increase mitochondrial mass and mtDNA copy number to meet the energy demand of cells, which largely depends on delicate regulations of a group of nuclear-encoded proteins (Lee and Wei, 2005). Mitochondrial biogenesis responds to environmental change (e.g. cold), exercise, calorie restriction and oxidative stress (Lee and Wei, 2005; Zhu *et al.*, 2013). Peroxide proliferator activates receptor γ coactivator 1 alpha (PCG-1α) is central to mitochondrial biogenesis pathways (Puigserver and Spiegelman, 2003; Jornayvaz and Shulman, 2010; Fernandez-Marcos and Auwerx, 2011). Major upstream signalling regulators of PCG-1α include AMP-activated protein kinase (AMPK), Sirtuin 1 (SIRT1), cAMP responsive element binding protein (CREB) and p38 mitogen-activated protein kinase (p38 MAPK) (Scarpulla, 2011; Scarpulla *et al.*, 2012; Zhu *et al.*, 2013). Under calorie restriction, AMPK detects the fluctuation of AMP/ATP ratio and phosphorylates PCG-1α; in addition, SIRT senses the increase in the NAD+ level and deacetylates PCG-1α, which both lead to upregulation of PCG-1α (Cantó and Auwerx, 2009).

Exercise stimulates PCG-1α expression by activating p38 MARK as well as AMPK (Fernandez-Marcos and Auwerx, 2011). Cold, on the other hand, engenders elevation of cAMP, which activates protein kinase A (PKA), phosphorylating CREB to further enhance PCG-1α expression (Zhu *et al.*, 2013).

Increased expression of PCG-1α improves mitochondrial biogenesis by upregulating a group of proteins, including nuclear respiratory factors NRF1 and NRF 2, oestrogen related receptor alpha (ERRα) and peroxisome proliferator activated receptors (PPARs) (Wu *et al.*, 1999; Zhu *et al.*, 2013). Enhanced expression of NRFs upregulates mitochondrial transcription factor A (TFAM), a vital transcription activator whose level is intimately associated with mtDNA copy number (Virbasius and Scarpulla, 1994; Pohjoismäki *et al.*, 2006).

1.4 Mitochondrial genetics

1.4.1 Mitochondrial genome

Unlike the nuclear genome, human mitochondrial DNA (mtDNA) is a circular, double-stranded sequence with a superhelical structure and is absent of introns and histone (Anderson *et al.*, 1981). The human mtDNA was initially sequenced in 1981 and reviewed in 1999 (Anderson *et al.*, 1981; Andrews *et al.*, 1999). With a length of approximate 16.6kb, the mitochondrial genome consists of 37 genes, encoding 13 polypeptides as key components of the RC complexes, 2 ribosomal RNAs and 22 transfer RNAs (Figure 1.3) (Anderson *et al.*, 1981). Nuclear-encoded proteins that are synthesised in the cytoplasm and imported to mitochondria are indispensable for the maintenance of mitochondrial function along with mtDNA-encoded proteins (Schon *et al.*, 2001; Alston *et al.*, 2017). Within the 13 mtDNA-encoded polypeptides, seven (ND1, ND2, ND3, ND4, ND4D, ND5 and ND6) of them are constituents of complex I; one (cytochrome *b*) is a component of complex III; three (COXI, COXII and COXIII) are subunits of complex IV and two (ATP6 and ATP8) are elements of complex V, i.e. the ATP synthase (Figure 1.3) (Wallace, 1992).

Each mitochondrion contains approximately 2 – 10 copies of mtDNA molecules that are packed into a cluster of proteins to form complexes termed “nucleoids” (Wang and Bogenhagen, 2006; Gilkerson *et al.*, 2013). Many protein components in nucleoids are essential for mtDNA replication and expression, such as TFAM, mitochondrial DNA helicase (TWINKLE), single-stranded DNA binding protein (mtSSB) and mitochondrial DNA polymerase (POLγ) (Gilkerson *et al.*, 2013). The number of mtDNA copies is related to cellular energy demand in somatic cells and can substantially vary between different cell

types (Shoubridge and Wai, 2007). For example, oocytes carry > 10^5 copies of mtDNA molecules, whereas most of somatic cells contain thousands of mtDNA copies (Shoubridge and Wai, 2007). Stem cells can have a lower mtDNA copy number due to the high nuclear: cytoplasmic ratio; however, the ratio of mitochondrial mass and cellular mass is estimated similar to somatic cells (Birket *et al.*, 2011; Xu *et al.*, 2013).

The double strands of mtDNA are defined as the heavy (H) strand and the light (L) strand based on their differentiated buoyant densities in graded caesium chloride solutions as a result of different guanine contents between the two strands (Kasamatsu and Vinograd, 1974). The majority of mitochondrial genes are located in the H-strand, except the genes encoding ND6 and eight tRNAs, which are resident in the L-strand (Figure 1.3) (Anderson *et al.*, 1981; Wallace, 1992). MtDNA also contains a triple-strand section named the displacement (D) loop with a short sequence complementary to L-strand inserted between the location of heavy and light strands, which is the only non-coding sector in the mitochondrial genome (Figure 1.3) (Anderson *et al.*, 1981; Shadel and Clayton, 1997). The D-loop is critical to mtDNA maintenance and expression, as it includes major transcriptional promotors and the site of the origin of H-strand replication (Figure 1.3) (Taanman, 1999; Falkenberg *et al.*, 2007).

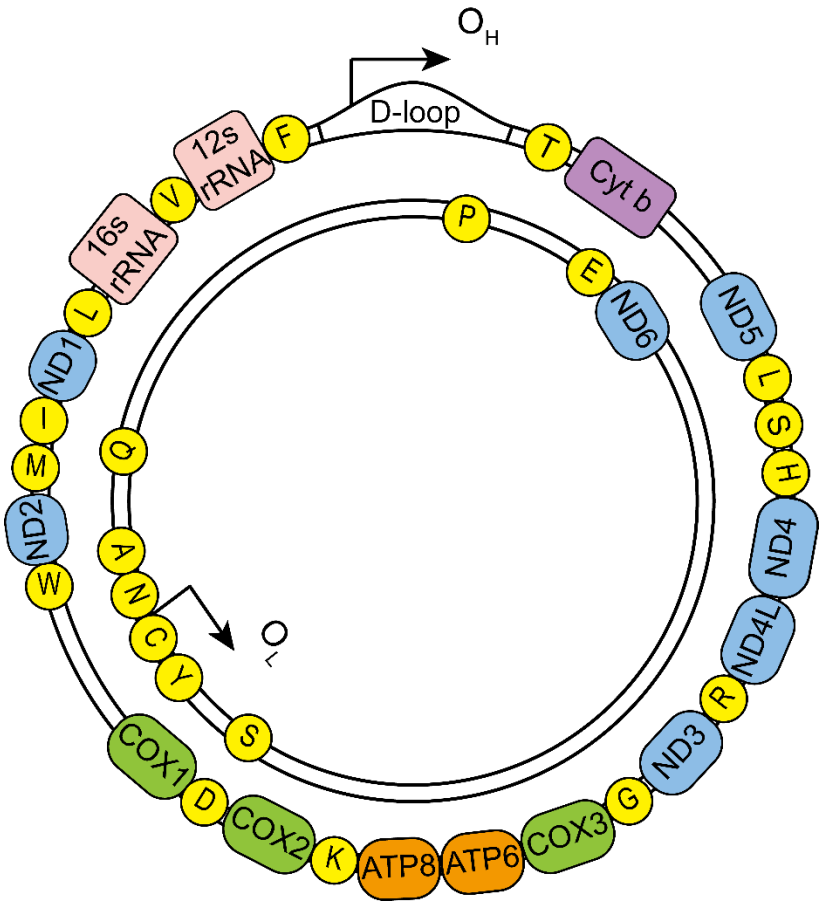

Figure 1.3 The human mitochondrial genome. The double-stranded genome encodes 37 genes, including 13 polypeptides (complex I genes in blue, complex III gene in purple, complex IV genes in green and complex V genes in orange), 22 tRNA (yellow) and 2 rRNA (pink). The sites of the origins of heavy (O_H) and light (O_L) strand replication are shown in the D-loop and the light strand respectively.

1.4.2 Mitochondrial DNA transcription

Transcription and replication of mtDNA are primarily regulated by the non-coding region of the mitochondrial genome. Transcription initiates at promotor domains, where heavy strand promoter (HSP) and light strand promotor (LSP) mediates the commencement of H-stand and L-strand transcription respectively to opposite directions (Montoya *et al.*, 1983; Falkenberg *et al.*, 2007). In detail, H-strand transcription initiates at two sites (HSP1 and HSP2). HSP2 produces transcripts that encompass information of all genes in the H-strand, whereas HSP2 only enables the transcription of two rRNAs and two tRNAs (Falkenberg *et al.*, 2007). LSP is the only commencing site for L-strand transcription, which produces transcripts for all genes in the L-strand. All three sites generate polycistronic transcriptional products (Taanman, 1999; Clayton, 2000).

Mitochondria have elegant transcription machinery containing TFAM, mitochondrial RNA polymerase (POLMRT) and mitochondrial transcription factors B1 and B2 (TFB1M and TFB2M) (Falkenberg *et al.*, 2002). Transcription is triggered by the binding of TFAM to the upstream of promoters, which leads to conformational changes in mtDNA, facilitating the incorporation of POLMRT and TFB1M/TFB2M. POLMRT forms a heterodimeric complex with either TFM1M or TFM2M to initiate transcription, though TFM2M is more potent than TFM1M (Taylor and Turnbull, 2007; Morozov *et al.*, 2014; Morozov *et al.*, 2015). POLMRT further conducts the elongation of the transcript assisted by mitochondrial elongation factor (TERM). The polycistronic transcriptional chain comprises protein-encoding and rRNA genes separated by tRNA genes, which needs to be processed and cleaved by RNAase to produce mature mRNA, tRNA and rRNA (Falkenberg *et al.*, 2007). This is proposed as the "tRNA punctuation model". The termination of transcription is mediated by mitochondrial transcription termination factors (mTERF) that are found to have four members (mTERF 1 - 4) (Martin Schmeing *et al.*, 2005; Falkenberg *et al.*, 2007). The entire process of transcription is highly accurate, and any minor imprecision may cause severe mitochondrial disease. For example, mitochondrial encephalomyopathy, lactic acidosis, and stroke-like episodes (MELAS) syndrome is principally caused by the m.3243A>G point mutation in the $tRNA^{Leu\ (UUR)}$ gene that is a binding location of mTERF. The mutation has been observed to weaken the binding affinity of mTERF to the sequence in vitro (Chomyn *et al.*, 1992a), which may impair mitochondrial protein synthesis.

1.4.3 Mitochondrial DNA translation

Mitochondria have their own translation apparatus to synthesise proteins encoded by mtDNA. This is carried out using the 22 mitochondrial encoded tRNA (Anderson *et al.*, 1981; Bibb *et al.*, 1981). Despite a smaller size compared with bacterial and cytosolic tRNA, most of them still have a classical cloverleaf architecture, comprising an acceptor stem with a CCA triplet, a D-loop, a T loop and an anticodon loop with their corresponding stems (Suzuki *et al.*, 2011). Mitochondrial translation in mammals occurs at mitoribosomes that are resident in the mitochondrial matrix (Smits *et al.*, 2010). Mitoribosomes are composed of a small 28S subunit (SSU) and a large 39S subunit comprising 12S and 16S mitochondrial rRNA respectively, with in total 82 nuclear-encoded mitochondrial ribosomal proteins (MRPs) (Greber and Ban, 2016). Despite similar functions, mitoribosomes have more protein components but harbour less rRNA compared with cytosolic ribosomes (Greber and Ban, 2016).

After transcription, mRNA and rRNA that are severed from polycistronic transcripts are prepared for mitochondrial translation through polyadenylation by mitochondrial poly (A) polymerase (Smits *et al.*, 2010). Mitochondrial translation is unique in many aspects, but it still follows the stepwise translation procedure, i.e. initiation, elongation and termination, which requires the involvement of nuclear-encoded initiation/elongation/release factors (Smits *et al.*, 2010). The mitochondrial translation system also necessitates nuclear-encoded aminoacyl-tRNA synthetase to attach amino acids to the CCA triplet of tRNA and methionyl-tRNA transformylase to formylate $tRNA^{Met}$, which are both required to commence the translational process (Hou, 2010; Smits *et al.*, 2010). As only 22 mitochondrial tRNA are available for mitochondrial translation, which is less than the minimum 31 tRNA for nuclear translation according to the "wobble hypothesis", mitochondria change several rules to compensate this shortage in translation (Barrell *et al.*, 1980; Smits *et al.*, 2010; Boos *et al.*, 2016). Typically, mitochondria use a codon pool that is slightly different from the universal codes (Xochitl *et al.*, 2008; Boos *et al.*, 2016). For example, AUA is a codon for arginine in the universal coding system, and AUU is a codon for isoleucine (Crick, 1966). However, they are recognised by formylated $tRNA^{Met}$ to initiate mitochondrial translation (Boos *et al.*, 2016). In contrast, nuclear translation commonly initiates at AUG that is the only codon for methionine according to the "wobble hypothesis" (Crick, 1966).

Mitochondrial translation is terminated when mitochondrial the translation release factor mtRF1a identifies the termination codons UAA and UAG (Soleimanpour-Lichaei *et al.*, 2007). However, many mRNA do not carry these stop codons but instead harbour AGA or AGG codons (Anderson *et al.*, 1981; Smits *et al.*, 2010). To terminate the translation of these mRNA, mitoribosomes can induce a frame shift to facilitate identification of the downstream UAG termination codon (Temperley *et al.*, 2010). The integrity of mitochondrial tRNA is critical for functional mitochondrial translation. Pathogenic mutations in mt-tRNA genes can ubiquitously impair synthesis of mtDNA-encoded protein and RNA products (Kauppila *et al.*, 2016).

1.4.4 Mitochondrial DNA replication

Mitochondrial DNA replication is independent of cell cycles, which is termed "relaxed replication" (Bogenhagen and Clayton, 1977). The turnover rate of mtDNA is higher in mitotic cells compared with that in post-mitotic cells, e.g. neurons (Wang *et al.*, 1997). Mammalian mtDNA replication is conducted by mitochondrial replisome that contains three

essential proteins: the mitochondrial TWINKLE helicase, the mitochondrial single-stranded DNA binding protein (mtSSB) and the mtDNA polymerase (POLγ) (Korhonen *et al.*, 2004; Falkenberg *et al.*, 2007; Falkenberg, 2018).

In mammalian cells, POLγ has a heterotrimeric structure comprising one catalytic subunit POLγA and two accessory subunits POLγB (Gray and Wong, 1992). The latter binds to double-stranded DNA and improves the catalytic activity and processivity of POLγA (Farr *et al.*, 1999; Yakubovskaya *et al.*, 2006). POLγA also contains a 3' – 5' exonuclease domain that endows it a proofreading ability, ensuring the fidelity of the polymerase (Gray and Wong, 1992; Longley *et al.*, 2001). The initiation of mtDNA replication at both the origin of heavy (O_H) and light strand replication (O_L) necessitates the RNA primers produced by POLRMT that also mediates mtDNA transcription (Chang and Clayton, 1985; Fusté *et al.*, 2010). POLγ is unable to use double-stranded DNA as a template, therefore, requires TWINKLE to unwind the double strands in the 5' to 3' direction ahead of it (Falkenberg, 2018). Once unwound, mtSSB binds to the single-stranded DNA to protect it from nucleolysis as well as enhance mtDNA synthesis by improving the function of TWINKLE and POLγ (Mignotte *et al.*, 1985; Farr *et al.*, 1999; Korhonen *et al.*, 2003). Mitochondrial DNA replication also needs proteins in addition to the essential apparatus to function. Paradigms for such proteins include the Ribonuclease H1 (RNASEH1) that removes RNA primers at the origins of replication and the mitochondrial topoisomerase (TOP1mt) that relieves torsional force of the strands during replication (Akman *et al.*, 2016; Falkenberg, 2018).

The complete mechanism of mtDNA replication has not been determined; however, three models for mtDNA replication have been proposed. The "strand-replacement" model (a.k.a. the asynchronous model) was the first model proposed in the early 1980s. According to this theory, transcription from LSP produces primers that trigger the replication of H-strand at O_H. When two-thirds of the new H-strand has been synthesised, the origin of L-strand replication (O_L) is exposed, enabling the continuous synthesis of a nascent L-strand. Once both strands are entirely synthesised, they combine to form another copy of mtDNA (Clayton, 1982). In the second model, the replication can initiate at multiple sites in a broad zone, where both new strands are synthesised simultaneously in opposite directions. More recently, RITOLS (ribonucleotide incorporation throughout the lagging strand) model has been proposed as the third model of mtDNA replication (Holt *et al.*, 2000; Bowmaker *et al.*, 2003). This model suggests that the new leading and lagging strands are not synthesised simultaneously, which is analogous to the "asynchronous" model. However, it suggests that the synthesis of the leading strand is concomitant with incorporation of RNA intermediates on the lagging strand. In due

course, the DNA synthesis of the lagging strand begins, primarily at O_L, where the RNA intermediates are substituted or converted to DNA (Holt and Reyes, 2012).

1.4.5 Mitochondrial DNA mutagenesis and repair

Different types of mutations can arise in mtDNA molecules, including mtDNA point mutations or DNA rearrangements, such as deletions, insertions and duplications (Schon *et al.*, 2012). Mitochondrial DNA point mutations are generally believed to the consequence of errors that occur during POLγ-mediated mtDNA replication (Zheng *et al.*, 2006), whereas deletions are proposed to arise from slippage replication or during repair of mtDNA with double-strand breaks (Krishnan *et al.*, 2008).

The mutation rate of mtDNA is higher than that of nDNA possibly due to the absence of histone and proximity to ROS generated by ETC (Brown *et al.*, 1979; Richter *et al.*, 1988). Such difference was also believed to result from a lack of any form of mtDNA repair system in the past (Clayton, 1982). However, recent studies show that mitochondria in fact share some mechanisms with nuclei for DNA repair, including base excision repair to remove damaged bases (e.g. oxidised lesions) (Stierum *et al.*, 1999; Liu *et al.*, 2008) and mismatch repair to remove unpaired nucleotide from POLγ replication errors (Liu and Demple, 2010; Zinovkina, 2018). In addition, accumulating evidence suggests the existence of homologous recombination and non-homologous end joining in the mtDNA repair system for fixing double-strand breaks (Liu and Demple, 2010; Zinovkina, 2018). Furthermore, Mitochondria can direct damaged mtDNA molecules for degradation to prevent the amplification of defective mtDNA (Shokolenko *et al.*, 2009).

1.4.6 Heteroplasmy and threshold effect

One cell generally contains thousands of copies of mtDNA, with 2-10 copies per mitochondria. This property of mtDNA refers to polyplasmy, which is distinct from nuclear DNA (Taylor and Turnbull, 2005). A state where all copies of mtDNA have identical genotypes is termed homoplasmy. More frequently, the mitochondrial population encompasses mtDNA copies with pathogenic mutations or polymorphic variants as well as wild-type copies (Holt *et al.*, 1988). This status is referred to as heteroplasmy and is commonly expressed as a fraction of the mutated mtDNA copies in tissue/cells. (Larsson and Clayton, 1995; Smeitink *et al.*, 2001).

A pathogenic heteroplasmic mtDNA mutation does not necessarily cause mitochondrial dysfunction and OXPHOS deficiency unless it accumulates to a certain threshold. This characteristic is termed as the threshold effect (Figure 1.4) (Sciacco *et al.*, 1994). Biochemical thresholds of mutations are affected by multiple factors, such as mutation type, cell types, the cellular energy demand and the remaining amount of wild-type mitochondrial genomes. Within a variety of pathogenic mutations, mutations in tRNA are generally tolerable compared with large-scale deletions. The threshold for tRNA mutations is ~90% (Yoneda *et al.*, 1995), but only ~70 – 80% for large-scale deletions in skeletal muscle (Sciacco *et al.*, 1994). The threshold for point mutations in protein-encoding genes can vary, which is specifically tailored for different mutations (Schon *et al.*, 2012). However, once the mutation load is above 95%, OXPHOS deficiency will occur for all pathogenic mutations (Schon *et al.*, 2012). Heteroplasmy and threshold effect have profound implications for the heterogeneous phenotypes of mitochondrial disorders.

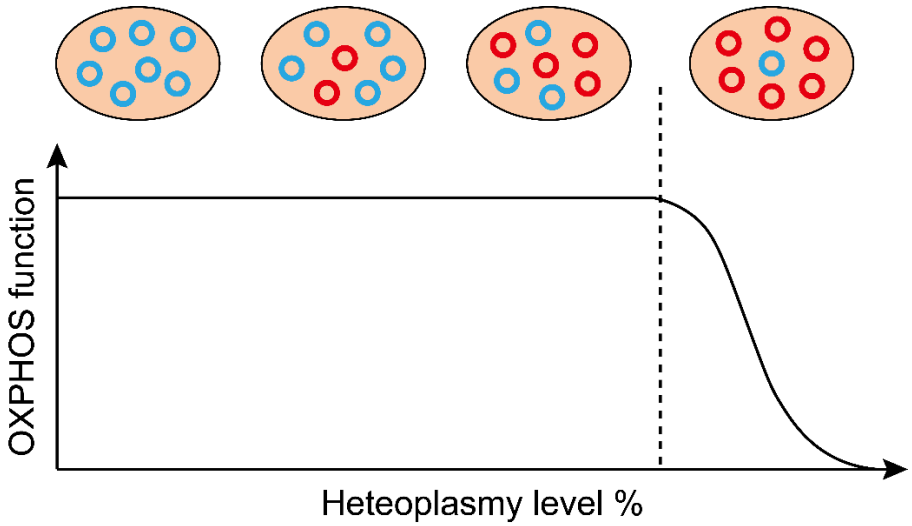

Figure 1.4 Mitochondrial threshold effect. Mitochondrial DNA mutations (red circles) can be recessive. Cells can maintain normal OXPHOS function by virtue of the compensation of a certain level of wild-type mtDNA molecules (blue circles) until the heteroplasmy of mtDNA mutations reaches a mutation-specific threshold level (dotted line), at which point OXPHOS function is compromised.

1.4.7 Maternal inheritance and bottleneck effect

It is commonly accepted that mtDNA is maternally transmitted, despite a study exceptionally reporting a small amount of paternal mtDNA leakage in the offspring of interspecific hybrids of two mice strains (Gyllensten *et al.*, 1991). Homoplasmic mutations are transmitted entirely, though they do not necessarily develop into congenital diseases. For example, among individuals who carry homoplasmic mutations that could cause Leber hereditary optic neuropathy (LHON), approximately only half of the males and only one-tenth of the females among them will contract the disease (Man *et al.*, 2003). In comparison, heteroplasmic inheritance of mtDNA is more frequent and complicated. In addition, the inherited risks for different types of mutations are differential. The transmission of single large-scale deletions of mtDNA is occasional, even rare, in light of the studies on a large cohort of patients (Chinnery *et al.*, 2004). In contrast, transmission of mtDNA point mutations is common, predisposing individuals to compromised physical function or even inherited mtDNA diseases depending on the number of mutations transmitted through the germline (Falkenberg *et al.*, 2007). The heteroplasmy levels can notably vary from generation to generation, and an unaffected mother possibly gives birth to affected offspring, which makes genetic counselling difficult. This is due to the bottleneck effect, where a small number of mutated mtDNA in primordial germ cells are substantially amplified through rapid replication, which is commonly believed to occur during oogenesis (Stewart and Larsson, 2014).

1.4.8 Clonal expansion

Clonal expansion refers to a process where a mutated mtDNA molecule clonally amplifies and becomes the dominant mitochondrial genotype in a cell (Mita *et al.*, 1989). It is crucial for the development of highly heterogeneous biochemical phenotypes of tissue/cells in both aged individuals and patients with mtDNA disease. The exact mechanism by which clonal expansion occurs remains unknown; however, several hypotheses have been proposed to explain this phenomenon.

The “survival of the smallest” model was proposed first, theorising that a mitochondrial genome with large-scale deletions takes advantage of its smaller size to replicate faster than the wild-type genome (Wallace, 1989). However, this hypothesis could not apply to the clonal expansion of mtDNA point mutations. In addition, a small genome that has lost many genes is unlikely to obtain enough ATP for its rapid replication, as it probably cannot produce intact proteins to support a functional OXPHOS system (Kowald and Kirkwood, 2000).

Alternative theories hypothesise that mutations in protein encoding or tRNA genes could cause a change in mitochondrial function to facilitate their clonal amplification (Shoubridge *et al.*, 1990; De Grey, 2005). Shoubridge initially proposed that mtDNA defects might induce compensatory enhancement of mitochondrial biogenesis, which leads to amplification of the defective genome. This is evidenced by identification of ragged red fibres (RRF) with proliferated mitochondria in the muscle of some patients with mtDNA disease (Shoubridge *et al.*, 1990). Further studies support this hypothesis, showing that non-selective proliferation of mtDNA content that contains mutated and wild-type DNA molecules could eventually lead to clonal expansion of mutated molecules when the mutation heteroplasmy exceeds a specific threshold, though, before the point, mtDNA biogenesis could be beneficial to maintain the amount of wild-type mtDNA in a comparatively normal range (Chinnery and Samuels, 1999; Durham *et al.*, 2007). An alternative hypothesis proposed by De Grey theorises that defective mtDNA has the advantage to elude from quality control systems, as it impairs the function of ETC, which diminishes the generation of oxidative stress that damages mitochondrial membrane, thus reducing the degradation of the dysfunctional mitochondria (De Grey, 2005). These two hypotheses have provided meaningful views that link mitochondrial functions to clonal expansion but to some extent overlook mitochondrial dynamics and underestimate quality control systems.

More recently *in silico* modelling has become a useful tool for studying the clonal expansion of mtDNA mutations, and has contributed to the proposal of "random genetic drift" hypothesis. Computer simulations suggest that relaxed mtDNA replication and non-selective distribution of mtDNA molecules into daughter cells during cell division can solely account for the clonal accumulation of mutated mtDNA in mitotic cells, including healthy buccal epithelial cells, cancer cells (Coller *et al.*, 2001) and intestinal stem cell populations (Stamp *et al.*, 2018). Unbiased replication of mtDNA can also result in a clonal expansion of mutations in post-mitotic cells (Elson *et al.*, 2001). Random genetic drift is suggested to take place early in life to allow a mutation to expand to a high level in tissue over a long time (Elson *et al.*, 2001; Greaves *et al.*, 2014).

1.4.9 Mitotic segregation

It is commonly believed that mitochondria are randomly segregated during cell division (Tuppen *et al.*, 2010). If a mitotic cell harbours heteroplasmic mutated mtDNA, mitotic/vegetative segregation will result in substantial variations in mutation levels between daughter cells (Figure 1.5). However, recent in vitro studies challenge the notion of mitotic segregation, showing that stem cells might be able to selectively separate aged mitochondria during division to maintain stem cell properties in part of the daughter cells (Katajisto *et al.*, 2015). However, this mechanism might not always be activated in vivo, as computer modelling suggests that mitotic segregation leads to clonal expansion of somatic mtDNA mutations in dividing cells including colonic stem cell populations (Coller *et al.*, 2001; Stamp *et al.*, 2018). On the contrary, patients with mtDNA disease are found to lose specific inherited mtDNA mutation in mitotic blood with age, suggesting contrasting fates between different types of mtDNA mutations during cell division (Rahman *et al.*, 2001; Grady *et al.*, 2018) (detailed in 3.1).

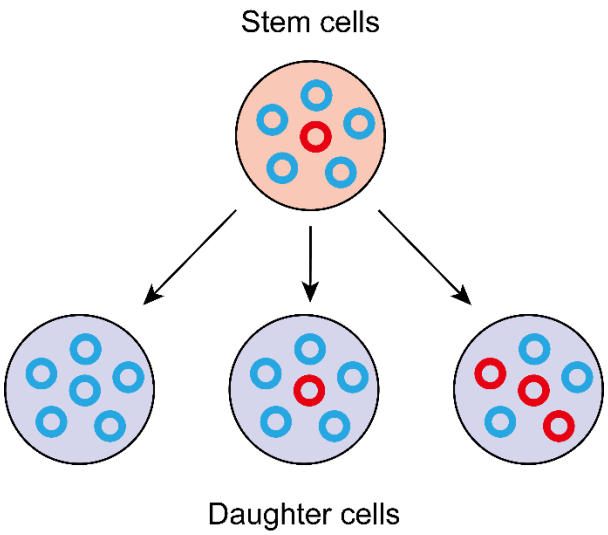

Figure 1.5 Shift of mutation levels in daughter cells during stem cell division as a result of mitotic segregation. Relaxed replication of mtDNA with random segregation during cell division allows stem cells with mutated mtDNA molecules (red circle) to produce daughter cells with variable heteroplasmy levels. Blue circles are wild-type mtDNA molecules.

1.5 Mitochondrial DNA mutations in ageing and disease

1.5.1 Somatic mtDNA mutations in humans and mice

1.5.1.1 Somatic mtDNA mutations in normal aged humans

Normal individuals accumulate OXPHOS deficiency in a variety of tissues with age, including post-mitotic skeletal muscle, heart and brain and mitotic blood, epithelium of stomach and intestines (Müller-Höcker, 1989; Müller-Höcker, 1990; Cottrell *et al.*, 2001; Taylor *et al.*, 2003; McDonald *et al.*, 2008; Gutierrez‐Gonzalez *et al.*, 2009). In colonic epithelium, OXPHOS defects increase exponentially with age (Taylor *et al.*, 2003). Crypts with COX deficiency are rarely observed in young adult (< 30 years old), whereas the number of COX-deficient crypts can rapidly increase afterwards to reach ~15% of the crypt population in aged humans (>70 years old) (Taylor *et al.*, 2003). Combined CI, CIII and CIV deficiency is the major type of OXPHOS defects in colonic crypts of aged humans, followed by isolated CIV deficiency, whereas isolated CI deficiency is a rare form of OXPHOS defects in the aged colonic epithelium (Greaves *et al.*, 2010). OXPHOS deficiency can affect the function and turnover of colonic epithelial cells, which is discussed in Chapter 6.

The OXPHOS defects are caused by the accumulation of miscellaneous somatic mtDNA mutations, including common mutations that cause mtDNA disease, such as the large-scale deletions spanning 4977 nucleotides (Schon *et al.*, 1989), and m.3243A>G and m.8344A>G point mutations (Münscher *et al.*, 1993; Zhang *et al.*, 1993). A study using an improved PCR technique with higher sensitivity demonstrates that the mutation level of m.3243A>G in the skeletal muscle, brain, heart, liver and kidney of middle-aged and elderly adults is 5- to 10-fold higher compared with infants (Liu *et al.*, 1997). Other studies show that somatic mtDNA mutations can occur early in life, which clonal expand to a high level in the soma (Greaves *et al.*, 2014).

The accumulation of somatic mtDNA mutations has a tissue-specific manner. Post-mitotic tissue tends to acquire mtDNA deletions (Pallotti *et al.*, 1996; Reeve *et al.*, 2009), whereas mitotic tissue tends to obtain point mutations (Taylor *et al.*, 2003). In addition, in mitotic tissue that is rapidly renewed by adult stem cells, mutations are likely to occur and accumulate in stem cells and expand in the rest of the tissue. Studies have shown a massive mtDNA heterogeneity in the clones of CD34+ positive haematopoietic stem cells (HSC) and progenitor cells in the bone marrow of adults compared with the clones of CD34+ cells in umbilical cord blood (Shin *et al.*, 2004a). Somatic mtDNA mutations are also shown to accumulate in gastric and intestinal stem cells that pass down the mutations to all their

progeny in gastric glands and intestinal crypts (Taylor *et al.*, 2003; McDonald *et al.*, 2008; Gutierrez‐Gonzalez *et al.*, 2009). Furthermore, somatic mtDNA mutations can spread via crypt or gland fission in the gastrointestinal epithelium, which is possibly associated with stem cell niches (Greaves *et al.*, 2006; McDonald *et al.*, 2008; Gutierrez‐Gonzalez *et al.*, 2009). The accumulation of somatic mtDNA mutations is intimately associated with ageing and age-related disease and cancer, but whether it plays a causal role in these processes is still contentious (Khrapko and Vijg, 2009; Baines *et al.*, 2014b).

1.5.1.2 mtDNA-mutator mice

To date, several mouse models have been developed, showing an accumulation of mtDNA mutations with age, such as Mito-PstI mice, "deletor mice" and mtDNA-mutator mice. The mito-PstI mice are created by induction of mtDNA double-strand breaks, which primarily causes mtDNA depletion (Pinto *et al.*, 2016). Accumulation of mtDNA deletions is also observed in the brain and muscle of these mice (Pinto *et al.*, 2016). The deletor mice have a p.A360T change or a duplication in TWINKLE expression, which correspond to the expression of genes with dup352-364 and A359T mutations in patients with PEO (Tyynismaa *et al.*, 2005). These changes lead to the accumulation of multiple DNA deletions and respiratory chain defects in the brain and skeletal muscle with age (Tyynismaa *et al.*, 2005). These mouse models emphasise the accumulation of deletions in post-mitotic tissue rather than point mtDNA mutations in mitotic tissue. As this thesis focuses on the dynamics of mtDNA point mutations in epithelial cells, the mtDNA-mutator mice with a notable accumulation of point mutations in mitotic tissue are discussed in more detail.

The mtDNA-mutator mice carry a knock-in missense mutation in the exonuclease domain of *Polg* that encodes mtDNA polymerase gamma (Polγ), impairing its proofreading ability, which results in an accumulation of somatic mtDNA mutations with age in a variety of mouse tissues (Kujoth *et al.*, 2005; Trifunovic *et al.*, 2005). These short-lived $PolγA^{mut/mut}$ mice harbour respiratory chain defects in various tissues and display a number of ageing phenotypes, including weight loss, kyphosis, hair loss, compromised hearing, reduced subcutaneous fat, osteoporosis, muscle loss and sterility (Trifunovic *et al.*, 2004; Kujoth *et al.*, 2005). The European strain with C57B1/6N background (Trifunovic *et al.*, 2004) displays more severe physiological and biochemical defects compared with the American strain with C57B1/6J background (Kujoth *et al.*, 2005), highlighting the impact of nuclear regulation on the phenotype manifestation.

In addition, these mice predominantly accumulate mtDNA point mutations and suffer hampered development of mitotic intestine, thymus and testicle (Kujoth *et al.*, 2005). The death of these mice is most often due to progressive anaemia that results from defective haematopoiesis, suggesting that the accumulation of somatic mtDNA mutations affect HSC functions (Trifunovic *et al.*, 2004; Kujoth *et al.*, 2005; Chen *et al.*, 2009). Further research showed that the homeostasis of different types of adult stem cells and progenitor cells are impeded in these mice (Chen *et al.*, 2009; Norddahl *et al.*, 2011; Ahlqvist *et al.*, 2012; Fox *et al.*, 2012; Su *et al.*, 2018). In particular, studies show an altered cell cycle and increased apoptosis in the small intestinal crypt of the mutator mice, which is comprised of intestinal stem cells (ISC) and transit-amplifying cells (Fox *et al.*, 2012). Impaired growth of the organoids (comprising stem cells and Paneth cells) that are developed from isolated crypts is also reported (Fox *et al.*, 2012). The functional changes in intestinal stem cells and progenitor cells result in extended cell migration, morphological alterations in the intestinal epithelium and hampered fat absorption of the mtDNA-mutator mice (Fox *et al.*, 2012). These findings together suggest that mtDNA mutagenesis can alter stem cell properties (self-renewal and differentiation ability), which could be through impairing mitochondrial functions and dynamics (Su *et al.*, 2018).

1.5.2 Selective pressures on mtDNA mutations

1.5.2.1 Selective pressures on mtDNA mutations during germline transmission

Mitochondrial DNA mutations can also accumulate in germline (Gustafsson *et al.*, 2016). Fortunately, the germline has a purifying selective pressure on extremely pathogenic mtDNA mutations, in particular, non-synonymous mutations in protein-encoding genes (Stewart *et al.*, 2008). Selection against the milder mutations in mt-tRNA genes are relatively less intense, but some studies have shown a strong selective pressure against certain mutations in tRNA genes during post-fertilisation embryonic development (Stewart *et al.*, 2008; Freyer *et al.*, 2012). The time point that the germline selection occurs remains elusive. To date, studies have indicated that the segregation of mtDNA mutations is unbiased during germ cell maturation, and negative selection occurs post-oogenesis (Fan *et al.*, 2008; Stewart *et al.*, 2008; Freyer *et al.*, 2012). In addition, females with a heavy mutation burden show impaired fertility, suggesting that mutations might also be selected against at the organismal level (Stewart *et al.*, 2008; Burr *et al.*, 2018). Furthermore, studies have reported a positive relationship between the number of mtDNA variants transmitted through the germline and

maternal age, suggesting a negative effect of female age on the selective pressure on mtDNA variants (Rebolledo-Jaramillo *et al.*, 2014).

The exact mechanism of the germline selection is unclear; however, several hypotheses have been proposed based on the current findings. The bottleneck effect in germline transmission is commonly believed to cause a shift of heteroplasmy between generations (Gustafsson *et al.*, 2016). It is powerful enough to fix a *de novo* DNA polymorphic variant in a maternal lineage within a few generations (Upholt and Dawid, 1977; Olivo *et al.*, 1983). Studies have provided evidence that the bottleneck effect changes the heteroplasmy level via stochastic sampling of a small number of mtDNA molecules in human and mice (Jenuth *et al.*, 1996; Chinnery *et al.*, 2000). Nevertheless, this is unable to explain the selective loss of some pathogenic mtDNA mutations through germline transmission (Freyer *et al.*, 2012). Studies on Drosophila suggest that the negative selective force might result from phenotypically compromised fitness of mitochondria, which is possibly mediated by a change in the mitochondrial membrane potential (Hill *et al.*, 2014; Ma *et al.*, 2014; Stewart and Larsson, 2014). A recent study has suggested that the switch from glycolytic to oxidative metabolism of primordial germ cells during their development is able to expose the pathogenicity of mtDNA mutations to facilitate their targeting for selective removal (Floros *et al.*, 2018). This study also reported the existence of a bottleneck effect in somatic cells during embryonic development, implying that mitotic cell populations might share some common mechanisms for the segregation of mtDNA molecules (Floros *et al.*, 2018). Despite limited quantity of evidence at present, it is hypothesised that the selection against mtDNA mutations within germline transmission can take place at the organismal level (compromised female fertility), the cellular level (impaired cell division or an inclination to cell death) and the mitochondrial level (unfitness of mitochondria) (Stewart *et al.*, 2008; Freyer *et al.*, 2012; Burr *et al.*, 2018; Floros *et al.*, 2018; Zhang *et al.*, 2018).

1.5.2.2 The absence of selective pressures on somatic mtDNA mutations

Mechanisms underlying the accumulation of somatic mtDNA mutations in normal ageing populations remains unclear. Harman initially proposed the free radical theory stating that impaired respiratory chain produces excessive ROS, which exacerbates mtDNA mutagenesis, generating more oxidative stress and forming a "vicious cycle" (Harman, 1972). This theory is challenged by some studies showing that the occurrence rate of somatic mtDNA mutations is unlikely to change with age (Greaves *et al.*, 2014). On the other hand, in silico modelling

suggests that random genetic drift can solely engender the clonal expansion of somatic mtDNA mutations in both dividing and non-dividing cells (Coller *et al.*, 2001; Elson *et al.*, 2004). However, these two hypotheses are not mutually exclusively.

The mechanism underpinning the accumulation of somatic mtDNA mutations is thought to be tailored for specific mutations and tissue/cell types. For example, some mutations are proposed to have an advantage for clonal expansion (detailed in 1.4.8). In addition, vegetative segregation in mitotic cell populations with perpetual relaxed replication complicate the dynamics of mtDNA mutations (detailed in 1.4.8 and 1.4.9) (Stewart and Chinnery, 2015). Furthermore, tissue-specific nuclear factors are found to manipulate the segregation of mtDNA mutations (Jokinen *et al.*, 2010).

Mitochondrial DNA mutations can also be inherited through the germline and cause mtDNA disease. During transmission, mutations are under strong purifying selective pressures, which eliminate those that are highly pathogenic, leaving the comparatively mild mutations/variants to pass down to the next generation (Fan *et al.*, 2008; Stewart *et al.*, 2008; Greaves *et al.*, 2012a). However, the acquired somatic mtDNA mutations in colonic epithelium are significantly more pathogenic than the germline variants (Greaves *et al.*, 2012a). In addition, the accumulated somatic mutations are randomly distributed in the mitochondrial genome (Greaves *et al.*, 2012a). These findings suggest no purifying selection against somatic mtDNA mutations.

1.6 Overview of mitochondrial disease

As mitochondrial function is maintained by proteins encoded by both mtDNA and nDNA, pathogenic mutations in either genome can cause mitochondrial disease. The minimum prevalence of mitochondrial disorders is estimated at one in 5000 as summarised from combined epidemiological data of both children and adults (Schaefer *et al.*, 2004). Recently studies show that in adult populations, the prevalence of mitochondrial disease caused by mitochondrial and nuclear DNA mutations is approximately one in 4300 (Gorman *et al.*, 2015). The actual prevalence could be higher as mitochondrial disease is an enormously heterogeneous group of disorders with miscellaneous phenotypic expressions in multiple systems and broad ages of onset with diverse clinical features, which tremendously hampers their diagnosis (Schaefer *et al.*, 2004). The massive heterogeneity of mitochondria disease is a result of multifaceted impacts of different factors, including the mutation type, heteroplasmy

and biochemical threshold, bottleneck effect, mitotic segregation and clonal expansion (Taylor and Turnbull, 2005).

Nuclear DNA encodes structural subunits for RC complexes as well as proteins for complex assembly, maintenance and expression of mtDNA and mitochondrial dynamics. Pathogenic mutations in nDNA can cause a variety of mitochondrial disorders (Lightowlers *et al.*, 2015). For instance, mutations in nuclear genes POLG and PEO1, which encodes POLγ and TWINKLE respectively, can cause secondary mtDNA depletion and deletions, resulting in severe mitochondrial disorders (Spelbrink *et al.*, 2001; Naviaux and Nguyen, 2004; Lightowlers *et al.*, 2015). This thesis focuses on mtDNA mutations, in particular, point mutations in mt-tRNA genes, which cause primary mtDNA disease. Thus, I will discuss these in more detail.

1.6.1 Overview of mtDNA disease

Pathogenic mtDNA mutations are estimated to be carried by a minimum of one in 200 individuals (Elliott *et al.*, 2008). Despite the presence of mitochondria in all eukaryotic cells, tissue with high energy-consumption like brain, heart, skeletal muscle and retina are more susceptible to mitochondrial dysfunction caused by mutations (DiMauro and Schon, 2003). Although the clinical manifestations of mtDNA disease are extremely heterogeneous, they share several common features, such as lactic acidosis and presence of ragged-red fibres (RRF) in skeletal muscles (DiMauro and Schon, 2003). The RRF are termed such for the appearance of myocytes with over-accumulated mitochondria at its subsarcolemmal region when they are stained using Gomori Trichrome (Cunningham, 1963; Mita *et al.*, 1989).

Diagnosis of mtDNA disease is facilitated by a variety of histochemical and biochemical assays, such as Gomori Trichrome stain, sequential COX/SDH histochemistry and quadruple immunofluorescence enormously. These have revealed many typical features of patients' tissue, in particular, muscle fibres, such as RRF, COX deficiency and decreased expression of RC complexes (Sciacco *et al.*, 1994; Rocha *et al.*, 2015). Determination of phenotypes is normally followed by genetic diagnosis using genome sequencing, with next-generation sequencing based techniques becoming prevalent (Alston *et al.*, 2017).

Though genetic diagnosis is of great potential, the diagnosis of mitochondrial disease is still difficult because there is no strict correlation between mutations and their clinical manifestations. Moreover, treatment is limited, auxiliary and possibly ineffective at present (DiMauro and Schon, 2003; Taylor and Turnbull, 2005). Hence, detection and prevention of

the transmission of mtDNA mutations becomes crucial, where prenatal diagnosis and assisted reproduction methods including pre-implantation genetic diagnosis (PGD), pronuclear transfer and polar body genome transfer are promising strategies (Craven *et al.*, 2010; Wang *et al.*, 2014)

1.6.2 Mutations in mtDNA disease

Mitochondrial DNA mutations, in essence, are a highly heterogeneous group of mutations that have distinct nature in many aspects. First, inheritance of mtDNA mutations can be different. For example, point mutations are normally transmitted through the germline, whereas single large-scale deletions are generally sporadic, arising during oogenesis or early embryogenesis and clonally expanding via rapid replication during cell division (DiMauro and Schon, 2003; Greaves *et al.*, 2012b; Schon *et al.*, 2012). Moreover, the biochemical thresholds of different mtDNA mutations vary (covered in 1.4.6). Furthermore, in contrast to the somatic mtDNA mutations that accumulate in mitotic tissue with age and cause OXPHOS deficiency, some inherited mutations tend to decrease in mitotic blood and certain epithelial cells with age (Larsson *et al.*, 1990; Grady *et al.*, 2018). Such loss is sometimes concomitant with recovered symptoms of patients (McShane *et al.*, 1991; Nørby *et al.*, 1994). Specific inherited mtDNA mutations are also distributed non-randomly between different tissues, which is intimately associated with dividing abilities of the tissue (Chinnery *et al.*, 1999). These intriguing phenomena that contrast the permissive accumulation of somatic mtDNA mutations suggest potential selective pressures against inherited mtDNA mutations in mitotic tissue, which are discussed in detail in Chapter 3. This feature is crucial to the development of tissue-specific phenotypes. Studying the mechanism of these features would benefit understanding of mtDNA disease progression and development of potential treatment. Therefore, this PhD work aims to further investigate the selective loss of inherited mtDNA mutations in mitotic tissue.

Various mtDNA mutations can cause primary mtDNA disease, including mtDNA point mutations or rearrangements (Schon *et al.*, 2012). Formation of these mutations is discussed in 1.4.5. Single large-scale deletions are the most prevalent form of mtDNA rearrangement in mtDNA disease (Schon *et al.*, 2012). Deletions can span the sites of several genes, causing severe mitochondrial disorders, such as Pearson syndrome (Rotig *et al.*, 1989), Kearns-Sayre syndrome (KSS) (Zeviani *et al.*, 1988) and chronic progressive external ophthalmoplegia (CPEO) (Moraes *et al.*, 1989). Point mutations could occur throughout the mitochondrial

genome, affecting genes that encode structural proteins of RC complexes, ribosomal RNA (rRNA) and tRNA, all of which could cause mtDNA disorders (Taylor and Turnbull, 2005). For example, Leber's Hereditary Optic Neuropathy (LHON), which is the most prevalent mitochondrial disorder, is primarily caused by point mutations in MT-ND1, MT-ND4 and MT-ND6 that encode subunits of RC complex I (Wallace *et al.*, 1988; Howell *et al.*, 1991; Johns *et al.*, 1992; Gorman *et al.*, 2015). A less frequent disorder, NARP (neurogenic weakness, ataxia and retinitis pigmentosa) are caused by point mutations at the nucleotide 8993 in mt-ATP6 gene that encodes CV subunit (Holt *et al.*, 1990; Schon *et al.*, 2001; Schon *et al.*, 2012).

1.6.2.1 Point mutations in mitochondrial tRNA genes

It is of interest that among mtDNA disease, more than half of the cases are caused by mutations in mitochondrial tRNA genes, whereas tRNA-coding sequences only occupy around 10% of the whole mtDNA coding section (Schon *et al.*, 2012). This phenomenon is probably due to a permissive environment for tRNA mutations during oogenesis (Stewart *et al.*, 2008).

Two common pathogenic mt-tRNA mutations m.3243A>G and m.8344A>G are widely investigated compared with other mt-tRNA mutations. The m.3243A>G mutation in $tRNA^{Leu(UUR)}$ gene is also the most common mtDNA point mutation, which is present in approximately 1 in 12800 individuals (Gorman *et al.*, 2015). This mutation is associated with most MELAS cases (Goto *et al.*, 1990; Goto *et al.*, 1991), though it more often causes the milder MIDD (maternally inherited diabetes and deafness) (van den Ouweland *et al.*, 1992). The m.8344A>G mutation in the $tRNA^{Lys}$ gene almost entirely leads to MERRF (myoclonus epilepsy and ragged red fibres) syndrome (Shoffner *et al.*, 1990; Schon *et al.*, 2012). However, only around one in 143000 individuals are estimated to harbour this mutation, suggesting it is generally an uncommon mutation (Gorman *et al.*, 2015). Both m.3243A>G and m.8344A>G can impair mtDNA expression, yet the exact mechanism is still being investigated (Lightowlers *et al.*, 2015). Pathogenicity of m.3243A>G could be associated with impaired termination of mtDNA transcription (discussed in 1.4.2) and/or lack of modification at the first position of the anticodon of $tRNA^{Leu}$ (Yasukawa *et al.*, 2000b). The m.8344A>G mutation is found to result in the unmodified base at the wobble site of the anticodon in the $tRNA^{Lys}$ (Yasukawa *et al.*, 2000a). As well as the common features of mitochondrial diseases like lactic acidosis and RRF, patients with MELAS also display symptoms of encephalopathy

like seizures and dementia, and those with MERRF may display myoclonus, ataxia and seizures (Hirano *et al.*, 1992; Hammans *et al.*, 1993). Heteroplasmy of m.3243A>G and m.8344A>G has been found to be related to the clinical manifestations and severity of the diseases (Hammans *et al.*, 1993; Whittaker *et al.*, 2009; de Laat *et al.*, 2012). Studies have shown that m.3243A>G and m.8344A>G mutations are associated with a defect in one or more of the respiratory chain complexes in patients, including CI, CIII and CIV (Berkovic *et al.*, 1989; Bindoff *et al.*, 1991; Hirano *et al.*, 1992). In addition, the CI level is more susceptible to m.3243A>G mutation compared with CIV (Mariotti *et al.*, 1995; Rocha *et al.*, 2015).

1.6.3 Mouse models of mtDNA disease

A number of mouse models of primary mtDNA disease have been established, which benefits the investigation of transmission and pathogenesis of disease-causing mtDNA mutations and phenotype development of mtDNA disease.

1.6.3.1 Mice with mtDNA large-scale deletions

Mito-mice with a large-scale deletion of size 4696bp were generated by introducing trans-mitochondrial cybrids containing somatic mtDNA mutations into mouse zygotes (Inoue *et al.*, 2000; Nakada *et al.*, 2004). These mice recapitulate certain phenotypes of the patients with large-scale deletions, such as hearing loss and lactic acidosis (DiMauro *et al.*, 1985; Larsson *et al.*, 1990; Nørby *et al.*, 1994; Inoue *et al.*, 2000; Nakada *et al.*, 2004). They also have a shortened lifespan due to severe renal failure, in accordance with markedly reduced COX activity in their kidney. Additionally, the skeletal and cardiac muscle fibres of the mito-mice show COX defects (Inoue *et al.*, 2000). However, some characteristics of the mito-mice are not consistent with those of mtDNA disease. The deletions were stably transmitted through germline with a cut-off limit of 90% heteroplasmy level (Inoue *et al.*, 2000), which is rare for large-scale deletions in humans (Taylor and Turnbull, 2005). This was thought to be associated with a co-existing mtDNA duplication in these mice (Inoue *et al.*, 2000). Moreover, unlike the patients with Pearson syndrome who lose the deletions in their blood with age (Larsson *et al.*, 1990; McShane *et al.*, 1991; Nørby *et al.*, 1994), no difference in the mutation level was found among a variety of mitotic and post-mitotic tissues of these mice, regardless of the age (Inoue *et al.*, 2000). Hence, this mouse model is not suitable for studying selective pressures on inborn mtDNA mutations.

1.6.3.2 Mice with point mutations in rRNA genes

Attempts to generate the embryos of mice with mtDNA point mutations were made by microinjecting stem cells that were fused with cytoplasts carrying pathogenic mtDNA mutations into blastocysts (Watanabe *et al.*, 1978; Marchington *et al.*, 1999). The cytoplasts with the pathogenic mutations that succeeded in producing chimeric mice originated from mouse cell lines with naturally occurring or mutagenized mtDNA mutations (Levy *et al.*, 1999; Sligh *et al.*, 2000; Kasahara *et al.*, 2006; Fan *et al.*, 2008; Yokota *et al.*, 2010; Freyer *et al.*, 2012; Lin *et al.*, 2012; Shimizu *et al.*, 2014; Shimizu *et al.*, 2015). The first mutation introduced by this method was a point mutation in the mitochondrial rRNA gene, which endows cybrids with resistance to chloramphenicol (CAP^R mutation) (Watanabe *et al.*, 1978; Marchington *et al.*, 1999). However, only mice with low chimerism were produced, as the resident wild-type mtDNA molecules in the stem cells were not eliminated, despite their small number (Watanabe *et al.*, 1978; Marchington *et al.*, 1999). This prompted the researchers to refine this procedure by pre-treating embryonic stem cells (ESCs) with Rhodamine-6-G (R-6-G) to deplete their endogenous wild-type mtDNA (Levy *et al.*, 1999; Sligh *et al.*, 2000). Using the modified method, chimeric mice with CAP^R mutation were successfully created, and they showed multiple phenotypes of mtDNA disease (Taylor and Turnbull, 2005), such as growth retardation, ophthalmological defects, myopathy and cardiomyopathy (Sligh *et al.*, 2000). Germline transmission of the CAP^R mutation was achieved, and pups with homoplasmic or heteroplasmic mutations were generated; however, none of them survived through the embryonic or perinatal period (Sligh *et al.*, 2000).

1.6.3.3 Mice with mutations in protein-encoding mtDNA

Fusing R-6-G pre-treated ESCs with cytoplasts containing pathogenic mtDNA mutations has been extensively used for establishing mouse models with mtDNA point mutations in protein-encoding genes. ESC cybrids were microinjected into embryos, which were then transplanted into pseudo-pregnant female mice to produce founder mice (Kasahara *et al.*, 2006). By subsequent mating the founder females with wild-type males, a mouse line with a homoplasmic m.6589T>C mutation in the COI gene was segregated with stable germline transmission (Kasahara *et al.*, 2006). The phenotype of these mice is very mild, only lactic acidosis and growth retardation, though biochemical and histochemical examinations revealed decreased COX level in the heart, brain, skeletal muscle and liver (Kasahara *et al.*, 2006).

Another mouse model with the same missense mutation in the COI gene was created by another research group using similar methods (Fan *et al.*, 2008). In addition to the homoplasmic COI mutation, some of these mice carried a more severe insertion in the ND6 gene, causing translational frameshift (Fan *et al.*, 2008). Other mice carried an ND6 revertant mutation, correcting the defects caused by the insertion, which enabled the determination of the functional changes caused by the mild COI missense mutation (Fan *et al.*, 2008). These mice confirmed the COX deficiency caused by m.6589T>C COI mutation and discovered complex I deficiency caused by the ND6 frameshift insertion (Fan *et al.*, 2008). These mice also showed abnormal mitochondrial proliferation and mitophagy in the heart with myofibrillar degeneration (Fan *et al.*, 2008), demonstrating the association between the function of mitochondria and somatic cells in disease development. Furthermore, the severe frameshift mutation was selectively removed in four generations with evidence that the loss of the mutation occurred in proto-oocytes before ovulation, whereas no selection was found against the revertant ND6 mutation and the mild COI mutation during germline transmission (Fan *et al.*, 2008). These findings improved our understanding of the selective pressures on mtDNA mutations with different pathogenicity through germline transmission. Unexpectedly, no selective pressure upon the ND6 frameshift mutation was found in the mitotic tissue of postnatal animals with age: the mutation was evenly distributed in various mitotic and post-mitotic tissues in aged trans-mitochondrial mice (Fan *et al.*, 2008), which is not the case in patients with certain mtDNA mutations (Chinnery *et al.*, 1999).

Similar strategies were also used to generate two mouse lines with a stable germline transmitted homoplasmic m.13997G>A mutation in the ND6 gene, which were designed for modelling the LHON disorder (Yokota *et al.*, 2010; Lin *et al.*, 2012). In the first study, despite a marked decline in the complex I level in the brain, kidney and muscle, the examined young mice only presented lactic acidosis with no sign of optic nerve atrophy that is a typical characteristic of LHON patients (Wallace, 1999; Yokota *et al.*, 2010). This phenotype was achieved in the second model, where the aged mice showed a weakened retinal response, abnormal retinal ganglion cells (RGCs) and atrophy of optic nerves with abnormal morphology and proliferation of mitochondria in RGCs (Lin *et al.*, 2012). These two studies highlight the effect of age on phenotype development in disease progression and the importance of investigating subjects at different stages of the lifespan. However, as these mouse lines harbour homoplasmic mutations in all tissues, they cannot be used to study the tissue-specific segregation of pathogenic mtDNA mutations (Yokota *et al.*, 2010; Lin *et al.*, 2012).

1.6.3.4 Mice with mutations in mt-tRNA genes

More recently, a mouse model with m.7731G>A mutation in the $tRNA^{Lys}$ gene was established using the technique of introducing pathogenic mtDNA mutation via R-6-G pre-treated ESCs (Shimizu *et al.*, 2014). This mutation is comparable with the m.8328G>A mutation and the common m.8344A>G mutation affecting the same tRNA gene in patients (Shimizu *et al.*, 2014). These mice showed a transmission threshold of 80% heteroplasmy level due to the fatal effect of a higher mutation load (Shimizu *et al.*, 2014). Phenotypically, young mice with high heteroplasmy levels displayed short body length and muscle weakness with defective OXPHOS in the muscle and kidney (Shimizu *et al.*, 2014), recapitulating features of myopathy in patients with mutated $tRNA^{Lys}$ gene (Houshmand *et al.*, 1999; Blakely *et al.*, 2007). Examinations of the aged animals revealed disease progression with age (Shimizu *et al.*, 2015). The aged mutants developed new phenotypes including anaemia, lactic acidosis and fatal renal failure (Shimizu *et al.*, 2015), some of which are typical characteristics of MERRF patients with mt-$tRNA^{Lys}$ mutation (Fukuhara *et al.*, 1980; Rosing *et al.*, 1985; Wallace, 1999). However, these mice had a comparatively normal lifespan and showed no ragged red fibres in the muscle (Shimizu *et al.*, 2015), a distinctive metabolic feature of MERRF patients (Fukuhara *et al.*, 1980; Rosing *et al.*, 1985). In addition, the mutation levels were uniform among various tissues in both young and old mice (Shimizu *et al.*, 2015), unlike MERRF patients who showed consistently lower mutation level in blood compared with skeletal muscles (Larsson *et al.*, 1992). Therefore, though these mice carry heteroplasmic mutations, they are not a perfect model for studying the tissue heterogeneity of mtDNA diseases caused by certain mtDNA mutations.

The most recent method for generating mouse models of inherited mtDNA mutations was to cross mtDNA-mutator females ($Polg^{mut/mut}$) with wild-type males, followed by continuous backcrossing with females to acquire mice with wild-type *Polg* but germline mtDNA mutations (Freyer *et al.*, 2012). The first generated mice carry pathogenic m.5245T>C point mutation in the $tRNA^{Cys}$ gene and m.3875delC in the $tRNA^{Met}$ gene that perturbed the expression of the corresponding tRNA (Freyer *et al.*, 2012). The m.5245T>C mutation was initially heteroplasmic but quickly expanded to homoplasmy in all organs of the mice (Freyer *et al.*, 2012). The m.3875delC maintained heteroplasmy with no offspring harbouring the mutation higher than 86% heteroplasmy level (Freyer *et al.*, 2012). The study suggested that selection against the m.3875delC mutation occurred during embryonic development after the formation of primary germ cells and oocytes (Freyer *et al.*, 2012), giving insights into the mechanism of the germline transmission of pathogenic mt-tRNA mutations. Surprisingly,

these mice did not show respiratory chain defects in the tissue possibly due to the compensatory upregulation of other RNA molecules (Freyer *et al.*, 2012). In addition, the heteroplasmy levels of the m.3875delC mutation in different tissues were similar and did not change with age (Freyer *et al.*, 2012). These findings contradict those regarding patients with certain inherited mt-tRNA mutations (Chinnery *et al.*, 1999; Grady *et al.*, 2018), limiting the use of this mouse model for investigating selective pressures upon inherited mtDNA mutations.

As discussed above, none of these mouse models shows clear evidence of losing inherited mtDNA mutations in mitotic tissue, thus are not suitable for investigating selective pressures against inherited mutations. Recently, a mouse model with an inherited m.5024C>T mutation has been developed and serve as a model of mtDNA disease (discussed in detail in Chapter 4) (Kauppila *et al.*, 2016). The mice with a high mutation load show a loss of the m.5024C>T mutation in blood with age (Kauppila *et al.*, 2016). Further characterisation of these mice is necessary to determine whether they are suitable for studying the mechanism underlying the selective pressures against inherited mtDNA mutations in mitotic tissue.

1.7 Gastrointestinal tract and GI stem cell populations

Stem cells are a group of cells that are able to renew themselves and differentiate into different progenies by either symmetric division or asymmetric division (Morrison and Kimble, 2006). The differentiation potential of different types of stem cells can vary. Embryonic stem cells (ESCs) isolated from the inner cell mass of early embryos are pluripotent, meaning that they have the capacity to differentiate into all three germ layers that will develop into any tissue or organs in animals (Wu and Izpisua Belmonte, 2016). Pluripotent stem cells could also be created by reprogramming fibroblasts with defined transcription factors. These reprogrammed cells are named induced pluripotent stem cells (iPSCs) (Takahashi and Yamanaka, 2006). Adult stem cells (ASCs) (a.k.a. somatic stem cells) are multipotent cells, which are able to generate certain types of progenitor cells in order to ultimately differentiate and replenish the somatic cells in tissue or organs (Goodell *et al.*, 2015). They are responsible for haematopoiesis and rapidly renewing various epithelial tissues, such as skin and gastrointestinal epithelium (Goodell *et al.*, 2015). These mitotic tissues are characterised by sufficient cell proliferation for tissue regeneration and injury repair (Campisi and di Fagagna, 2007). In contrast, post-mitotic tissues like the brain or different types of muscles (e.g. skeletal muscle, myocardium and smooth muscle) consist of

terminally differentiated cells with limited ability to repair and regenerate though some of them have quiescent stem cells (Roth *et al.*, 2000; Campisi and di Fagagna, 2007).

The human alimentary tract consists of two main parts: the upper and lower gastrointestinal (GI) tract, which is demarcated by the Ligament of Treitz (Warrell *et al.*, 2003). The upper GI tract is composed of the oesophagus, stomach and duodenum and the lower part consists of the jejunum, ileum, caecum, colon, rectum and anal canal (Warrell *et al.*, 2003). The duodenum, jejunum and ileum constitute the small intestine, while the large intestine is composed of the caecum, appendix, colon and rectum (Warrell *et al.*, 2003). The components of the GI tract share similar histological features with four general layers: mucosa (containing epithelium, lamina propria and muscularis mucosae), submucosa with blood vessels and nerves embedded, muscularis externa (including the inner circular and outer longitudinal smooth muscle) and serosa, though they still have their own specific features in particular in the mucosal layer (James S. Lowe, 2015). It is commonly accepted that gastrointestinal epithelium is a mitotic tissue renewed by gastrointestinal stem cells.

1.7.1 Oesophagus

The epithelium of the oesophagus is comprised of stratified squamous cells with a basal layer of cells adjacent to the basement membrane, which is markedly dissimilar to that of the digestive tract from stomach to rectum (Figure 1.6) (Treuting and Dintzis, 2011). However, the segment of the oesophageal epithelium below the diaphragm has a transition from squamous cells to columnar cells as a junction to the stomach. The lamina propria projects into the epithelium to form papillae with irregular epithelial borders (James S. Lowe, 2015). Moreover, unlike the other components of the GI tract that are encircled by smooth muscle, the upper third of oesophagus is encircled by striated muscle for voluntary swallowing (James S. Lowe, 2015). After the transition of the middle third part, the lower third section is finally encompassed by smooth muscle.

The regeneration of oesophageal epithelium is believed to initiate at the basal layer of epithelium (Figure 1.6) (Eastwood, 1977). It is commonly thought that in GI stem cell populations, there is a small portion of dormant stem cells that are only activated to replenish the loss of normal stem cells after trauma (Li and Clevers, 2010). However, there seem no quiescent stem cell populations in the oesophageal epithelium (Doupé *et al.*, 2012; DeWard *et al.*, 2014). Studies show that the cells at the basal layer divide stochastically to produce proliferating and differentiated daughter cells approximately twice per week, and wounds

caused by physiological or chemical irritations can enhance the regeneration (Doupé *et al.*, 2012). More recently, Deward *et al.* found Itgb4^{High} and CD73^{+} stem cell populations in mouse oesophagus that are resident in the basal cell layer of epithelium with transit-amplifying cells (Figure 1.6) (DeWard *et al.*, 2014). These Itgb4^{High} and CD73^{+} stem cells divide actively, though at a lower frequency compared with amplifying cells (DeWard *et al.*, 2014). Although the overall turnover of oesophageal epithelium is considered fast, it is still ~5 times slower than that of intestinal epithelium (Creamer *et al.*, 1961; Squier and Kremer, 2001).

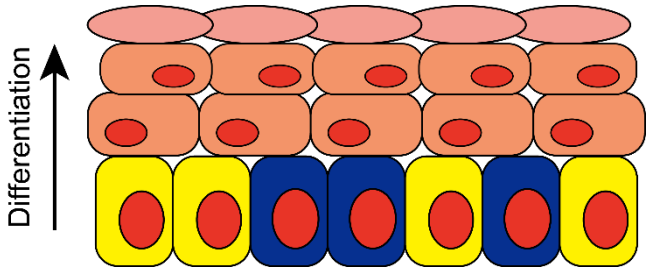

Figure 1.6 Diagram of oesophageal epithelial cells. Oesophageal epithelium consists of stratified squamous epithelial cells, which is strikingly different from the gastric or intestinal epithelium. Cell regeneration occurs at the basal layer of the epithelium, where stem cells (blue) and transit amplifying cells (yellow) actively produce nascent cells that migrate upwards to replace old cells.

1.7.2 Stomach

Macroscopically, the human stomach is demarcated as four regions: cardia, fundus, corpus and antrum (Treuting and Dintzis, 2011), but histologically there are two types of gastric mucosa: fundic and pyloric mucosa. Fundus and corpus shares fundic mucosa whereas cardia and antrum have pyloric mucosa (Treuting and Dintzis, 2011). Mouse stomach is different compared with humans, comprising a forestomach and glandular stomach. The latter is histologically similar to human stomach except for lack of cardia and is examined in this project (Treuting and Dintzis, 2011). In both species, the fundic epithelium is the major type of glandular mucosa (Treuting and Dintzis, 2011).

Compared with the small and large intestines, the stomach has an extra layer of oblique smooth muscle, lying in between the other two muscle layers, in order to mix food with gastric acid and digestive enzymes (James S. Lowe, 2015). The epithelium of stomach is also unique, containing numbers of gastric units, which are comprised of gastric pits and glands

with several glands merged and opened to the base of the pit (Kouznetsova *et al.*, 2011). Gastric units are comprised of the pit, downward to the isthmus, the neck and the base (Bartfeld and Koo, 2017). The main types of cells in gastric epithelium include mucus cells that supply protective mucus, parietal/oxyntic cells that secret acid, chief cells that produce pepsin and various enteroendocrine cells (Barker *et al.*, 2010a; Bartfeld and Koo, 2017). The pit is lined by mucus-secreting cells, which is the same between the corpus and the pylorus (Bartfeld and Koo, 2017). The narrow isthmus region contains a group of proliferative gastric stem cell population (Bartfeld and Koo, 2017). The location of the isthmus differs between different types of gastric epithelium. In fundic epithelium, the isthmus segment lies in the upper third of the unit, whereas it sinks to the lower third of epithelium in the pylorus (Mills and Shivdasani, 2011; James S. Lowe, 2015). In addition, the cell component, of the neck and the base particularly, is distinct between fundic and pyloric gastric units. The fundic units have a typical architecture of gastric units, containing myriads of chief cells and parietal cells. In contrast, the pyloric units have abundant mucus-secreting cells with only scattered parietal cells and lack chief cells (Treuting and Dintzis, 2011; James S. Lowe, 2015).

The replenishment of gastric epithelial cells relies on gastric stem cells that are traditionally considered to reside at the isthmus mixed with neck mucous cells (Thompson *et al.*, 1990; McDonald *et al.*, 2008). Within each gastric unit, multiple stem cells contribute to tissue renewal, the progenies of which migrate bilaterally along gastric units (McDonald *et al.*, 2008). Using lineage tracing in vivo, Barker et al. have reported a second potential stem cell population labelled by *Lgr5*, at the pyloric base of adult mice (Barker *et al.*, 2010b). In addition, gastric epithelium regeneration has plasticity. Chief cells labelled by *Tnfrsf19* (encoding TROY) are able to gain stemness and dedifferentiate into actively cycling stem cells for tissue regeneration, particularly after injury (Stange *et al.*, 2013). Of note, in addition to normal lineage tracing method through the activation of a reporter gene to chromatically label all lineages of specific cells, lineage tracing using mtDNA mutations has been validated as a convincing method for the biological study of gastrointestinal stem cells (Taylor *et al.*, 2003; McDonald *et al.*, 2008). However, to date, markers for gastric stem cells have not been exhaustively studied (Mills and Shivdasani, 2011).

Although all cells within a gastric unit are renewed by gastric stem cells, the turnover of different cells in the gastric epithelium occurs at a differential rate (Hoffmann, 2008). The turnover of surface mucous cells in gastric pits is ~3 days, whereas it can take months to renew parietal cells and chief cells in gastric glands (Lee and Leblond, 1985a; Lee and Leblond, 1985b; Hoffmann, 2008; Barker *et al.*, 2010a). This leads to different turnover rates

between different sections of gastric units and between different types of gastric epithelium with distinct cell components (Hoffmann, 2008). For example, the turnover of pyloric epithelium is markedly more rapid than that of fundic epithelium (Teir and Rasanen, 1961; Hansen *et al.*, 1976; Patel *et al.*, 1993).

1.7.3 Intestines

The small intestine is the main nutrient-absorptive organ with typical common histological characteristics of the GI tract, containing three parts: the duodenum that connects the pylorus of the stomach, the jejunum and the ileum that connects to the large intestine (caecum, colon and rectum). The jejunum is the main site for nutrition to be absorbed with paradigmatic finger-shaped villi to amplify the surface area for absorption. The bases of the villi extend to crypts that project into the lamina propria at the mucosa of the small intestines. A variety of cells constitute this epithelium (crypts and villi), including enterocytes with microvilli for absorption, goblet cells that produce mucus for lubrication, Paneth cells with immune function and endocrine cells that secret hormones (Figure 1.7) (James S. Lowe, 2015). Intestinal epithelium also contains M (microfold) cells and tuft cells, which are uncommon but play an important role in immune defence (von Moltke *et al.*, 2015; Gerbe *et al.*, 2016).

The histological structure of the large intestine is similar to that of the small intestine. The primary difference is that colonic epithelium comprises only crypts with no villi, and crypts are more distinct and straight (Figure 1.7) (James S. Lowe, 2015). In addition, due to the different function of the colon, which is to reabsorb water and electrolytes to shape faeces, the cell components are also distinct from small intestinal epithelium. Columnar cells with absorptive ability are the major cell type within colonic crypts. The rest of the cells in crypts include goblet (mucous) cells for mucus production in the colon, scattered endocrine cells and tuft cells (Figure 1.7) (James S. Lowe, 2015).

As the intestinal epithelium is rapidly renewed every 3 – 5 days, it serves as a fascinating prototype for mitotic tissue (Gehart and Clevers, 2019). In both small and large intestinal epithelium, newly differentiated cells migrate upwards to replace apoptotic aged cells during intestinal renewal except the Paneth cells that migrate downwards in the crypt of small intestines (Potten *et al.*, 1997).

1.7.3.1 Intestinal stem cells

Intestinal stem cells (ISCs) are responsible for replenishing all types of cells in the small and large intestines, with more than one ISC involved in this process per crypt (Taylor *et al.*, 2003; Barker *et al.*, 2007). It is commonly accepted that ISCs are situated at the base of crypts (Figure 1.7). In the small intestine, there are two functionally distinct ISC subpopulations residing at different positions relative to Paneth cells. Taking advantage of the tritiated thymidine labelling, Chen et al. pioneered the identification of ISCs and proposed that the crypt base columnar (CBC) cells with stem cell characters are interspersed between Paneth cells (Cheng and Leblond, 1974). Barker et al. ultimately confirmed the CBC cells via *in vivo* lineage tracing using the *Lgr5-EGFP-ires-cre-ERT2/R26R-lacZ* mouse model, showing their ability to self-renew and differentiate into all cell lineages of the intestinal epithelium (Barker *et al.*, 2007). This study has also revealed *Lgr5* as an exceedingly specific marker for CBC cells (Barker *et al.*, 2007). In addition, *ex vivo* culture of fluorescence-activated cell sorting (FACS)-isolated $Lgr5^+$ CBC cells from the *Lgr5-EGFP* reporter mice can develop into self-maintainable organoids with functional crypts and villi, further corroborating the identity of CBC cells (Sato *et al.*, 2009). *Olfm4* and *Ascl2* were also suggested to be promising candidates to label CBC cells (van der Flier *et al.*, 2009; Schuijers *et al.*, 2014). The behaviour of CBC cells is substantially regulated by Wnt signalling (Mah *et al.*, 2016). With *Lgr5* as an important member in Wnt signalling pathway, CBC cells display a marked Wnt signature in their gene expression, including many Wnt target genes, such as *Sox9*, *Ascl2*, *EphB2* and *Rnf43* (Korinek *et al.*, 1998; Barker *et al.*, 2007; Van der Flier *et al.*, 2007; Muñoz *et al.*, 2012). The majority of $Lgr5^+$ cells intersperse between Paneth cells, but some are detected above Paneth cells (Figure 1.7) (Barker *et al.*, 2007). For colonic crypts with no Paneth cells, the $Lgr5^+$ ISC lie exclusively at the base of crypts (Barker *et al.*, 2007; Barker, 2014). The $Wnt^{high}Lgr5^+$ CBC cells actively divide for self-renewal and epithelium regeneration under basal conditions and are sensitive to DNA damage caused by chemotherapy or irradiation (Yan *et al.*, 2012; Tao *et al.*, 2015). To prevent the catastrophe of losing susceptible CBC cells, intestines contain a functionally distinct ISC population, reserve stem cells that are able to repopulate CBC cells after injury and in non-pathological circumstances (Sangiorgi and Capecchi, 2008a; Tian *et al.*, 2011; Yan *et al.*, 2012; Yousefi *et al.*, 2016). These stem cells reside around the +4 position (four cells from the crypt base), above Paneth cells but below the transit amplifying cell zone in crypts, and are commonly referred to as +4 stem cells (Potten *et al.*, 1997; Medema and Vermeulen, 2011; Gehart and Clevers, 2019). Unlike CBC cells, the reserve stem cells are primarily quiescent, damage-

resistant, injury-inducible and irresponsive to Wnt signalling (Yan *et al.*, 2012; Li *et al.*, 2016; Mah *et al.*, 2016; Yousefi *et al.*, 2016; Yousefi *et al.*, 2017). Potential markers for reserve stem cell populations include Bmi1, mTert and Hopx; however, the reliability of these markers are still debatable, as these markers are not expressed exclusively in +4 stem cells (Sangiorgi and Capecchi, 2008b; Montgomery *et al.*, 2011; Takeda *et al.*, 2011; Muñoz *et al.*, 2012; Grün *et al.*, 2015).

Unlike the unidirectional grading differentiation in the haematopoietic system, intestinal regeneration has plasticity within the hierarchy, where committed cells can dedifferentiate back to stem cells to maintain epithelial regeneration after injury-induced loss of CBC cells (van Es *et al.*, 2012b; Buczacki *et al.*, 2013; Tetteh *et al.*, 2016; Yan *et al.*, 2017; Yousefi *et al.*, 2017). In addition to intestinal stem cells populations, chief cells in the stomach are also able to acquire stemness and regenerate gastric epithelium (Stange *et al.*, 2013; Barker, 2018).

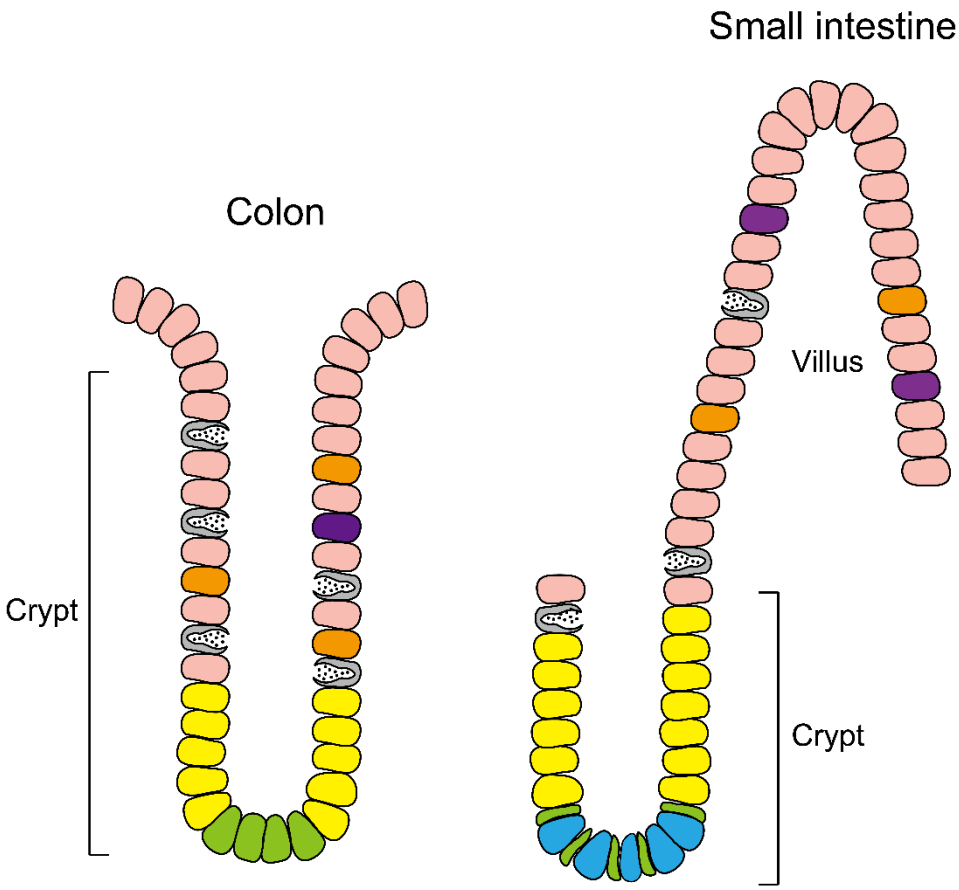

Figure 1.7 Structure of the epithelium of small intestine and colon. Stem cells (green) are located at the base of intestinal crypts. Stem cells differentiate into transit-amplifying cells (yellow) that rapidly divide to renew all types of cells in the crypt (pink enterocytes, orange enteroendocrine cells, grey goblet cells and purple tuft cells). In the small intestine, stem cells are intercalated with Paneth cells (blue), which produce progenies to migrate upwards beyond the crypt to form villus.

1.7.3.2 Intestinal stem cell niche

Stem cells not only need intrinsic signalling to regulate their division and differentiation but also require an appropriate microenvironment to maintain their function (Spradling *et al.*, 2001). The microenvironment where the stem cells are located is defined as the stem cell niche (Spradling *et al.*, 2001). In intestines, the proximal epithelial cells and stromal cells interact with ISC through a series of intercellular signalling pathways, such as WNT, EGF (epidermal growth factor), BMP (bone morphogenetic protein) and Notch signalling, to regulate ISC activity and epithelial regeneration (Sato *et al.*, 2010; Barker, 2014; Valenta *et al.*, 2016; Gehart and Clevers, 2019). In particular, WNT signalling is indispensable for stem cell maintenance and differentiation (Kuhnert *et al.*, 2004; van Es *et al.*, 2012a; Pinto *et al.*, 2016). Enhanced WNT signalling induces immoderate epithelial proliferation and adenoma formation (Moser *et al.*, 1995; Barker *et al.*, 2008), and mutations in WNT signalling are exceedingly common (93%) in colon cancer (The Cancer Genome Atlas *et al.*, 2012). At the crypt base, WNT and the WNT activator R-spondin are produced by Paneth cells and mesenchymal cells (Sato *et al.*, 2010; Aoki *et al.*, 2016; Valenta *et al.*, 2016; Stzepourginski *et al.*, 2017). Due to the poor diffusion of the WNT signal, it displays a decreasing gradient from the crypt base to the opening of the lumen (Mah *et al.*, 2016; Gehart and Clevers, 2019). Opposing to the WNT gradient, BMP signals have the most robust expression at the distal end of the crypt, which neutralises the proliferative signals from the stem cell niche and drives cell differentiation (He *et al.*, 2004; Kosinski *et al.*, 2007). EGF signals are also critical for intestinal epithelium turnover as they control the rate of intestinal stem cell proliferation (Gehart and Clevers, 2019). Excessive EGF signalling in the oncogenic *Kras* mutant mice have been shown to accelerate stem cell division, and endow stem cells carrying the mutation an advantage to dominate the niche (Snippert *et al.*, 2014). To ensure the strict regulation of EGF signalling, CBC cells abundantly express its receptor ERBB1 alongside its inhibitor LRIG1 (Wong *et al.*, 2012). Notch signalling plays an important role in intestinal stem cell maintenance and the adjustment of secretory to absorptive lineage ratio (Gehart and Clevers, 2019). In colonic crypts, in the absence of Paneth cells, the deep crypt secretory cells act as their alternatives to supply WNT, EGF and Notch signals in the niche (Sasaki *et al.*, 2016).

Cells in the niche not only communicate with stem cells through signalling pathways but also support stem cell metabolism. CBC cells primarily rely on OXPHOS during proliferation and differentiation. In contrast, Paneth cells undergo glycolysis and generate lactate that can be utilised by CBC cells as a resource for OXPHOS (Rodríguez-Colman *et al.*, 2017).

There are multiple stem cells resident in the niche of each crypt; approximately five of them are effective stem cells that divide actively for routine epithelial renewal, which results in the initial heterogeneous phenotype of each crypt (Winton *et al.*, 1988; Park *et al.*, 1995; Kozar *et al.*, 2013; Stamp *et al.*, 2018; Gehart and Clevers, 2019). Unlike general somatic stem cells, intestinal stem cells inherently divide symmetrically with identical phenotypes; however, due to restricted space in the niche, stem cells are stochastically lost and replaced by other stem cells or dominate the niche, resulting in niche succession where a single stem cell and its clones entirely occupy the stem cell pool (Figure 1.8) (Lopez-Garcia *et al.*, 2010; Snippert *et al.*, 2010; Stamp *et al.*, 2018). As a result, all the cells within the crypt derive from this stem cell and its clones, and the crypt inherits the phenotype of this stem cell and displays homogenous phenotype, which is termed monoclonal conversion (Figure 1.8). This is initially supported by a study reporting the presence of crypts with complete XY genotype or XO genotype in XO/XY mosaic patients (Novelli *et al.*, 1996). Further studies show that in the R26R-Confetti/Cre recombinase reporter mice that allow the induction of the random expression of a variety of fluorescent markers, individual crypts that originally contain multiple colours of fluorescence only present monochrome fluorescence after 30 weeks (Snippert *et al.*, 2010). In addition, lineage tracing studies where the expression of the reporter gene is linked to frameshift mutations during DNA replication show that the number of partially-labelled intestinal crypts remains steady with age, whereas the number of wholly-labelled crypts increases with age (Kozar *et al.*, 2013). Of note, in non-physiological circumstances, for example, the occurrence of an oncogenic mutation that increases proliferative capacity of a stem cell, the niche competition can be biased, and the mutation-harbouring stem cell may acquire an advantage over other stem cells to take over the niche (Snippert *et al.*, 2014). Monoclonal conversion is not an exclusive feature for intestinal crypts but also applies to gastric glands (discussed in Chapter 5 in more detail) (Nomura *et al.*, 1998; Bjerknes and Cheng, 2002; McDonald *et al.*, 2008).

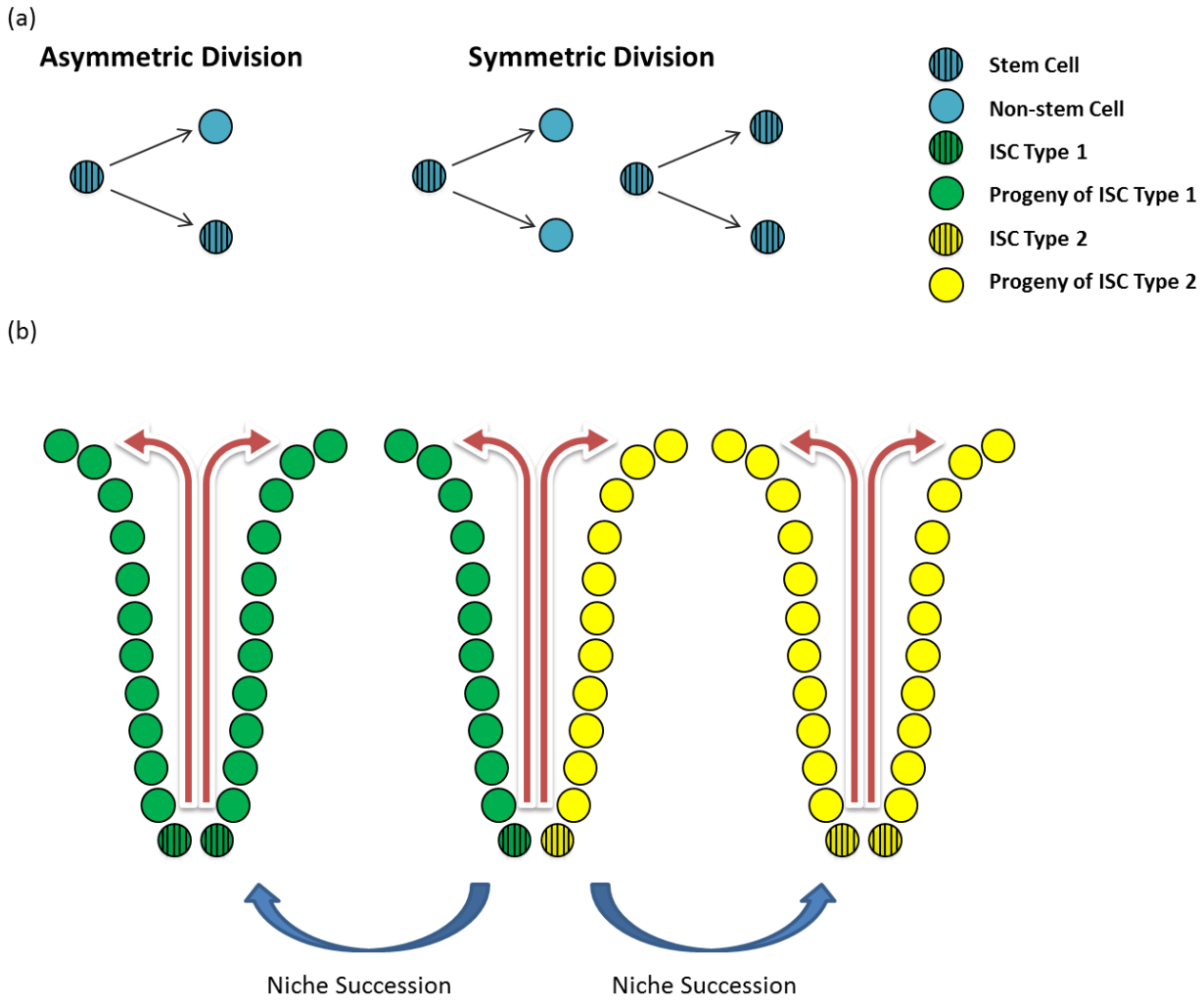

Figure 1.8 Schematics of (a) the division model of stem cells and (b) niche succession. (a) Immortal stem cells only divide asymmetrically for self-renewal. Whereas, in a niche, stem cells undergo either asymmetric division or symmetric division (Kim and Shibata, 2002). If a single stem cell symmetrically divides into two daughter cells, then this stem cell is lost in the niche. (b) By niche succession, an initially heterogeneous crypt can change into a homogeneous crypt, where one of the stem cells dominate the niche, and all differentiated cells eventually derive from this stem cell and its clones. The red arrows denote the directions of cell migration. ISC, intestinal stem cell.

1.8 Overall aims and objectives

The overall aim of this thesis is to further the understanding of tissue-specific phenotypes and distribution of mtDNA mutations during the development of mtDNA disease and more specifically, to understand the selective loss of inherited mtDNA mutations in mitotic tissue using gastrointestinal epithelium as a model, with a specific focus on intestines. This includes three aspects:

1. Ascertain whether patients with inherited m.3243A>G and m.8344A>G mutations selectively lose the mutations in their gastrointestinal epithelium.
2. Genetically and biochemically characterise $tRNA^{Ala}$ mutant mice with an inherited m.5024C>T mutation to determine whether they are qualified candidates for the investigation of mechanisms underpinning the selective pressures against inherited mtDNA mutations in mitotic cell populations.
3. Using the colonic epithelium of $tRNA^{Ala}$ mutant mice to investigate potential mechanisms underlying the selective loss of inherited mtDNA mutations with age.

Chapter 2 Materials and Methods

2.1 Equipment and software

2.1.1 Equipment

ABI verti-96 well Thermo Cycler	Applied Biosystems
3510 Benchtop pH meter	Jenway
2100 Antigen Retriever	Aptum Biologics
Aperio CS2 Scanner	Leica
Autoclave	Prior Clave
ChemiDoc Imaging System	Bio-Rad
Eppendorf Thermomixer	Eppendorf
Eppendorf® Refrigerated Microcentrifuge 5417R	Eppendorf
Eppendorf Centrifuge 5418	Eppendorf
GeneAmp PCR system 9700	Applied Biosystems
Horizontal gel electrophoresis tank	Peqlab
IKA™ Aluminum Alloy Basic Magnetic Hotplate Stirrer	Fisher Scientific
Microflow biological safety hood	J. Marston engineers
Nanodrop ND-1000 Spectrophotometer	Labtech International
A1 Confocal Laser Microscope System	Nikon
OHAUS adventurer® balance	OHAUS
OTF5000 Cryostat	Bright
PALM MicroBeam	Zeiss
PURELAB® flex	ELGA LabWater
PyroMark Q24 Pyrosequencer	Qiagen
PyroMark Q24 Vacuum Workstation	Qiagen
QBD2 Dry Block Heating System	Grant
UV Cabinet	BioAir
Vortex genie 2	Scientific Industries
Vwr Microscope Compound Bi Adv V031	VWR
Zeiss Axio Imager M1 microscope	Zeiss

2.1.2 Software

Aperio ImageScope	Leica
AxioVision	Zeiss

ImageJ	National Institutes of Health
ImageLab v.4.1	Bio-Rad
Minitab v17.1.0	Minitab
ND-1000 software	Labtech International
NIS-Element AR Imaging Software v4.40	Nikon
Palm Robo v4.6	Zeiss
Prism v6.01	GraphPad
PyroMark Q24 Software 1.0.10	Qiagen
R v3.3.0	R
R Studio v0.99.896	RStudio
ZEN blue	Zeiss

2.2 Consumables

0.2ml Thin-walled PCR tubes	STARLAB
0.5ml Thin-walled PCR tubes	STARLAB
1.5ml Eppendorf	Eppendorf
2ml Eppendorf	Eppendorf
24-Well PCR Plate, Non-Skirted, Elevated Wells, Natural	STARLAB
96-well plate Semi-Skirted with Raised Rim	STARLAB
Colourcoat+ adhesion microscope slides	CellPath
Coverslips (22x40mm and 22x50mm)	VWR
DNeasy Blood & Tissue Kits	QIAGEN
ErgoOne® Single-channel Pipettes (P10, P20, P200, P1000)	STARLAB
Falcon Tubes (15ml and 50ml)	BD Biosciences
Gloves	STARLAB
MicroAmp® Optical Cap Strips	Applied Biosystems
PEN membrane slides	Leica Microsystems
PIPETMAN P2	Gilson
PAP Pen Liquid Blocker	Newcomer Supply
Scalples	Swann Morton
SlideRita 5 Mailer	CellPath
Superfrost Plus slides	Thermo Scientific
TipOne® Pipette Tips	STARLAB
Weigh boats	VWR

Xtra-Clear Advanced Polyolefin StarSeal	STARLAB

2.3 Chemicals and solutions

2.3.1 Chemicals

2.3.1.1 Tissue processing

Liquid Nitrogen	BOC
OCT™ medium	Raymond Lamb

2.3.1.2 Histological and histochemical reagents

Avidin/biotin blocking kit	Vector Laboratories
Catalase	Sigma
Cytochrome *c*	Sigma
3,3’ Diaminobenzidine tetrahydrochloride	Sigma
DPX mounting media	Merck
Eosin	CellPath
Ethanol	Fisher Scientific
Ethylenediaminetetraacetic acid (EDTA) disodium salt dehydrate	Affymetrix
Histoclear™	National Diagnostics
Hoechst 33342, Trihydrochloride, Trihydrate	Life Technology
Hydrochloric acid	VWR
Hydrogen peroxide solution 30% (w/w) in H2O	Sigma
Mayer’s haematoxylin	TCS Bioscience Ltd.
Methanol	Merck
Nitro Blue Tetrazolium	Sigma
Normal goat serum	Sigma
Paraformaldehyde solution 4% in PBS	Santa Cruz Biotechnology
Phenazine methosulphate	Sigma
Phosphate buffered saline tablets	Sigma
Prolong Gold mounting medium	Life Technologies
Sodium azide	Sigma
Sodium chloride	Sigma
Sodium succinate	Sigma

Tri-sodium citrate dihydrate	VWR
Trizma base	Sigma
Tween-20	Sigma

2.3.1.3 Molecular biology reagents

Agarose	Bioline
Bromophenol Blue	Sigma
dNTP Mix	Promega
DNA Away	Thermo Fisher
GoTaq polymerase	Promega
PCR Ranger 100 bp DNA Ladder	Norgen Biotek Corp
Proteinase K	Invitrogen
PyroMark Annealing buffer	Qiagen
PyroMark Binding buffer	Qiagen
PyroMark Gold Q24 Reagents (5 x 24)	Qiagen
PyroMark Wash buffer (x10)	Qiagen
Streptavidin sepharose^{TM} high performance beads	GE Healthcare
SYBR Safe DNA Gel Stain	Thermo Scientific
Tris acetate EDTA (10x TAE)	Sigma
TRIS hydrochloride	Sigma

2.3.2 Solutions

Cell lysis buffer	50 mM Tris-HCL pH 8.5 0.5% Tween-20 20mg/ml proteinase K
DNA loading buffer	0.25% (w/v) Bromophenol Blue 30% (v/v) Glycerol
DNA electrophoresis running buffer (1L)	100 ml 10x TAE 900ml ultrapure water
DNA electrophoresis running buffer (1L)	100ml 10x TAE 900ml ultrapure water
EDTA antigen retrieval buffer pH 8.0	1 mM EDTA

Phosphate buffered saline (PBS)	1 PBS tablet in 100ml ultrapure water
Scott's tap water	0.2% (w/v) Sodium Bicarbonate 2% (w/v) Magnesium Sulphate)
Sodium citrate antigen retrieval buffer pH 6.0	10 mM tri-sodium citrate
TBST pH 7.4	5 mM Trizma base 100 mM Sodium chloride 0.1% (v/v) Tween®-20

2.4 Human samples

2.4.1 Patients

Ileum tissue was obtained from patient 1 with m.3243A>G via ileectomy. Gastrointestinal tissue specimens were collected from two patients (P2 and P3) with inherited m.3243A>G and one patient with m.8344A>G at post-mortem. Details of patients and tissue they provided are summarised in Table 2.1.

Patient	Age (years)	Gender	MtDNA genotype	Tissue	Tissue component
P1	30	F	m.3243A>G	Ileum	E and M
P2	36	F	m.3243A>G	Oesophagus Stomach Jejunum	E and M
P3	64	F	m.3243A>G	Colon	E and M
P4	56	M	m.8344A>G	Colon	E and M

Table 2.1 Information of the patients with inherited mitochondrial point mutations and the tissue thereof. E, epithelium; M, muscle. The age indicates the age of the patients when the tissue was collected.

2.4.2 Controls

Control tissue confirmed by histopathologists as "normal" was collected through endoscopy from patients who had digestive complaints but showed no evidence of intestinal disease or through resection 20cm away from the tumour area of patients with colonic cancer. No mitochondrial disorders were reported in any control subjects. Information of the control subjects and the tissue thereof is detailed in Table 2.2.

2.4.3 Ethical approval

Informed consent from all participants was received prior to collecting the tissue. Ethical approval for this project was granted from Newcastle and North Tyneside Local Research Ethics Committees.

Control	Age (years)	Gender	MtDNA genotype	Tissue	Tissue component
C1	30	F	WT	Small intestine	E
C2	31	F	WT	Small intestine	E
C3	31	F	WT	Small intestine	E
C4	34	F	WT	Small intestine	E
C5	37	F	WT	Small intestine	E
C6	37	F	WT	Small intestine	E
C7	59	F	WT	Colon	E and M
C8	61	F	WT	Colon	E and M
C9	62	M	WT	Colon	E and M
C10	64	F	WT	Colon	E and M
C11	64	M	WT	Colon	E
C12	41	M	WT	Oesophagus Stomach	E
C13	44	M	WT	Oesophagus Stomach	E
C14	57	F	WT	Oesophagus	E
C15	58	F	WT	Oesophagus	E

Table 2.2 Summary of the control individuals and their tissue. E, epithelium; M, muscle.

2.5 $tRNA^{Ala}$ mutant mice with m.5024C>T mutation

All mice were bred by Dr James Stewart and Prof Nils-Göran Larsson, Max Planck Institute for Biology of Ageing, Cologne, Germany. A mouse lineage (*PolgA*$^{mut/+}$) (Trifunovic *et al.*, 2005) was used to generate $tRNA^{Ala}$ mutant mice (Kauppila *et al.*, 2016), which is a mouse model of mitochondrial disease with m.5024C>T point mutation. The former lineage (*PolgA*$^{mut/mut}$) carries a knock-in mutation in the exonuclease domain of the mtDNA polymerase γ (*Polg*), which compromises its proofreading ability and causes an age-dependent accumulation of mtDNA mutations (Trifunovic *et al.*, 2005). *PolgA*$^{mut/mut}$ mice have similar germline and somatic mutation load, which is 16 – 20 mutations per molecule (Stewart *et al.*, 2008; Ross *et al.*, 2013). To facilitate segregating single mtDNA mutations via screening correlated phenotypes, *PolgA*$^{mut/+}$ mice that carry approximately 3 mutations per mtDNA molecule were employed to generate the new mouse line (Kraytsberg *et al.*, 2009; Ross *et al.*, 2013; Kauppila *et al.*, 2016). Male *PolgA*$^{mut/+}$ mice were mated with wild-type C56Bl/6N (*PolgA*$^{+/+}$) females to obtain female *PolgA*$^{mut/+}$ mice which had the mutator allele but no inherited mtDNA mutations, which were then backcrossed with wild-type *PolgA*$^{+/+}$ mice to produce females with wild-type mtDNA polymerase that transmitted mtDNA mutations (N1) (Figure 2.1) (Kauppila *et al.*, 2016). After breeding these mice for at least three generations, the phenotype of the colonic epithelium was screened (Figure 2.1) and mouse lineages with no COX-deficient crypts were discontinued (Kauppila *et al.*, 2016). Three out of twelve mouse lines showed COX deficiency, which were further subjected to whole mtDNA genome sequencing to screen candidate mutations (Figure 2.1) (Kauppila *et al.*, 2016). A mouse line ($tRNA^{Ala}$ mice) with a stable transmission of m.5024C>T in the $tRNA^{Ala}$ gene (> 6^{th} generation) was segregated and used for this project (Figure 2.1) (Kauppila *et al.*, 2016).

An ear notch biopsy was taken from mice at ≈3 weeks and its mutation level was measured via pyrosequencing by Dr James Stewart, Max Planck Institute for Biology of Ageing, Cologne, Germany. Mutant mice in two age groups (~10 weeks and ~ 50 weeks) and their age-matched wild-type controls were sacrificed by cervical dislocation and the organs were harvested to obtain both frozen and formalin-fixed paraffin-embedded (FFPE) tissue, which was performed by Dr Laura Greaves and Dr James Stewart. Each organ was divided in two, and one half was snap-frozen in isopentane cooled to -180°C in liquid nitrogen. Frozen tissue was then stored at -80°C. The second half was fixed in 10% neutral buffered formalin for 24 hours, prior to dehydration and embedding in paraffin. Five $tRNA^{Ala}$ mice with high ear heteroplasmy (>70%) and two mice with intermediately high ear heteroplasmy (60%) in each

age group were included in the study. Information of each mouse and acquired organs was summarised in Table 2.3. Details of the frozen and FFPE gastrointestinal tissue from 10-week and 50-week $tRNA^{Ala}$ mice were concluded in Table 2.4 and Table 2.5 respectively.

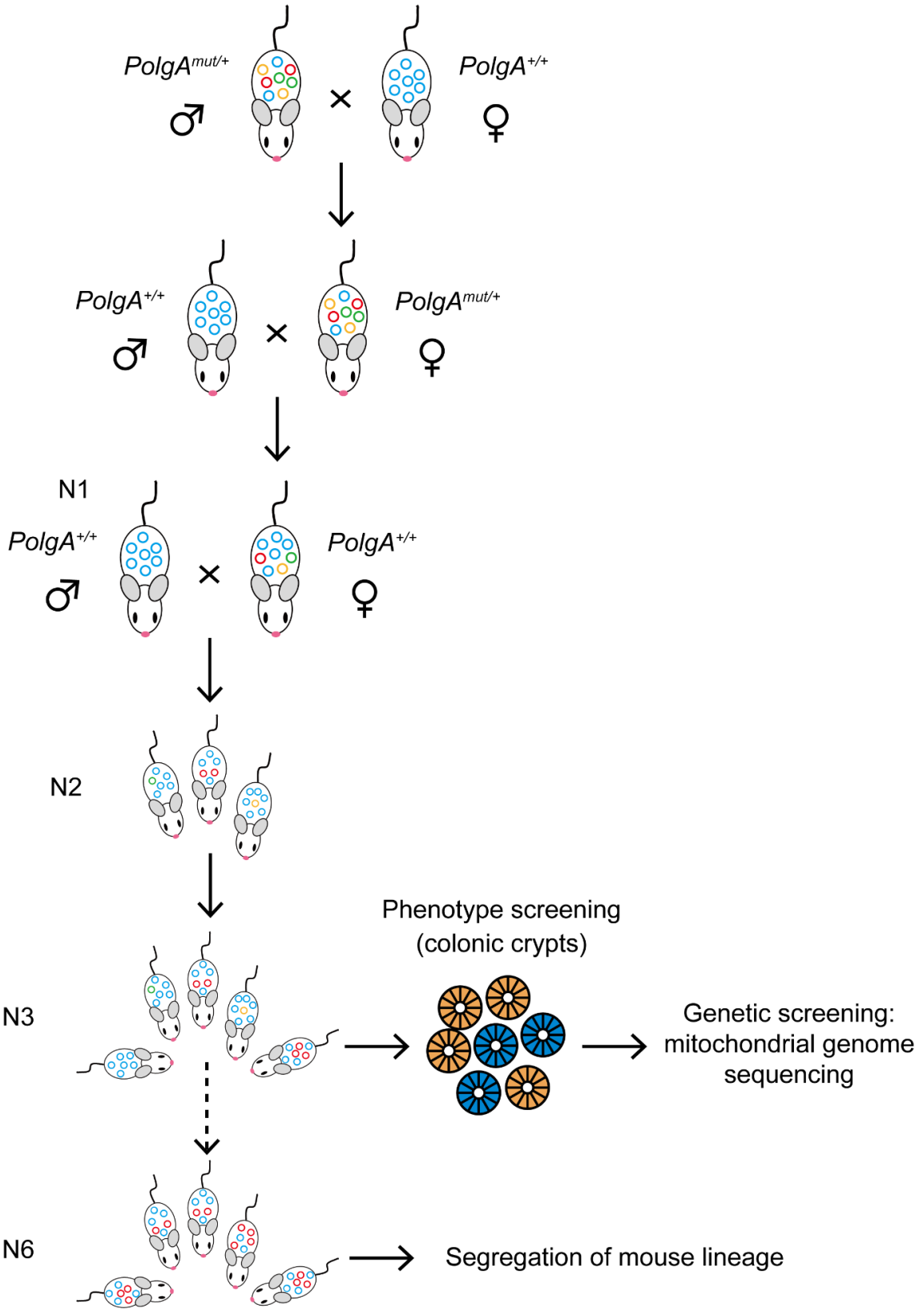

Figure 2.1 Breeding and screening strategy for $tRNA^{Ala}$ mutant mice. Rings in blue indicate wild-type mtDNA. Rings in red are mtDNA molecules with m.5024C>T mutation. Rings in the other colours are mtDNA with different types of pathogenic or non-pathogenic mutations. N indicates the generation. A $tRNA^{Ala}$ mutant mouse line with stably transmitted m.5024C>T was segregated after the 6^{th} generation of the maternal lineage.

ID	Mut% in ear (3w)	Age (w)	Sex	Spleen	Pancreas	Kidney	Liver	Heart	Lung	Brain	SKM
B933	79	10	F	o	o	o	o	o	o	o	o
B934	77	10	F	o	o	o	o	o	o	o	o
B938	77	10	F	o	-	o	o	o	o	o	o
B945	74	10	F	o	o	o	o	o	-	o	o
B948	71	10	F	o	o	o	o	o	o	o	o
B949	65	10	M	o	o	o	o	o	o	o	o
B952	68	10	M	o	o	o	o	o	o	o	o
351	60	53	M	o	o	o	o	o	o	o	o
353	73	53	M	o	o	o	o	o	o	o	o
365	79	49	F	o	o	o	o	o	o	o	o
369	71	49	F	o	o	o	o	o	o	o	o
370	73	49	M	o	o	o	o	o	o	o	o
372	80	49	M	o	o	o	o	o	o	o	o
373	69	49	M	o	o	o	o	o	o	o	o

Table 2.3 Information of the $tRNA^{Ala}$ mice and the organs obtained from the whole body dissection. “o”, tissue used in the study; “-”, tissue unavailable. Mice in two age groups (≈10 weeks and ≈ 50 weeks) were used in this project. SKM, skeletal muscle.

ID	Mut% in ear (3w)	Age (w)	Sex	Colon (frozen)	Colon (FFPE)	Caecum (frozen)	SI (frozen)	Gastric fundus (frozen)	Gastric pylorus (frozen)
B933	79	10	F	o	o	N/A	o	o	-
B934	77	10	F	o	o	N/A	o	o	-
B938	77	10	F	o	o	N/A	o	o	-
B945	74	10	F	o	o	N/A	o	o	o
B948	71	10	F	o	o	N/A	o	o	o
B949	65	10	M	o	N/A	N/A	o	o	-
B952	68	10	M	o	N/A	N/A	o	o	o
B988	WT	9	F	N/A	o	N/A	N/A	N/A	N/A
B994	WT	9	F	N/A	o	N/A	N/A	N/A	N/A
B995	WT	9	F	N/A	o	N/A	N/A	N/A	N/A

Table 2.4 Gastrointestinal tracts dissected from the 10-week $tRNA^{Ala}$ mice. Frozen tissue was used for sequential COX/SDH histochemistry and pyrosequencing. FFPE tissue was used for immunofluorescence. “o”, tissue used for assays; “-”, tissue unavailable; “N/A” tissue not used.

ID	Mut% in ear (3w)	Age (w)	Sex	Colon (frozen)	Colon (FFPE)	Caecum (frozen)	SI (frozen)	Gastric fundus (frozen)	Gastric pylorus (frozen)
351	60	53	M	-	N/A	o	o	o	-
353	73	53	M	o	o	o	o	o	o
365	79	49	F	-	o	o	o	o	o
369	71	49	F	-	o	o	o	o	-
370	73	49	M	o	o	o	-	o	-
372	80	49	M	o	o	o	-	-	o
373	69	49	M	-	N/A	o	o	o	-
24769	WT	47	M	N/A	o	N/A	N/A	N/A	N/A
24283	WT	47	M	N/A	o	N/A	N/A	N/A	N/A
WT201	WT	54	F	N/A	o	N/A	N/A	N/A	N/A
WT214	WT	59	F	N/A	o	N/A	N/A	N/A	N/A

Table 2.5 Gastrointestinal canal obtained from the 50-week $tRNA^{Ala}$ mice with m.5024C>T. Frozen tissue was used for sequential COX/SDH histochemistry and pyrosequencing. FFPE tissue was used for immunofluorescence. “o”, tissue used for assays; “-”, tissue unavailable; “N/A” tissue not used.

2.6 Cryosection

Frozen tissue was mounted on Whatman™ filter paper with a small amount of OCT™ medium (VWR) in liquid nitrogen. Tissue was then placed in OTF5000 Cryostat (Bright) to warm to -19°C before sectioning. Sections for histochemical assays were cut at a thickness of 10 µm using the OTF5000 Cryostat (Bright) and were mounted on Superfrost Plus slides (Thermo Scientific). Sections for laser microdissection were cut at 20 µm and mounted on polyethylene naphthalate (PEN) membrane slides (Leica Microsystems). Specimens were then air-dried for an hour and stored in sealed slide mailers at -80°C until required.

2.7 Histochemistry

2.7.1 Haematoxylin and eosin staining

Tissue sections were brought up to room temperature and air-dried for an hour. Sections were then submerged into Mayer's haematoxylin (TCS Bioscience Ltd.) for 5 minutes and rinsed with tap water. Sections were subsequently blued in Scott's tap water (0.2% (w/v) Sodium Bicarbonate, 2% (w/v) Magnesium Sulphate) for 30 seconds followed by a wash with running tap water. Sections were then immersed in Eosin (CellPath) for 2 minutes and rinsed with tap water. Sections were dehydrated through a gradient of ethanol solutions (70%, 95%, and 2x 100%) for 1 minute in each and cleared in Histoclear (National Diagnostics) twice with 1 minute in each and mounted in DPX (Merck) with a coverslip.

2.7.2 COX, SDH and sequential COX/SDH histochemistry

Tissue sections (10 µm) were removed from the freezer and air-dried at room temperature for an hour. Sections were then circled in hydrophobic barriers using a PAP liquid blocker pen (Newcomer Supply). COX stock solutions (500 µM cytochrome *c* and 5 mM diaminobenzidine tetrahydrochloride (DAB) in 0.2M phosphate buffer, pH 7.0) were thawed at 55°C for 5 minutes. COX medium (100 µM cytochrome *c*, 4 mM DAB in 0.2M phosphate buffer, pH 7.0) were prepared by adding a 200 µl cytochrome *c* to 800 µl DAB with 20 µg/ml catalase. Each section was incubated in 100 µl COX medium at 37°C in a humid chamber. Tissue sections were then washed with phosphate buffered saline (PBS) for 3 x 5 minutes. SDH aliquots (800 µl 1.5 mM nitroblue tetrazolium (NBT), 100 µl 1.5M sodium succinate, 100 µl 2 mM phenazine methosulphate (PMS) and 10 µl 100 mM sodium azide in 0.2M phosphate buffer, pH 7.0) were defrosted at 55°C for 5 minutes and combined to make an SDH solution with a final concentration of 1.2 mM NBT, 130 mM sodium succinate, 200 µM

PMS and 1 mM sodium azide in 0.2M phosphate buffer, pH 7.0. Each section was covered with 100 µl SDH solution and incubated in a humid atmosphere at 37°C, then washed by PBS 3 x 5 minutes. Optimised incubation times of COX and SDH medium for various tissues were listed in the Table 2.6. Sections were subsequently dehydrated through graded ethanol solutions (70%, 95% and 2 x 100%) and cleared in two changes of the Histoclear (National Diagnostics) for 5 minutes in each, then mounted with DPX (Merck) with coverslips.

For individual COX or SDH histochemistry, sections were incubated only with COX medium or SDH medium and washed with PBS 3 x 5 minutes, then dehydrated and mounted as above.

For the tissue prior to laser microdissection, sections (20 µm) were subjected to the sequential incubation of COX and SDH medium and were dehydrated in the ethanol gradient as above. Sections were then air-dried for an hour, sealed in slide mailers and stored at -80°C.

Tissue	Species	COX medium incubation time (minutes)	SDH medium incubation time (minutes)
Small intestine (E)	Human	60	35
Colon (E)	Human	50	35
Stomach (E)	Human	50	35
Oesophagus (E)	Human	60	35
GI Smooth muscle	Human	50	35
Stomach (fundus) (E)	Mouse	5	11
Stomach (pylorus) (E)	Mouse	25	25
Small intestine (E)	Mouse	25	30
Large intestine (E)	Mouse	25	30
GI smooth muscle	Mouse	25	25

Table 2.6 Optimised incubation time for different types of tissues in COX/SDH medium. E, epithelium; GI, gastrointestinal.

2.8 Immunofluorescence

2.8.1 Immunofluorescence on frozen tissue

Frozen tissue sections were allowed to warm to room temperature and air-dried for an hour. Sections were fixed in 4% paraformaldehyde (Santa Cruz Biotechnology) for 10 minutes at 4°C to preserve morphology. Sections were gently rinsed with distilled water and then washed in TBST (5 mM Trizma base, 100 mM Sodium chloride and 0.1% (v/v) Tween®-20) for 10 minutes. Specimens were further permeabilised in a methanol gradient in sequence: 70% for 10 minutes, 95% (with 0.3% H_2O_2 (v/v)) for 10 minutes, 100% for 20 minutes, 95% for 10 minutes and 70% for 10 minutes. Subsequently, sections were washed by TBST and encircled with a hydrophobic pen (Newcomer Supply). To reduce non-specific binding between secondary antibodies and endogenous antigens, tissue was incubated with a protein block solution for an hour at room temperature. The blocking solution is the diluted serum of the animal species for producing the secondary antibody, which is 10% normal goat serum (NGS) (Sigma Aldrich) diluted in TBST in this study. A combination of primary antibodies was diluted in the 10% NGS to the required concentrations (Table 2.7) and applied to the specimens at 4°C overnight in a moist chamber. A no primary control (NPC) corresponding to each case was incubated in 10% NGS with no primary antibodies added and was subjected to the same subsequent procedure. Sections were then washed 3 x 5 minutes with TBST and incubated with a cocktail of diluted secondary antibodies at 4°C for 2.5 hours in a humid container in the dark. Sections were then washed 3 x 5 minutes with TBST in dark. When a biotinylated secondary antibody was used, a streptavidin-conjugated tertiary antibody was diluted and applied to the specimens, followed by 3 x 5 minute wash in TBST. Tissue was then mounted with Prolong Gold mounting medium (Life Technologies) and stored at -20°C.

2.8.2 Immunofluorescence on formalin-fixed paraffin-embedded (FFPE) tissue

FFPE tissue sections at a thickness of 4 µm were deparaffinised and rehydrated by one-hour incubation at 60°C, followed by immersion 2 x 10 minute in Histoclear (National Diagnostics), an ethanol gradient (2 x 5 minute in 100%, 1 x 5 minute in 95%, 1 x 5 minute in 70%) and then distilled water for 5 minutes. Specimens were submerged in 1 mM EDTA (pH 8.0) and placed in 2100 retriever unit (Election Microscopy Sciences) for antigen retrieval. Sections were left in the retriever to cool for 40 minutes after the program finished, as a sharp change in temperature might detach the tissue from the slide. Tissue was then washed with TBST three times with 5 minutes each and incubated in 10% NGS for an hour. Sections were then washed 3 x 5 minute with TBST. Endogenous biotin and avidin binding sites were

blocked using an Avidin/Biotin blocking kit (Vector Laboratories), when biotinylated secondary antibody was used. Sections were covered with the avidin block solution for 15 minutes at room temperature followed by a 3 x 3 minute wash. Sections were then incubated with the biotin block reagent for 15 minutes and washed three times with 3 minutes each. Primary antibody cocktails were applied to tissue overnight at 4°C, followed by 3 x 10 minute wash. Sections were then incubated with secondary antibodies for 2 hours at 4°C, followed by a 3 x 10 minute wash in dark. A streptavidin conjugated tertiary antibody was applied to tissue followed by a 3 x 10 minute wash in dark, when a biotinylated secondary antibody was included in the cocktail of secondary antibodies. Sections were then mounted with Prolong Gold (Life Technologies) using a coverslip and stored at -20°C.

2.8.3 Counterstain Hoechst for immunofluorescence

Counterstaining sections with Hoechst to label nuclei was performed after washing the last set of antibodies. Tissue was incubated with 0.01 mg/ml Hoechst (Life Technology) for 15 minutes at room temperature in dark followed by a 3 x 5 minute wash. Tissue was then mounted with Prolong Gold on a glass slide and stored at 20°C.

Primary antibody	Host	Isotype	Dilution (Human)	Dilution (Mouse)	Manufacturer	Code
Anti-NDUFB8	M	IgG1	1:50	1:50	Abcam	ab110242
Anti-SDHA	M	IgG1	1:200	1:200	Abcam	ab14715
Anti-COX4+COX4L2	M	IgG2a	1:200	-	Abcam	ab110261
Anti-MTCO1	M	IgG2a	1:100	1:100	Abcam	ab14705
Anti-VDAC1	M	IgG2b	1:100	1:100	Abcam	ab14734
Anti-β-catenin	R	IgG	1:100	N/A	Abcam	ab6302
Anti-β-catenin	M	IgG2b	N/A	1:300	Santa Cruz Biotechnology	sc-393501
Anti-Alpha smooth muscle Actin	R	IgG	1:100	N/A	Abcam	ab5694
Anti- E-cadherin	R	IgG	1:400	N/A	Abcam	ab40772
Anti-Ki-67	R	IgG	N/A	1:300	Cell Signaling Technology	#12202
Anti-Caspase 3, active (cleaved) form	R	IgG	N/A	1:40	Merck	AB3623
Anti-TOMM20	R	IgG	N/A	1:100	Abcam	ab186734
Anti-Tom20	M	IgG2a	N/A	-	Santa Cruz Biotechnology	sc-17764
Anti-TOMM22	M	IgG2a	N/A	1:100	Abcam	ab57523
Anti-Tim23	M	IgG2b	N/A	1:20	Santa Cruz Biotechnology	sc-514463
Anti-Parkin	M	IgG2b	N/A	1:50	Merck	MAB5512
Anti-Parkin	M	IgG2b	N/A	-	Abcam	ab77924
Anti-Parkin	M	IgG2b	N/A	-	Santa Cruz Biotechnology	sc-32282
Anti-PGC-1	R	IgG	N/A	-	Abcam	ab3242
Anti-PINK1	R	IgG	N/A	1:100	Abcam	ab23707

Table 2.7 Information of primary antibodies and their optimised dilutions for immunofluorescence. M, mouse; R, rabbit; "-", failed to be optimised; “N/A”, not used on the tissue.

Secondary/tertiary antibody	Target	Host	Dilution (Human)	Dilution (Mouse)	Manufacturer	Code
Biotin-XX	Mouse IgG1	Goat	1:200	1:400	Life Technologies	A10519
Biotin-XX	Rabbit IgG	Goat	1:200	1:400	Vector Labs	BA-1000
Alexa Fluor 647	Mouse IgG1	Goat	1:200	1:400	Life Technologies	A21240
Alexa Fluor 488	Mouse IgG2a	Goat	1:200	1:400	Life Technologies	A21131
Alexa Fluor 546	Mouse IgG2a	Goat	1:200	1:400	Life Technologies	A21133
Alexa Fluor 488	Mouse IgG2b	Goat	1:200	1:400	Life Technologies	A21141
Alexa Fluor 546	Mouse IgG2b	Goat	1:200	1:400	Life Technologies	A21143
Alexa Fluor 647	Mouse IgG2b	Goat	1:200	1:400	Life Technologies	A21242
Alexa Fluor 405	Rabbit IgG	Goat	1:200	1:400	Life Technologies	A31556
Alexa Fluor 488	Rabbit IgG	Goat	1:200	1:400	Life Technologies	A11008
Alexa Fluor 546	Rabbit IgG	Goat	1:200	1:400	Life Technologies	A11010
Alexa Fluor 647	Rabbit IgG	Goat	1:200	1:400	Life Technologies	A21244
Streptavidin, Alexa Fluor 405 conjugate	Biotin	N/A	1:100	1:200	Life Technologies	S32351
Streptavidin, Alexa Fluor 488 conjugate	Biotin	N/A	1:100	1:200	Life Technologies	S32354
Streptavidin, Alexa Fluor 647 conjugate	Biotin	N/A	1:100	1:200	Life Technologies	S21374

Table 2.8 Details of secondary/tertiary antibodies and their optimised dilutions used in the study.

2.9 Microscopy and image analysis

2.9.1 Brightfield imaging

Whole-section scanning was conducted using Aperio CS2 (Leica). Aperio ImageScope (Leica) was used for snapshotting and quantifying COX deficiency in gastrointestinal epithelium. Using the counter tool in the graphical user interface, the number of COX-defective gastrointestinal crypts and the total number of crypts on an intact section were counted to calculate the COX deficient percentage in the epithelium. For each patient and mouse, counting was performed on two serial sections.

2.9.2 Fluorescence microscopy and image analysis

Fluorescent images were taken by a monochrome camera (AxioCam MRm) integrated in a Zeiss Axio Imager M1 microscope at a magnification of 10x. For human and animal studies, AxioVision and Zen blue (updated version of AxioVision) were used for controlling the microscope respectively. Cubes for filtering fluorescence at a wavelength 405 nm, 488 nm, 546 nm and 647 nm were selected according to the fluorescent dyes. Exposure time was set based on no primary controls to minimize background fluorescence and antibody-treated sections with the strongest optical density to avoid pixel saturation, and was kept consistent between each subject. Files were saved as .zvi format and exported as tagged image file format (TIFF) images for quantitative analysis. Pictures for each channel were then imported to ImageJ. Regions of interest (ROI) were selected and the mean fluorescence intensity within the ROI was automatically measured by the software.

2.9.3 Confocal microscopy and image analysis

Sections were imaged using an upright A1+ Confocal Laser Microscope System (Nikon Instruments) comprising of a Nikon Ni-E body, confocal scan head laser and detector (PMT / GASP detectors) units providing lasers at four wavelengths (405nm, 488nm, 561nm and 647nm). Images were captured using NIS-Elements Imaging Software (v4.40) (Nikon) through an apochromatic lens with x20 magnification, numerical aperture 0.75 and working distance 1.0 mm (Nikon). Each section was scanned in a z-stack fashion for 9 steps with 1 µm interval between sections. Individual colours were scanned in sequence to reduce ‘cross-talk’ between each channel where photons resulting from the excitation of one dye may be collected in the channel of another. Laser settings including laser power, photon amplification gain (HV) and offset adjustment was tuned according to the brightest image in a set of

experiments to avoid pixel saturation, and were maintained identical for each sample. Confocal scan settings are summarised in the Table 2.9. Images were saved as .nd2 format for analysis using NIS-Element AR Imaging Software (v4.40) (Nikon). Z-stack images were integrated to obtain maximum intensity projection at each pixel site. Colonic crypts were selected as ROI and were masked with a minimum threshold of pixel intensity to remove the lumen area. The masking strategy was remained the same for each case in a set of experiments. Mean pixel intensity was measured for each channel. Punctate signals were manually counted.

Pinhole size (µm)	**Scan size**	**Zoom factor**	**Optical sectioning (µm)**	**Pixel size (µm)**	**Scan speed (pixel dwell time)**
21.2	1024 x 1024	2	2.83	0.31	2.4 µs

Table 2.9 Camera settings for confocal imaging.

2.10 DNA extraction and cell lysis

2.10.1 Laser microdissection

Sections were air-dried for an hour and loaded on the Zeiss Laser Capture Microdissection microscope. Sterile 200 µl PCR tubes were filled with cell lysis buffer (50 mM Tris-HCL pH 8.5, 0.5% Tween-20, 20mg/ml proteinase K and distilled water) in their caps (10 µl for a single crypt or a small area of smooth muscles; 20 µl for a collection of large areas of epithelium or muscle from several fields of view) and installed on the motorised rack of the microscope. Tissue was selected manually and laser-cut under the mode of "Robo-LPC" using Palm Robo v4.6 at 20x magnification. Tissue-specific laser power was optimised until the cutting line was thin and smooth. A reagent negative control with no tissue added in the lysis buffer was prepared for pyrosequencing (2.11.1). Tissue was then catapulted into the lid of the tube and kept on ice to be prepared for cell lysis.

2.10.2 Cell lysis and DNA extraction from laser-cut tissue

Tissue with the lysis buffer (2.10.1) was centrifuged at 14000 rpm for 10 minutes at 4°C, then lysed at 55°C for 5 hours, 95°C for 10 minutes to inactivate the proteinase K and held at 4°C until being transferred into a -20°C freezer.

2.10.3 DNA extraction from tissue homogenate

Frozen mouse organs were sectioned at 10 µm in OTF5000 Cryostat (Bright), the morphology of which was checked under a Brightfield microscope (VWR). A small piece of tissue was then cut and transferred to a sterile freezing 1.5 ml Eppendorf tube in OTF5000 Cryostat (Bright). DNA extraction was conducted using a DNeasy Blood & Tissue Kits (QIAGEN) following the manufacturer's instruction. DNA concentration was measured using Nanodrop spectrophotometer (Thermo Scientific) with a minimal concentration 2 ng/µl to ensure sufficient DNA for the genetic study. Extracted DNA was stored at -80°C.

2.11 PCR and sequencing

2.11.1 PCR amplification for pyrosequencing

DNA extracted from the microdissected tissue (2.10.2) and the organ homogenate (2.10.3) was used as a template to determine mutation levels in these tissues. A single round of PCR was performed using a Thermal cycler (Applied Biosystems) to generate enough PCR products for pyrosequencing. A no-template control with no DNA added in the mastermix was set for each PCR plate (STARLAB). A lysis-reagent negative control (2.10.1) was run together if the DNA was obtained from the micro-dissected tissue. Triplicates were set for all samples. Information of primer sequences for the pre-pyro PCR was summarised in Table 2.13. Details of the mastermix and the PCR programme for each point mutation is described in the subsections below.

2.11.1.1 Assay for m.3243A>G

PCR was performed to amplify a 210 bp PCR fragment spanning the m.3243 mutation locus using a forward biotinylated and a reverse primer. The volume of the PCR solution for this assay is 25µl: 12.8 µl distilled water, 5 µl 5x GoTaq Reaction buffer (Promega), 2.5 µl 10x dNTP (0.2 mM) (Promega), 1.25 µl of each primer (10 µM), 0.2 µl GoTaq polymerase (Promega) and 2 µl DNA lysate. Details of PCR programme is summarised in Table 2.10.

Step	Temperature	Duration	Cycles
Initial denaturation	95°C	10 minutes	1
Denaturation	95°C	30 seconds	40
Annealing	63°C	30 seconds	
Extension	72°C	30 seconds	
Final Extension	72°C	10 minutes	1
Hold	4°C	∞	

Table 2.10 PCR condition for expanding PCR fragments at m.3243 locus.

2.11.1.2 Assay for m.8344A>G

A PCR assay to amplify a 147 bp segment spanning m.8344 mutation site was carried out in a 25 µl solution containing 12.8 µl distilled water, 5 µl 5x reaction buffer (Promega), 2.5 µl 10x dNTP (0.2 mM) (Promega), 1.25 µl of the forward biotinylated and the reverse primer each (10 µM), 0.2 µl GoTaq polymerase (Promega) and 2 µl DNA lysate. PCR condition is concluded in Table 2.11.

Step	Temperature	Duration	Cycles
Initial denaturation	95°C	10 minutes	1
Denaturation	95°C	30 seconds	40
Annealing	62°C	30 seconds	
Extension	72°C	30 seconds	
Final Extension	72°C	10 minutes	1
Hold	4°C	∞	

Table 2.11 PCR condition for the m.8344A>G assay.

2.11.1.3 Assay for mt.5024C>T

A PCR fragment in a size of 178 bp spanning m.5024 locus was amplified using 1 µl DNA lysate and 24 µl mastermix including 13.8 µl distilled water, 5 µl 5x reaction buffer (Promega), 2.5 µl 10x dNTP (0.2 mM) (Promega), 1.25 µl of the forward biotinylated and the reverse primer each (10 µM) and 0.2 µl GoTaq polymerase (Promega). PCR programme was listed in Table 2.12. A wild-type control was set for each plate with DNA extracted from a wild-type mouse (by courtesy of Dr Craig Stamp).

Step	Temperature	Duration	Cycles
Initial denaturation	95°C	10 minutes	1
Denaturation	95°C	30 seconds	38
Annealing	62°C	30 seconds	
Extension	72°C	30 seconds	
Final Extension	72°C	10 minutes	1
Hold	4°C	∞	

Table 2.12 Thermal cycler programme for amplifying DNA segments spanning mt.5024 mutation site.

2.11.2 Agarose gel electrophoresis

PCR products were separated on a 2% (w/v) agarose gel and visualised using SYBR Safe DNA Gel Stain (Thermo Scientific) under ultraviolet light. Each PCR product (3 µl) was mixed with 1 µl loading dye (0.25% (w/v) bromophenol blue and 30% (v/v) glycerol) and loaded in the gel. PCR products were run with 5 µl of PCR Ranger 100 bp DNA Ladder (Norgen Biotek Corp). At least one gap was left between the PCR products generated from DNA and the no-template negative control to avoid contamination. Gel was immersed in 1x TAE buffer (40 mM Tris-acetate and 1 mM EDTA, pH 8.3) (Sigma-Aldrich) and subjected to electrophoresis at 100V for 45 minutes. PCR products were visualised using a ChemiDoc Imaging System (Bio-Rad). Enough amount of PCR products showing clear bands and absence of contamination were confirmed before pyrosequencing (Figure 2.2).

Figure 2.2 An image of gel electrophoresis showing PCR products (178bp) spanning m.5024 position with no contamination in the reagent negative control (no DNA in the lysis buffer) and the no-template negative control (no DNA template added). DNA used for pre-pyro PCR were extracted from small intestines of $tRNA^{Ala}$ mutant mice. HE, homogenate of epithelium; HSM, homogenate of smooth muscle; WT, wildtype; RNC, reagent negative control; Neg, no-template negative control.

2.11.3 Pyrosequencing

PCR products (10 µl) were added into 70 µl mastermix consisting of 29 µl distilled water, 40 µl PyroMark binding buffer (Qiagen) and 1 µl Streptavidin Sepharose High Performance beads (GE Healthcare) to form a total 80 µl solution. The mix was homogenised on a shaker for 10 minutes to facilitate PCR products binding to the beads. Samples were then transferred to a PyroMark Q24 Vacuum Workstation (Qiagen) equipped with a hedgehog head connected to a 2511 Dry Vacuum Pump/Compressor (Welch). Samples was aspirated using the hedgehog head and beads bound with PCR products were filtered and collected at the tip of its probes, which were then flushed successively through 70% ethanol for 5 seconds, denaturation solution (0.2M NaOH) for 5 seconds, 1x PyroMark wash buffer (Qiagen) for 10 seconds. Beads were then released from the probes into a 25 µl annealing solution consisting of 0.75 µl sequencing primers (Table 2.13) and 24.25 µl PyroMark annealing buffer (Qiagen), and were placed on a QBD2 Dry Block Heating System (Grant) to denature at 80°C for 2 minutes. Samples were then placed in the PyroMark Q24 Pyrosequencer (Qiagen) and annealed at room temperature for at least 5 minutes to allow the primers to bind to PCR amplicons. PyroMark Gold Q24 Reagents (Qiagen), including dNTPs, enzyme compounds (DNA polymerase, ATP sulfurylase, luciferase and apyrase) and substrate compounds (adenosine 5' phosphosulfate and luciferin), were loaded in a PyroMark Q24 Cartridge (Qiagen) in volumes calculated by PyroMark Q24 Software 1.0.10 (Qiagen) according to the sample size. Pyrosequencing was performed on PyroMark Q24 Pyrosequencer (Qiagen) equipped with the PyroMark Q24 Cartridge (Qiagen) following the corresponding assays selected for each mutation. Raw data were exported and analysed using the allele quantification algorithm in PyroMark Q24 Software 1.0.10 (Qiagen). WT controls were included to ensure the stringency of the assay with errors less than 3%. Final mutation levels of each sample were the mean value of triplicates.

Mutation	Genbank Accession number	Primer	Sequence (5'→ 3')
m.3243A>G	NC_012920	5'-biotin forward primer (nt3143-3163)	TAAGGCCTACTTCACAAAGCG
		Reverse primer (nt3331-3353)	GCGATTAGAATGGGTACAATGAG
		Sequencing primer (nt3244-3258)	ATGCGATTACCGGGC
m.8344A>G	NC_012920	5'-biotin forward primer (nt8240-8264)	TTTGAAATAGGGCCCGTATTTACC
		Reverse primer (nt8363-8387)	CGGTAGTATTTAGTTGGGGCATTT
		Sequencing primer (nt8347-8367)	ATTTCACTGTAAAGAGGTGT
mt.5024C>T	NC_005089	5'-biotin forward primer (nt4891-4913)	TTCCACCCTAGCTATCATAAGC
		Reverse primer (nt5114-8091)	CGTAGGTTTAATTCCTGCCAATCT
		Sequencing primer (nt5001-5020)	TGTAGGATGAAGTCTTACA

Table 2.13 Primer sequences and their locations for pre-pyro PCR and pyrosequencing.

2.12 Statistical analyses

2.12.1 R statistical analysis for immunofluorescence

Raw data exported from imageJ (2.9.2) was processed through an R-script written by Dr John Grady (Rocha *et al.*, 2015). Optical density (OD) for each channel in sections treated with primary antibodies was subtracted by OD in the NPC for each case to remove the background caused by non-specific binding of secondary antibodies, which was then normalised by logarithm transformation. Normal populations were established by randomly sampling equal numbers of measured items from each control. The number was defined according to the control with the smallest size. Mean and standard deviation (SD) of normal populations were obtained as estimates for calculating z-scores of patient and control cohorts with or without normalisation of mitochondrial mass markers. Boundaries for categorising levels of OXPHOS subunits were set according to statistical confidence levels (Table 2.14) and specified in individual result chapters. Levels of mitochondrial mass (Tom20) or nuclear encoded mitochondrial markers (SDHA and COX4) were classified as "very low" (z-score < -3), "low" (-3 ≤ z-score < -2), "normal" (-2 ≤ z-score ≤ 2), "high" (2 < z-score ≤ 3) and "very high" (z-score > 3).

Z-score (SD)	Confidence level
< -2 or > 2	95%
< -2.6 or > 2.6	99%
< -3 or > 3	≈99%
< -3.3 or > 3.3	99.9%

Table 2.14 Confidence levels corresponding to significant z-scores defined as the number of SD that a sample is away from the mean of a population.

2.12.2 General data analysis

Immunofluorescence data was formatted using Minitab v17.1.0 before being exported for R analysis. Prism v6.01 was used for the remaining statistical analyses and generating figures. Normality tests were performed on data sets and sample sizes were taken into account for selecting corresponding parametric or non-parametric tests.

Chapter 3 Inherited mtDNA mutations in the gastrointestinal tract from patients with mitochondrial disease

3.1 Introduction

3.1.1 Somatic mtDNA mutations in normal individuals during ageing

In normal ageing humans, OXPHOS deficiency has been found in both mitotic (Taylor *et al.*, 2003; McDonald *et al.*, 2008; Gutierrez‐Gonzalez *et al.*, 2009; Greaves *et al.*, 2010) and post-mitotic tissues (Müller-Höcker, 1989; Müller-Höcker, 1990; Cottrell *et al.*, 2001). Mitochondrial DNA mutations, some of which are highly pathogenic, have been shown to accumulate clonally to high levels of heteroplasmy or to homoplasmy in individual cells, resulting in a respiratory chain defect (Taylor *et al.*, 2003; Kraytsberg *et al.*, 2006; Greaves *et al.*, 2010). These somatic mtDNA mutations are associated with ageing (Khrapko and Vijg, 2009; Baines *et al.*, 2014b), age-related disease (Cha *et al.*, 2015) and cancer (Popadin *et al.*; Chatterjee *et al.*, 2006), though whether these mutations play a causal role in ageing and the development of these diseases remains unknown. Adult stem cells responsible for regular tissue regeneration contribute to the accumulation of somatic mtDNA mutations in mitotic tissue. Studies have shown that the accumulation of somatic mtDNA mutations occurs in stem cells, particularly haematopoietic (Shin *et al.*, 2004a; Shin *et al.*, 2004b) and intestinal stem cells (Taylor *et al.*, 2003). In addition, stem cell niches are involved in the spread of these mutations in gastric and colonic epithelium (Greaves *et al.*, 2006; McDonald *et al.*, 2008). Limited numbers of studies on human samples show the functional changes caused by the accumulated somatic mtDNA mutations in stem cells and their progenies, and their findings are controversial (McDonald *et al.*, 2008; Gutierrez‐Gonzalez *et al.*, 2009; Nooteboom *et al.*, 2010). Mouse models with mtDNA mutagenesis show a typical ageing phenotype, with the homeostasis of either stem cells per se or downstream precursors severely affected (Trifunovic *et al.*, 2004; Kujoth *et al.*, 2005; Wang *et al.*, 2013b; Pinto *et al.*, 2016). These studies suggest a strong association between age-dependent mtDNA mutagenesis and stem cell ageing, yet the underlying mechanism is unclear (Su *et al.*, 2018).

The mechanism by which somatic mtDNA mutations occur and clonally expand within individual cells with age is largely unknown. Somatic mtDNA mutations may be generated in a tissue-specific way: in neurons with a high demand of energy, mutations are thought to occur through repairing the mtDNA molecules that are damaged by ROS (Krishnan *et al.*, 2008), whereas in mitotic tissue, mutations originate from replication errors (Reeve *et al.*, 2009). Clonal expansion of the somatic mtDNA mutations can be entirely explained by a model of random genetic drift in both dividing and non-dividing cells (Coller *et al.*, 2001;

Elson *et al.*, 2001; Stamp *et al.*, 2018), but this does not rule out the traditional free radical hypothesis where respiratory chain defects produce excessive ROS to damage mtDNA, which in turn causes more oxidative stress to form a vicious cycle (Harman, 1972; Vincent *et al.*, 2018). Somatic mtDNA mutations in a variety of mitotic tissue, such as the epithelium of colon, small intestine, stomach and prostate, and bladder urothelium are not subjected to any purifying selection as in germline transmission, since comparing different spectra of mtDNA mutations show that the somatic mtDNA mutations are remarkably more pathogenic compared to variants transmitted through germline in general populations (Greaves *et al.*, 2012a; Baines *et al.*, 2014a). To date, little is known about the dynamics of the accumulation of somatic mtDNA mutations during ageing and the mechanism underlying the absence of negative selection against them.

3.1.2 Inherited mtDNA mutations in patients with mitochondrial disease

In addition to the somatic mutations discussed above, mtDNA mutations can also be inherited through the germline or occur sporadically during oogenesis or embryogenesis and cause mitochondrial DNA disease (DiMauro and Schon, 2003; Taylor and Turnbull, 2005). Large-scale deletions and mtDNA point mutations are the two most frequent causes of primary mtDNA disorders (Alston *et al.*, 2017). Despite only about 10% of the mtDNA genome being tRNA genes, more than half of the inherited pathogenic point mutations are in tRNA encoding sequences, the two most prevalent of which are m.3243A>G in the $tRNA^{Leu}$ gene and m.8344A>G in the $tRNA^{Lys}$ gene (Schon *et al.*, 2012; Gorman *et al.*, 2015).

In contrast to the somatic mtDNA mutations that accumulate with age, patients with mtDNA disease have been shown to lose specific mtDNA mutations in specific mitotic tissues, with some evidence suggesting the involvement of stem cells (Su *et al.*, 2018). For example, patients with Pearson syndrome caused by single large-scale deletions suffer from fatal pancytopenia as the mutation severely affects the haematopoietic progenitor cells in the bone marrow (Pearson *et al.*, 1979; Rotig *et al.*, 1989). However, patients can gradually recover from the abnormal haematopoiesis and show a normal blood phenotype and a marked lower mutation load in blood than in muscle, but they may then develop Kearns-Sayer syndrome that predominantly affects post-mitotic tissue (Larsson *et al.*, 1990; McShane *et al.*, 1991; Nørby *et al.*, 1994). For mtDNA point mutations, the loss of the mutation was first suggested by a contrast in the distribution of the mutation across different tissues in affected foetuses and adult patients. During foetal development (12 – 25 gestation weeks), the inherited

mtDNA point mutations are uniform across tissues, regardless of whether they are mitotic or post-mitotic (Matthews *et al.*, 1994; Cardaioli *et al.*, 2000; Monnot *et al.*, 2011). In contrast, non-random distribution of the mutation was reported in adult patients, with the mutation load in post-mitotic skeletal muscle higher than that in several mitotic tissues, such as hair follicles, buccal mucosa and blood (Chinnery *et al.*, 1999). Furthermore, both cross-sectional and longitudinal studies show a decrease in the mutation level in blood with age in symptomatic patients and asymptomatic carriers with the germline m.3243A>G mutation (t Hart *et al.*, 1996; Rahman *et al.*, 2001; Frederiksen *et al.*, 2006; de Laat *et al.*, 2012; Grady *et al.*, 2018). This was also shown to be the case in a few samples containing mitotic cells, including urine, buccal mucosa and cervical smears (Olsson *et al.*, 2001; Frederiksen *et al.*, 2006; de Laat *et al.*, 2012; Grady *et al.*, 2018). In contrast, the mutation level of m.3243A>G in post-mitotic muscle was shown to be stable with age with no correlation between them (Frederiksen *et al.*, 2006; Grady *et al.*, 2018). As mitotic tissue is regularly renewed by somatic stem cells, this contrast in the behaviour of the inherited mtDNA mutation between mitotic and post-mitotic tissue implies that stem cells might be involved in the loss of the mutation.

The loss of inherited mutations in blood with age suggests a selective pressure against them, which is in contrast to the accumulation of somatic mtDNA mutations during ageing in stem cell populations with no evidence of any selective pressure on them (Greaves *et al.*, 2012a). This highlights the difference in the organismal response to mtDNA mutations under ageing and pathogenic mitochondrial conditions, which is likely associated with stem cell biology. Investigating the age-related behaviour of inherited mtDNA mutation in mitotic tissue and more specifically, somatic stem cells, is crucial, as it benefits the understanding of both ageing and mitochondrial disease. Intestinal epithelium with a rapid turnover rate has proved to be a good model for stem cell research (Barker, 2014). With all cells in a crypt originating from the stem cells at its base, it can go through a process termed monoclonal conversion where the stem cell niche of an individual crypt is dominated by a single stem cell (Novelli *et al.*, 1996; Kim and Shibata, 2002; Snippert *et al.*, 2010; Kozar *et al.*, 2013). These traits make each crypt monoclonal, which is a good representative of the characteristics of the mother stem cell.

3.2 Aims

Although studies have suggested selection against inherited mtDNA mutations in blood as well as a few types of epithelial cells, such as those in the buccal mucosa, urine and cervix, it is unknown whether this is generic to other mitotic tissue, where the selection occurs in the tissue and what effect it is on tissue phenotype. Using gastrointestinal (GI) tissue from patients with inherited mtDNA mutations, I aimed to:

1. Determine the heteroplasmy of inherited mtDNA mutations in the epithelium of different GI segments and compare this with post-mitotic tissue in the same patient.
2. Determine whether the selection against inherited mtDNA mutations occurs in intestinal stem cell populations by analysing isolated intestinal crypts.
3. Determine the effect of a decrease in heteroplasmy on OXPHOS function in the mitotic epithelium.

3.3 Methods

3.3.1 Tissue samples

Post-mortem GI tissue was obtained from two patients with m.3243A>G (patient 2 and patient 3) and one patient with m.8344A>G (patient 4). An ileum sample was collected from patient 1 by ileectomy. Control tissue with no evidence of pathology was collected from age-matched normal individuals for biochemical assays. Details of the patients and controls with the samples they provided are tabulated in Table 2.1 and Table 2.2 respectively. The case history is described in the Appendix 8.1. The study was approved by Newcastle and North Tyneside Local Research Ethics Committees.

3.3.2 Sequential COX/SDH histochemistry

Frozen tissue from patients subjects was sectioned (detailed in 2.6) for histochemical assays. Tissue sections from controls 12 – 15 (Table 2.2) were provided by Dr Stuart A.C. McDonald. Sections were subjected to haematoxylin and eosin staining (2.7.1) to assess the morphology. Sequential COX/SDH histochemistry for determining the COX activity was then performed on patients' tissue sections and two to four control samples as a reference for tissue with normal and defective COX activity (described in 2.7.2). The percentage of COX deficiency in the tissue was determined as the number of the COX-deficient intestinal crypts or gastric pits by the total number of the crypts/pits. The counting was performed on two sections to prevent loss of information from the imperfect morphology of the tissue due to post-mortem degradation or sectioning. Only crypts/gastric pits with no COX activity in blue were counted to quantify the level of COX defects, as this is the method to quantify COX deficiency caused by the accumulation of somatic mtDNA mutation in normal ageing individuals in the published data (Taylor *et al.*, 2003). In addition, it is imprecise to define the tissue with partial COX deficiency labelled as bluish brown, as differentiating the hue of blue in brown pigment by eye is very subjective. Therefore, though this histochemical assay is advantageous for determining the functional defects in enzymes, the immunofluorescence assay described below is required, which allows for an exact quantification of the protein level of the respiratory chain complexes.

3.3.3 Immunofluorescence

Antibodies for the immunofluorescence assay were always optimised prior to final experiments. Details of primary and secondary/tertiary antibodies with their optimised concentrations are summarised in Table 2.7 and Table 2.8 respectively. Antibody cocktails used in the formal experiments were listed in Table 3.1. The optical density of each intestinal crypt/gastric unit was measured using ImageJ. For oesophageal epithelium and muscle, the optical density of the section was measured by dividing it into small areas of similar sizes (≈ 50000 μm^2) as a unit in multiple fields, as it was not feasible to include the whole section in one field of view. Fluorescence data of all subjects were background corrected according to the no primary controls. The number of age-matched controls for each patient and the number of the examined intestinal crypts/gastric units in each subject is listed in Table 3.2. The detailed procedure of the immunofluorescence assay and image analysis are described in section 2.8.1 and 2.9.2. Z-scores of the optical density in each examined unit were calculated using data from the control population established by random sampling of the same number of units from each control subject (detailed in 2.12.1) and categorised as follows: for NDUFB8 labelling the respiratory chain complex I and COX1 marking the complex IV, the subunit level was classified by z-scores as "negative" (< -3SD), "Intermediate" (-3SD ~ -2SD) and "positive" (> -2SD); for the non-mtDNA encoded proteins COX4 and SDHA, the level was categorised as "low" (< -2SD), "normal" (-2SD ~ 2SD) and "high" (> 2SD).

	Primary antibody	Secondary antibody	Tertiary antibody
Combination one	Anti-NDUFB8 (ab110242)	Biotin-XX (A10519)	Streptavidin, Alexa Fluor 488 conjugate (S32354)
	Anti-COX4+COX4L2 (ab110261)	Alexa Fluor 546 Mouse IgG2a (A21133)	N/A
	Anti- E-cadherin (ab40772)	Alexa Fluor 647 Rabbit IgG (A21244)	N/A
Combination two	Anti-MTCO1 (ab14705)	Alexa Fluor 488 Mouse IgG2a (A21131)	N/A
	Anti-SDHA (ab14715)	Alexa Fluor 647 Mouse IgG1 (A21240)	N/A
	Anti- E-cadherin (ab40772)	Alexa Fluor 546 Rabbit IgG (A11010)	N/A

Table 3.1 Antibody combinations used for formal experiments. Details of the primary and secondary/tertiary antibodies with their optimised concentrations on human tissue are summarised in Table 2.7 and Table 2.8 respectively.

Tissue	Patient ID & the number of controls	The number of units for the examination of NDUFB8 and COX4		The number of units for the examination of MTCO1 and SDHA	
		Patient	Controls	Patient	Controls
Ileum E	Patient 1 with 4 controls	70	128	20	83
Oesophagus E	Patient 2 with 3 controls	n/a	n/a	n/a	n/a
Stomach E	Patient 2 with 2 controls	6	36	7	44
Small intestine E	Patient 2 with 3 controls	28	48	30	47
Colon E	Patient 3 with 3 controls	20	91	20	79
Colon M	Patient 3 with 3 controls	n/a	n/a	n/a	n/a

Table 3.2 The summary of the number of age-matched controls for each patient and the number of crypts/gastric units included for fluorescence quantification. n/a = the epithelium of the oesophagus and the colonic smooth muscle on a whole section were included for the measurement.

3.3.4 Pyrosequencing

Gastrointestinal epithelium and muscle were randomly selected and collected by laser microdissection (Figure 3.1) (detailed in 2.10.1) and subjected to cell lysis (2.10.2) to extract DNA. Five crypts/gastric glands were collected and pooled. The oesophageal epithelium in a whole field of view and muscles were divided into areas of similar sizes and collected as a unit (≈ 50000 μm^2). DNA extracted from the tissue was then subjected to PCR amplification (described in 2.11.1). Enough amount of PCR product was visualised by DNA electrophoresis (detailed in 2.11.2) and used for pyrosequencing described in 2.11.3 to measure the mutation load of the tissue.

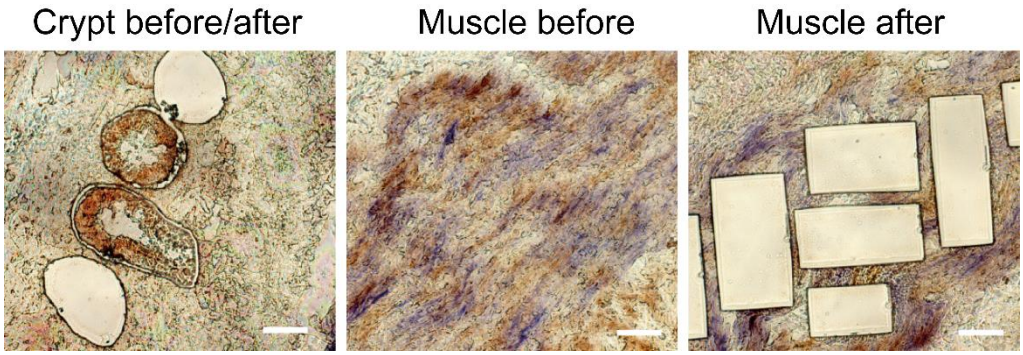

Figure 3.1 Laser microdissection of the intestinal crypts and smooth muscle. The left panel shows the laser-microdissected intestinal crypts before and after collection. The middle and the right images show the smooth muscle before and after microdissection. Tissue was randomly selected regardless of the COX activity. Scale bar: 50μm.

3.4 Results

3.4.1 Heteroplasmy levels of mitotic and post-mitotic tissue in the alimentary canal

The mutation level in the homogenate of different segments of the alimentary canals from two patients with the m.3243A>G point mutation was reported to be lower than that in smooth muscle (Betts *et al.*, 2008). As the homogenate contains all types of tissues in the segment, including epithelium, connective tissue as well as smooth muscle, this finding suggests that the epithelium and/or connective tissue might have a lower mutation load that depresses the average. To determine whether this is due to the decrease in the mutation load in the GI epithelium, I collected the mucosal epithelium and smooth muscle from different GI segments of three patients with the inherited m.3243A>G mutation (patient 1 - 3) and one patient with the m.8344A>G mutation (patient 4) by laser microdissection and lysed them to obtain their DNA. I further performed pyrosequencing using the DNA to measure heteroplasmy in the tissue. The pyrosequencing technique provides a rapid and accurate measurement for the heteroplasmy of mtDNA point mutations based on the "sequencing by synthesis" principle, where it quantifies the light signal generated when a nucleotide is incorporated to the DNA template strand (Ronaghi *et al.*, 1998). The Newcastle Wellcome Centre pyrosequencing assay for the m.3243A>G and m.8344A>G mutations have been validated to be highly sensitive and specific and proved capable of precisely measuring the heteroplasmy of the mutations in small areas of tissue and even in single cells (Chrysostomou *et al.*, 2015; de Laat *et al.*, 2016). The sensitivity of the assay suggests that any measurements showing heteroplasmy levels lower than 2% should be considered as "no detectable mutation", which is confirmed by comparing to the wild-type control. The dissected tissue was randomly selected regardless of its COX activity to ensure the measured mutation level objectively reflects the true heteroplasmy of the tissue.

The mutation level was significantly lower in the mitotic epithelium compared with that in the post-mitotic muscle fibres in the oesophagus ($p < 0.0001$, Mann-Whitney U test); the stomach ($p < 0.0001$, unpaired t-test); the small intestines (SI) ($p < 0.05$ for patient 1 and $p < 0.0001$ for patient 2, unpaired t-test and Mann-Whitney U test respectively); and the colon ($p < 0.005$, unpaired t-test) (Figure 3.2). For the patient with the m.8344A>G mutation, the heteroplasmy level was also markedly lower in the colonic crypts compared with the smooth muscle ($P < 0.0001$, unpaired t-test) (Figure 3.2).

The data show a substantial variation in the heteroplasmy level between different crypts/areas of the oesophageal epithelium in contrast to the tight distribution within the muscle of the patients (Figure 3.2). The variance in the gastric glands was smaller compared with the other

epithelial tissues (Figure 3.2C). In addition, some intestinal crypts and oesophageal epithelium carried no detectable mutation (< 2% is considered as no mutation) (Figure 3.2A and 2B). Furthermore, each epithelial tissue shows an upper limit for the heteroplasmy level. Neither crypts harbouring an m.3243A>G% higher than 86% nor gastric glands with m.3243A>G% higher than 89% were observed. The oesophageal epithelium shows a lower limit (51%) for the m.3243A>G mutation. The upper limits for m.3243A>G and m.8344A>G were similar in the colonic epithelium, which was ~80%. The upper limit of the mutation in the epithelium was always lower than the average heteroplasmy level in the muscle of the same GI segment in the patients with high levels of the mutation in muscle (patient 2, 3 and 4). In patient 1 who had an intermediate mutation load (< 80%) in the muscle, the upper limit of m.3243A>G in the epithelium (77%) was higher than the mean mutation load in the muscle and was similar to the highest mutation level in the muscle (78%).

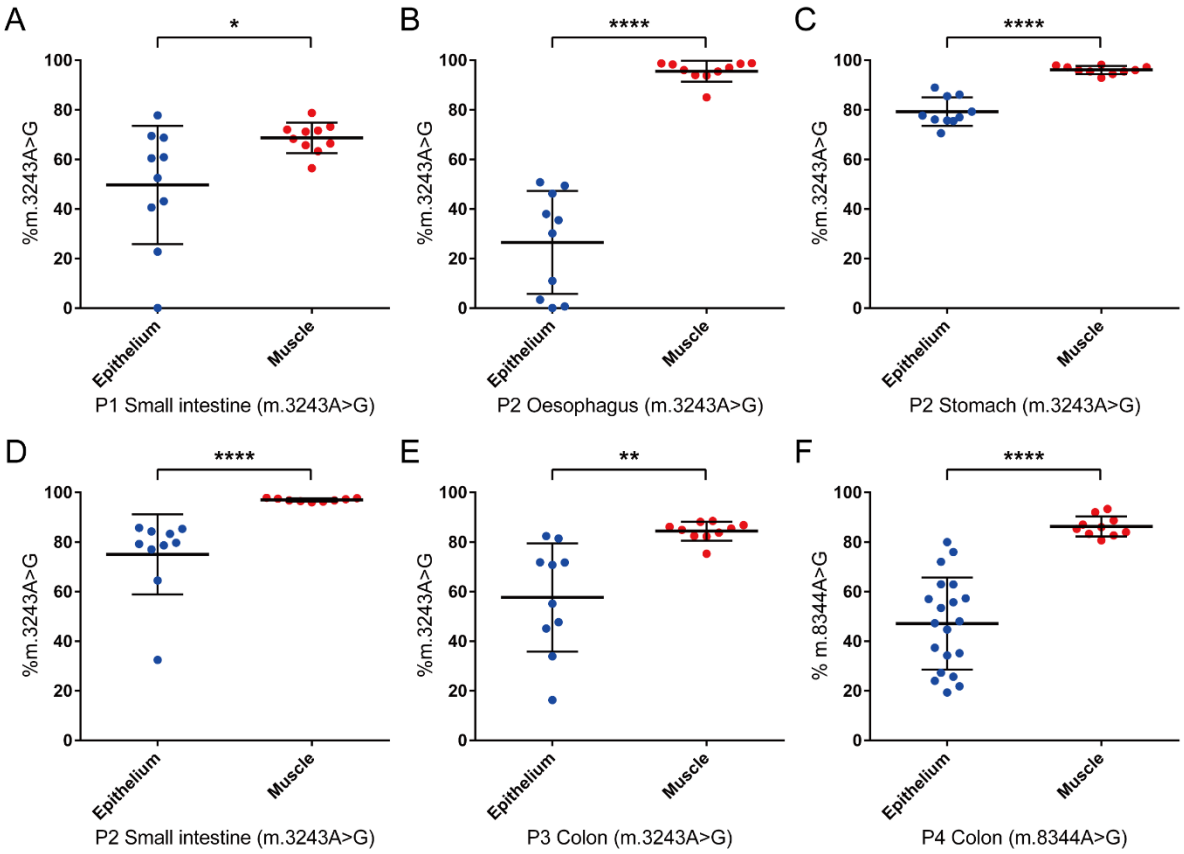

Figure 3.2 Heteroplasmy in the epithelium and the smooth muscle of different parts of the digestive tracts from patients with inherited m.3243A>G and m.8344A>G point mutations. The DNA for each replicate was extracted from 5 intestinal crypts/gastric glands/areas of oesophageal epithelium or muscle. P1 SI (ne=10, nm=10), P2 oesophagus (ne=10, nm=10), P2 stomach (ne=10, nm=10), P2 SI (ne=10, nm=9), P3 colon (ne=10, nm=10), P4 colon (ne=20, nm=10). *, P<0.05, **, P<0.005 and ****, P<0.0001.

3.4.2 COX activity in the gastrointestinal tract

The m.3243A>G mutation is pathogenic, and once it reaches a heteroplasmy threshold, it causes OXPHOS deficiency in both mitotic and post-mitotic tissue (Hämäläinen *et al.*, 2013). To investigate whether the reduction of the mutation load in the GI epithelial tissue makes any difference to the OXPHOS level, I performed sequential COX/SDH histochemistry and quantitative immunofluorescence on the tissue to determine the COX activity and protein levels of the respiratory chain subunits respectively. Haematoxylin and eosin staining was first carried out on sections of the patients' GI tract to assess the morphology of the tissue. Sequential COX/SDH histochemistry was then performed on patients' GI tissue, which allows visualisation of the in situ enzyme activity of cytochrome *c* oxidase (COX) and succinate dehydrogenase (SDH) in the tissue. In this assay, the electron donor, 3,3'-diaminobenzidine (DAB) will be oxidised by COX with normal enzyme activity to form brown polymer compounds saturating the cells and preventing the subsequent reactions of the SDH assay. When a cell contains dysfunctional COX that fails to produce polymer precipitates, the electron acceptor, nitroblue tetrazolium (NBT) will be reduced to blue formazan products, allowing visualisation of the SDH activity within the cell.

The ileum sample from patient 1 was very well preserved with intact morphology (Figure 3.3). Post-mortem tissue from patients 2 – 4 had various degree of degradation. The epithelium of the colon samples from patients 3 and 4 was poorly preserved and failed to be labelled by the SDH (Figure 3.4) and COX assay (Appendix 2, Figure 8.2) respectively. The COX and SDH assays were optimised separately on the epithelium and muscle of the GI tissue from patients 1 and 2 with comparatively good morphology (Figure 3.3 and Figure 3.5 respectively).

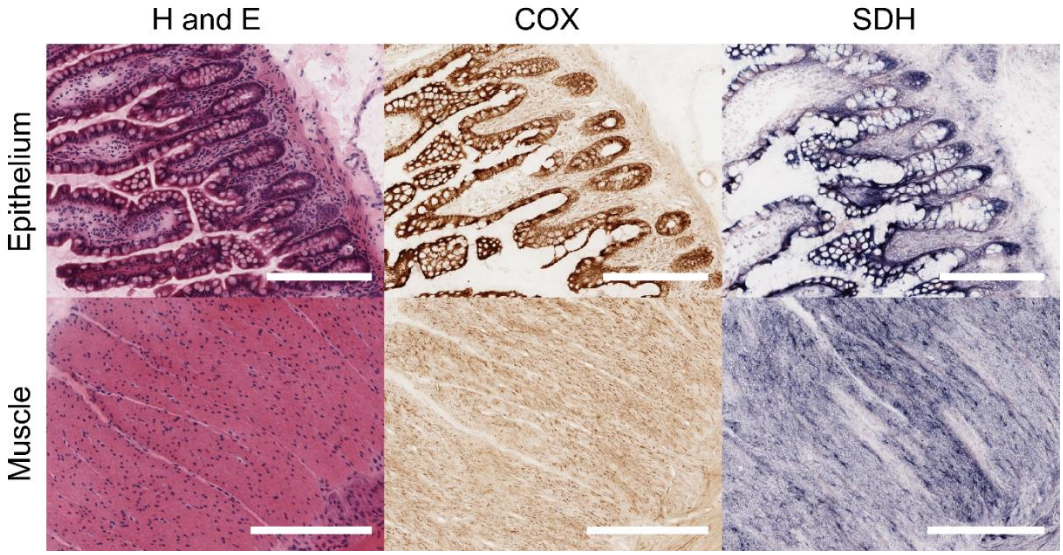

Figure 3.3 Haematoxylin and eosin staining, COX and SDH assay on the ileum from patient 1 with inherited m.3243A>G. Haematoxylin and eosin staining revealed the intact morphology of the tissue. The middle and right panel shows the optimised COX and SDH assay respectively on the epithelium and smooth muscle. Scale bar: 200µm.

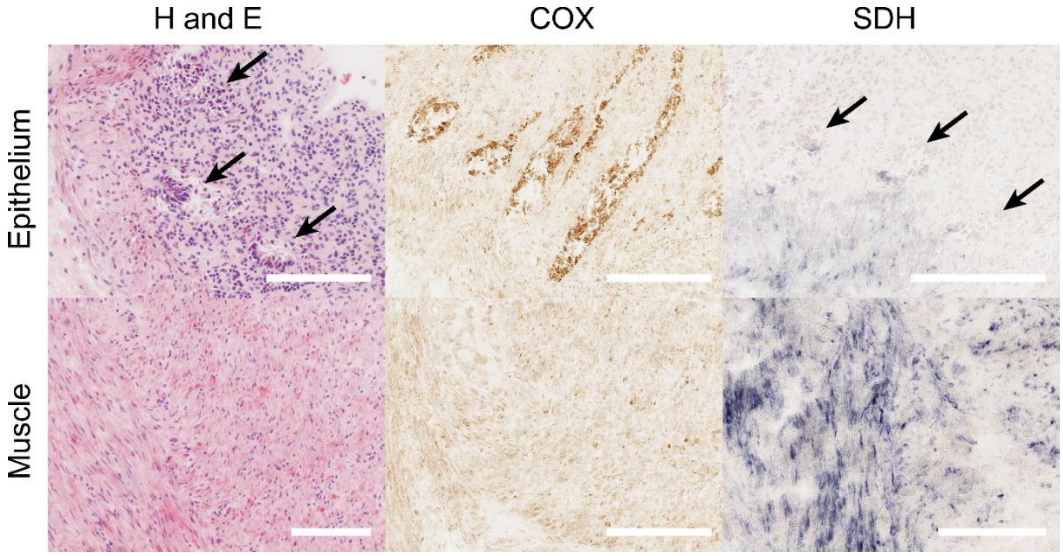

Figure 3.4 Haematoxylin and eosin staining, COX and SDH assay on the colon of patient 3 with the m.3243A>G mutation. H&E staining revealed fragmented colonic crypts with severe post-mortem degradation (indicated by the black arrows). SDH histochemistry failed the optimisation due to the poor morphology. Scale bar: 200µm.

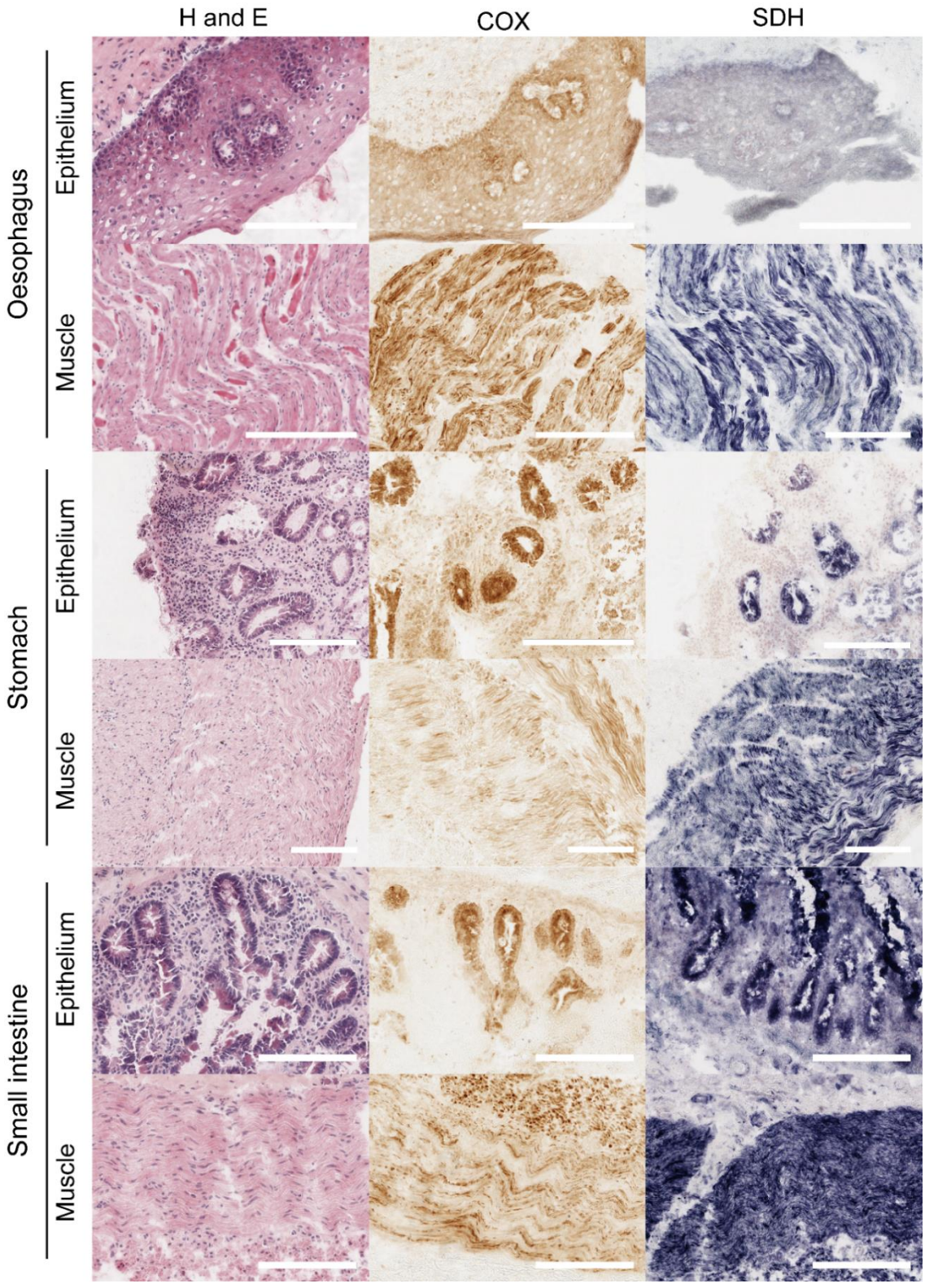

Figure 3.5 Haematoxylin and eosin staining, optimised COX assay and SDH assay on the epithelium and muscle of the oesophagus, stomach and jejunum (small intestine) from patient 2 with m.3243A>G. The morphology of the oesophageal epithelium was comparatively better than the gastric and intestinal epithelium. Many gastric pits, as well as the villi of the small intestine, were degraded. Scale bar: 200µm.

Sequential COX/SDH histochemistry revealed numerous blue COX-defective muscle fibres along the GI tract, whereas almost no COX deficiency was observed in the epithelium (Figure 3.6). To confirm this observation, all intestinal epithelial crypts and gastric pits in a whole section were examined, and COX deficiency was quantified as the ratio of the COX-defective crypts/gastric pits and all crypts/gastric pits on the section. It shows zero to very low levels of COX deficiency in each epithelial tissue (Table 3.3).

These results indicate that the COX activity was mainly preserved in the mitotic GI epithelial tissue from the patients, despite the pathogenicity of the m.3243A>G mutation shown by the severe COX deficiency in the post-mitotic muscle.

Patient (m.3243A>G)	Tissue (epithelium)	COX deficiency
P1	Ileum	1.25%
P2	Stomach	2.67%
	Jejunum	0.00%
P3	Colon	2.59%

Table 3.3 COX deficiency in the epithelial tissue of patients with the inherited m.3243A>G mutation. COX deficiency was quantified as the number of the COX-deficient intestinal crypts/gastric pits over the total number of the crypts/pits on a section. The counting was performed on two sections and averaged as the final result.

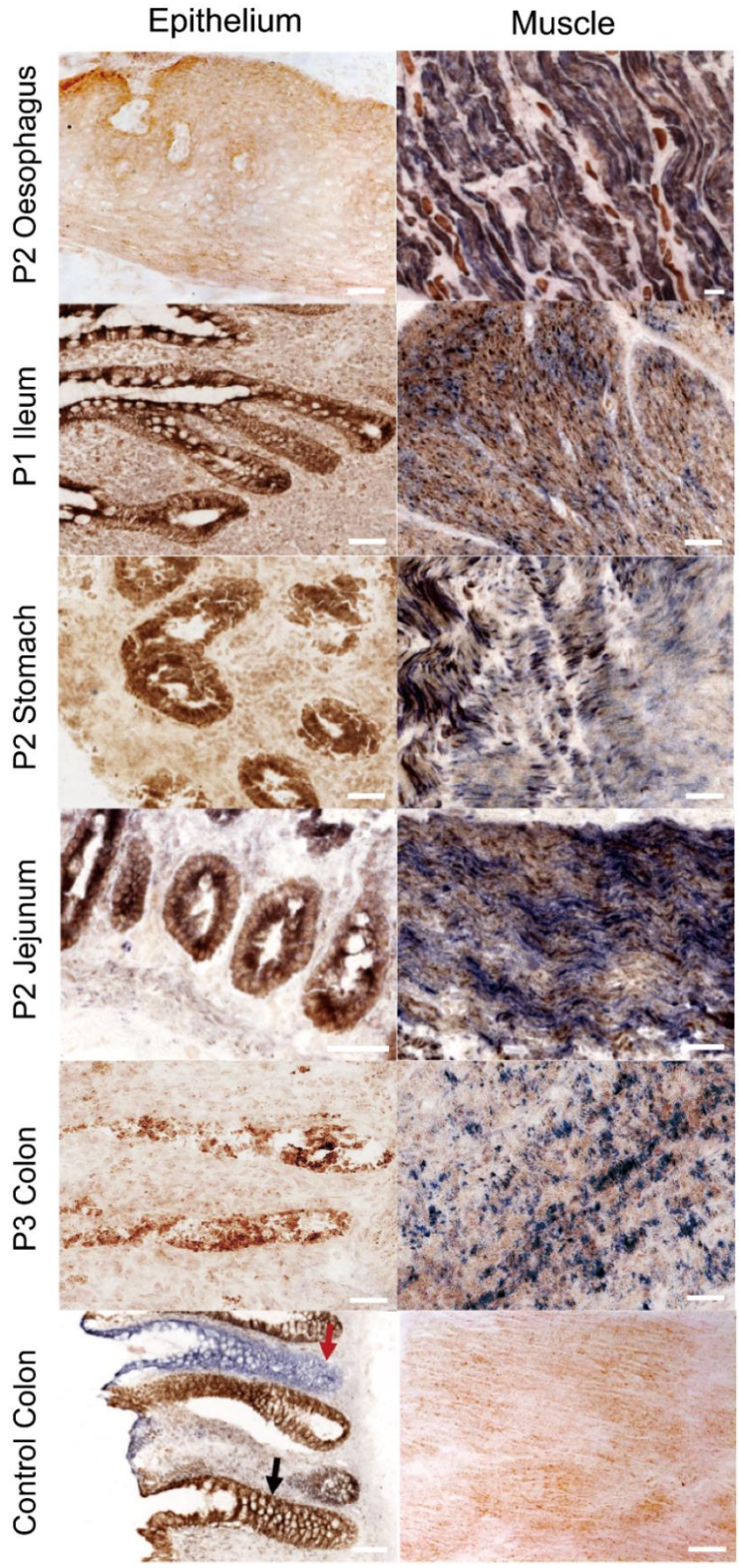

Figure 3.6 Sequential COX/SDH histochemistry on the epithelium and muscle of the GI segments from all three patients with inherited m.3243A>G mutation. Tissue with COX activity was labelled brown, and that with COX deficiency was in blue. A control section was used as a reference for the pigment. The black and red arrow refers to the COX-normal and COX-deficient crypt respectively. Scale bar: 50µm.

3.4.3 Optimisation of immunofluorescence and verification of mitochondrial markers

The histochemical results have demonstrated the preservation of the COX function in accordance with the decreased mutation load in the epithelial cells. To further investigate whether the OXPHOS level was influenced by the loss of the inherited mtDNA mutations, immunofluorescence was carried out on the GI tissue from three patients with the m.3243A>G mutation. The poor morphology of the tissue due to the post-mortem degradation was a significant challenge and required considerable time and effort to optimise the antibodies. Antibodies were incubated on tissue in a gradient of dilutions, and the antibody concentration that gave the optimal optic effect under the identical imaging exposure time was selected for the formal experiment (an example is shown in Figure 3.7A). Epithelial tissue and muscle were identified by labelling with antibodies for E-cadherin and Actin respectively (Figure 3.7, A and B). The E-cadherin marker nicely labelled the crypts in the ileal resection of patient 1 but failed to label some of the crypts in the post-mortem intestines of patient 2 (Figure 3.7C) and patient 3. Despite this, it helped me differentiate the epithelial tissue in the fluorescence imaging. Another intestinal epithelium marker, beta-catenin, also failed to mark the post-mortem epithelium.

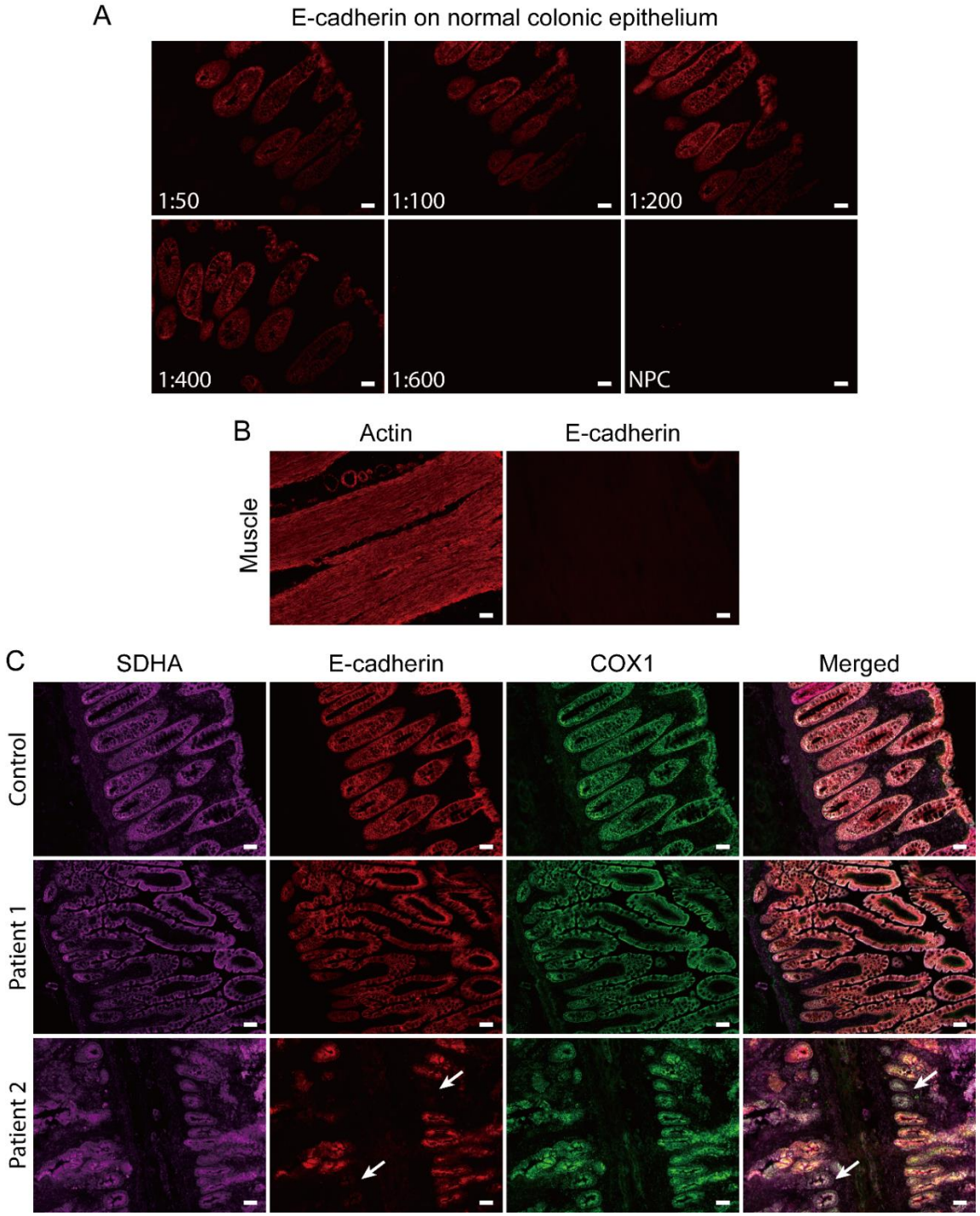

Figure 3.7 (A) E-cadherin optimisation as an example to show the optimisation strategy for antibodies used in immunofluorescence. Epithelial tissue was marked by E-cadherin in a dilution gradient, in which the one (1:200) that had the best labelling effect was chosen for the final experiment. (B) Identification of muscle using actin with no labelling of the epithelial marker (E-cadherin). (C) E-cadherin failed to label the epithelium in the post-mortem tissue. The images in the top and middle row show the clear labelling of SDHA, E-cadherin and COX1 on the control and the ileum section of patient 1 from resection respectively. The bottom row shows that E-cadherin failed to label a few intestinal crypts taken from patient 2 at post-mortem. Scale bar: 50μm.

Labelling tissue with a nuclear-encoded mitochondrial marker that is not affected by mtDNA mutations is necessary as it enables the OXPHOS deficient tissue to be visualised and selected for quantification in fluorescence imaging. In addition, as mitochondrial proliferation was reported in patients with mtDNA mutations (Egger *et al.*, 1981; Moraes *et al.*, 1992), it is important to investigate whether the loss of the inherited mtDNA mutation has any impact on nuclear-encoded mitochondrial components. Porin is a nuclear-encoded protein that constitutes the ion channel at the outer membrane of mitochondria, and was firstly used as a mitochondrial marker. However, the antibody of porin failed to label the epithelium of the post-mortem GI tissue (Figure 3.8). SDHA and COX4, the nuclear-encoded subunits that proved to be preserved in tissue with mtDNA defects (Betts *et al.*, 2008; Chrysostomou *et al.*, 2015), were used as alternatives. Although they are encoded by nDNA, they are subunits of the respiratory chain complexes and might be disabled by the inherited mtDNA mutation, despite a low possibility. To verify SDHA and COX4 as mitochondrial markers, I performed an immunofluoresence assay to examine their protein level together with porin in the ileum section of patient 1 that was obtained by ileectomy. Z-scores of the optical density in individual intestinal crypts were calculated based on the control population for each marker to normalise the inherent difference in the level of each protein. Neither of them showed any deficiency in the patient when compared with four age-matched controls, and their protein level was as steady as that of the porin (Figure 3.9). This proves that COX4 and SDHA are appropriate mitochondrial markers for immunofluorescence assay.

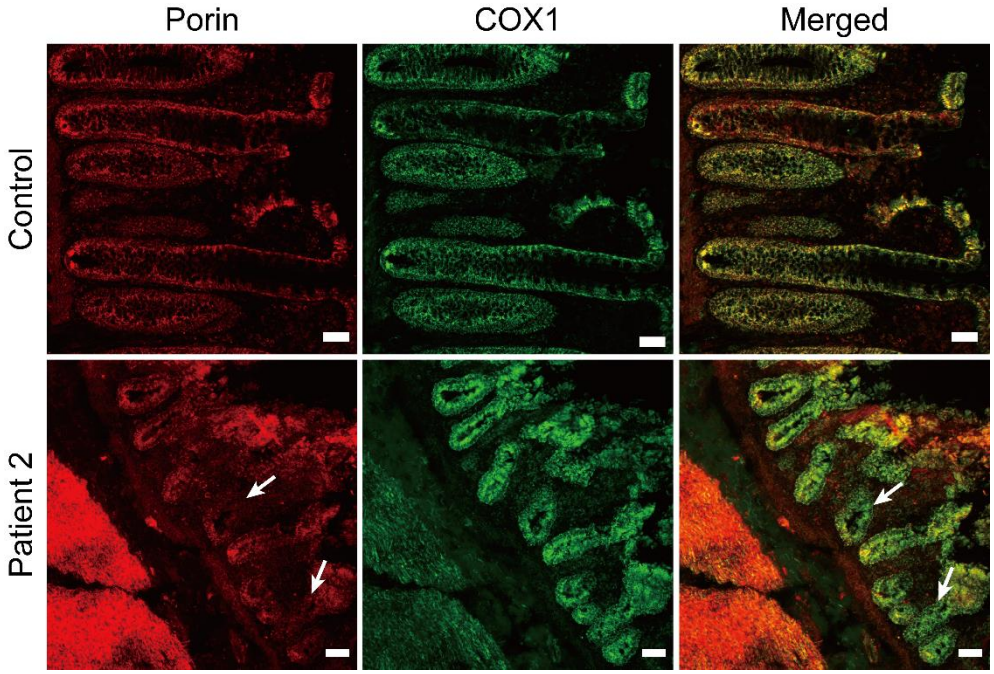

Figure 3.8 Porin failed to label the mitochondria on the post-mortem section of patient 2. The white arrows indicate some intestinal crypts showing no fluorescent signal of the porin marker that labels the mitochondria but strong signals of the respiratory chain complex IV (marked by COX1 antibody). The top panel shows the normal labelling of the porin and COX1 antibodies in the colonic crypts of a control. Scale bar: 50μm.

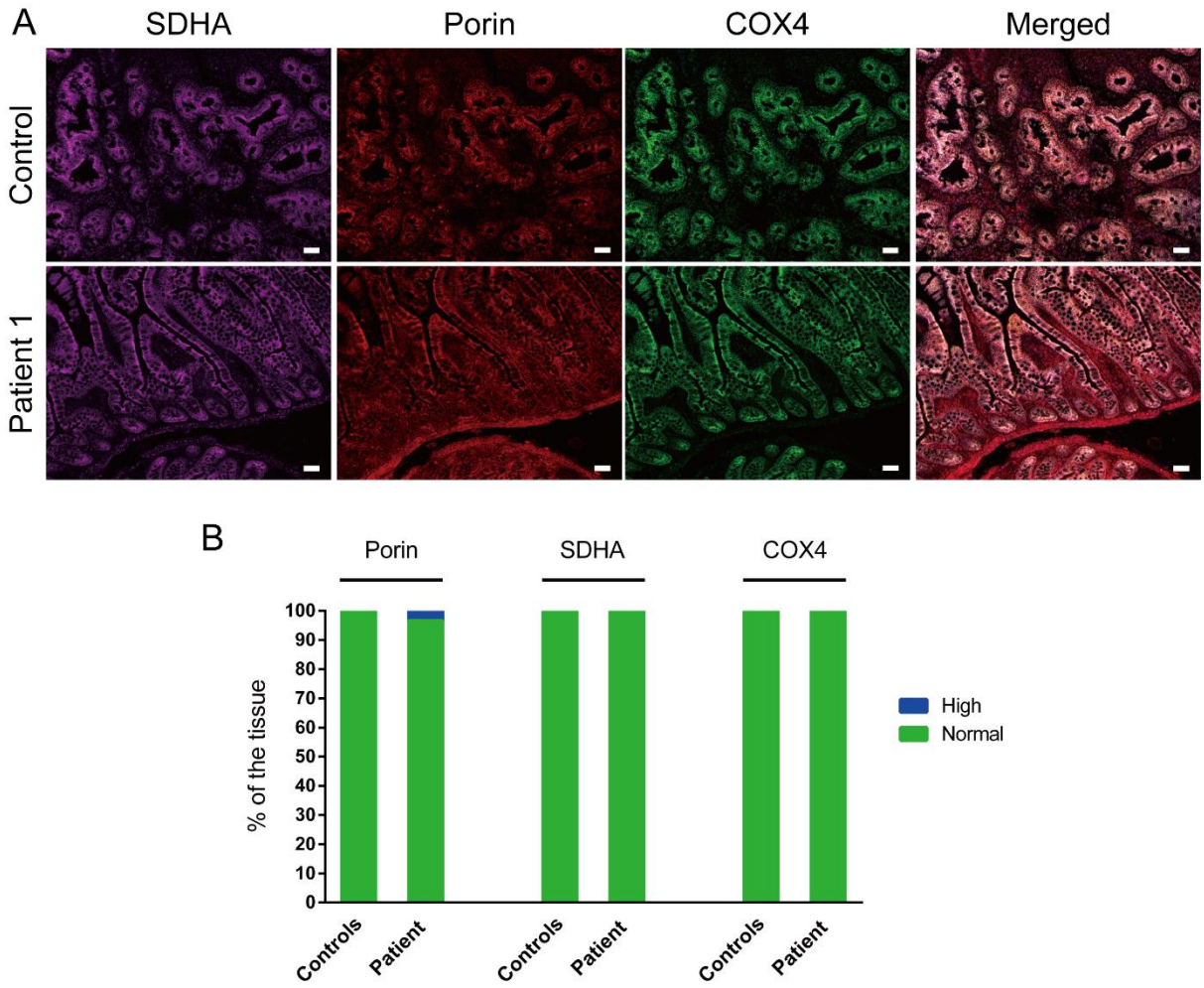

Figure 3.9 Verification of SDHA and COX4 as mitochondrial markers. (A) Immunofluorescence images of SDHA, porin and COX4 in a combination on the ileum section of patient 1. SDHA and COX4 show clearer borders of the intestinal crypts than porin. Scale bar: 50µm. (B) Immunofluorescence quantification of porin, SDHA and COX4. Fluorescence of individual crypts was quantified using ImageJ. Z-scores were calculated using the raw data and categorised according to the control population. Crypts: n (control) = 40 from four age-matched individuals, n (patient) = 30. Z-scores were classified as "low" (< -3SD), "normal" (-3SD ~ 3SD) and "high" (> 3SD).

3.4.4 Level of the respiratory chain complexes I and IV in gastrointestinal tract

Respiratory chain complexes I (CI) and IV (CIV) contain subunits that are encoded by mtDNA and are predisposed to mtDNA mutations (James *et al.*, 1996; Rocha *et al.*, 2015). To determine whether the loss of the inherited mtDNA mutation in the GI epithelium has any influence on the protein levels of these complexes, I performed quantitative immunofluorescence to measure the level of complexes I and IV using the antibodies against NDUFB8, a subunit of complex I that is critical to the complex assembly and often lost when there is a respiratory chain defect, and COX1, a mitochondrial encoded subunit of complex IV, respectively (Perales-Clemente *et al.*, 2010; Rocha *et al.*, 2015; Guerrero-Castillo *et al.*, 2017). Nuclear-encoded mitochondrial markers, COX4 and SDHA, were verified (3.4.3) and co-labelled with NDUFB8 and COX1 respectively to visualise tissue with a loss of complex I or IV subunits (Figure 3.10 and Figure 3.12 respectively). Raw data of the optical density was transformed to z-scores based on the control population and categorised according to different confidence levels.

No CI-deficient epithelium was found in any GI segments of any of the three patients with the inherited m.3243A>G mutation, including the oesophagus, stomach, small intestine and colon (Figure 3.10 and Figure 3.11). In contrast, half of the muscle fibres in the colon of patient 3 were complex I-deficient (Figure 3.10 and Figure 3.11). Except for the oesophageal epithelium of patient 2, which had a higher mean CI level than controls, the average CI level in patients' GI epithelium was similar to controls (Figure 3.11B).

In the epithelium of the oesophagus, stomach and small intestine of the patients, complex IV level was normal compared with controls (Figure 3.12 and Figure 3.13). A low level of COX1 deficiency (5%) was detected in the colonic epithelium of patient 3 (Figure 3.13). Surprisingly, no COX1 deficiency in the colonic muscle was observed (Figure 3.12 and Figure 3.13). The mean COX1 level in the epithelium of the oesophagus was higher than that in the control, though it was still within the normal range (z-score ≈ 2) (Figure 3.13B).

These results demonstrate that the protein levels of complex I and IV were preserved in the epithelium of the GI tracts from the patients, which is consistent with the normal COX activity and the low m.3243A>G mutation level in the epithelium discussed in 3.4.2 and 3.4.1.

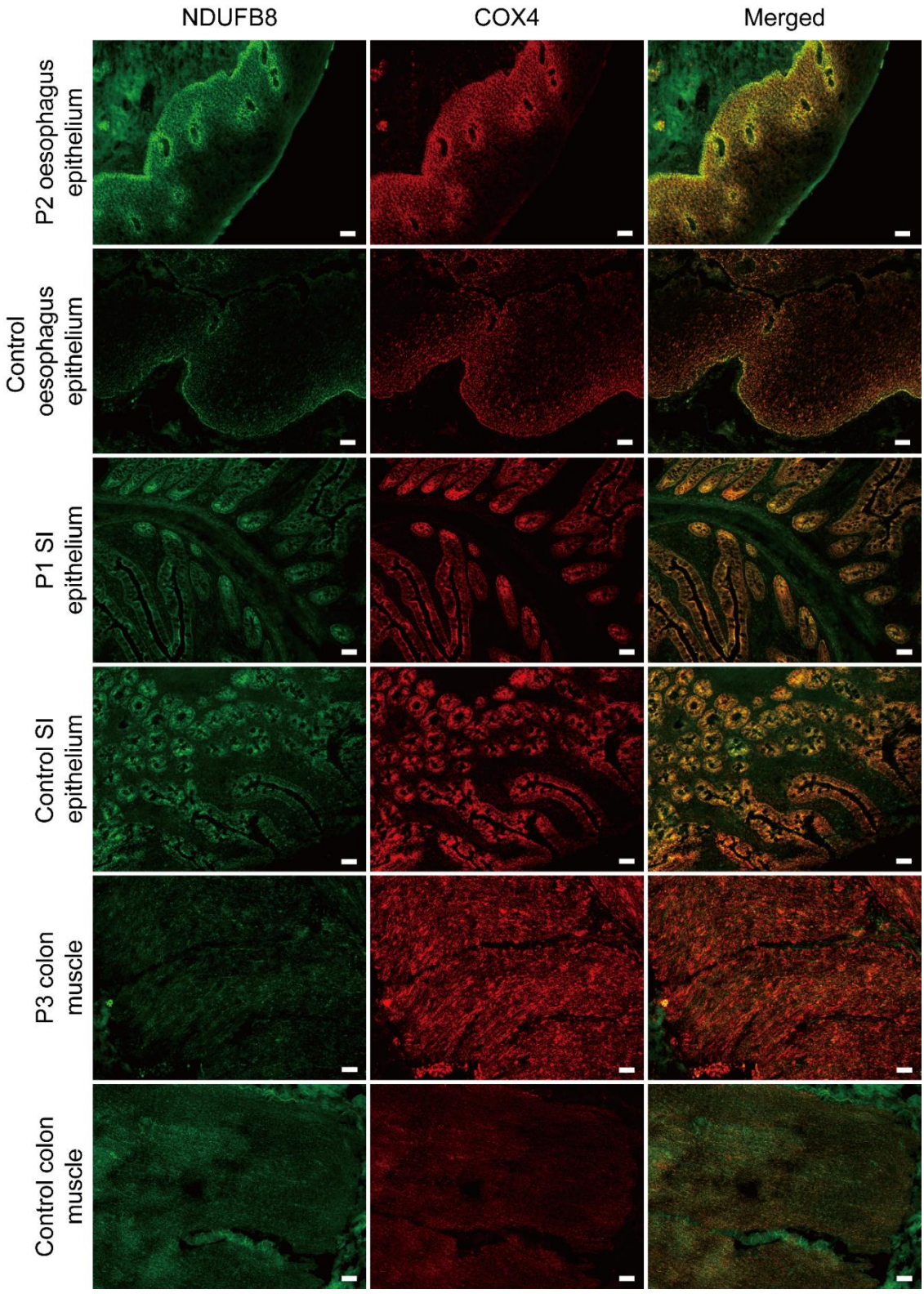

Figure 3.10 Immunofluorescence images of complex I (marked by NDUFB8 green) co-labelled with the mitochondrial marker COX4 (red) on the oesophageal and small intestinal epithelium, and the colonic smooth muscle from patients with m.3243A>G mutation compared with age-matched controls. The merged image is shown in the right panel. Scale bar: 50μm.

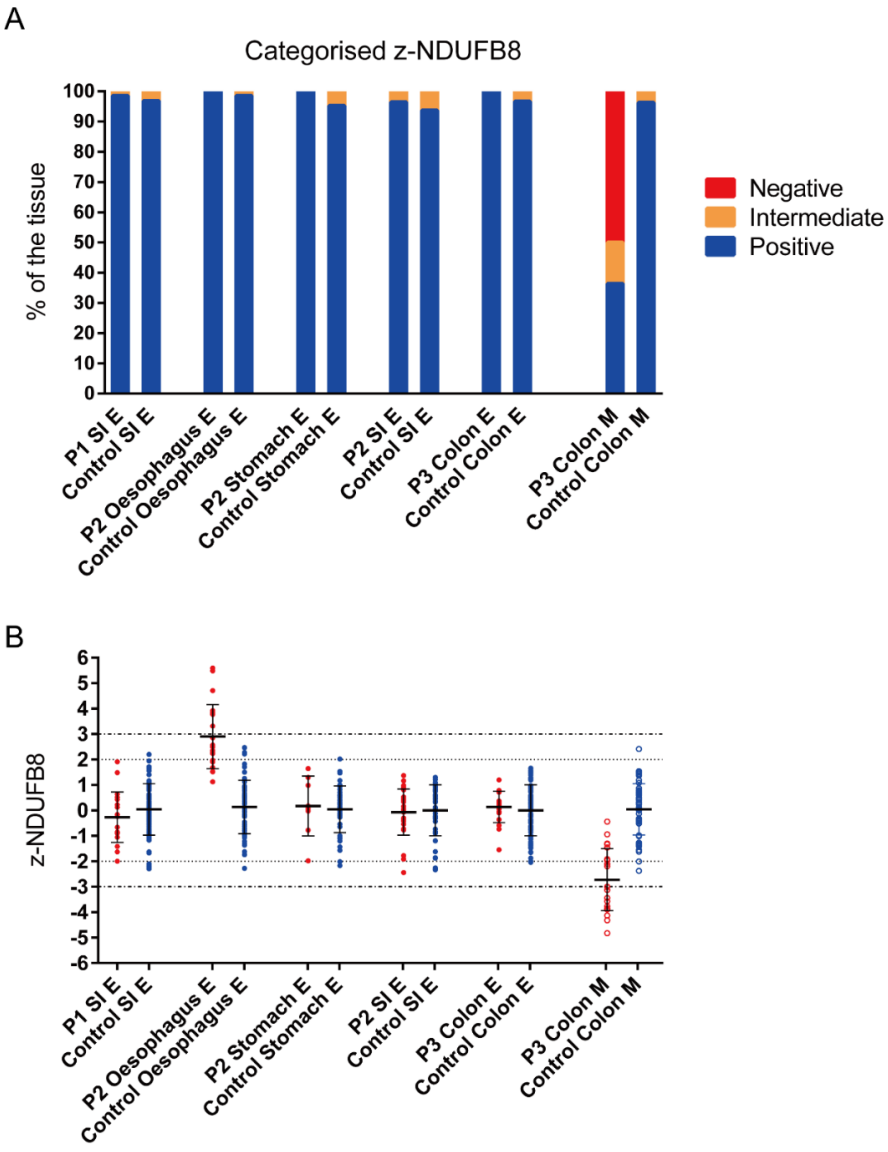

Figure 3.11 Quantification of complex I in the epithelium along the GI tract and the colonic smooth muscle of patients with m.3243A>G and controls. (A) Categorised z-scores of complex I (NDUFB8). The optical density of the tissue was measured using ImageJ, which was transformed to z-scores according to the control population. Categorisation of the z-scores was based on the 95% and 99% confidence levels: “negative” (< -3SD), “Intermediate” (-3SD ~ -2SD) and “positive” (> -2SD). (B) An overview dot plot showing the mean and distribution of the CI data. Individual intestinal crypts/gastric pits were selected for optical quantification. The oesophageal epithelium and colonic smooth muscle on the whole section were selected and quantified as areas of similar sizes. The number of selections for measurement: n (P1 SI) = 70; n (control) =128; n (P2 SI)= 28, n (control) = 48; n (P2 stomach) = 6, n (control) = 36; n (P3 colon)=20, n (control) = 91. Patients were compared with two controls for the stomach, three controls for the colon, the oesophagus and the small intestine of the patient 2, and four controls for the SI of the patient 1. SI, small intestine; E, epithelium; M, muscle.

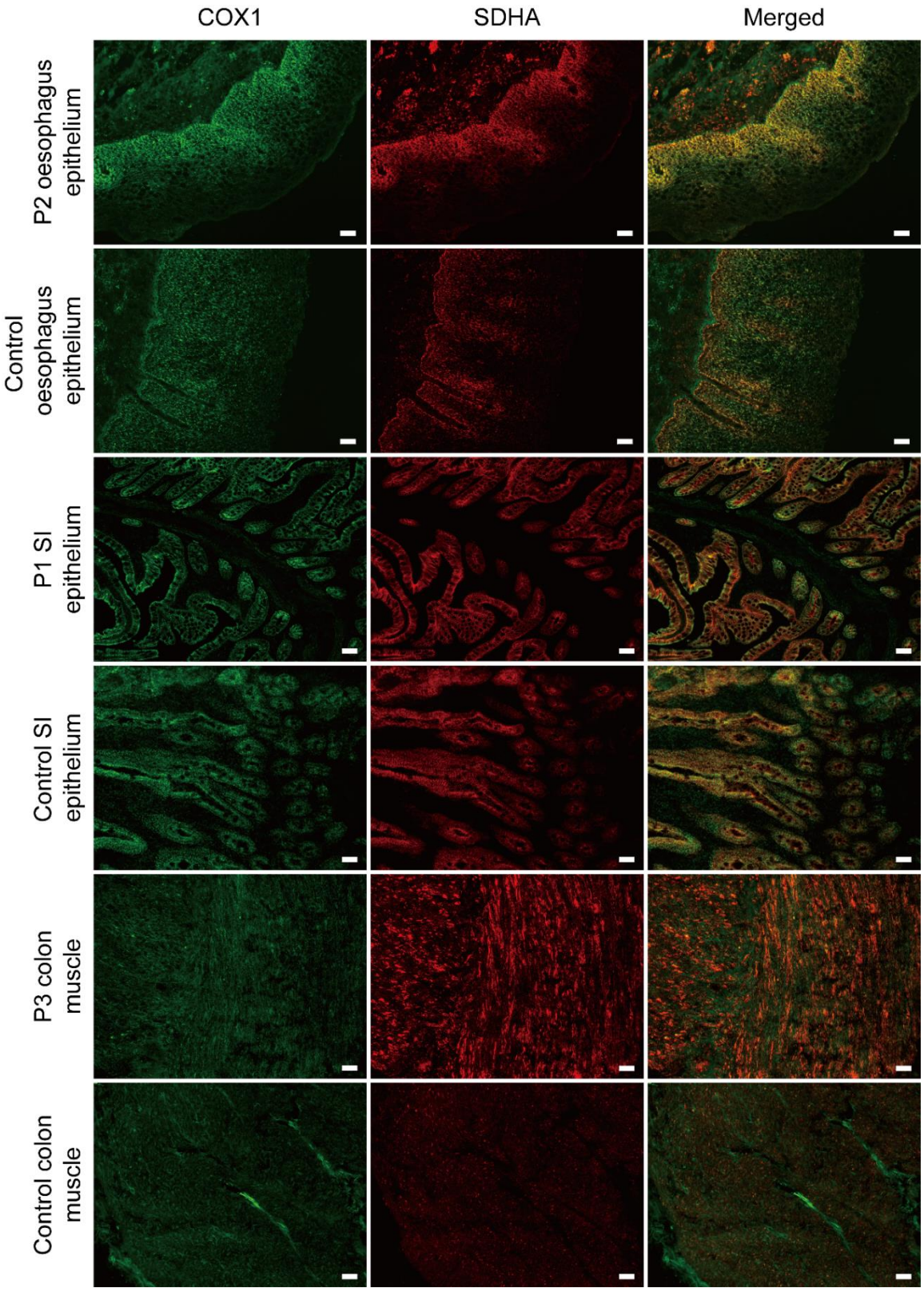

Figure 3.12 Example pictures showing combined COX1 (green) and SDHA (red) labelling on the epithelium of the oesophagus and the stomach, and the muscle of the colon from patients with inherited m.3243A>G in comparison to controls. The right panel shows the merged image. Scale bar: 50µm.

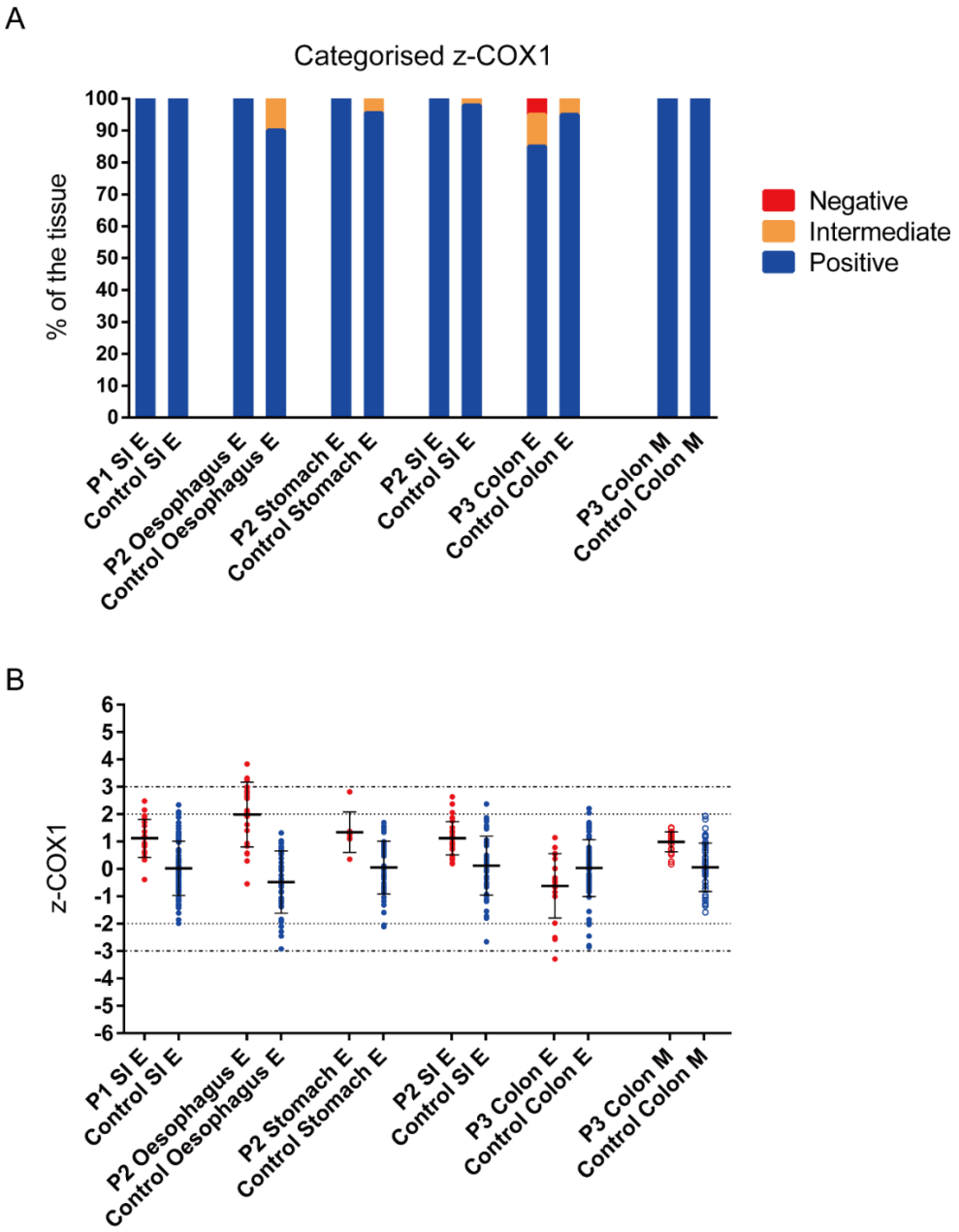

Figure 3.13 Quantification of COX1 (labelling complex IV) in the GI epithelium and the colon muscle of patients with m.3243A>G in comparison to controls. (A) Classification of the z-scores was set corresponding to the 95% and 99% confidence levels: "negative" (< -3SD), "Intermediate" (-3SD ~ -2SD) and "positive" (> -2SD). (B) A summary of the z-scores of the COX1 level showing the mean and the distribution of the data. The COX1 level was measured in individual crypts/gastric units and areas of the oesophageal epithelium and smooth muscle in the whole section. The number of analysed subjects: n (P1 SI) = 20; n (control) = 83; n (P2 SI)= 30, n (control) = 47; n (P2 stomach) = 7, n (control) = 44; n (P3 colon)=20, n (control) = 79. Two controls were included for the stomach, three controls for the colon, the oesophagus and the small intestine of patient 2, and four controls for the SI of patient 1. SI, small intestine; E, epithelium; M, muscle.

3.4.5 Level of nuclear-encoded mitochondrial markers

The nuclear-encoded respiratory chain subunit COX4 showed increased levels in the epithelium of the small intestine (8.57% of the tissue with a high level of COX4 in patient 1 and 14.29% in patient 2) and the oesophagus (40.91%) but not the muscle from the patients with the inherited m.3243A>G mutation (Figure 3.14A). The average level of COX4 in patients' GI epithelium and muscle were within the normal range (z-scores between -2 to 2), except a marked upregulation in the oesophageal epithelium (Figure 3.14B). SDHA, a subunit of complex II that is entirely encoded by nDNA, was also elevated in the epithelium of patients' GI segments, including the oesophagus (47.62%), stomach (14.29%), and small intestine (10%) (Figure 3.15A). It also augmented in the colonic muscle of the patient 3 (27.27%) (Figure 3.15A). The mean level of SDHA was notably higher in the oesophageal epithelium and the smooth muscle of the patients compared with controls, but it was still below the threshold of abnormality (<2) (Figure 3.15B). Of note, both of the mitochondrial markers was increased in the epithelium of the oesophagus and the small intestine of the patients compared to controls(Figure 3.14 and Figure 3.15).

Surprisingly, 5% and 15% of the crypts in the small intestine of patient 1 and the colon of patient 3 respectively showed low SDHA expression (95% confidence level) (Figure 3.15A), though none of them dropped below -3 (99% confidence level) (Figure 3.15B). A slight increase in the mitochondrial markers was noticed in the epithelium of different GI segments from controls, which might be a compensatory response to age-related OXPHOS deficiency (Figure 3.14 and Figure 3.15).

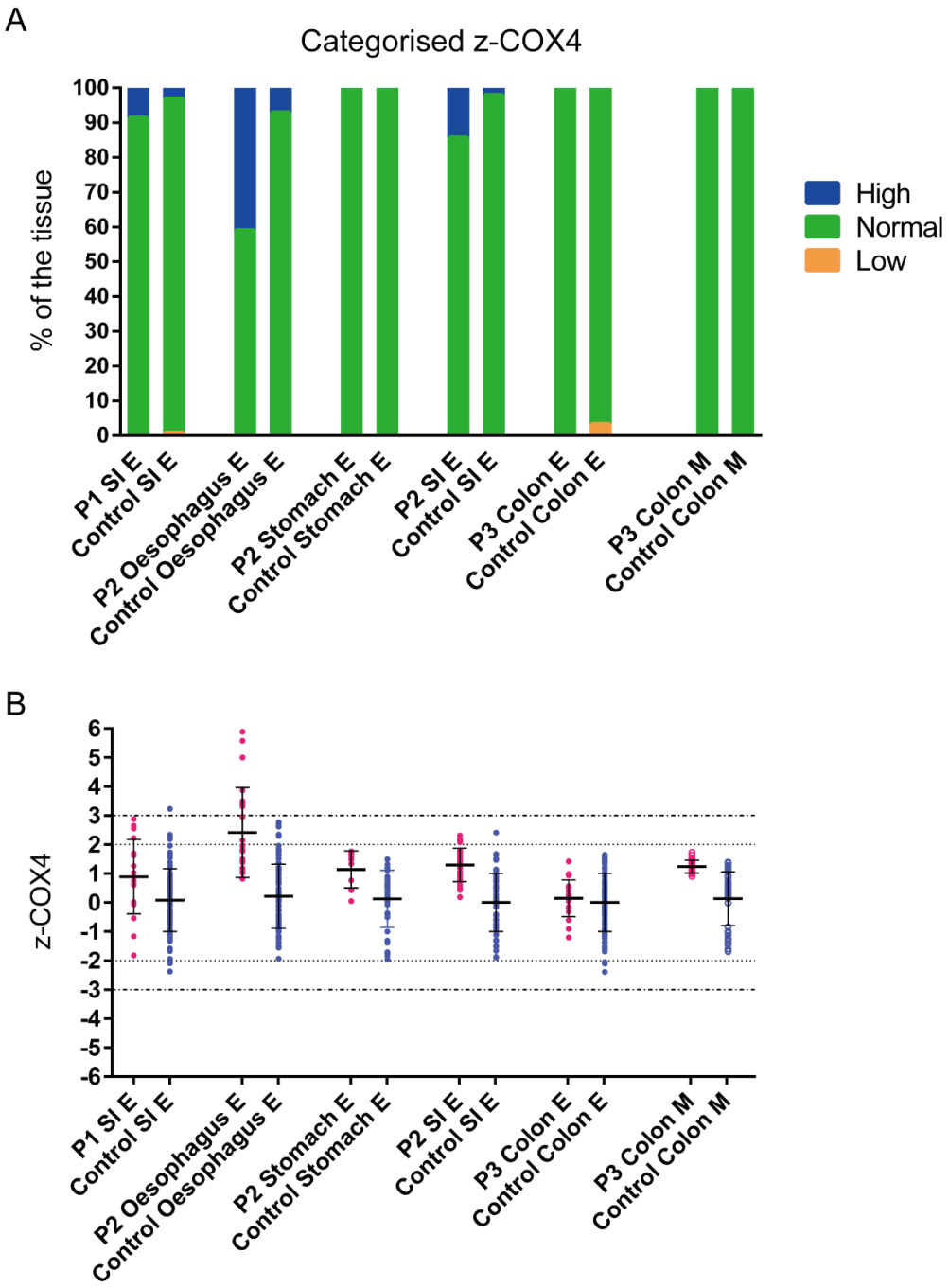

Figure 3.14 Z-scores of COX4 levels in the epithelium and muscle of the GI tract from the patients with the inherited m.3243A>G mutation and controls. (A) Categorised z-scores based on the control population: "low" (< -2SD), "normal" (-2SD ~ 2SD) and "high" (> 2SD). (B) An overview of the distribution and the average level of the data. Patients were compared with 2 controls for the stomach, 3 controls for the colon, the oesophagus and the small intestine (P2), and 4 controls for the SI (P1). The number of crypts/gastric pits/oesophageal epithelium or muscle areas for analysis: n (P1 SI) = 70; n (control) =128; n (P2 SI)= 28, n (control) = 48; n (P2 stomach) = 6, n (control) = 36; n (P3 colon)=20, n (control) = 91. SI, small intestine; E, epithelium; M, muscle.

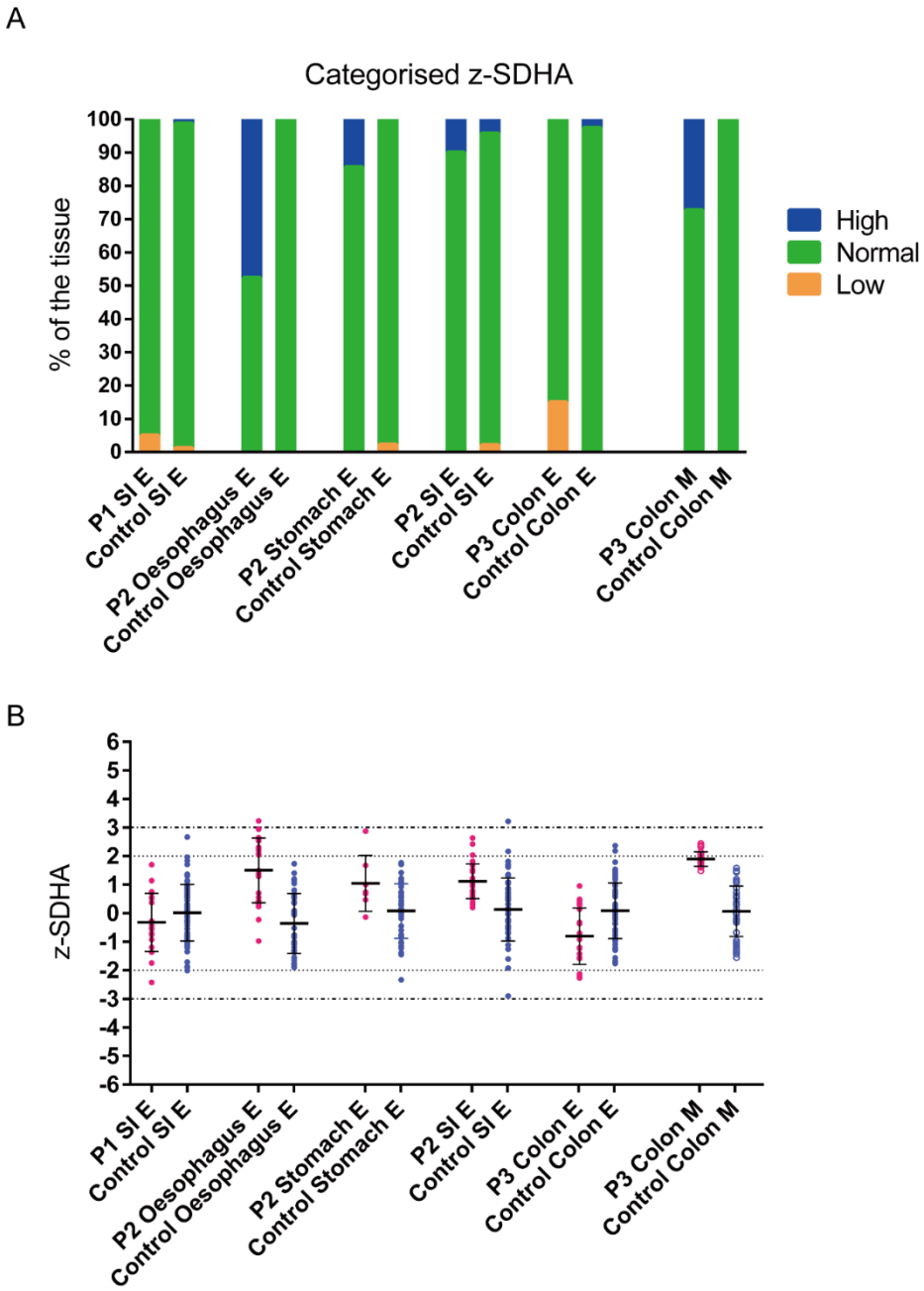

Figure 3.15 The level of SDHA in the epithelial and muscle tissue of patients with m.3243A>G compared with controls. (A) The raw optical density data was transformed into z-scores and categorised according to the control population: "low" (< -2SD), "normal" (-2SD ~ 2SD) and "high" (> 2SD). (B) The plot showing the mean and the variation of the data. Two controls were used for the stomach, three controls for the colon, the oesophagus and the small intestine (P2), and four controls for the SI (P1). The number of analysed crypts/gastric pits/areas of the oesophageal epithelium or smooth muscles: n (P1 SI) = 20; n (control) = 83; n (P2 SI)= 30, n (control) = 47; n (P2 stomach) = 7, n (control) = 44; n (P3 colon)=20, n (control) = 79. SI, small intestine; E, epithelium; M, muscle.

3.4.6 Correlation between the level of complex I/IV and mitochondrial markers

Linear regression and correlation analysis were performed to determine whether the maintenance of complex I and IV in patients' GI epithelium was associated with the nuclear-encoded mitochondrial markers, COX4 and SDHA respectively. Both patients and controls showed positive correlations between complex I and COX4 in the epithelium and muscle (Figure 3.16). The linear models are of good fitness for most of the tissue (Table 3.4). The slope of the linear model for the epithelium of the small intestine, the oesophagus and the colon in patients is not different from controls (Figure 3.16 A, B, D and E, and Table 3.4), indicating the level of complex I in the patients increased with COX4 at the same speed as in controls. In regards to the gastric epithelium and the smooth muscle, the slope of the patients' model is significantly steeper compared with controls, meaning that complex I increased faster with the elevation of COX4 in patients compared with controls (Figure 3.16 C and F, and Table 3.4).

COX1 had a strong positive correlation with SDHA in the epithelium of the small intestine, oesophagus and stomach in both patients and controls, but it showed no correlation with SDHA in the colonic epithelium of patient 3 (Figure 3.17 A-E and Table 3.5). COX1 was also significantly correlated with SDHA in the smooth muscle of both patients and controls (Figure 3.17F and Table 3.5). For all epithelial tissues with the correlation between COX1 and SDHA, the slope of the linear model is the same between patients and controls with a good fit of the data to this model indicated by the high R^2 value (Figure 3.17 A-D and Table 3.5).

These data suggest that in most of the epithelial tissue in the GI tract and the colonic smooth muscles, the levels of complex I and IV are positively correlated with the level of mitochondrial markers.

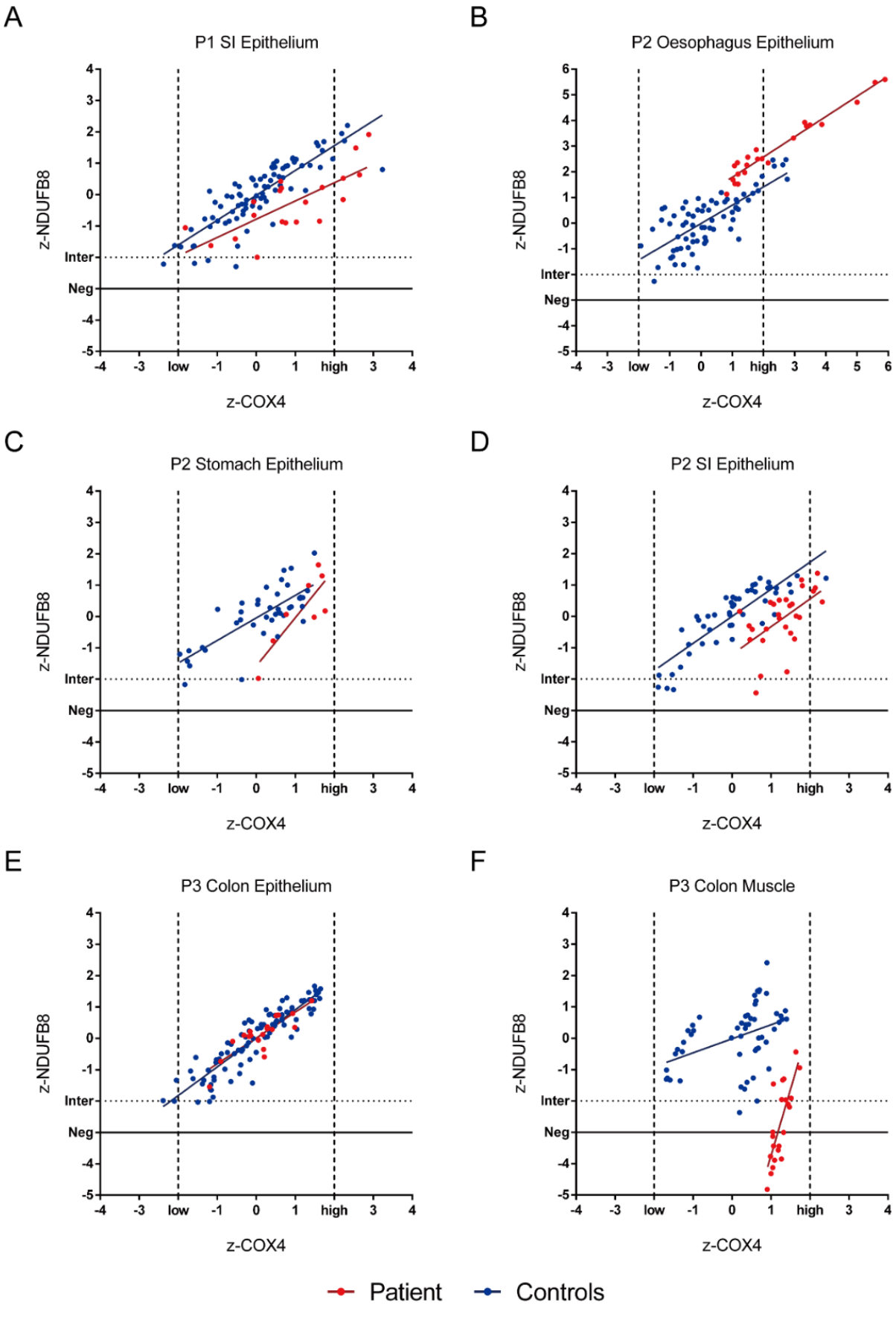
A
P1 SI Epithelium
B
P2 Oesophagus Epithelium
C
P2 Stomach Epithelium
D
P2 SI Epithelium
E
P3 Colon Epithelium
F
P3 Colon Muscle
z-NDUFB8
z-COX4
Inter
Neg
low
high
Patient
Controls

Figure 3.16 Linear modelling showing the correlation between complex I (marked by NDUFB8) and the nuclear encoded COX4 in the epithelium of (A) the small intestine of patient 1, (B) the oesophagus, (C) the stomach and (D) the small intestine of patient 2, (E) the colonic crypts and (F) the smooth muscle of patient 3 compared with controls. Each dot represents a single crypt/gastric pit or an area of the oesophageal epithelium and the smooth muscle. Equations of the linear models in each tissue: (A) patient, Y = 0.5824*X - 0.7855; controls, Y = 0.7916*X - 0.02390; (B) patient: Y = 0.7884*X + 0.9989; controls, Y = 0.7121*X - 0.01499; (C) patient: Y = 1.542*X - 1.584; controls, Y = 0.7189*X - 0.04683; (D) patient, Y = 0.8860*X - 1.217; controls, Y = 0.8642*X - 4.883e-008; (E) patient, Y = 0.8234*X + 0.01112; controls, Y = 0.9118*X - 4.140e-010; (F) patient, Y = 4.236*X - 7.986; controls, Y = 0.4476*X - 0.01741. Patient 1 was compared with 4 controls. Patient 2 was compared with 2 controls for the stomach and 3 controls for the oesophagus and the small intestine. Patient 3 was compared with 3 controls. The number of crypts/gastric pits/areas of oesophageal epithelium and muscle for analysis: n (P1 SI) = 70; n (control) =128; n (P2 SI)= 28, n (control) = 48; n (P2 stomach) = 6, n (control) = 36; n (P3 colon)=20, n (control) = 91. SI, small intestine.

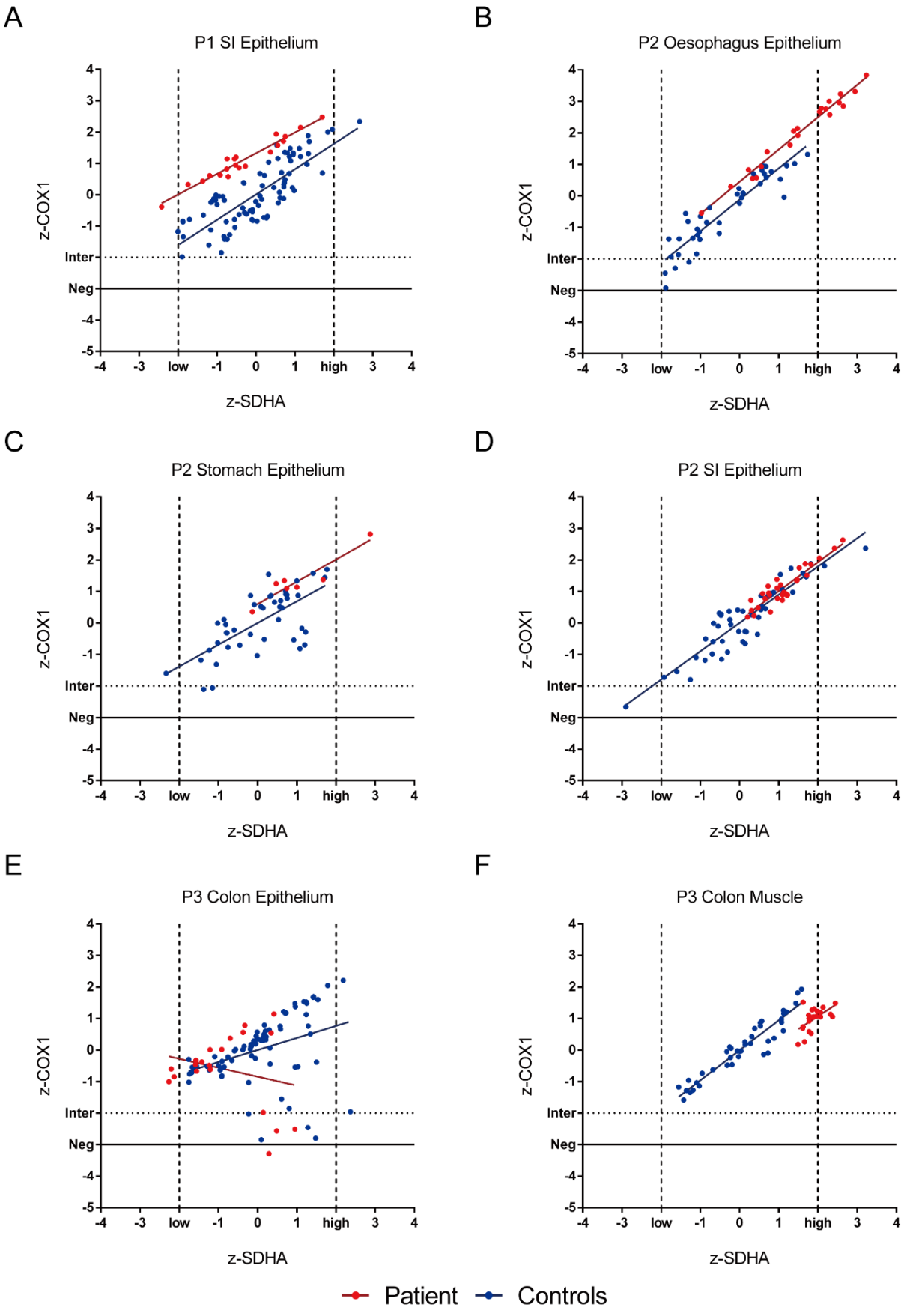
A
P1 SI Epithelium
B
P2 Oesophagus Epithelium
C
P2 Stomach Epithelium
D
P2 SI Epithelium
E
P3 Colon Epithelium
F
P3 Colon Muscle
z-COX1
z-SDHA
Inter
Neg
low
high
Patient
Controls

Figure 3.17 Linear regression showing the correlation between complex IV (labelled by COX1) and mitochondrial marker, SDHA in the GI tract of patients with the m.3243A>G mutation and controls. Equations of the linear relationship: (A) small intestine epithelium: patient 1, Y = 0.6608*X + 1.327; four controls, Y = 0.8109*X + 0.005016; (B) oesophageal epithelium: patient 2, Y = 1.024*X + 0.4491; three controls, Y = 1.001*X - 0.1228; (C) gastric epithelium: patient 2, Y = 0.7077*X + 0.5981; two controls, Y = 0.6882*X - 0.004174; (D) small intestinal epithelium: patient 1, Y = 0.6608*X + 1.327; three controls, Y = 0.8109*X + 0.005016; (E) colonic epithelium: patient 3, Y = -0.2840*X - 0.8434 (P> 0,05, no linear correlation); three controls, Y = 0.3824*X + 0.0006270; (F) colonic smooth muscle: patient 3, Y = 0.8107*X - 0.5503; three controls, Y = 0.9494*X - 0.008117. The number of crypts/gastric pits/areas of the oesophageal epithelium or smooth muscles for the analysis: n (P1 SI) = 20; n (control) = 83; n (P2 SI)= 30, n (control) = 47; n (P2 stomach) = 7, n (control) = 44; n (P3 colon)=20, n (control) = 79. SI, small intestine.

Tissue	**Patient**		**Controls**		**Any difference between P & C (P value)?**	
	P value	R^2	P value	R^2	Slope	Intercept
SI E (P1)	0.0001	0.5624	< 0.0001	0.7186	No	< 0.0001
Oesophagus E	< 0.0001	0.9505	< 0.0001	0.5641	No	< 0.0001
Stomach E	0.0090	0.7065	< 0.0001	0.5954	0.0305	N/A
SI E (P2)	0.0019	0.3135	< 0.0001	0.7469	No	< 0.0001
Colon E	< 0.0001	0.7021	< 0.0001	0.8314	No	No
Colon M	< 0.0001	0.6062	0.0020	0.1692	< 0.0001	N/A

Table 3.4 Parameters of the linear regression of complex I and COX4 in the epithelium and the muscle of patients' GI segments compared with controls. P, patient; C, controls.

Tissue	Patient		Controls		Any difference between P & C (P value)?	
	P value	R^2	P value	R^2	Slope	Intercept
SI E (P1)	< 0.0001	0.9420	< 0.0001	0.6540	No	< 0.0001
Oesophagus E	< 0.0001	0.9766	< 0.0001	0.8542	No	< 0.0001
Stomach E	0.0022	0.8701	< 0.0001	0.4690	No	0.0372
SI E (P2)	< 0.0001	0.8456	< 0.0001	0.8451	No	No
Colon E	>0.05	0.05700	0.0011	0.1298	0.0128	N/A
Colon M	0.0053	0.3282	< 0.0001	0.8957	No	< 0.0001

Table 3.5 Parameters of the linear models of COX1 and SDHA in the epithelium and muscle of the GI segments from patients with m.3243A>G and controls. P, patient; C, controls.

3.4.7 The difference in the OXPHOS level between gastric pits and glands

A difference in the OXPHOS level between the gastric pits and glands in the stomach from patient 2 was observed as a secondary finding. In contrast to the well-preserved OXPHOS function in the gastric pits (discussed in 3.4.2, 3.4.4 and 3.4.6), sequential COX/SDH histochemistry revealed COX deficiency in the gastric glands (Figure 3.18). In addition, the quantitative immunofluorescence assay demonstrated lower levels of complex I and IV in the gastric glands compared with controls (Figure 3.19A and B). Furthermore, the level of the nuclear-encoded mitochondrial markers COX4 and SDHA decreased in the gastric glands compared with controls (Figure 3.19C and D), which was not the case in the gastric pits (discussed in 3.4.5). No correlation was found between the levels of complex I and COX4 in the gastric glands (P-value = 0.4294, R^2 = 0.1617) (Figure 3.19E), though the level of complex IV was still positively correlated to SDHA (P < 0.0001, R^2 = 0.8067) (Figure 3.19F). The linear relationship between complex IV and SDHA in the gastric glands of the patient is the same compared with controls (P = 0.3836 for the slope and P = 0.5715 for the intercept). However, as a secondary discovery, these data are still preliminary due to the small sample size. To draw a comprehensive conclusion, more gastric glands should be included for analysis in future work.

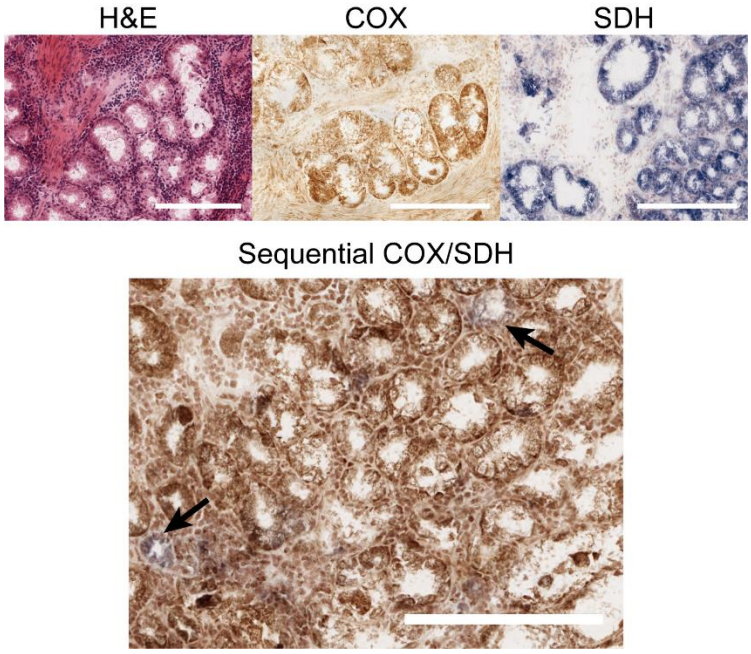

Figure 3.18 The COX activity in the gastric glands of patient 2 compared with controls. Haematoxylin and eosin staining, a COX assay, an SDH assay and sequential COX/SDH histochemical assay were performed on the gastric gland sections of patient 2. The black arrows indicate the COX-defective glands.

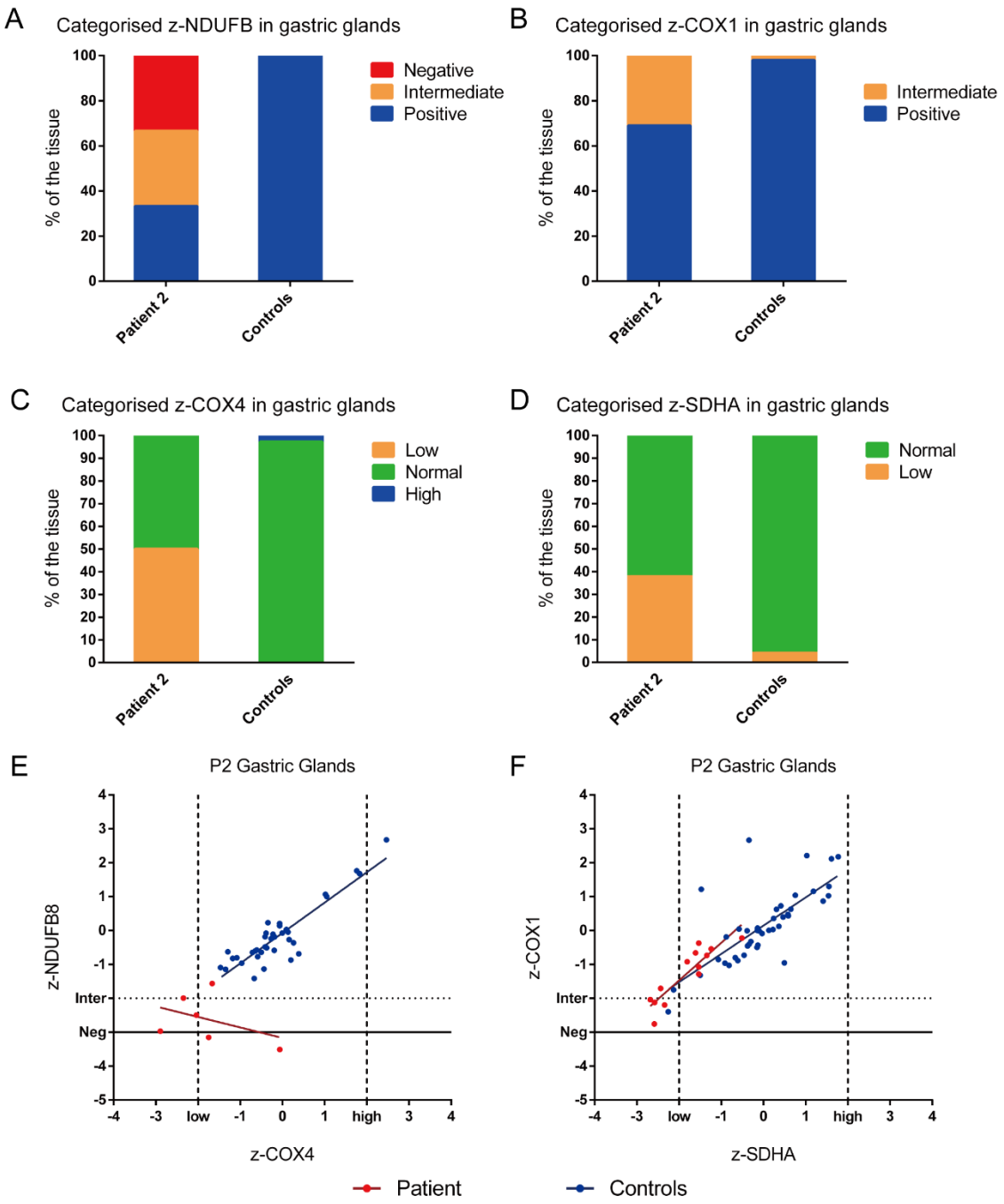

Figure 3.19 Categorical z-scores of the level of (A) complex I (marked by NDUFB8), (B) complex IV (marked by COX1), (C) COX4 and (D) SDHA in the gastric glands of patient 2 in comparison to two age-matched controls. Classification for NDUFB8 and COX1: "negative" (< -3SD), "Intermediate" (-3SD ~ -2SD) and "positive" (> -2SD). Hierarchy for nuclear encoded COX4 and SDHA: "low" (< -2SD), "normal" (-2SD ~ 2SD) and "high" (> 2SD). (E) Linear regression of NDUFB8 and COX4 in the gastric pits of the patient and controls. Equations of the linear models: patient, $Y = -0.3097*X - 3.170$ ($P > 0.05$, $R^2 = 0.1617$); controls, $Y = 0.8963*X - 0.07408$ ($P < 0.0001$, $R^2 = 0.8028$). (F) Correlation between COX1 and SDHA in the glands of the stomach from the patient and controls. Linear formulas: patient, $Y = 1.110*X + 0.7457$ ($P < 0.0001$, $R^2 = 0.8067$); controls, $Y = 0.8337*X + 0.1424$ ($P < 0.0001$, $R^2 = 0.5499$).

3.5 Discussion

Understanding the behaviour of mtDNA mutations in various tissues is crucial to understanding the development of both ageing and primary mitochondrial disorders. In contrast to the somatic mtDNA mutations that accumulate under no selective pressures with age (Greaves *et al.*, 2012a), patients with mitochondrial disease lose certain inherited mutations in mitotic blood (McShane *et al.*, 1991; Rahman *et al.*, 2001; Grady *et al.*, 2018). However, the age-related behaviour of the inherited mtDNA mutations in other mitotic tissue remains mostly unknown. Here I have investigated whether the loss of the inherited mtDNA mutations also occurs in mitotic gastrointestinal epithelium and whether it has any impact on the biochemical defect caused by the mutation.

Previous studies have shown that the m.3243A>G mutation was uniformly distributed in various tissues of foetuses, regardless of whether they are mitotic or not (Matthews *et al.*, 1994; Cardaioli *et al.*, 2000; Monnot *et al.*, 2011). In contrast, this study shows a lower m.3243A>G mutation load in the mitotic epithelium compared with the post-mitotic muscle in different GI segments from the patient group (age ranging from 36 years to 64 years). Given that there is no evidence the mutation load in muscle changes with age (Frederiksen *et al.*, 2006; Grady *et al.*, 2018), this contrast suggests a loss of the mutation in the patients' GI epithelial tissue, which is consistent with previous studies on epithelial cells in the buccal mucosa, urine and cervical smears (Olsson *et al.*, 2001; Frederiksen *et al.*, 2006; de Laat *et al.*, 2012; Grady *et al.*, 2018).

The intestinal epithelium is a good model for stem cell research as each crypt is an independent unit with all cells deriving from the stem cell at the crypt base. In addition, intestinal crypts often undergo niche succession where a single stem cell dominates the stem cell pool, and monoclonally produces daughter cells in a crypt (Novelli *et al.*, 1996; Kim and Shibata, 2002; Snippert *et al.*, 2010; Kozar *et al.*, 2013). Given the monoclonal attribute of the intestinal crypt, the considerable variation in the heteroplasmy level between different crypts with some of the crypts carrying no m.3243A>G mutation suggests that the loss of the inherited mtDNA mutation occurs in intestinal stem cells. This is consistent with a previous study where *in silico* simulations suggest that the loss of m.3243A>G mutations in blood occurs in haematopoietic stem cells (Rajasimha *et al.*, 2008). However, the analysis of the clinical data in this study also shows that the level of m.8344A>G mutation does not tend to decrease with age in patient blood (Rajasimha *et al.*, 2008), despite a consistent slightly lower heteroplasmy level in the blood compared with that in the muscle of the patients shown in the other study (Larsson *et al.*, 1992). The results here demonstrate that the heteroplasmy level of

m.8344A>G is significantly lower in the colonic epithelium of the patient compared with the muscle with a large variation in different crypts, which suggests that the selection against the m.8344A>G mutation may be stronger in the intestinal epithelium than blood. Nevertheless, due to the shortage of tissue samples, the results need to be confirmed when tissue specimens from more patients are available.

My results also show an upper limit of heteroplasmy level in the GI epithelium of the patients, which is likely tissue-specific, as in the same patient, the limit in the oesophageal epithelium is substantially different from that in the gastric or intestinal epithelium. The upper limit of the heteroplasmy level could also be individual-specific and might be associated with the overall mutation burden in the patient, since the limit in the small intestinal epithelium of patient 1 with an intermediate mutation load in the muscle is approximately 10% lower compared with patient 2 with a high mutation burden in the muscle. The upper cut-off limit of the mutation level in patients' GI epithelium suggests that once cells have reached this level of mutation load, they might be eliminated or activate some pathways to remove the mutation. The upper limits for m.3243A>G and m.8344A>G are similar in the colonic epithelium from the patients with comparable mutation burdens in the muscle; however, due to the small sample size, the factors that determine the limit of the mutation are still unknown.

Whether the loss of the inherited mtDNA mutations influences the phenotype of the tissue has not been documented in previous research on blood or epithelial cells, given the technical difficulties in examining the biochemical level in these tissues. Defective respiratory chain complex I and complex IV caused by mtDNA mutations are frequently reported (Hämäläinen *et al.*, 2013; Rocha *et al.*, 2015). In this study, I have demonstrated that the loss of the inherited mtDNA mutation in the mitotic GI epithelium of the patients corresponds to the well-preserved COX activity and protein levels of complexes I and IV in the epithelium. By contrast, the patients had a severe COX defect and complex I deficiency in accordance with the high mutation load in the post-mitotic muscle. Since studies indicate that high levels of m.3243A>G mutation can cause severe COX and complex I deficiency in mitotic intestinal epithelium as well as post-mitotic muscle and neurons (Hämäläinen *et al.*, 2013), the finding here suggests that the biochemical defects in the patients' GI epithelium might be reversible with the loss of the inherited mtDNA mutations. The data here also shows that the colonic smooth muscle with severe complex I deficiency displays a relatively normal level of complex IV, together with previous studies (James *et al.*, 1996; Hämäläinen *et al.*, 2013; Rocha *et al.*, 2015), suggesting that complex I is more susceptible to m.3243A>G mutation than complex IV.

This study also shows that the nuclear-encoded subunits COX4 and SDHA are as stable as porin as a mitochondrial marker for the patient cases with the m.3243A>G mutation, which is consistent with previous studies (Chrysostomou *et al.*, 2015). The results have revealed increased levels of COX4 and SDHA in the epithelium of different GI segments from patients compared with controls, which has a strong positive correlation to the level of complex I and complex IV respectively in most of the GI epithelial tissues of the patients. These data suggest an adaptive response of the nuclear-encoded subunits to inherited mtDNA mutations, which might improve the phenotype of the tissue and buffer the OXPHOS deficiency caused by the mutation. Such compensation was also observed in the smooth muscle of patient 3, which is in accordance with previous research on skeletal muscles (Moraes *et al.*, 1992). No increase in either of the mitochondrial markers was observed in the colonic epithelium of patient 3 (64y, the oldest among all the cases). In addition, the tissue has a low level of COX1 deficiency with no correlation between COX1 and SDHA. These data suggest a limit in the compensatory response that might be associated with ageing, yet the mechanism remains unknown. The gradient of the linear models between the mitochondrial markers and NDUFB8/COX1 in most of the patients' tissue is the same as for controls, suggesting that the rising rate of NDUFB8/COX1 concomitant with the increase in the mitochondrial markers in patients are the same compared with controls. For gastric pits and colonic smooth muscle, NDUFB8 rises faster with the elevation of COX4 in patients compared with controls, indicating some adaptability in the relationship. The correlation between COX1 and SDHA is robust in the epithelium of different GI segments from patient 1 and 2, indicated by the consistent high R^2 value. NDUFB8 and COX4 are also strongly correlated in the GI epithelium of the patients, but the correlation is comparatively weaker than that between COX1 and SDHA. Nevertheless, whether COX1 is more associated with mitochondrial mass than NDUFB8 needs to be confirmed by correlating them with the same mitochondrial mass marker.

In this study, despite severe COX deficiency shown by sequential COX/SDH histochemistry in the colonic smooth muscle of the patient, the level of COX1 determined by immunofluorescence is unexpectedly normal compared with controls. One possibility is that the COX deficiency indicated by the histochemical assay is exaggerated by the overpowering labelling of the upregulated SDH activity to some extent. Moreover, as the histochemical assay determines the enzyme activity of complex IV, whereas the immunofluorescence assay quantifies the protein level, a more likely explanation is that the muscle contains dysfunctional complex IV even though the protein expression is unaffected by the mtDNA

mutation. This has also been reported in other studies (Hämäläinen *et al.*, 2013), suggesting that for clinical diagnosis or laboratory examination of the OXPHOS function, the histochemical assay should not be replaced by techniques that solely examine the protein level of complex IV. Another explanation is that COX1 fails to mark the true level of complex IV for cases with m.3243A>G mutations. This is unlikely, as the mtDNA-encoded subunit COX1 has been well documented to be an ideal marker for the respiratory chain complex IV in patients with the m.3243A>G mutation (Rocha *et al.*, 2015).

The findings in this study also reveal tissue specificity in the rate of losing the inherited mtDNA mutations. The mutation level of m.3243A>G in the oesophageal epithelium is notably lower compared with that in the gastric or intestinal epithelium from the same patient, which is concomitant with the significant upregulation of complex I/IV and the mitochondrial markers. The reason why the epithelium of the oesophagus loses the mutation much faster than other parts of the alimentary tract remains unknown, but the data here suggests that the rate of losing the mutation is unlikely to be solely determined by the tissue turnover rate under normal physiological conditions, as the normal renewal speed of the oesophageal epithelium is much slower than that of the intestinal epithelium (Creamer *et al.*, 1961; Squier and Kremer, 2001). On the other hand, it might be associated with the increased cell proliferation during wound healing in the oesophageal epithelium (Doupé *et al.*, 2012), considering that it is often exposed to the high temperature and hardness of food, which predisposes it to more damage compared with the other part of the GI tract.

The gastric epithelium is composed of numerous gastric units that comprise gastric pits and glands (James S. Lowe, 2015). A noticeable difference in the OXPHOS level between the gastric pits and glands of the same patient was observed as a secondary finding, which highlights the specificity within epithelial tissue. Although gastric stem cells at the neck zone of a gastric unit produce daughter cells that undergo a bidirectional migration to form all the cells within the unit, gastric pits and glands are distinct in terms of the cell composition and function (Kouznetsova *et al.*, 2011; James S. Lowe, 2015). Thus, they may have different demands for energy, and their sensitivity and response to the m.3243A>G mutation may be different accordingly. Another possibility is that the gastric pit and gland may have different levels of the mutation, which suggests an involvement of amplifying or differentiated cells in altering the load of the inherited mtDNA mutation within a gastric unit. Unfortunately, in this study, no gastric pits were available for the pyrosequencing measurement to determine the heteroplasmy level. In addition, the interpretation is only based on the data of one patient with

a limited number of gastric units being analysed. Hence, the hypotheses above need to be confirmed when tissue specimens from more patients become available in the future.

The limitations of this study are due to the quality of the tissue and the small sample size. The tissue from only four patients was available. The severe post-mortem degradation of the tissue was a challenge in all of the assays for DNA or protein analysis. DNA extracted from a single intestinal crypt/gastric gland was not sufficient for genetic analysis. Thus five pooled crypts/glands were used for the measurement of the mutation load, which might compromise the interpretations. The poor morphology of the tissue generally compromised the protein assays and incapacitated the antibodies of the ideal mitochondrial mass marker porin and several epithelial markers. The poor tissue quality and the lack of GI stem cell markers for humans restrict the study to stem cell progenies rather than stem cells per se. In addition, this is not a longitudinal study, and the age-related changes in the mutation level in the patients are extrapolated based on previous literature. These limitations make it necessary to confirm the findings using tissue from more patients when it is available and to use animal models for mechanistic studies.

3.5.1 Future work

There are still many questions in regards to the loss of inherited mtDNA mutations in mitotic tissue. Here only the two common mtDNA-tRNA mutations were investigated, and it is necessary to expand the sample size. Furthermore, studies have reported that for two mutations at the site m.8993 in a protein-encoding gene mt-ATP6, there is no tissue-specific segregation or age-related changes in the mutation load in blood (White *et al.*, 1999). To gain the understanding of the biological features of pathogenic mtDNA mutations and the phenotype of mitochondrial disease, it would be beneficial to determine whether the age-dependent loss of the mutation in the GI stem cell populations is generic to other types of inherited mtDNA mutations. Longitudinal studies show that, despite a possibility that the mutation might have been lost before the examination, not all subjects with the inherited m.3243A>G lose the mutation in blood (Grady *et al.*, 2018). There was a large variance in the change in the mutation level with age between individuals, and the mutation level in some of the subjects drifted slightly up or was sustained as a plateau (Grady *et al.*, 2018). This seems not to be the case here, and more samples need to be examined to consolidate the conclusion. Studying the variance in the heteroplasmy in different segments of GI epithelium would possibly reveal the difference in the selective pressure against inherited mtDNA mutations

between different stem cell populations. Answering all these questions requires tissue from more patients and carriers with inherited mtDNA mutations.

The interpretations in regards to GI stem cell populations in this study is based on the extrapolation from the stem cell progenies and the presumption of monoclonal conversion of the intestinal crypt. It would be valuable to confirm the findings on stem cells per se. Isolating intestinal stem cells will also benefit mechanistic studies. Available techniques that allow isolation of intestinal stem cells from fresh biopsies of patients have been published recently, though it requires validation (Jung *et al.*, 2015). However, it is challenging to acquire such tissue in the clinic.

Investigating the mechanism underlying the loss of the inherited mutation in mitotic tissue is still at an early stage. Although there is a visible upper limit in the mutation load of different intestinal crypts from patients, the pattern of the data appears to resemble the distribution caused by random genetic drift. Investigating the distribution of the mutation level in crypts is very important to understanding the mechanism of the age-related loss of the inherited mtDNA mutations. Verifying whether the variation in the mutation load of different crypts is due to random genetic drift could be achieved by either statistically comparing the data in this study with known distributions caused by random genetic drift or establishing in silico simulations.

The ultimate question is why only inherited but not somatic mtDNA mutations that accumulate in normal ageing are under negative selective pressures. Due to the limitations of the human study, the investigation of the mechanism requires the use of animal models. A mouse model of mitochondrial disorders ($tRNA^{Ala}$ mutant mice) carrying hereditary m.5024C>T was established recently (Kauppila *et al.*, 2016), which may be of use in further investigating selective pressures. Full characterisation of the mouse model is indispensable for determining whether this mouse model is suitable for the mechanistic study. This will be discussed in Chapter 4 and Chapter 5.

3.6 Conclusion

In this study, I have presented genetic and biochemical evidence for the selective loss of the inherited mtDNA mutations in the mitotic GI epithelium. The substantial variation in the mutation load of different intestinal crypts with some of them carrying no inherited mutation suggests that the selection against the mutation occurs in intestinal stem cells. This study benefits the understanding of the phenotype and the progression of mtDNA disease. It also highlights the contrast in the selective pressures on inherited and somatic mtDNA mutations. Investigating the mechanism underlying this difference would be valuable in the understanding of both ageing and mitochondrial disorders.

Chapter 4 Genetic characterisation of a tRNA^{Ala} mutant mouse model for investigating selective pressure on inherited mtDNA mutations

4.1 Introduction

Mitochondrial diseases characterised by mitochondrial dysfunction are highly heterogeneous (Alston *et al.*, 2017). Patients with mitochondrial disorders can carry identical genetic mutations but present various tissue-specific phenotypes and symptoms with different ages of onset (Alston *et al.*, 2017). mtDNA diseases are a primary group of mitochondrial disorders caused by germline mtDNA mutations (Taylor and Turnbull, 2005). Many factors are believed to be involved in the heterogeneity of mtDNA diseases, including heteroplasmy level, clonal expansion, the biochemical threshold and tissue specificity with mitotic segregation (Taylor and Turnbull, 2005); however, the exact mechanism underlying disease heterogeneity remains uncertain. Studying the dynamics of mtDNA mutations in different tissues with age is critical to understanding the factors accounting for the diversity of mtDNA diseases. In addition, it is important to understanding ageing, ageing-related degenerative disease and cancer that are intimately related to the age-dependent accumulation of acquired somatic mtDNA mutations. However, it is difficult to study these using human samples, due to the invasive sampling methodology. Developing mitochondrial models of ageing and mtDNA disease and comparing normal aged individuals with those with mtDNA disease regarding the dynamics of mtDNA mutations would be enormously helpful to understanding mtDNA disease and ageing. A mouse model of ageing (mtDNA-mutator mouse) has been established, which recapitulates the accumulation of somatic mtDNA mutations during ageing (Kujoth *et al.*, 2005; Trifunovic *et al.*, 2005). These mice carry a knock-in mutation in the mtDNA polymerase γ (*Polg*) sequence, which impairs proofreading during mtDNA synthesis, predisposing them to acquired mtDNA mutations with age (Kujoth *et al.*, 2005; Trifunovic *et al.*, 2005). The mtDNA-mutator mice have been ubiquitously utilized to study the association between mtDNA mutations and ageing (Su *et al.*, 2018); however, establishing reliable models of mtDNA disease is a considerable challenge for mitochondrial researchers.

A breakthrough was the creation of rho zero (ρ^0) cells, a cell line depleted of mtDNA through exposure to ethidium bromide (King and Attardi, 1989). These cells were fused with cytoplasts with exogenous mtDNA to form trans-mitochondrial cybrids, enabling the study of different introduced mutant mtDNAs in the same nuclear background (King and Attardi, 1989). This model has proved valuable for studying the effect of heteroplasmy level on cellular function and phenotype (Hayashi *et al.*, 1991; Chomyn *et al.*, 1992b), the genetic causes of mitochondrial disorders (Tiranti *et al.*, 1995; Taanman *et al.*, 1997) and the

influence of nuclear factors on the dynamics of pathogenic mtDNA mutations in cells (Dunbar *et al.*, 1995).

Another cell model of mitochondrial disease has been established with the development of stem cell research where induced pluripotent stem cells (iPSCs) were generated through reprogramming fibroblasts from patients with mtDNA disease (Hämäläinen *et al.*, 2013). This technique enables the generation of teratomas containing different types of tissues with similar heteroplasmy levels and the same nuclear background from the iPSCs, and it also allows the monitoring of biochemical changes in the respiratory chain and the mtDNA dynamics during stem cell differentiation (Hämäläinen *et al.*, 2013). This model has proved useful for studying the influence of cell-specific factors and tissue development on the progression of mtDNA disease (Hämäläinen *et al.*, 2013).

4.1.1 Mouse models of mDNA disease

Although these in-vitro models are beneficial to the understanding of the pathogenesis of mtDNA disorders, mammalian models that simulate the actual in-vivo environment are undoubtedly the ultimate models of mtDNA disease. Mice are commonly utilised for disease modelling given their high genetic and physiological homology to humans, fast reproductive rate and manageable breeding strategy. Mouse models of mtDNA disease would be hugely advantageous to research into the mechanisms underlying the germline transmission as well as the pathogenesis of specific mtDNA mutations, and in particular, the progression of disease with age. It is difficult to investigate mtDNA disease progression at the tissue level in human patients due to the invasive nature of obtaining samples. Therefore, having a mouse model allows the study of the age-related phenotype development and the tissue heterogeneity through tissue sampling of mice at serial stages of the lifespan. This could potentially inform on prevention, diagnosis and treatment of mtDNA diseases. With continuous effort, researchers have succeeded in generating several mouse models of mtDNA disorders carrying different types of mtDNA mutations, including large-scale deletions, point mutations in protein-encoding and rRNA sequences and mutations in tRNA genes (Watanabe *et al.*, 1978; Levy *et al.*, 1999; Marchington *et al.*, 1999; Inoue *et al.*, 2000; Sligh *et al.*, 2000; Nakada *et al.*, 2004; Kasahara *et al.*, 2006; Fan *et al.*, 2008; Yokota *et al.*, 2010; Freyer *et al.*, 2012; Lin *et al.*, 2012; Shimizu *et al.*, 2014; Shimizu *et al.*, 2015; Kauppila *et al.*, 2016). These mouse models are reviewed in detail in 1.6.3 of Chapter 1. The mouse models of mtDNA disease mentioned above have given useful insights into the germline transmission as well as the pathogenesis of mtDNA mutations. However, none of them has proven suitable for studying

the tissue-specific distribution of mtDNA mutations and the selective loss of mutations in mitotic tissue of patients (Chinnery *et al.*, 1999; Grady *et al.*, 2018). Some of them carry homoplasmic mutations consistently in all organs (Kasahara *et al.*, 2006; Yokota *et al.*, 2010; Freyer *et al.*, 2012; Lin *et al.*, 2012), and the rest of them show uniformly distributed heteroplasmic mutations among different tissues, regardless of the age (Inoue *et al.*, 2000; Fan *et al.*, 2008; Freyer *et al.*, 2012; Shimizu *et al.*, 2015). Therefore, the establishment of a mouse model with heteroplasmic mtDNA mutations that shows age-related and tissue-specific segregation of the mutation is in demand to comprehensively investigate the development of tissue-specific phenotypes during the progression of mtDNA disease.

4.1.2 Mice with m.5024C>T mutation in the tRNA^{Ala} gene

Most of the existing mouse models of mtDNA disease were created by introducing pathogenic mutations that naturally occurred or mutagenized in a cell line into embryonic stem cells (ESC), which were subsequently microinjected into mouse embryos (Levy *et al.*, 1999; Sligh *et al.*, 2000; Kasahara *et al.*, 2006; Fan *et al.*, 2008; Yokota *et al.*, 2010; Lin *et al.*, 2012; Shimizu *et al.*, 2014; Shimizu *et al.*, 2015). Recently, a phenotypic-driven methodology has been developed, which avoids the laborious manipulation of ESCs and ensures the stable maternal transmission of the mutation (Kauppila *et al.*, 2016). This approach involves the use of the *Polg*$^{mut/+}$ (heterozygous mtDNA-mutator) mice with lower burdens of somatic and germline mtDNA mutations compared with the *Polg*$^{mut/mut}$ mice (Ross *et al.*, 2013). The *Polg* heterozygous male mice were mated with wild-type females to produce *Polg* heterozygous females with reintroduced germline wild-type mtDNA, which were then backcrossed with wild-type males for three generations (N3) (Kauppila *et al.*, 2016) (Figure 4.1). Due to the permissive environment for clonal expansion of pathogenic mtDNA mutations in colonic crypts (epithelium), mouse colonic crypts were collected from N3 mice and screened for COX deficiency (Kauppila *et al.*, 2016) (Figure 4.1). Mouse lines with normal COX activity were halted, and those with defective COX in their colonic epithelium were screened genetically via complete mitochondrial genome sequencing (Kauppila *et al.*, 2016) (Figure 4.1). The qualified candidates with pathogenic mtDNA mutations were reproduced for more than six generations to segregate the mouse lineage (Kauppila *et al.*, 2016) (Figure 4.1). Via this approach, a mouse line was generated carrying a pathogenic m.5024C>T mutation in their mitochondrial tRNA^{Ala} gene and a non-pathogenic m.13715C>T mutation in the ND6 polymorphic sequence (Kauppila *et al.*, 2016). The pathogenic m.5024C>T mutation locates in the same base pair as the m.5650G>A mutation

which causes mitochondrial myopathy in patients (Finnilä *et al.*, 2001; McFarland *et al.*, 2008). These mice demonstrated reduced body mass and cardiomyopathy with respiratory chain defects in the heart and the colonic smooth muscle that were highly correlated with the heteroplasmy level (Kauppila *et al.*, 2016). This mutation also impaired the translation of all mitochondrial encoded proteins (Kauppila *et al.*, 2016). The m.5024C>T mutation was stably transmitted through the germline with a maximum of 80% mutated mtDNA molecules transmitted to the offspring (Kauppila *et al.*, 2016). Although the mutation level in various tissues appeared to be similar in 20-week mice, the heteroplasmy level of the mitotic colonic epithelium was around 20% lower than that of the post-mitotic smooth muscle in the old mice (> 40 weeks) (Kauppila *et al.*, 2016). In addition, a loss of the mutation was observed with age in the blood of the mice with a high mutation load (>60%) but not in those with a low to intermediate mutation load (<60%) (Kauppila *et al.*, 2016), suggesting selective pressures against the pathogenic m.5024C>T mutation in the blood as in patients with other mt-tRNA mutations (Rahman *et al.*, 2001; Grady *et al.*, 2018). Therefore, this mouse model can potentially be a good model for the mechanistic study of the tissue-specific segregation of mtDNA mutations. However, it remains unclear whether the selective loss of the mutation also occurs in other mitotic tissue, for example, gastrointestinal epithelium, as reported in patients with mt-tRNA mutations (Chapter 3) and how the mutation is segregated in different types of tissues with age. A thorough characterisation of this mouse lineage to answer these questions would determine whether they are suitable for studying the development of tissue-specific phenotypes and the mechanism of the selective pressure upon the inherited mtDNA mutations in mitotic tissue, which would also be useful for understanding the absence of selection against somatic mtDNA mutations during ageing.

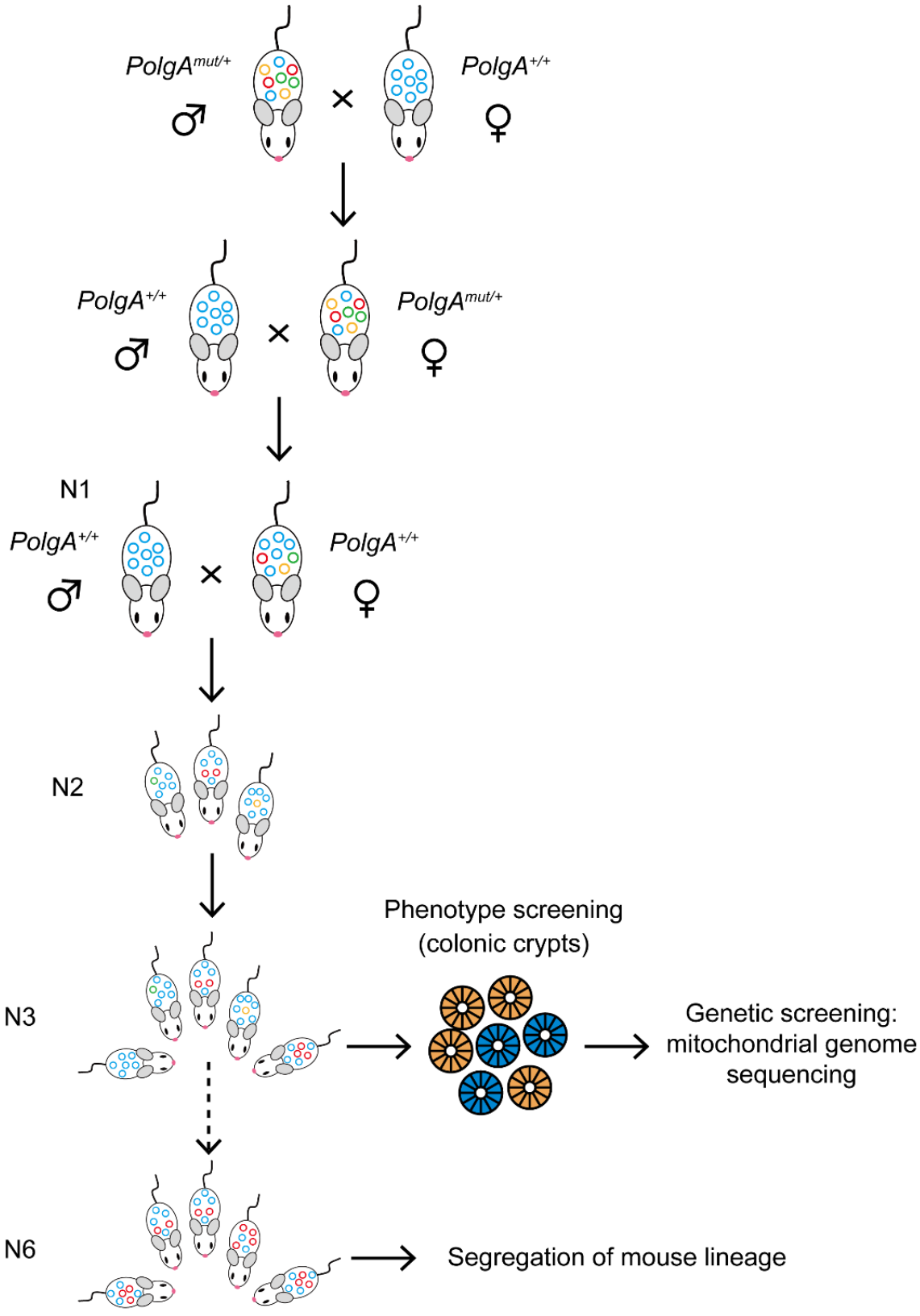
PolgA^mut/+
PolgA^+/+
PolgA^+/+
PolgA^mut/+
N1
PolgA^+/+
PolgA^+/+
N2
Phenotype screening
(colonic crypts)
N3
Genetic screening:
mitochondrial genome
sequencing
N6
Segregation of mouse lineage

Figure 4.1 Establishment of the mouse line with inherited m.5024C>T mutation in the $tRNA^{Ala}$ gene. *Polg* heterozygous females accumulate a multitude of somatic mtDNA mutations in the germline over generations. The previous heavy mutation burden must be removed from the germline of the *Polg* heterozygous females to facilitate the segregation of individual mutations. To this end, *Polg* heterozygous males were mated with *Polg* wild-type females to obtain *Polg* heterozygous females with reintroduced wild-type germline mtDNA. The newly generated females that accumulated a small number of age-related mutated mtDNA molecules in the germline were then backcrossed with *Polg* wild-type males to acquire *Polg* wild-type females with inherited mtDNA mutations. Mice were sacrificed after three generations to examine the COX deficiency in the colonic epithelium using sequential COX/SDH histochemistry (COX-defective crypts in blue and COX-normal crypts in brown). The breeding of the mice with no OXPHOS defects was discontinued. Tail biopsies were collected from the mice with defective COX activity in the colonic crypts, which were subjected to whole mitochondrial genome sequencing to identify the mutations in mtDNA. Qualified candidates with inherited m.5024C>T point mutation in the $tRNA^{Ala}$ gene were bred for at least six generations to segregate the mouse lineage with the stable maternal transmission. Rings in red signifies mtDNA molecules with the m.5024C>T mutation and those in other colour indicate molecules with various pathogenic mutations or polymorphism.

4.2 Aims

The $tRNA^{Ala}$ mutant mice show a loss of the m.5024C>T mutation in blood over time and a lower mutation load in colonic epithelium compared with the smooth muscle when they age. To date it is the only mouse model that has shown potential selective pressure against the inherited mtDNA mutation somatically, similar to patients with mtDNA disease.

This study aimed to genetically characterise the dynamics of the m.5024C>T mutation with age in the $tRNA^{Ala}$ mutant mice and determine whether these mice are a suitable model for studying the mechanism of the selection against the inherited mtDNA mutations. The characterisation included:

1. Determine whether there is any tissue-specific and age-related segregation of the m.5024C>T mutation by measuring the heteroplasmy levels of multiple tissue/organ homogenates from the young and old $tRNA^{Ala}$ mutant mice.
2. Determine whether the m.5024C>T is lost in gastrointestinal epithelium with age and whether GI stem cells are involved in this process through single crypt/gastric unit analysis.

4.3 Methods

4.3.1 Mice with m.5024C>T mutation in the mitochondrial tRNA^{Ala} gene

All the tRNA^{Ala} mutant mice were bred by Dr James Stewart and Nils-Göran Larsson, Max Planck Institute for Biology of Ageing, Cologne, Germany. Figure 4.1 illustrates the breeding strategy, which was expatiated in 2.5. The young (≈ 10 weeks) and old mice (≈ 50 weeks) were culled, and their organs were collected and frozen by Dr Laura Greaves and Dr James Stewart for the subsequent genetic analysis. The number of mice included for the examination of different tissue homogenates is summarised in Table 4.1. An ear notch was collected for each mouse at weaning (three weeks of age), of which the heteroplasmy level was measured by Dr James Stewart using pyrosequencing as a reference of the initial mutation load in each animal.

4.3.2 Quantification of the heteroplasmy level in tissue homogenates

A small tissue block was cut from the frozen organs of the tRNA^{Ala} mutant mice and was homogenised for DNA extraction (detailed in section 2.10.3). In regards to the homogenate of the GI epithelium and muscle, sections were labelled via sequential COX/SDH histochemistry. Then large areas of the epithelial tissue and smooth muscles spanning a couple of fields of view (≈ 5 x 10^5 µm^2 in total) were laser-microdissected and collected (described in 2.10.1), followed by cell lysis to acquire the DNA (detailed in 2.10.2). A pyrosequencing assay designed to quantify the heteroplasmy level of the m.5024C>T mutation was performed (delineated in section 2.11) using the extracted DNA described above. The number of mice included for the statistical analysis of each tissue is summarised in Table 4.1.

Tissue/organ homogenate	N (10-week mutants)	N (50-week mutants)
Ear notch	7	7
Gastric smooth muscle	7	7
SI smooth muscle	7	6
Heart	7	7
SKM	7	7
Brain	7	7
Kidney	7	7
Pancreas	6	7
Lung	6	7
Liver	7	7
Spleen	7	7
Fundic epithelium	7	6
Pyloric epithelium	3	3
SI epithelium	7	5

Table 4.1 The number of the 10-week and 50-week mice included for the analysis of the heteroplasmy level in each tissue/organ. Ear notches of the mice were collected at weaning (three weeks). N, number; SI, small intestine; SKM, skeletal muscle.

4.3.3 Genetic analysis of single intestinal crypts/gastric units

Tissue was sectioned in a cryostat at a thickness of 20 µm (specified in section 2.6). Single intestinal crypt/gastric units and small areas of GI smooth muscles (≈ 50000 μm^2 as a unit) were laser-microdissected and collected in PCR tubes (detailed in 2.10.1), which were lysed (2.10.2) for pyrosequencing to measure their heteroplasmy levels (2.11). The number of crypts/gastric units/muscle areas for the statistical analysis is concluded in Table 4.2.

ID	Small intestine		Stomach		
	N of crypts	N of muscles	N of fundic unit	N of pyloric unit	N of muscles
B933	10	10	n/a	n/a	n/a
B934	10	10	n/a	n/a	n/a
B945	10	9	n/a	n/a	n/a
B948	10	10	n/a	n/a	n/a
B952	10	10	n/a	n/a	n/a
B949	10	10	n/a	n/a	n/a
365	10	10	10	10	10
353	10	9	10	10	10
370	12	10	10	-	10
369	15	12	10	-	10
373	10	10	10	-	10
351	12	15	10	-	10
372	n/a	n/a	n/a	10	10

Table 4.2 The number of intestinal crypts/gastric units of fundus or pylorus/areas of smooth muscles included for statistical analysis. B933, B934, B945, B948, B952, B949 were sacrificed at 10 weeks. 365, 353, 370, 369, 373, 351 and 372 were culled at 50 weeks. "n/a" indicates the tissue that was not used in the study. "-" designates the tissue that was unavailable.

4.4 Results

4.4.1 Variations in the mutation level between tissues/organs in young and old mice

No discernible difference in the m.5024C>T mutation level was observed between seven tissues/organs, including the blood, spleen, skeletal muscle, heart, kidney, liver and the tail, within each 20-week $tRNA^{Ala}$ mutant mice (Kauppila *et al.*, 2016). To determine whether there is any tissue-specific age-related changes in the mutation load, I measured the heteroplasmy levels of the homogenates of various tissues/organs of the 10-week and 50-week $tRNA^{Ala}$ mutant mice, including the mitotic tissue, such as gastrointestinal epithelium and spleen; post-mitotic tissue including GI smooth muscle, heart, skeletal muscle and brain; and the organs that contain a mixture of mitotic and post-mitotic tissue or have limited regeneration under normal physiological conditions, such as kidney, pancreas, lung and liver (Benigni *et al.*, 2010; Kotton and Morrisey, 2014; Forbes and Newsome, 2016; Zhou and Melton, 2018). The heteroplasmy level of the post-mitotic ear notch measured by Dr James Stewart, Max Planck Institute for Biology of Ageing, Cologne, Germany, at 3 weeks of age, was included as a reference of the initial mutation burden of each mouse. Only mice with high mutation burden in the ear notch (60% - 80%) were used in this study since the loss of the mutation was not found in the blood of the mice with intermediate-low tail heteroplasmy (< 60%) (Kauppila *et al.*, 2016).

The mutation was evenly distributed in different tissues/organs of the 10-week mutant mice ($p = 0.1267$, one-way ANOVA) (Figure 4.2A). This is in contrast to the case of the 50-week mutant mice ($p < 0.0001$, one-way ANOVA), where the mutation level in the small intestinal epithelium was significantly lower compared with those in all the other tissues except for the spleen and pyloric epithelium of the stomach ($p < 0.01$, one-way ANOVA) (Figure 4.2B). The heteroplasmy level in the spleen was found to be lower than that in the ear notch and the gastric smooth muscle ($p < 0.05$, one-way ANOVA) (Figure 4.2B). To determine the change in the m.5024C>T heteroplasmy in each type of the tissue with age, I compared the mutation level of each tissue from the 10-week and 50-week $tRNA^{Ala}$ mutant mice. This revealed a decline in the mutation load in the small intestinal epithelium in the 50-week mutants compared with the 10-week mutants ($p < 0.01$, unpaired t-test) (Figure 4.3). However, no significant difference in the heteroplasmy level was observed in the other tissues between the 10-week and 50-week mice (Figure 4.3).

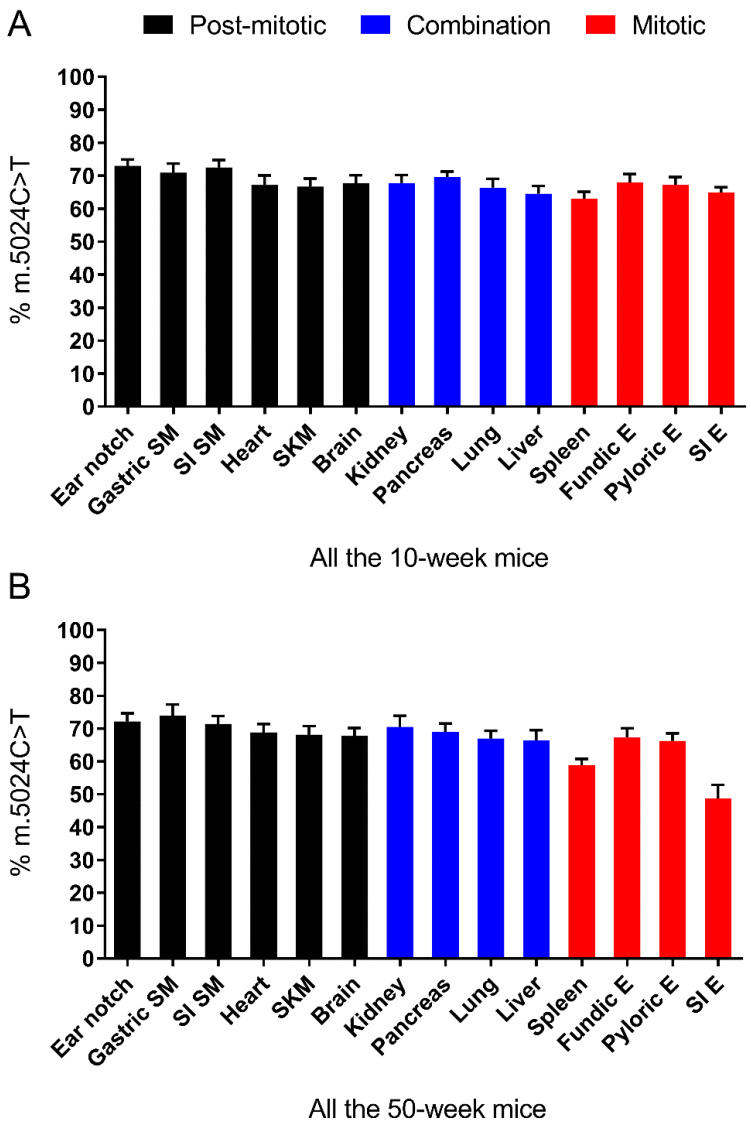

Figure 4.2 Mutation levels in different tissues/organs of (A) 10-week and (B) 50-week $tRNA^{Ala}$ mutant mice. Tissues/organs were categorised into "mitotic", "combination" and "post-mitotic" based on the general thoughts of the cell component and the renewal ability of the tissue/organ. Frozen tissue was homogenised and subjected to DNA extraction, which was used for pyrosequencing assay to measure the heteroplasmy level. The gastric epithelium was classified into fundic and pyloric epithelium because of the different cellular components and functions. All the mice in this study carried high levels of m.5024C>T mutation in the three-week ear notch (% m.5024C>T ranging from 60% to 80%). The number of mice included for analysing the data of each tissue is concluded in Table 4.1. SI, small intestine; SM, smooth muscle; E, epithelium; SKM, skeletal muscle. For the small intestinal epithelium of the 50-week mutants, $p < 0.0001$ compared with the ear notch (3 weeks) and gastric smooth muscle, $p < 0.001$ compared with the intestinal smooth muscle, kidney, pancreas and heart, $p < 0.01$ compared with the skeletal muscle, brain, lung, liver and gastric fundic epithelium; for the spleen of the 50-week mutants, $p < 0.05$ compared with the ear notch and gastric smooth muscle, determined by Tukey's multiple comparison test for one-way ANOVA.

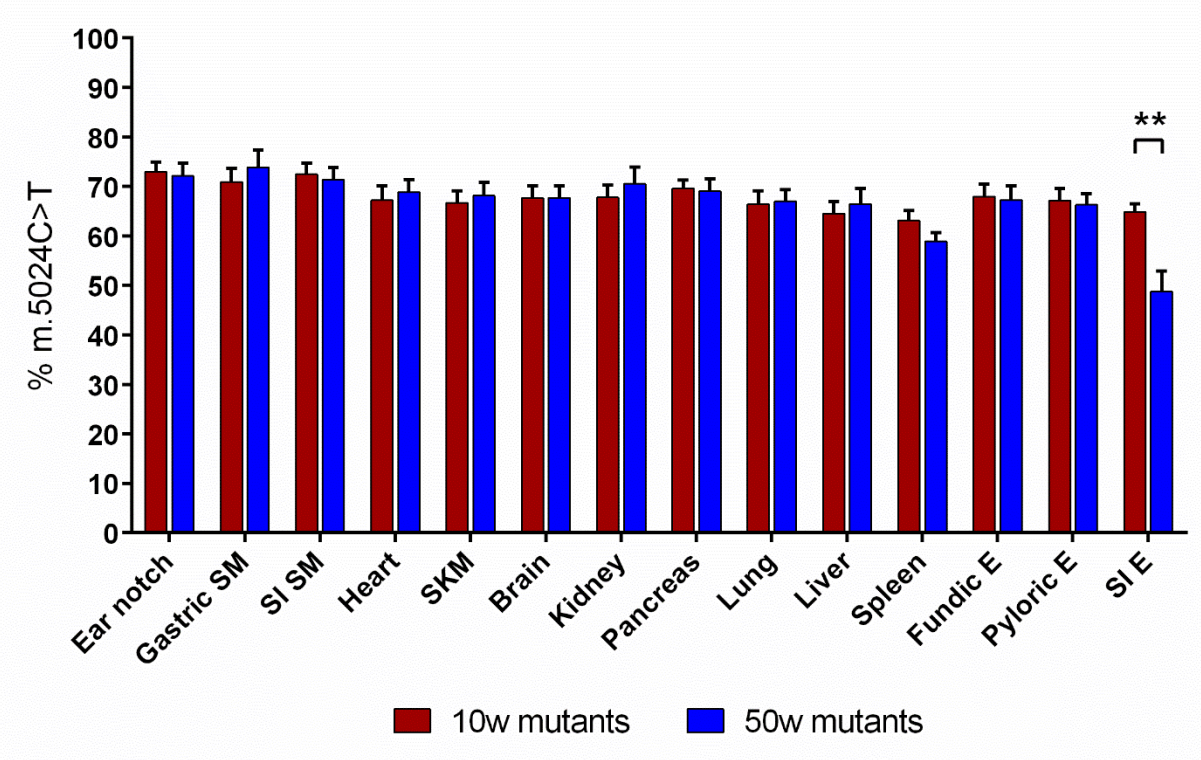

Figure 4.3 Comparison of the m.5024C>T mutation level in different tissues/organs between 10-week and 50-week $tRNA^{Ala}$ mutant mice. The heteroplasmy level of each tissue homogenate was measured by pyrosequencing. The number of mice for the analysis is tabulated in Table 4.1. SI, small intestine; SM, smooth muscle; E, epithelium; SKM, skeletal muscle. **, $P < 0.01$.

4.4.2 Assay verification and data normalisation

The data in this study show that the mutation level in the majority of the tissues was lower than that of the ear notch from the $tRNA^{Ala}$ mutant mice (Figure 4.2); however, previous studies have shown that the heteroplasmy of various tissues was often higher than that of the tail obtained at three weeks (Kauppila *et al.*, 2016). As the mutation level of the ear notch was measured by the pyrosequencing assay in the Max Planck Institute for Biology of Ageing, Cologne, Germany, whereas the data in this study were acquired using the assay of the Newcastle Wellcome Centre, this difference could be due to the variation between different Pyrosequencers and assays. To verify the pyrosequencing assay used in this study, I measured the heteroplasmy level in the ear notch using the same DNA that was used in the previous study and compared it to that measured by the Cologne assay. The mutation level in the ear notch of each mouse quantified by the Newcastle assay was consistently slightly lower than that quantified by the Cologne assay (Figure 4.4), which explains the difference in the findings (mean of difference with standard deviation: 3.71 ± 1.13; $p < 0001$, paired t-test).

The other concern is that the difference in the initial mutation burden of the mice might affect the comparison of the heteroplasmy level in different tissues between the 10-week and 50-week mutant mice. In the blood of the patients with different mutation burdens, a substantial variation was observed in the age-related change in the m.3243A>G heteroplasmy (Grady *et al.*, 2018). In addition, the loss of the m.5024C>T mutation in the blood of the $tRNA^{Ala}$ mutant mice was notably different between the mice with high and low tail heteroplasmy level (Kauppila *et al.*, 2016). Although the mice at different ages that were examined in this study all carried high levels of the mutation in their ear notch (putative original mutation level), the remaining variations in the heteroplasmy of the ear notch may still affect the analysis. Therefore, I normalised the data by subtracting the heteroplasmy level of the three-week ear notch from the mutation level of each tissue collected when they were culled, which was then compared between each mouse (Figure 4.5). In this way, the mutation level of the tissue from each mouse was normalised relative to its own initial heteroplasmy level.

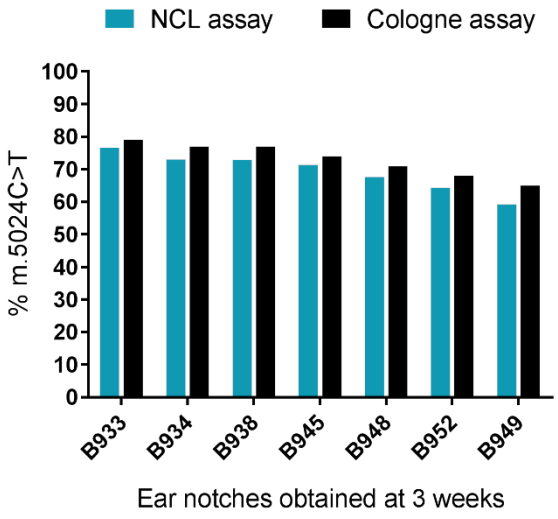

Figure 4.4 Comparison of the pyrosequencing assays used in the Max Planck Institute for Biology of Ageing, Cologne, Germany and the assay used in Wellcome Centre for Mitochondrial Research, Newcastle, UK. The same DNA was used for both assays, which was extracted from the three-week ear notch of seven 10-week $tRNA^{Ala}$ mutant mice by Dr James Stewart.

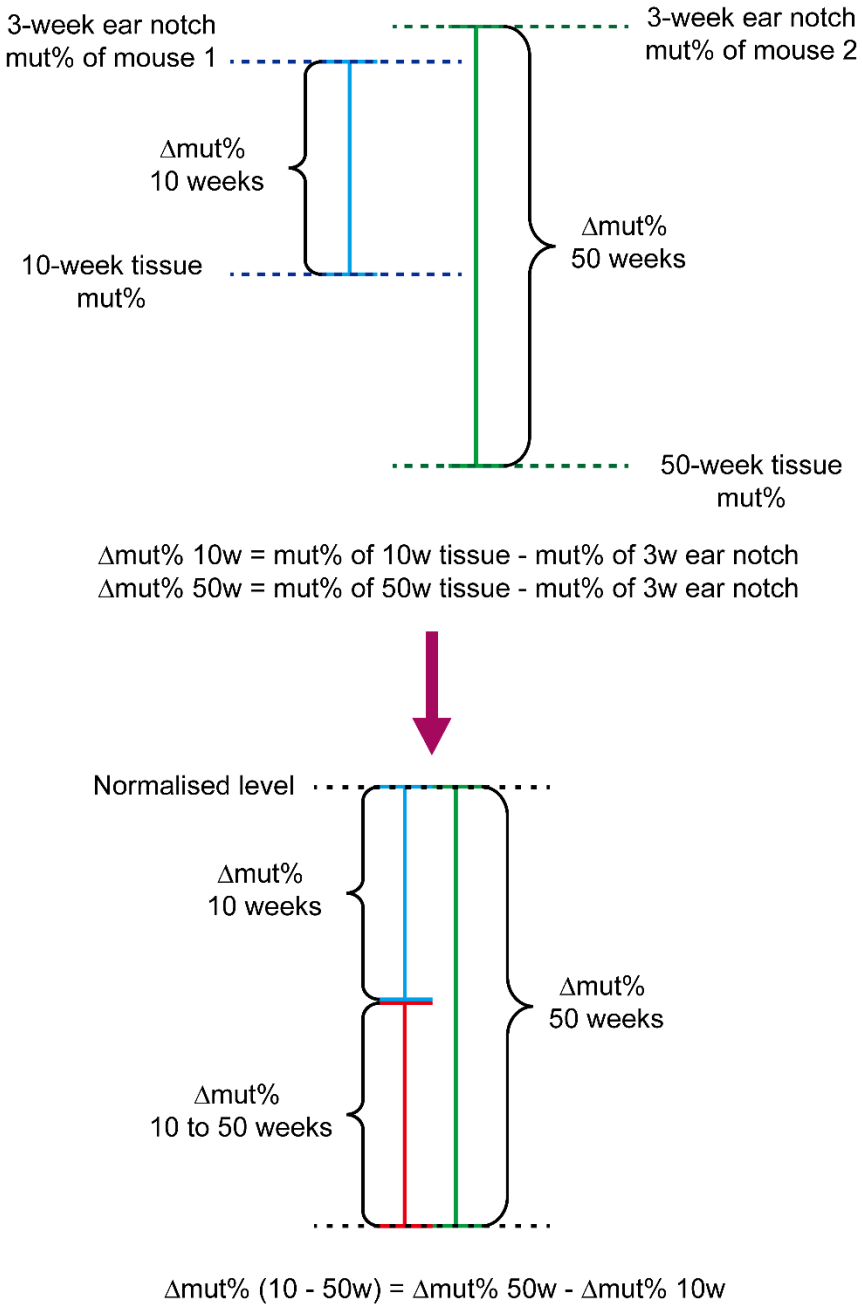

Figure 4.5 Diagram of the normalisation methodology of the initial mutation burden. For each $tRNA^{Ala}$ mutant mouse, the heteroplasmy level in each tissue relative to the initial mutation burden (Δmut% 10 weeks or 50 weeks) was normalised by subtracting the mutation load in the three-week ear notch from that in each tissue. The change in the mutation level from 10 weeks to 50 weeks in each tissue was calculated by subtracting the "Δmut% 10 weeks" from the "Δmut% 50 weeks".

4.4.3 Changes in the mutation loads in different tissues over time

The mutation level of each tissue collected from different tRNA^{Ala} mutant mice at 10 weeks and 50 weeks relative to their ear notch heteroplasmy was determined and compared (Figure 4.6), from which the change in the mutation load in each tissue with age was calculated (Figure 4.5 and Figure 4.7). This revealed a significant age-related decline in the heteroplasmy level in some canonical mitotic tissues, such small intestinal epithelium (-13.5%, $p < 0.001$), the pyloric epithelium (-7.2%, $p < 0.05$) and the spleen (-3.37%, $p < 0.05$) (unpaired t-test) (Figure 4.7). In contrast, the mutation load slightly drifted up in the kidney (3.6%) and the gastric smooth muscle (3.83%) ($p < 0.05$, unpaired t-test) (Figure 4.7). The heteroplasmy levels in the other tissues/organs, including the post-mitotic heart, skeletal muscle, intestinal smooth muscle and brain remained stable from 10 weeks to 50 weeks (Figure 4.7). Surprisingly, the mutation level in the putatively mitotic epithelium of the gastric fundus did not decrease with age (Figure 4.7).

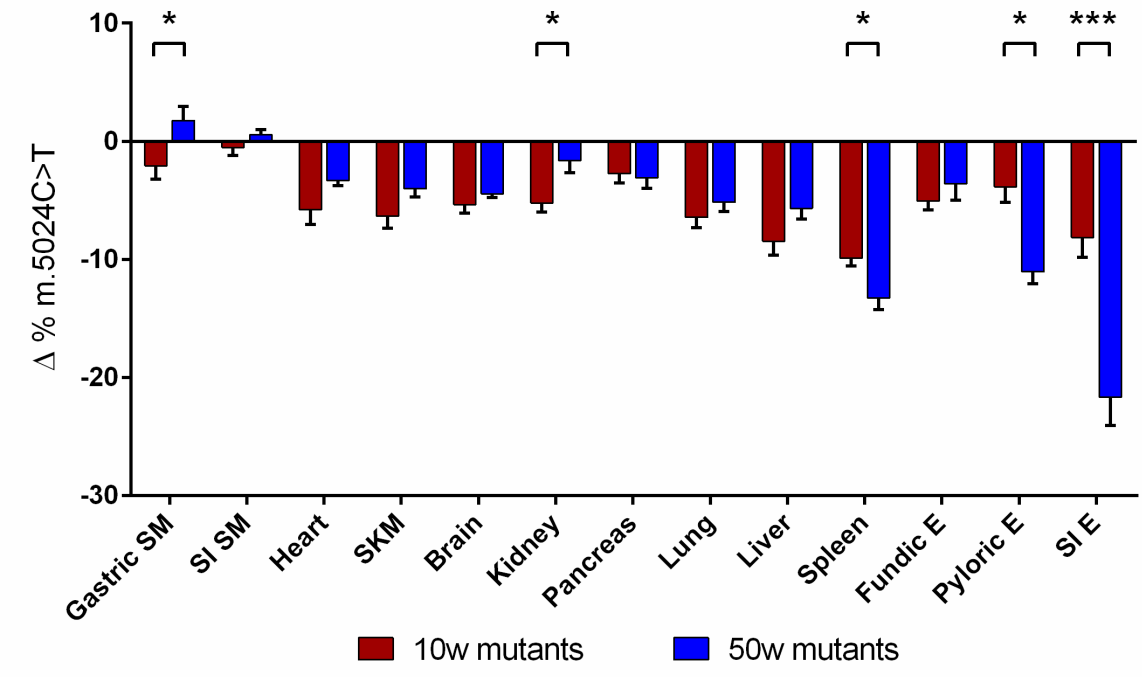

Figure 4.6 Comparison of the mutation levels in various tissues/organs of 10-week and 50-week tRNA^{Ala} mutant mice relative to the heteroplasmy of their three-week ear notches. The number of mice for the analysis is concluded in Table 4.1. SI, small intestine; SM, smooth muscle; E, epithelium; SKM, skeletal muscle. *, $P < 0.05$; **, $P < 0.01$; ***, $P < 0.001$.

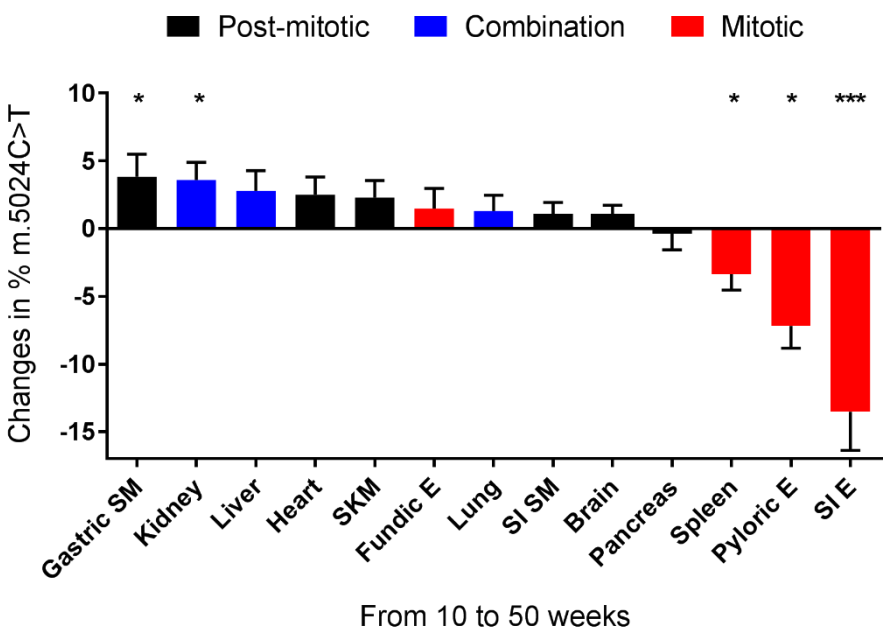

Figure 4.7 Changes in the mutation level in different tissues/organs of the $tRNA^{Ala}$ mutant mice from 10 weeks to 50 weeks. Tissues/organs were classified into "mitotic", "combination" and "post-mitotic" based on the main cell type in the tissue/organ and the general beliefs in their regeneration capability. The number of mice for the analysis is summarised in Table 4.1. SI, small intestine; SM, smooth muscle; E, epithelium; SKM, skeletal muscle. *, $P < 0.05$; **, $P < 0.01$; ***, $P < 0.001$.

4.4.4 Distribution of the m.5024C>T mutation in intestinal crypts and smooth muscles

To determine the distribution of the m.5024C>T mutation in the intestinal crypts and the smooth muscle of the $tRNA^{Ala}$ mutant mice and whether it mimics that in the patients with mt-tRNA mutations (Chapter 3), I laser-microdissected individual crypts and patches of the smooth muscle fibres from the $tRNA^{Ala}$ mutant mice and measured their heteroplasmy levels using pyrosequencing. Mice aged 10 weeks and 50 weeks were investigated, and each age group included two mice with intermediate-high (60% - 70%) and four mice with high (79% - 80%) mutation loads in the ear. Statistical analysis confirmed the match of the heteroplasmy level in the intestinal smooth muscle (no difference in the mean and variation between two populations, unpaired t-test) (Figure 4.8).

The study of the individual mice showed that in the 10-week $tRNA^{Ala}$ mutant mice, the average mutation level of the intestinal crypts was similar to or slightly lower than that of the smooth muscle (mean difference ≈ 10%) (Figure 4.9), whereas, in 50-week mutant mice, the mean heteroplasmy level in the crypts was significantly lower compared with the smooth muscle (mean difference ranging from 16.84% to 25.70%) (Figure 4.10). This is consistent

with the results of the tissue homogenate (Figure 4.2). In addition, the single crypt analysis showed that the variation in the mutation level of each crypt in individual 50-week mouse (SD ranging from 5.4 to 8.2) (Figure 4.10) was markedly larger compared with that in individual 10-week mutant mice (SD ranging from 2.4 to 3.8) (Figure 4.9). The statistical analysis on the pooled data of all the 10-week and 50-week mice confirmed the findings of the individual mouse investigation discussed above showing (1) a notable decrease in the heteroplasmy level in the intestinal epithelium from 10 weeks to 50 weeks (mean difference = 14.67%, $p < 0.0001$, one-way ANOVA with Tukey's multiple comparison test); (2) a tight distribution of the mutation in individual crypts of the 10-week mice and (3) a scattered mutation distribution in the 50-week crypts (difference in SD = 10.78, $p< 0.0001$, unpaired t-test with F-test) (Figure 4.8). The mutation load of some crypts dropped to 3% in 50-week mice, but no crypts harbouring the mutation higher than 83% heteroplasmy was found in mice at either age (Figure 4.8). The same maximum threshold also applied to the smooth muscles (Figure 4.8).

Of note, in two 10-week mice with intermediate-high mutation level in the ear, the heteroplasmy levels in single crypts followed a normal distribution with the means similar to the mutation load in their smooth muscle and the three-week ear notch, indicating that the heteroplasmy level drifted evenly in both directions (Figure 4.9, E and F). In contrast, in 10-week mice with high mutation load in the ear, the populations of the crypt heteroplasmy deviated from the muscle heteroplasmy (Figure 4.9, A-D), which became obvious in all 50-week mice (Figure 4.10). This difference in the distribution of the mutation between the 10-week mice with different initial mutation burdens prompted me to investigate the association between the rate of the losing the m.5024C>T mutation in the intestinal epithelium and the original mutation burden in the $tRNA^{Ala}$ mice. The former factor was reflected by the difference in the mutation level between the intestinal epithelium and the three-week ear notch of each mouse. However, no correlation was found between the loss rate of the mutation and the initial mutation burden in either 10-week ($p = 0.36$) or 50-week ($p = 0.75$) $tRNA^{Ala}$ mice (Spearman's rank correlation analysis) (Figure 4.11).

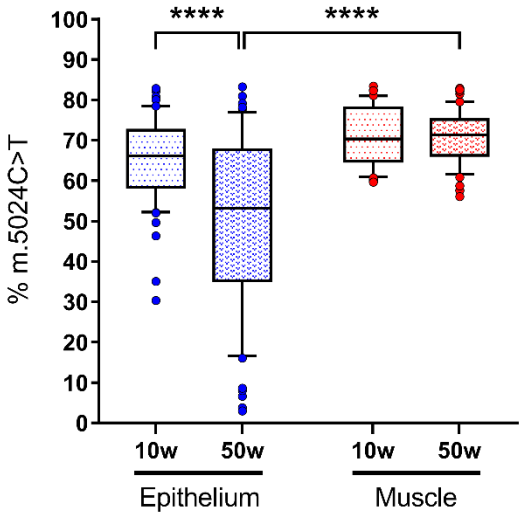

Figure 4.8 Comparison of the distribution of the m.5024C>T mutation in individual crypts and smooth muscle areas of the small intestines from the 10-week and 50-week $tRNA^{Ala}$ mutant mice. Single crypts and small areas of smooth muscles of the small intestines were laser-cut, collected and lysed to extract DNA. Pyrosequencing was performed using the DNA to measure the mutation level in the tissue. n (10-week crypts) = 60, n (50-week crypts) = 69, n (10-week muscle areas) = 59, n (50-week muscle areas) = 66; ****, $P < 0.0001$.

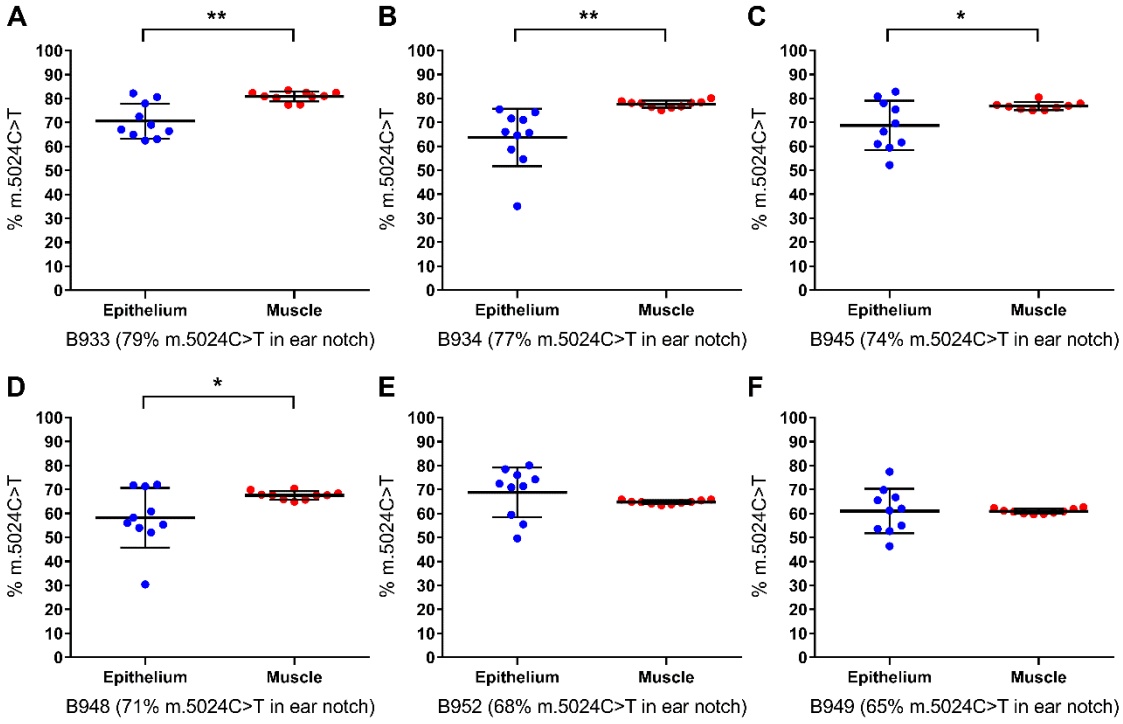

Figure 4.9 Quantification of the m.5024C>T heteroplasmy level in individual small intestinal crypt/areas of smooth muscles of each 10-week $tRNA^{Ala}$ mutant mice. The number of the crypts/muscle areas for the analysis is summarised in Table 4.2. *, $P < 0.05$; **, $P < 0.01$.

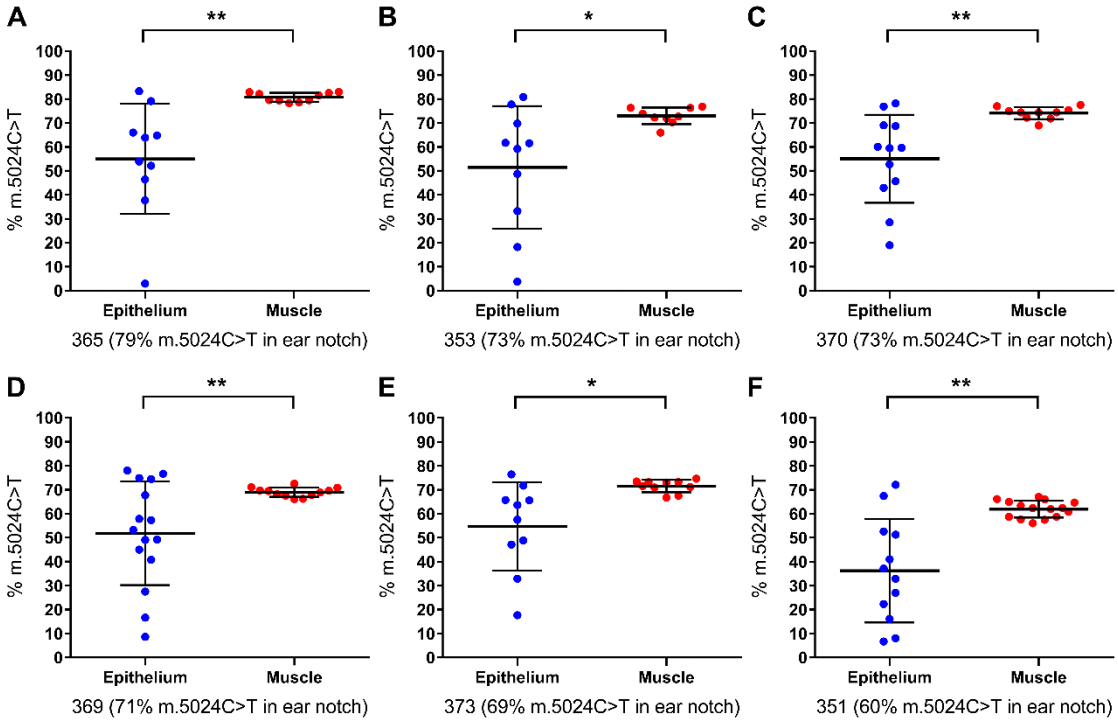

Figure 4.10 Quantification of the m.5024C>T heteroplasmy level in individual small intestinal crypt/areas of smooth muscles of each 50-week $tRNA^{Ala}$ mutant mice. The summary on the number of the crypts/muscle areas for the analysis is in Table 4.2. *, $P < 0.05$; **, $P < 0.01$.

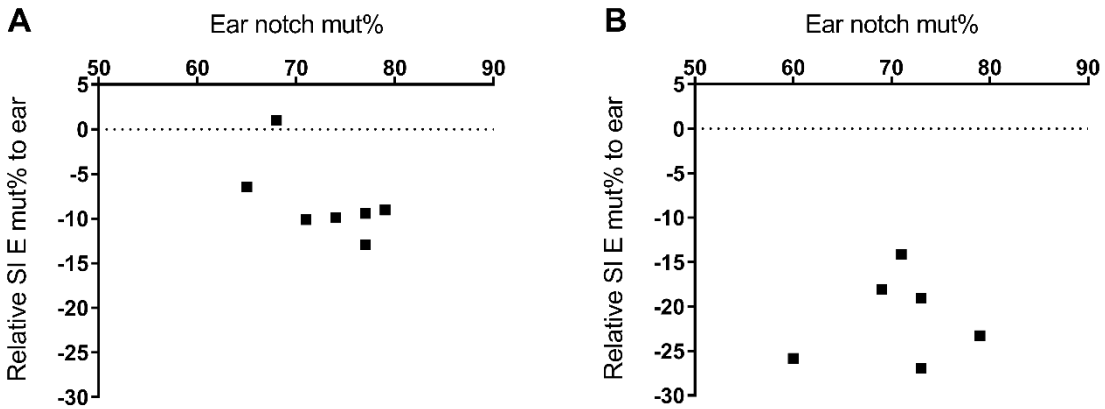

Figure 4.11 Associations between the initial mutation burden and the rate of losing the m.5024C>T mutation in the (A) 10-week and (B) 50-week $tRNA^{Ala}$ mutant mice. The loss rate of the mutation in each mouse is specified as the difference in the heteroplasmy level between the epithelium of the small intestine and the ear notch obtained at 3 weeks. Each square represents an individual mouse. n (10-week mice) = 7, n (50-week mice) = 6.

4.4.5 Distribution of m.5024C>T mutation in gastric units and smooth muscles

As the heteroplasmy level changed differently in the homogenate of the fundic and the pyloric epithelium of the stomach from the $tRNA^{Ala}$ mutant mice (Figure 4.7), I investigated the distribution of the mutation in the gastric epithelium of the 50-week mutant mice by quantifying the heteroplasmy in laser-microdissected single units of the gastric fundus and pylorus using pyrosequencing. Analysis of individual mice showed no difference in the mean heteroplasmy level between the fundic epithelium and gastric smooth muscle (Figure 4.12), confirming the previous study on tissue homogenate (Figure 4.2B). In addition, it revealed that the m.5024C>T mutation was tightly distributed in the fundic units, regardless of the initial mutation burden of the mice (Figure 4.12), with notably less variation compared with that in the pyloric units (Figure 4.13, Figure 4.14A and B) and intestinal crypts (Figure 4.10). The highest heteroplasmy level in the fundic units was 86% (Figure 4.14C), which is higher than that in the pyloric units (82%) and intestinal crypts (83%) (Figure 4.14C and Figure 4.8), indicating different tolerance to the mutation even in the same type (epithelial) of the tissue. Analysis of the collective data of all 50-week $tRNA^{Ala}$ mutant mice confirmed (1) a trend of a lower mutation level in the pyloric epithelium compared with the fundic epithelium and (2) a significant larger variation in the distribution of the mutation in individual pyloric units compared with that in individual gastric units of the fundus (difference in SD = 7.70, $p< 0.0001$, unpaired t-test with F-test) (Figure 4.14). It is worth mentioning that there were only three mice containing pyloric epithelium in their tissue sections and more mice should be included in the further study of this topic.

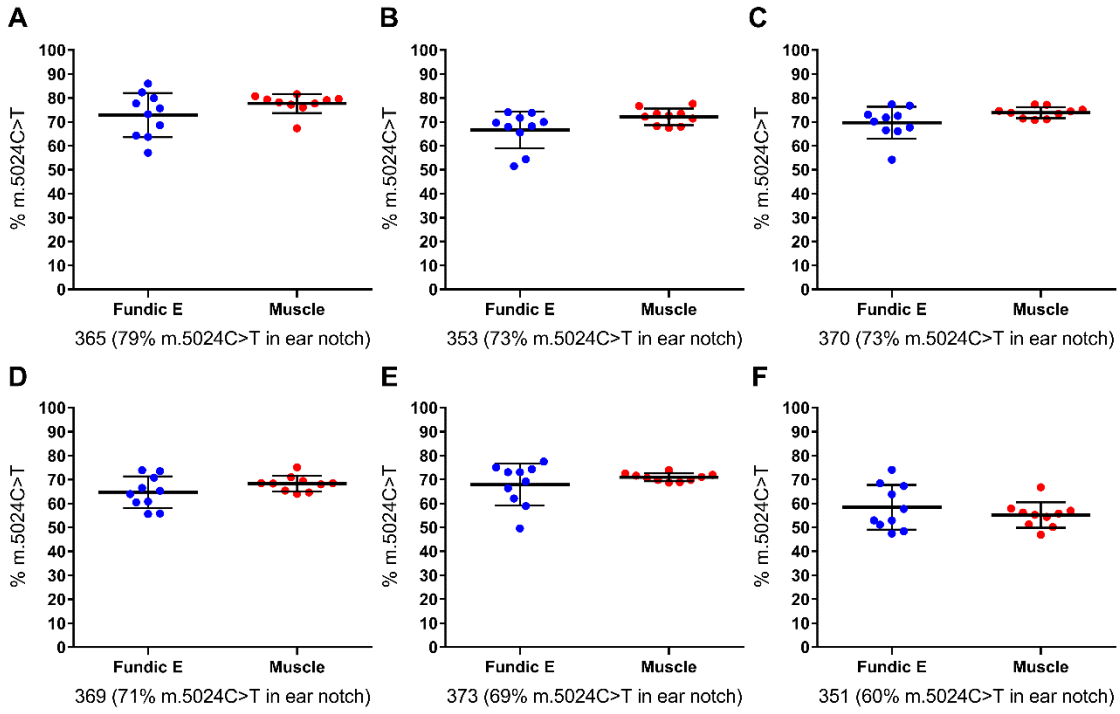

Figure 4.12 Heteroplasmy levels in individual fundic units compared with the smooth muscle fibres of the stomach from the 50-week $tRNA^{Ala}$ mutant mice. The number of the analysed gastric units of the fundus and the smooth muscle areas is summarised in Table 4.2. E, epithelium.

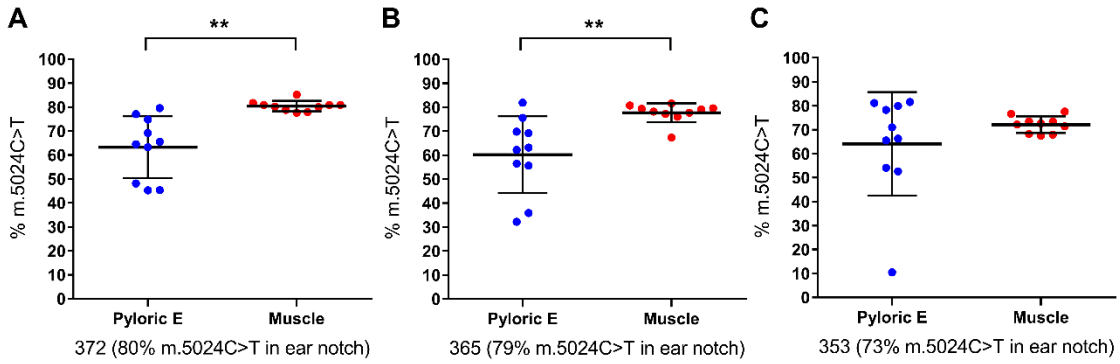

Figure 4.13 The m.5024C>T mutation level in individual pyloric units of the stomach and gastric smooth muscle of $tRNA^{Ala}$ mutant mice. The quantity of the analysed gastric units of the pylorus and the smooth muscle areas is concluded in Table 4.2. **, $P < 0.01$.

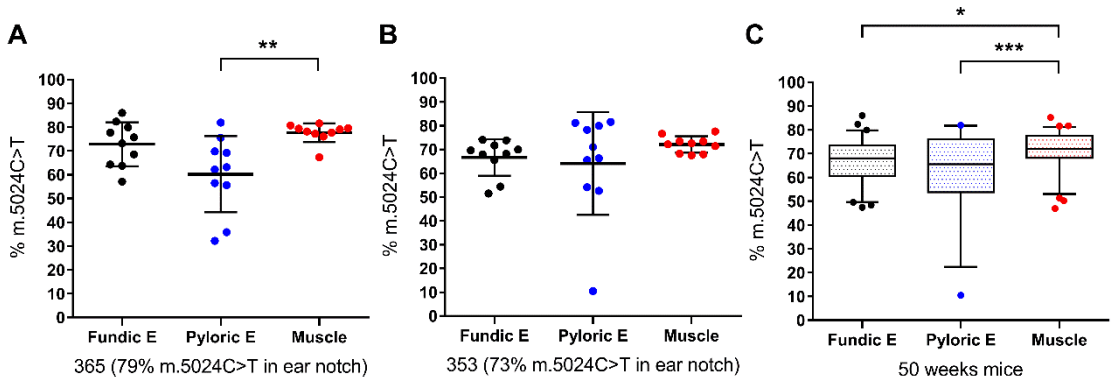

Figure 4.14 Comparison of the heteroplasmy level between individual fundic and pyloric units, and gastric smooth muscles of the 50-week tRNA^{Ala} mutant mice. (A) (B) show the data of two mice with both fundic and pyloric epithelium in the tissue samples. Figure (C) shows the pooled data of all 50-week mice whose stomachs were examined. n (fundic units) = 60, n (pyloric units) = 30, n (smooth muscle areas) = 70; *, $P < 0.05$; **, $P < 0.01$; ***, $P < 0.001$.

4.5 Discussion

The establishment of the mt-tRNA^{Ala} mutant mouse model with the heteroplasmic pathogenic m.5024C>T mutation is crucial to the investigation of the mechanism and the pathogenesis of mtDNA disorders. In addition, a selective loss of the inherited m.5024C>T had been previously reported in the mitotic blood of the mice with high mutation load in the tail, suggesting this mouse model could be potentially valuable for studying the dynamics of mtDNA heteroplasmy in mtDNA disease progression, including age-related mitotic segregation and tissue-specific distribution of mtDNA mutations. Furthermore, these mice could be useful for studying the mechanism of selection against inherited mtDNA mutations, which might reveal the cause of the difference in the selective pressure on inherited and somatic mtDNA mutations, and benefit our understanding of stem cell physiology and ageing. All of these potential applications need to be substantiated through a thorough genetic characterisation of the tRNA^{Ala} mutant mice in terms of the dynamics of mtDNA heteroplasmy with age. In this study, I have accomplished this by determining the heteroplasmy level in different tissues/organs of the tRNA^{Ala} mutant mice at two stages of lifespan and investigating the distribution of the m.5024C>T mutation in monoclonal intestinal crypts and gastric units that are regularly renewed by gastrointestinal stem cells.

The m.5024C>T is homogeneously distributed in various tissues/organs of the young (10-week) tRNA^{Ala} mutants, which becomes more heterogeneous with age, showing a detectable

lower mutation level in some mitotic tissues/organs, such as the spleen and the small intestinal epithelium, compared with the post-mitotic tissue in the 50-week mice. This is consistent with the reports of the non-random distribution of the m.3243A>G and the m.8344A>G mutation in different tissues of the adult patients (Larsson *et al.*, 1992; Chinnery *et al.*, 1999). The difference in the distribution of the mutation in tissue between the young and old mice is able to account for the effect of age on the development of the phenotypes in patients with mtDNA disease, where more symptoms involving mitotic tissues are observed in paediatric patients compared with adult patients who have symptoms mainly in post-mitotic organs (Taylor and Turnbull, 2005). Moreover, in both young and old $tRNA^{Ala}$ mutant mice, the high mutation loads in the kidney, pancreas, lung and liver that are similar to those in post-mitotic muscle and brain correlate with the renal, endocrinal, respiratory and hepatic symptoms in patients with mtDNA disease (Taylor and Turnbull, 2005).

The comparison between the young and the old $tRNA^{Ala}$ mutant mice regarding the heteroplasmy level in each tissue that is normalised by the initial mutation burden reveals a steady mutation level in the majority of the post-mitotic tissues with age, including the brain, heart, skeletal muscle and intestinal smooth muscle, in contrast to a significantly decreased mutation loads in the mitotic spleen, the epithelium of the gastric pylorus and the small intestine, suggesting the selection against the m.5024C>T mutation in the mitotic tissue of the $tRNA^{Ala}$ mutant mice. This is in accordance with the selective loss of the m.3243A>G mt-tRNA point mutation in mitotic blood and epithelial tissues in patients (discussed in Chapter 3) (Olsson *et al.*, 2001; Frederiksen *et al.*, 2006; de Laat *et al.*, 2012; Grady *et al.*, 2018). The strong selection against the m.5024C>T mutation only shows in the mitotic tissue that is rapidly renewed by somatic stem cells, whereas in organs that contain a mix of mitotic and post-mitotic tissues or/and are in a mitotically quiescent status physiologically, such as the kidney (Benigni *et al.*, 2010), pancreas (Zhou and Melton, 2018), lung (Kotton and Morrisey, 2014) and liver (Forbes and Newsome, 2016), the age-related selective loss is undetectable. This possibly accounts for the emerging or sustained symptoms relevant to these organs in patients with age (Taylor and Turnbull, 2005). The heteroplasmy level of the kidney and the gastric smooth muscle in the $tRNA^{Ala}$ mutant mice slightly drifted up from 10 weeks to 50 weeks, possibly as a result of the clonal expansion (Elson *et al.*, 2001), but this process is not obvious in these mice, as the rest of the post-mitotic tissues/organs consistently shows no age-dependent change in their mutation loads.

The genetic analysis of the single intestinal crypt demonstrates a tight distribution of the m.5024C>T mutation in individual crypts of the young mice. In contrast, the old $tRNA^{Ala}$

mutant mice show a considerable variation in the heteroplasmy level between individual crypts with some crypts harbouring extremely low levels of the mutation (≈ 3%), suggesting the involvement of stem cells. The skewed population of the crypt heteroplasmy with the mean deviating from the heteroplasmy of the three-week ear notch in the old mutant mice and an upper threshold of the mutation (≈ 83%) found in the intestinal crypts suggest the selection against the m.5024C>T mutation in the intestinal epithelium prevents the mutation level from drifting above the limit. These findings are analogous to the case in the patients with inherited m.3243A>G mutation (Chapter 3).

The genetic upper limit of the mutation load in crypts (≈ 83%) is different from the histochemical threshold of COX deficiency in the intestinal epithelium (≈ 70%) (Baines, 2014), suggesting that the biochemical defect does not solely regulate the elimination of the mutation. The similar distribution of the m.5024C>T in individual intestinal crypts and pyloric units implies that different GI epithelial tissues might share the same mechanism of the selective loss. In addition, the investigation of the individual mouse of two age groups with different initial mutation burdens delineates a gradual process of the segregation of the m.5024C>T mutation in individual crypts over time. The tight normal distribution of the heteroplasmy in the crypts with the mean value the same as that of the smooth muscle and the three-week ear notch in two young $tRNA^{Ala}$ mutant mice with intermediate-high mutation burdens suggests that all the intestinal crypts initially harbour the same quantity of mutations which segregate symmetrically to both directions with age until they meet the limit where the selection arrests this process.

The only mitotic tissue that does not have a detectable selective loss of the m.5024C>T mutation in the $tRNA^{Ala}$ mutant mice is the epithelium of the gastric fundus. This is unexpected, as the fundic epithelium is regularly renewed by gastric stem cells that are primarily located in the isthmian area of a gastric unit (Hoffmann, 2008). In contrast, the loss of the m.5024C>T mutation was observed in the antral epithelium of the gastric pylorus, revealing a difference in the selective pressure within the different epithelial tissues. The fundic and pyloric units have different cell components and are morphologically and functionally distinct (reviewed in 1.7.2 of Chapter 1). Many reasons could potentially account for the difference in the selection between them. One likely explanation is that the turnover rate of the fundic epithelium is much longer than that of the antral epithelium (Hansen *et al.*, 1976; Patel *et al.*, 1993; Hoffmann, 2008). In particular, the renewal timescale of the zymogenic cells that are the main cell type in the fundic gland is three times longer than that of the antral gland cells (Karam, 1999). Moreover, lineage tracing in hemizygous lacZ

transgenic mice with induced mutations that can hamper the expression of lacZ enzyme shows that despite homogeneous stem cell populations that lack lacZ activity, the mature parietal and zymogenic cells with normal lacZ function can last for a long time, resulting in the mosaic lacZ activity in some fundic units (Bjerknes and Cheng, 2002). Hence, though the gastric stem cells undergo a monoclonal conversion that might have lost the mutation (Thompson *et al.*, 1990; Nomura *et al.*, 1998; Bjerknes and Cheng, 2002), the heteroplasmy level of single fundic units can still be enormously affected by the slowly renewed mature glandular cells with high levels of mutated mtDNA. The difference in the heteroplasmy in the two epithelial tissues of the stomach with comparatively similar unit structure but different turnover rates suggests the involvement of transit-amplifying cells and differentiated epithelial cells in the selective loss of the m.5024C>T mutation in the mitotic tissue of the $tRNA^{Ala}$ mutant mice.

This study shows that the loss of the m.5024C>T mutation is more evident in young mice with high initial mutation levels compared with those with intermediate-high mutation loads. This is compatible with the data of patients' blood showing that most of the individuals with a heavy mutation burden in the first examination lost the m.3243A>G mutation in blood over time, whereas the heteroplasmy level does not tend to decrease in blood in those with the mutation load less than 20% (Grady *et al.*, 2018). However, despite a trend of correlation between the initial mutation burden and the rate of losing the m.5024C>T mutation in the small intestinal epithelium of the 10-week mice, the 50-week mice do not show any such evidence. This may be due to the small numbers of mice in the study. Therefore, further investigations are required using more mice with low, intermediate and high mutation load in the three-week ear.

4.5.1 Future work

Here I have genetically characterised the $tRNA^{Ala}$ mutant mouse model and demonstrated the dynamics of the m.5024C>T mutation in different tissues with age; however, the biochemical and histochemical consequence of the age-related change in the heteroplasmy level is unknown. It is interesting to study whether the phenotype of the mitotic tissue is reversible concomitant with the age-dependent decrease in the mutation load, which is observed in the blood of the patients with large-scale deletions (Larsson *et al.*, 1990; McShane *et al.*, 1991; Nørby *et al.*, 1994). Hence, it is essential to determine the biochemical and histochemical phenotype in the intestinal epithelium that loses the mutation most rapidly among all mitotic tissues at multiple stages of the lifespan to validate whether this mouse model is

phenotypically ideal for studying the selection against inherited mtDNA mutations. This will be discussed in Chapter 5.

Other questions that would be crucial to understanding the dynamics of mtDNA mutations and the tissue heterogeneity in mtDNA disease are what the loss rates of the mutation in different mitotic tissues are and whether they are consistent or variable with age. In this study, I have only characterised the mice at 10 weeks and 50 weeks. Answering these questions needs a further genetic characterisation of different mitotic tissues at multiple ages, for example, 30 weeks and 70 weeks. The subsequent establishment of the regression models using these data would reveal the relationship between the rate of losing the mutation and age.

Many factors might be associated with the loss rate of the m.5024C>T mutation. The data in this study illustrate a potential relationship between the initial mutation burden and the rate of the selective loss in the intestinal epithelium of the 10-week $tRNA^{Ala}$ mutant mice, which is overturned by the result showing they are not correlated in the 50-week mice. Nevertheless, a conclusion cannot be drawn considering the small number of mice included in the study that all carry similarly high levels of the mutation. Future work to elucidate this question should involve the investigations of an increased number of the $tRNA^{Ala}$ mutant mice with different initial levels of mutated mtDNA, for instance, "< 20%", "20% - 40%", "40%-60%" and "> 60%".

The different dynamics of the m.5024C>T mutation in the fundic and the antral epithelium with different turnover rates of the glandular cells in the mutants' stomach suggests the contributions of transit-amplifying cells and differentiated epithelial cells to the loss of the inherited mutation in mitotic tissue in addition to that of the stem cells. It is undoubtedly crucial to investigate the mechanism underpinning this phenomenon. Cell proliferation and apoptosis manipulate the turnover the stem cell progenies, and mitochondria play an important role in their regulation (Lu *et al.*, 2009; Mishra and Chan, 2014). In addition, studies have shown that apoptosis reacts differently to respiratory chain deficiency in normal ageing individuals and patients with mtDNA disease (Auré *et al.*, 2006; Nooteboom *et al.*, 2010), suggesting that this difference might contribute to the difference in the selective pressure on the somatic and the inherited mtDNA mutations. Thus, it would be valuable to investigate the balance of the cell proliferation and apoptosis in the fast-renewing intestinal crypt using corresponding markers, such as Ki-67 and cleaved caspase-3, for immunofluorescence (Chapter 6). Meanwhile, it is essential to confirm the contribution of the stem cells in the process of losing the mutation by pyrosequencing individual stem cells that are isolated by fluorescence-activated cell sorting at different ages.

Finally, it would be worth thoroughly characterising the histochemical and biochemical phenotypes, mitochondrial proliferation and abnormalities of mitochondrial microstructure in different tissues of the $tRNA^{Ala}$ mutant mice by sequential COX/SDH histochemistry, immunofluorescence and electron microscopy to verify whether this mouse model is ideal for studying the mechanism of mtDNA disease in other aspects.

4.6 Conclusions

In this study, I have genetically characterised $tRNA^{Ala}$ mutant mice with the inherited m.5024C>T mutation and demonstrated the dynamics of this mutation in a variety of tissues with different regeneration capability. I have shown that the heteroplasmy levels remain steady with age in the majority of tissues/organs of the $tRNA^{Ala}$ mutant mice that are post-mitotic, contain post-mitotic cells or mitotically quiescent. In contrast, I have found a selective loss in the mitotic spleen, pyloric epithelium of the stomach and intestinal epithelium. Moreover, I have illustrated that the distribution of m.5024C>T mutation in the individual intestinal crypts of the $tRNA^{Ala}$ mutant mice is very similar to what I found in the GI epithelium of patients with the m.3243A>G and the m.8344A>G mutation, which shows some crypts harbouring extremely low levels of the mutation and an upper threshold of the heteroplasmy level, suggesting the involvement of stem cells and a selective loss of the mutation above the upper limit. Furthermore, I have shown that the fundic unit of the $tRNA^{Ala}$ mutant mice maintains the mutation load over time probably because of the low turnover rate of the differentiated glandular cells, suggesting the involvement of the progenies of stem cells in the process of losing the m.5024C>T mutation in mitotic tissue. These results have corroborated that the $tRNA^{Ala}$ mouse model is genetically ideal for studying the mechanism underlying the selective pressure against the inherited mtDNA mutations. To date, this is the only mouse model of mtDNA disease that shows such tissue-specific distribution of the mutation and the age-dependent selective loss of the mtDNA mutation in mitotic tissue, which perfectly recapitulates the findings of the patients with certain mtDNA disease.

Chapter 5 Characterisation of the OXPHOS level in the gastrointestinal epithelium of the tRNA^{Ala} mutant mice

5.1 Introduction

As previously discussed in Chapter 3, I found a significantly lower mutation load of the m.3243A>G mt-tRNA point mutation in the mitotic gastrointestinal (GI) epithelium compared with that in the post-mitotic smooth muscle of patients with mtDNA disease. This correlated with normal COX activity and the protein level of respiratory chain (RC) complexes I and IV in the epithelium but defective COX function and decreased complex I protein subunit levels in the muscle. However, as it is a cross-sectional study, the effect of the age-dependent loss of inherited pathogenic mtDNA mutations on OXPHOS function needs further investigation.

In Chapter 4, I have shown a significant decrease in the heteroplasmy of the m.5024C>T mt-tRNA point mutation in the mitotic intestinal epithelium of the old tRNA^{Ala} mutant mice compared with the young mutants. Previously Dr Holly Baines has characterised COX activity in the colonic epithelium of the young and old mutant mice using sequential COX/SDH histochemistry. She found partial COX deficiency in the colonic epithelium of all tRNA^{Ala} mutant mice (Baines, 2014). Around a quarter of crypts ($\leq$ 27%) were found to have defective COX activity (Figure 5.1) (Baines, 2014). However, complete loss of COX activity is rare: two thirds of the mutant mice with a high tail heteroplasmy level ($\geq$ 60%) (representing the initial mutation load similar to the ear notch) did not have any crypts with complete COX deficiency; and a very low level of complete COX deficiency ($\leq$ 5% crypts) was detected in the rest of the mice (Baines, 2014). The heteroplasmy level of the m.5024C>T mutation segregated with COX activity in the colonic crypts, where crypts with defective COX activity harbour high m.5024C>T heteroplasmy and those with normal COX function carry low levels of the mutation (Baines, 2014). This has confirmed the pathogenicity of the m.5024C>T mutation and its correlation with COX function in the tRNA^{Ala} mutant mice (Baines, 2014). Surprisingly, even with the lower mutation load in the colonic epithelium compared with the smooth muscle in the aged mutant mice, there was no difference in the percentage of the colonic crypts with COX defects, including both entire and partial COX deficiency, between the young and old mutant mice (Figure 5.1) (Baines, 2014). However, the percentage of COX defective colonic crypts did correlate with the tail heteroplasmy in the young but not the old mutant mice (Baines, 2014). Since the sequential COX/SDH assay is for determining COX enzyme function and is semi-quantitative, further characterisation of the protein expression of the RC complexes using immunofluorescence was required. Moreover,

it is unknown whether other fast-renewing tissue, for example, the epithelium of small intestine, has any change in OXPHOS function with age correlating with the decrease in the m.5024C>T heteroplasmy level.

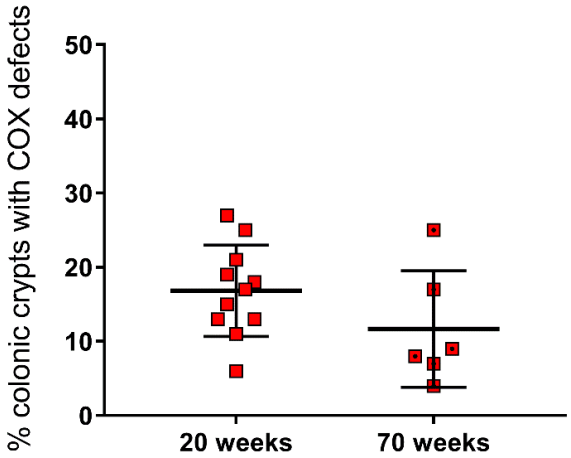

Figure 5.1 Defective COX activity in the colonic epithelium of the young and old $tRNA^{Ala}$ mutant mice. Sequential COX/SDH histochemistry was carried out on colon sections of the 20-week and 70-week $tRNA^{Ala}$ mutant mice. The percentage of COX defects is quantified as the ratio of the number of the COX defective crypts, including those with complete and partial loss of the COX activity, and the total number of colonic crypts (~500 crypts per sample). Raw data was obtained by Dr Holly Baines for the analysis ($p = 0.15$, unpaired t-test).

5.2 Aims

This study aimed to investigate the effect of the age-related decrease in the heteroplasmy level of the m.5024C>T mutation on OXPHOS function in the gastrointestinal epithelium of $tRNA^{Ala}$ mutant mice. This was achieved by detailed characterisation of OXPHOS protein expression, including:

1. Determine COX activity in the small intestinal epithelium in the young (10 weeks) and old (50 weeks) mutant mice by sequential COX/SDH histochemistry.
2. Determine COX activity in the epithelium of the gastric fundus and pylorus in the old mutant mice by sequential COX/SDH histochemistry for the reason that the age-related dynamics of the m.5024C>T mutation in these epithelial cells are different compared with that in the intestinal epithelium and it is worth investigating whether biochemical phenotypes of these tissues reflect the difference at the genetic level.
3. Determine the protein level of the respiratory chain complex I and IV, and the level of mitochondrial mass in the colonic epithelium of young and old mutant mice by immunofluorescence.

5.3 Methods

5.3.1 Sequential COX/SDH histochemistry and semi-quantification of COX defects

Frozen small intestines of seven 10-week $tRNA^{Ala}$ mutant mice and six 50-week mutants and stomach tissue of seven 50-week mice were sectioned in a cryostat at 10 µm. Each age group includes two mice with intermediately high ear m.5024C>T heteroplasmy (60% - 69%) and the remainder with high ear heteroplasmy (71% - 79%). COX and SDH histochemistry assays were optimised individually for use in the sequential COX/SDH assay. The optimisation strategy is shown in Figure 5.2. For the COX assay, sections were incubated in the COX solution for a sequential period of time (11 min, 15 min, 19 min, 22 min and 25 min). For SDH assay, sections were incubated in the SDH solution for 5 min, 10 min, 15 min, 20 min and 25 min. The timespan for each assay that provided cells with strong labelling and avoided over-pigmentation was selected for the sequential assay. The optimal incubation time for the COX/SDH assay is cell-specific, which is summarised in Table 2.6.

Sequential COX/SDH histochemistry was performed on sections. Crypts were analysed in a semi-quantitative manner using the following criteria: “complete deficiency” (blue), “partial deficiency” (bluish brown or containing blue/bluish brown cells) and “normal activity” (brown). Longitudinally and obliquely sectioned epithelial tissue, where the small intestinal crypts at the base of the mucosa could be identified, was included for the semi-quantification. A total number of approximately 120 crypts were examined in each mouse. The number of crypts with defective COX activity, including crypts with complete COX deficiency and partial COX deficiency, were counted. The percentage of crypts with COX defects was calculated as the number of COX defective crypts over the number of total examined crypts.

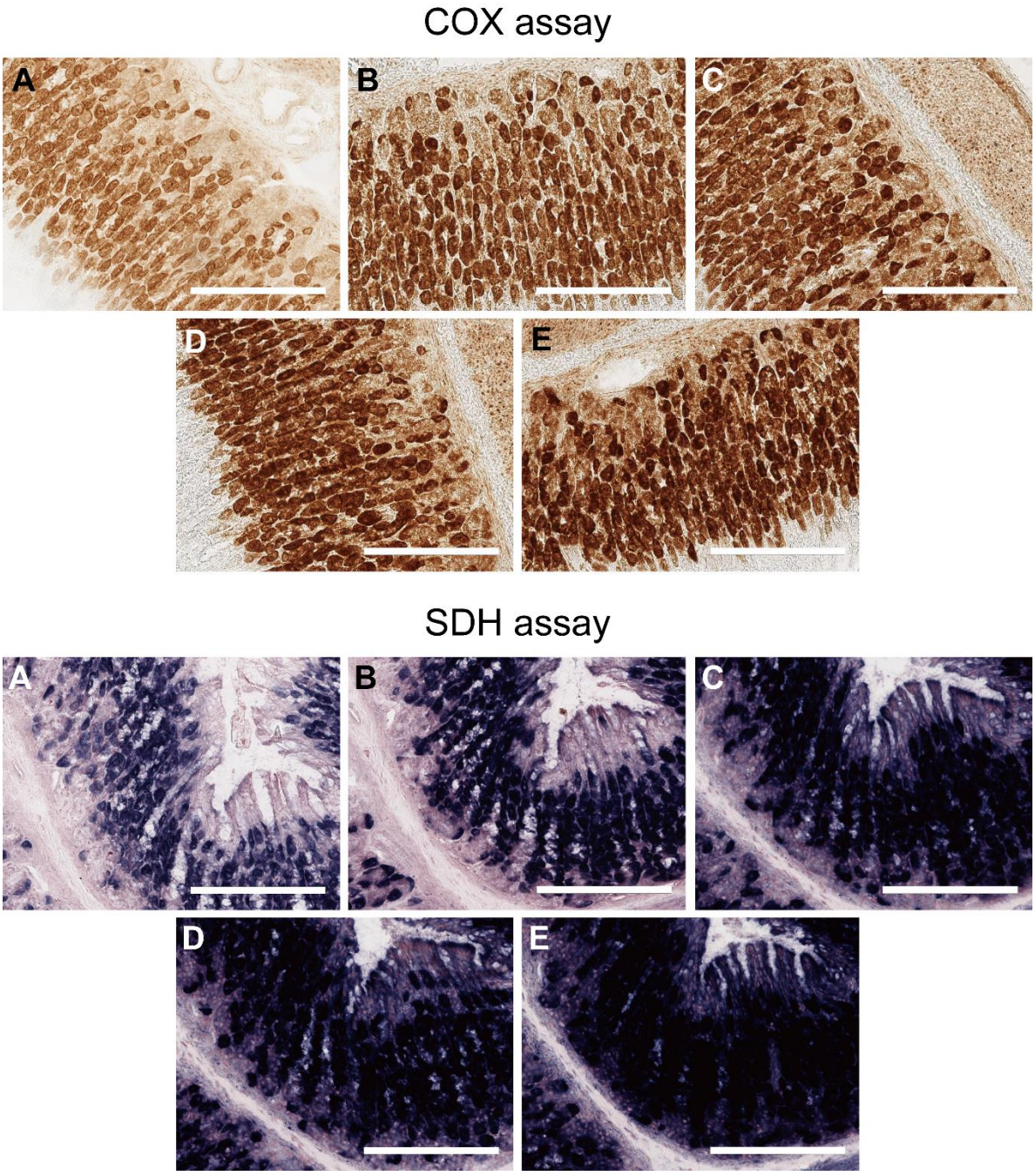

Figure 5.2 Optimisation of the incubation time for COX and SDH assays. For the COX assay, sections of the fundic epithelium were incubated in the COX solution for (A) 11 min, (B) 15 min, (C) 19 min, (D) 22 min and (E) 25 min. (A) 11 min was selected for the sequential COX/SDH assay. For the SDH assay, sections were incubated in the SDH solution for (A) 5 min, (B) 10 min, (C) 15 min, (D) 20 min and (E) 25 min. (A) 5 min was chosen for the final sequential assay. Scale bar = 200 µm.

5.3.2 Immunofluorescence

Formalin-fixed and paraffin-embedded (FFPE) colon tissue (4 µm) from $tRNA^{Ala}$ mutant mice was sectioned by myself for the optimisation of the immunofluorescence (IF) assay and by Anna Smith for final experiments. The optimised combination of antibodies in the IF study is in Table 5.1. Five mutant mice with high m.5024C>T heteroplasmy in the ear (71% - 80%) were examined in each age group (10 weeks and 50 weeks) and compared with three age-matched wild-type mice. Information about the mice included in the IF study and the number of colonic crypts scrutinised is summarised in Table 5.2. Due to a shortage of frozen colon tissue from the 10-week $tRNA^{Ala}$ mutant mice for determining the mutation level in the colonic epithelium, the heteroplasmy in intestinal crypts used in the analyses of this study was the average mutation level of individual small intestinal crypts from Chapter 4. Paired t-tests showed no difference in the mutation load in the small and large intestinal crypts in five 50-week mutants, proving the reliability of substituting heteroplasmy of small intestinal crypts for that of colonic crypts in the analyses (Figure 5.3).

Antibody combination		
Primary antibody	**Secondary antibody**	**Tertiary antibody**
Anti-NDUFB8 (ab110242)	Biotin-XX (A10519)	Streptavidin, Alexa Fluor 647 conjugate (S21374)
Anti-MTCO1 (ab14705)	Alexa Fluor 546 (A21133)	N/A
Anti-TOM20 (ab186734)	Alexa Fluor 488 (A21141)	N/A

Table 5.1 Information about the antibodies used for the immunofluorescence. Antibodies in the same row are the matching primary and secondary/tertiary antibodies. Details of each antibody and their optimised concentration are summarised in the Table 2.7 and Table 2.8.

10 weeks			
Mouse ID	Ear mut%	Intestinal E mut%	N of crypts
B933	79	70.63	150
B934	77	63.69	148
B938	77	67.57	154
B945	74	68.71	152
B948	71	58.17	146
B988	WT	n/a	144
B994	WT	n/a	142
B995	WT	n/a	145
50 weeks			
Mouse ID	Ear mut%	Intestinal E mut%	N of crypts
372	80	55.99	158
365	79	55.04	157
353	73	51.49	147
370	73	55.07	145
369	71	51.78	135
24283	WT	n/a	155
24769	WT	n/a	126
WT210	WT	n/a	144

Table 5.2 A summary of the mouse information and the number of examined colonic crypts in each mouse in the immunofluorescence study. Colon tissue of five $tRNA^{Ala}$ mutant mice with high m.5024C>T heteroplasmy and three age-matched wild-type mice in each group was used. Mut, mutation. N, number.

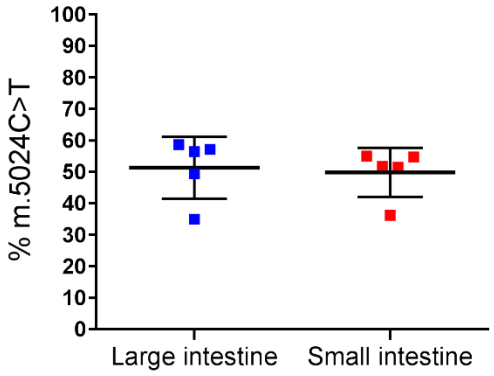

Figure 5.3 Mutation load in the crypts of small and large intestines from five 50-week tRNA^{Ala} mutant mice (mouse 351 353 365 369 and 373). Heteroplasmy of 10 small and large intestinal crypts of each mouse was determined by pyrosequencing and averaged for comparison. Each square signifies a mouse.

5.3.3 Imaging and statistical analysis

As the 10-week and the 50-week mouse tissue was fixed by Dr Laura Greaves and Dr James Stewart respectively, the fixation conditions of the tissue were slightly different. All blocks of tissue were sectioned and collected using adhesive glass slides by Anna Smith. However, possibly due to different fixation conditions, under an epifluorescence microscope, some cells of the 50-week sections slightly floated above the focal panel of the majority of the cells. To fix this issue, sections that were labelled by fluorophore-conjugated antibodies were imaged using an upright Confocal Laser Microscope System in a z-stack fashion, which covered a range of focal panels (detailed in 2.9.3). The stacked images were then incorporated to acquire the maximum projection at each pixel site, which represents the pixel intensity at the optimal focus of the tissue at each pixel point. Individual crypts were drawn on the images as regions of interest (ROI) covered with a mask defining the minimum pixel intensity to remove the lumen of the crypts. Mean pixel intensity within the ROI was measured using NIS-Element AR Imaging software (detailed in 2.9.3).

Three independent experiments were performed on non-serial sections to comprehensively determine the level of RC complexes and mitochondrial mass in the colonic crypts of the tRNA^{Ala} mutant mice. The raw data of the pixel intensity in each crypt was background corrected and log-transformed to fit the R-script written by Dr John Grady for calculating z-scores (specified in 2.12.1). Transforming data into z-scores allows the integration of the data of the three experiments. The z-scores of the absolute protein level of RC complexes and the level of Tom20 in individual crypts were calculated according to the parameters (mean and SD) of the control population that was established by randomly sampling an equal number of

measurements of the 10-week wild-type controls (described in 2.12.1). For calculating the z-scores of the relative level of RC complexes to the mitochondrial mass marked by Tom20 antibodies, a linear regression was established between the data of the RC complexes and Tom20 to provide a predicted level of RC complexes based on the Tom20 level. An estimate of the deviation of the level of RC complexes against Tom20 level from the predicted level was presented as the z-scores. The classification of the z-scores is shown in Table 5.3, which is based on the confidence level (detailed in section 2.12.1).

To determine the relationship between age, mouse genotype, the absolute/relative level of complex I/IV and the level of mitochondrial mass, mixed-effect generalised linear models were established by Dr Alasdair Blain. Random factors accounting for the variation between experimental sets and mouse individuals were added to enable the best fitness of the model (tested using Akaike Information Criterion).

Classification	z-score boundaries
Tom20	
Very low	$z < -3.0$
Low	$-3.0 \leq z < -2.0$
Normal	$-2.0 \leq z \leq 2.0$
High	$2.0 < z \leq 3.0$
Very high	$3.0 < z$
NDUFB8 and MTCO1	
Positive	$-2.0 \leq z$
Intermediate positive	$-2.6 \leq z < -2.0$
Intermediate negative	$-3.3 \leq z < -2.6$
Negative	$z < -3.3$

Table 5.3 Categorisation of the boundaries of the z-score. The z-scores of the absolute level and the relative level of RC complexes share the same classification.

5.4 Results

5.4.1 Defective COX function in the small intestine and stomach

Previously, Dr Holly Baines found no difference in the percentage of the COX defective colonic crypts between the young and old $tRNA^{Ala}$ mutant mice (Baines, 2014). As the m.5024C>T mutation load significantly decreased in the small intestinal epithelium of the old mutants compared with the young mice (Chapter 4), I performed sequential COX/SDH histochemistry on the sections of the small intestinal crypts of the 10-week (n = 7) and 50-week (n = 6) $tRNA^{Ala}$ mutant mice to investigate whether there is any change in the COX function concomitant with the reduced mutation load. Each age group consisted of two mice with intermediately high heteroplasmy in the ear (60% - 69%) and the remaining mice with high ear heteroplasmy (71% - 79%). Villi of the small intestine were excluded since the cells of each villus stem from several stem cells niches, whereas each crypt comprises of a single stem cell niche that undergoes monoclonal conversion, a few Paneth cells and the transit-amplifying cells that originate from these stem cells (Barker, 2014). Partial COX deficiency (bluish brown crypts or crypts containing blue/bluish brown cells) was detected in all the mutant mice, but complete COX deficiency (blue crypts) was barely observed in the intestinal epithelium (<2%) (Figure 5.4A). No difference in the percentage of the COX-defective small intestinal crypts, including those with complete and partial loss of the COX activity, was found between the 10-week and 50-week $tRNA^{Ala}$ mutant mice (Figure 5.4B). No correlation was found between the level of COX defects and the m.5024C>T heteroplasmy level in the ear or crypts in either 10-week or 50-week $tRNA^{Ala}$ mutant mice ($p > 0.05$, Spearman's rank analysis).

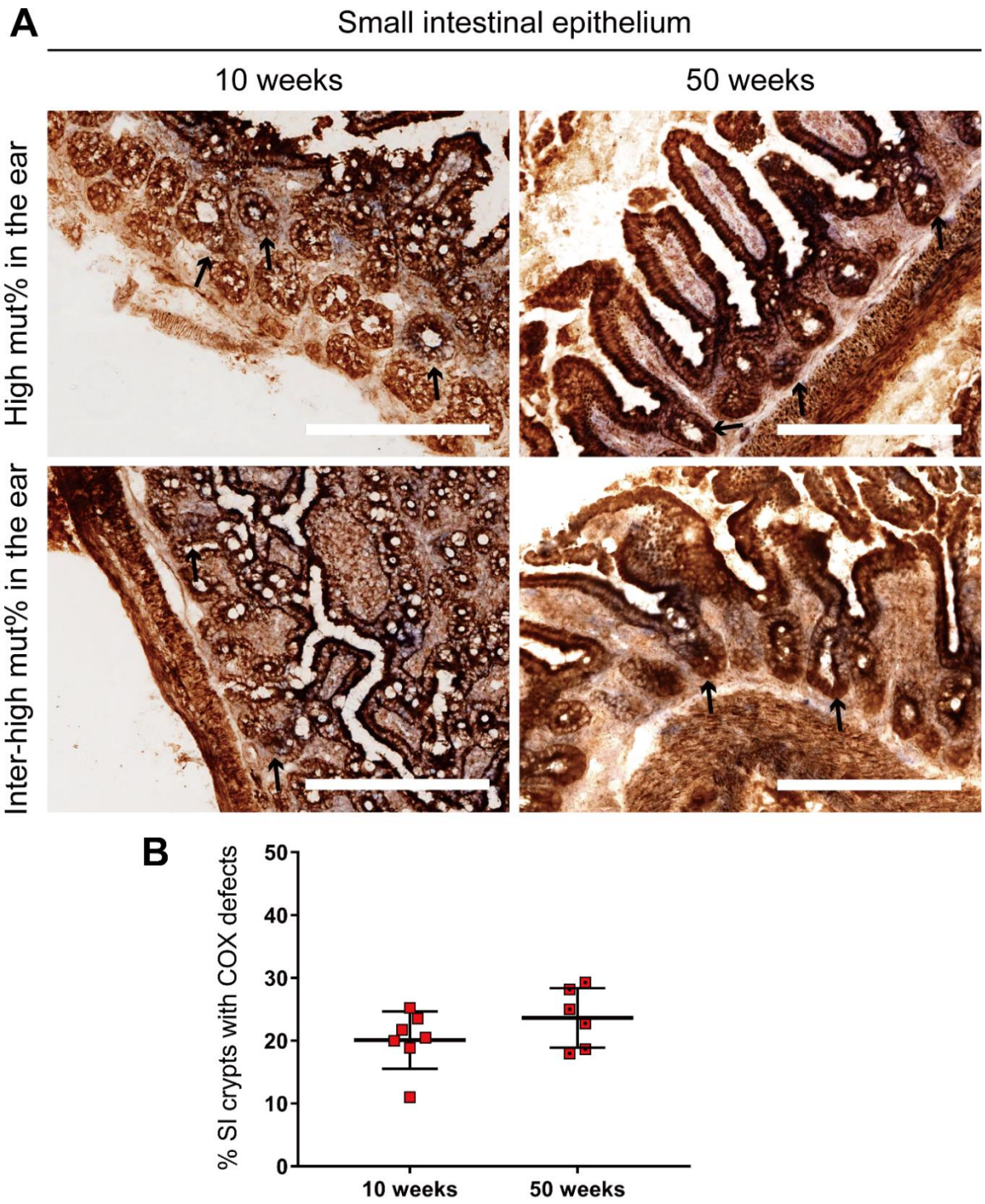

Figure 5.4 COX defects in the small intestinal epithelium of the 10-week and 50-week $tRNA^{Ala}$ mutant mice labelled by sequential COX/SDH histochemistry. (A) Example images of COX defective crypts in the 10-week and 50-week mice with high and intermediately high ear heteroplasmy level. Black arrows indicate small intestinal crypts with partial COX deficiency that contain bluish brown or blue cells. Scale bar = 200 µm (B) Quantification of the percentage of the crypts with COX defect (entire and partial loss of COX activity). Seven 10-week mice (B933, B934, B938, B945, B948, B949 and B952) and six 50-week mice (365, 353, 370, 369, 373 and 351) were included for statistical analysis. Each square represents a single mouse.

The mutation load of fundic epithelium remained high from 10 weeks to 50 weeks in the $tRNA^{Ala}$ mutant mice, which was in contrast to the pyloric epithelium in which the mutation level decreased with age (Chapter 4). To ascertain whether the genetic finding is correlated with the COX activity in these two types of epithelial tissues in the stomach, I performed sequential COX/SDH histochemistry on the sections of gastric fundus (n = 6) and pylorus (n = 3) of the 50-week $tRNA^{Ala}$ mutant mice. Gastric epithelium of the 10-week mutant mice was not examined in this study, since the mutation level was similar in all tissues of the 10-week mutants. Both the fundic and pyloric units of all examined mice contained many evident blue cells that had a complete absence of COX activity (Figure 5.5 and Figure 5.6), which is in contrast to the milder COX defect in the small intestinal crypts with lower mutation load (Figure 5.4). Due to the distinct cell component between the fundic, pyloric and small intestinal epithelium, the semi-quantification by subjective colour differentiation and manual counting would be unreliable. The indefinite boundaries of the fundic units would further lessen the accuracy of the semi-quantification. Thus, semi-quantification was not carried out on the images of the fundic and pyloric epithelium. Quantitative immunofluorescence would be required for precise determination of the OXPHOS level in these tissues in the future.

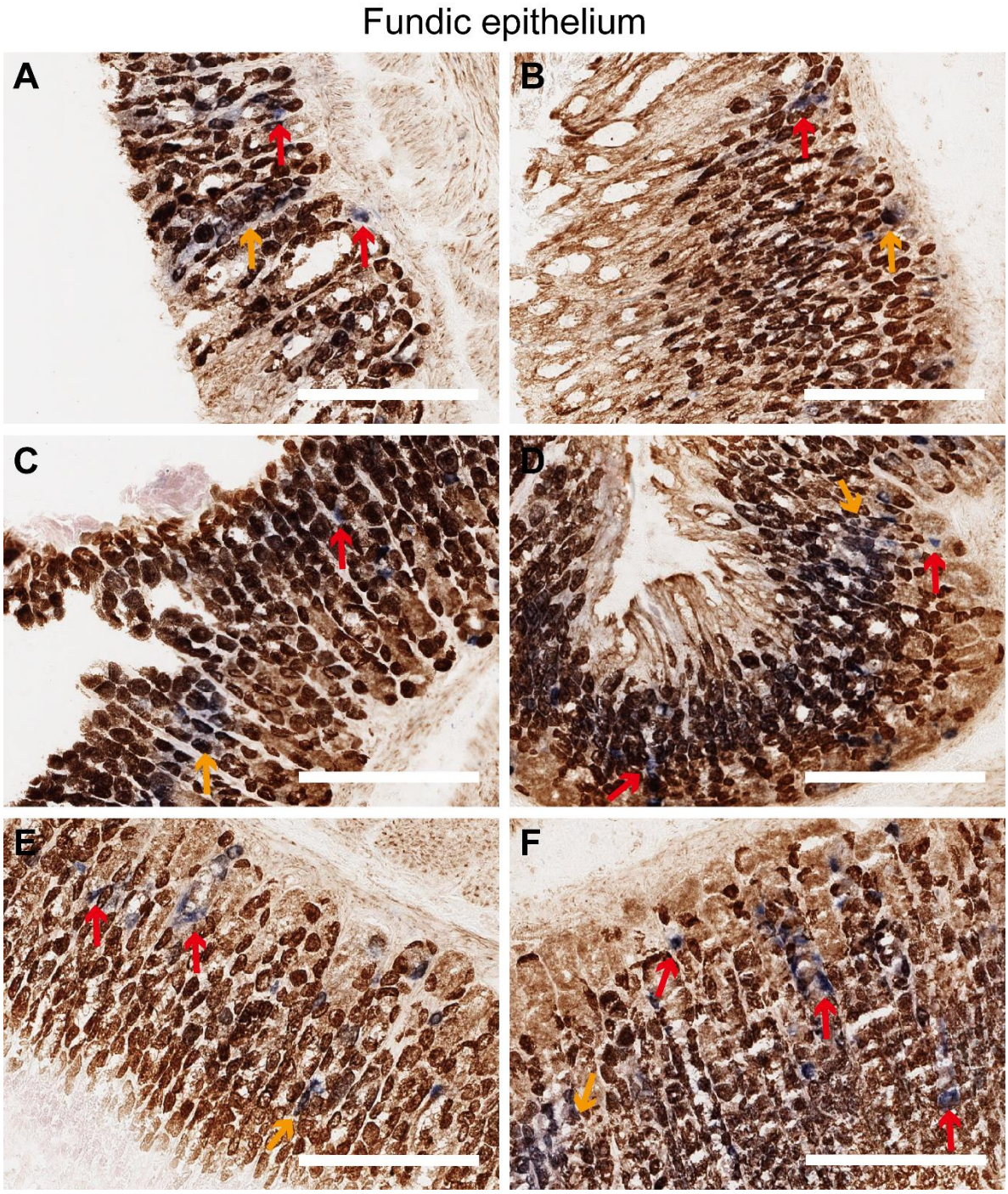

Figure 5.5 Images showing COX deficiency in the epithelium of the gastric fundus in the 50-week $tRNA^{Ala}$ mutant mice. Sections were labelled using sequential COX/SDH assay. Six mice were examined: (A) 365 (ear m.5024C>T% = 79%), (B) 353 (ear m.5024C>T% = 73%), (C) 370 (ear m.5024C>T% = 73%), (D) 369 (ear m.5024C>T% = 71%), (E) 373 (ear m.5024C>T% = 69%) and (F) 351 (ear m.5024C>T% = 71%). Cells with complete COX deficiency are blue (red arrows), and those with partial COX deficiency are bluish-brown (yellow arrows). Scale bar = 200 µm.

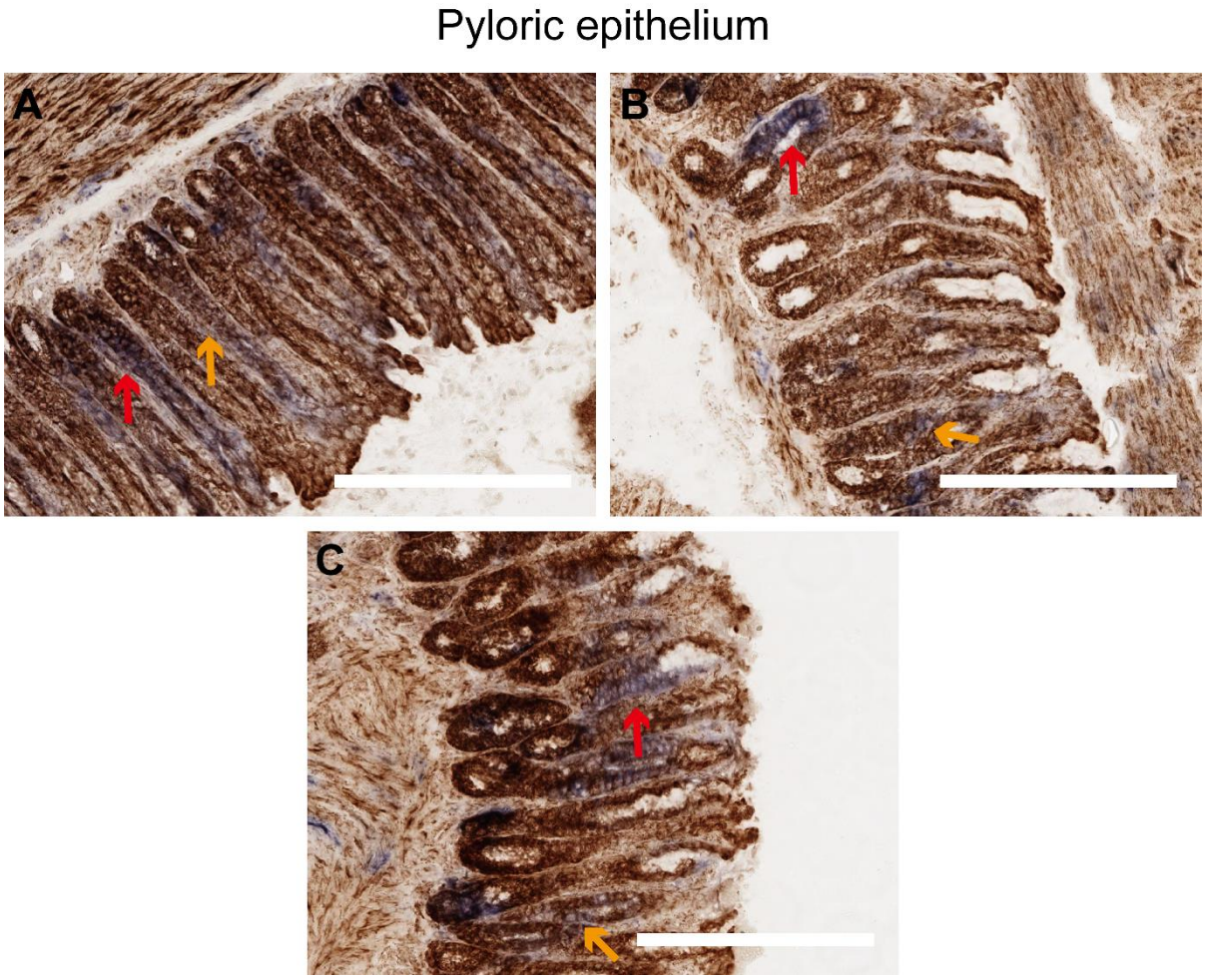

Figure 5.6 Images showing the COX defects in the epithelium of the gastric pylorus of the 50-week $tRNA^{Ala}$ mutant mice. Sequential COX/SDH assay was performed on the sections. Three mice were examined: (A) 372 (ear m.5024C>T% = 80%), (B) 365 (ear m.5024C>T% = 79%) and (C) 353 (ear m.5024C>T% = 73%). Cells that entirely lost COX function are blue (red arrows), and those with partial COX deficiency are bluish-brown (yellow arrows). Scale bar = 200 μm.

5.4.2 Quantification of absolute level of RC complexes in the colonic crypts

5.4.2.1 Absolute level of complex I

As the semi-quantification of COX function was based on subjective assessment of COX and SDH labels, I performed a more reliable quantitative immunofluorescence to investigate the expression of RC complexes on sections of the colonic epithelium of the $tRNA^{Ala}$ mutant mice. I performed three independent experiments on non-serial colon sections of 10-week and 50-week wild-type (n = 3 in each age group) and $tRNA^{Ala}$ mutant mice (n = 5 in each age group) and examined approximately 150 crypts in total in each mouse. The 10-week and 50-week mutants both displayed complex I deficiency (labelled by NDUFB8 antibody) compared with the age-matched wild-type controls (Figure 5.7 complex I panel). The 10-week mice displayed a general decrease in complex I expression, whereas the 50-week mice had some crypts with strong complex I labelling and some crypts that had completely lost complex I expression (Figure 5.7 complex I panel), possibly as a result of the monoclonal conversion. Pixel intensity of individual crypts was measured in each independent experiment, which was transformed into z-scores and pooled for statistical analysis (detailed in 5.3.3). The level of RC complexes was classified into four groups: "positive", "intermediate positive", "intermediate negative" and "negative" with the boundaries corresponding to 95%, 99% and 99.9% confidence level (detailed in 5.3.3). Categorical quantification of the absolute protein level of complex I showed mild complex I deficiency in the 10-week mutant mice (3.20% CI-negative and 3.33% CI-intermediate-negative) similar to that in the 50-week mutant mice (3.91% CI-negative and 3.37% CI-intermediate-negative crypts) (Figure 5.8A). Analysis of the z-score distribution revealed a higher median level of complex I in the 50-week mutants (median = 1.33) than the 10-week mutants (median = 0.44), suggesting an improvement of complex I expression in the mitotic colonic epithelium of the $tRNA^{Ala}$ mutant mice with age (Figure 5.9B).

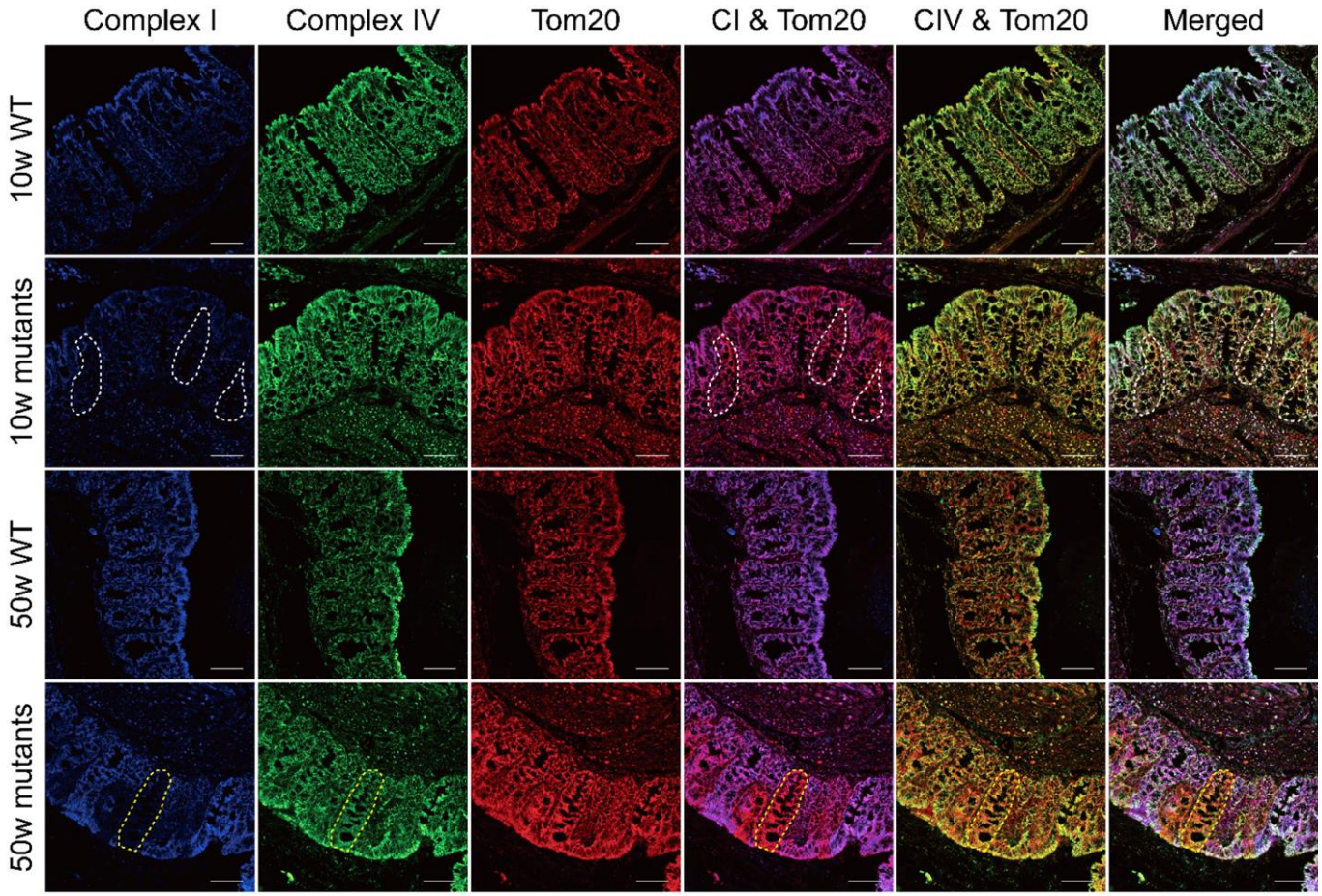

Figure 5.7 Example immunofluorescence images showing the level of respiratory chain complex I (labelled by NDUFB8 in blue) and IV (labelled by MTCO1 in green) co-labelled with the mitochondrial mass marker Tom20 (red) in the colonic epithelium of the 10-week and 50-week $tRNA^{Ala}$ mutant and wild-type mice. The panel of complex I/IV alone indicates the absolute complex level in the tissue. The "CI & Tom20" and "CIV & Tom20" panel show the complex I/IV level relative to the mitochondrial mass. White dotted line circle the crypts with isolated complex I deficiency. Yellow dotted lines circle the crypts with absolute and relative complex I deficiency and relative complex IV defect. Scale bar = 50 µm.

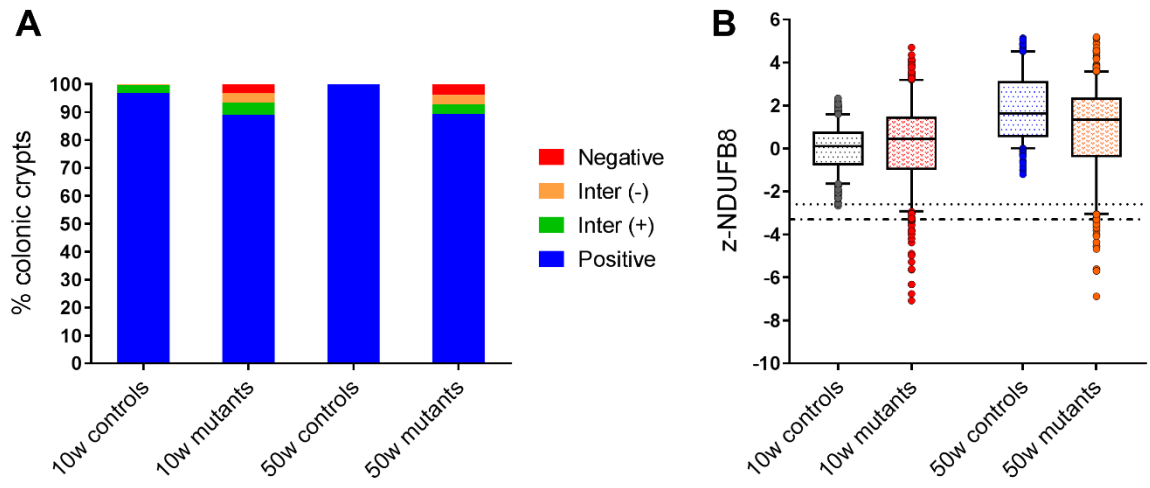

Figure 5.8 Quantification of the absolute complex I protein level (labelled by NDUFB8) in the colonic epithelium of the $tRNA^{Ala}$ mutant mice. (A) Categorical z-scores of complex I levels in the $tRNA^{Ala}$ mutants compared with the wild-type controls at 10 weeks and 50 weeks. The complex I level was classified as "positive", "intermediate positive", "intermediate negative" and "negative". The boundaries of the z-scores for each category are summarised in the Table 5.3. (B) Whisker-and-box plot of the z-NDUFB8 showing the median and distribution of the complex I level in the colonic epithelium. Each point signifies a measurement of an individual crypt. The dotted lines are the boundaries for defining "intermediate negative" and "negative".

An overview of the absolute complex I level in individual mice is shown in Figure 5.9. Modelling of the whole dataset with factors "variation in experiment sets" and "variation in individual mice" included (detailed in 5.3.3) showed a negative linear relationship between the ear heteroplasmy and the z-scores of complex I in the colonic crypts of both 10-week ($p < 0.001$) and 50-week ($p < 0.001$) mutants, indicating a decrease in the absolute complex I level in the colonic epithelium concomitant with an increase in the initial mutation load. The relationship was much stronger in the 10-week mice ($r = 0.418$) compared with the 50-week mice ($r = 0.140$), suggesting a weakened influence of the initial mutation burden m.5024C>T with age on the complex I level. In addition, it showed a weak negative linear relationship between the complex I level and the average mutation level in intestinal crypts (Table 5.2) in the 10-week mutants ($r = 0.086$, $p = 0.013$), which became stronger in the 50-week mutants ($r = 0.117$, $p < 0.001$), suggesting that the association of the mutation level and the absolute complex I level in the colonic crypts increased with age.

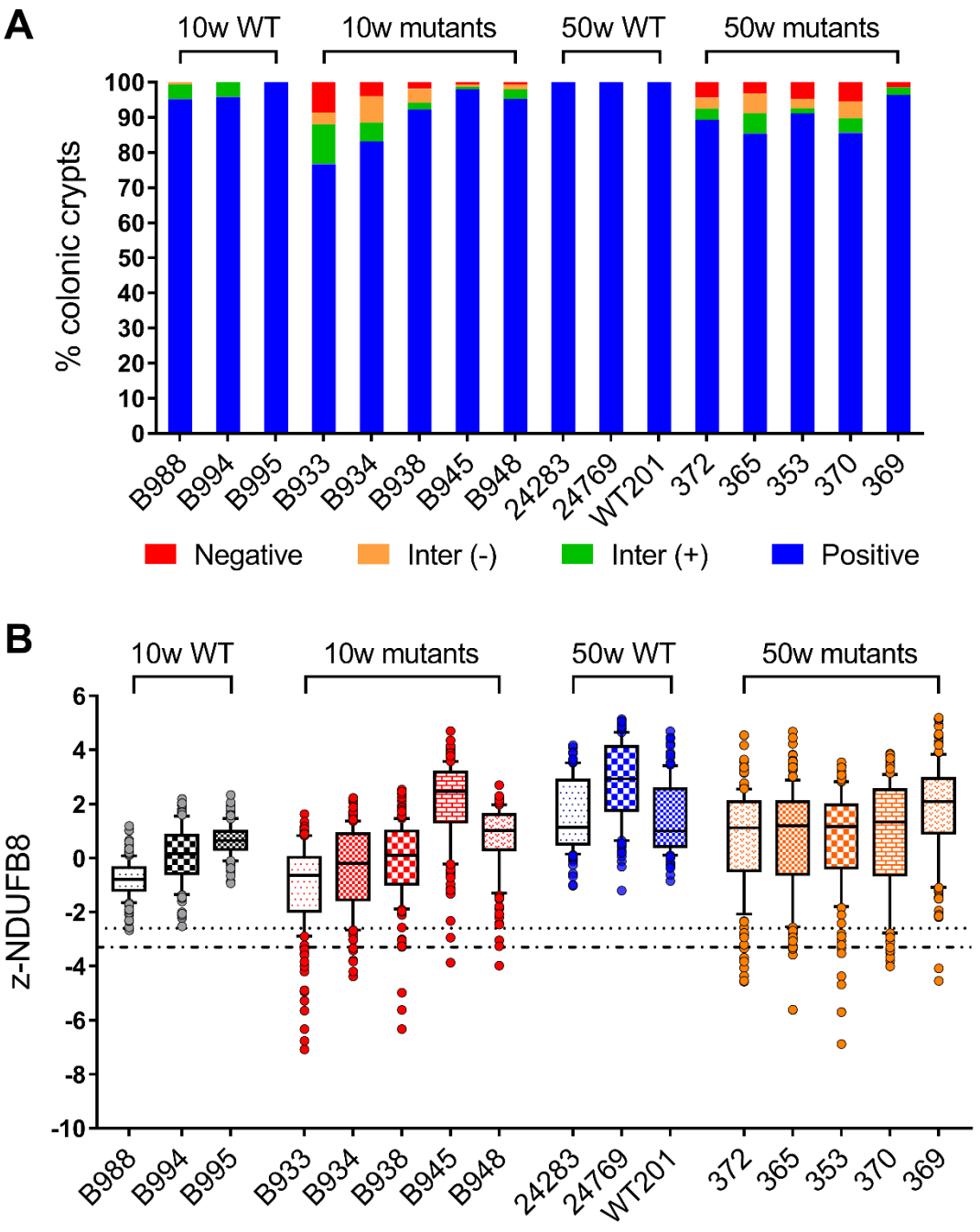

Figure 5.9 Quantification of the respiratory chain complex I level in the colonic epithelium of individual $tRNA^{Ala}$ mutant mice. (A) Categorical z-scores of the complex I level. Complex I level was classified as "positive", "intermediate positive", "intermediate negative" and "negative". The boundaries of the z-scores for each category are summarised in the Table 5.3. (B) An overview of z-NDUFB8 showing the median and the distribution of the complex I level in the colonic epithelium. Each point represents a measurement of an individual crypt. The 10-week mutant mice, B933, B934, B938, B945 and B952 carried 79%, 77%, 77%, 74% and 71% m.5024C>T in the ear respectively. The 50-week mutants, 372, 365, 353, 370 and 369 carried 80%, 79%, 73%, 73% and 71% m.5024C>T in the ear respectively.

5.4.2.2 Absolute level of complex IV

Since COX deficiency was observed in all the examined $tRNA^{Ala}$ mutant mice, in addition to RC complex I, I also measured RC complex IV level (labelled by the MTCO1 antibody) in the colonic epithelium by quantitative immunofluorescence assay. I observed no difference in the complex IV level between the 10-week wild-type controls, 10-week $tRNA^{Ala}$ mutants and 50-week mutants, but a notably decreased complex IV level in the 50-week wild-type controls on the images (Figure 5.7 complex IV panel). Quantification of the z-scores revealed 10.59% complex IV-negative and 6.12% intermediate-negative colonic crypts in the aged controls (Figure 5.10A). In contrast, there were barely any crypts with a complex IV defect in either 10-week (0.54% negative and 0.93% intermediate negative) or 50-week (0.67% negative and 3.24% intermediate negative) $tRNA^{Ala}$ mutants (Figure 5.10A). The distribution of the z-MTCO1 showed that the median level of complex IV was slightly higher at 10 weeks than 50 weeks in both controls and $tRNA^{Ala}$ mutants (Figure 5.10B). The data of the 50-week wild-type mice had a marked larger variation with the z-MTCO1 of numerous crypts below the "negative" line (< 3.3) (Figure 5.10B), suggesting an effect of ageing on OXPHOS function. This is in contrast to the other groups where the z-MTCO1 of most of the crypts was within the normal range (quartiles between -2 and 2) (Figure 5.10B).

Individual mouse analysis confirmed that the absolute complex IV level was not affected in the 10-week mutant mice, and was slightly decreased in the 50-week mutants (Figure 5.11). In contrast, the categorical data showed a significantly reduced complex IV level in two aged wild-type mice (23.27% CIV-negative and 5.81% intermediate-negative crypts in 24283; 6.25% negative and 11.81% intermediate negative in WT201), which was confirmed by the distribution data (Figure 5.11). No complex IV deficiency was found in the other 50-week wild-type mouse 24769. More aged wild-type mice will be included to confirm these findings in the future.

These results indicate that the aged $tRNA^{Ala}$ mutants with inherited m.5024C>T mutation did not display as pronounced a complex IV defect as the aged wild-type mice did.

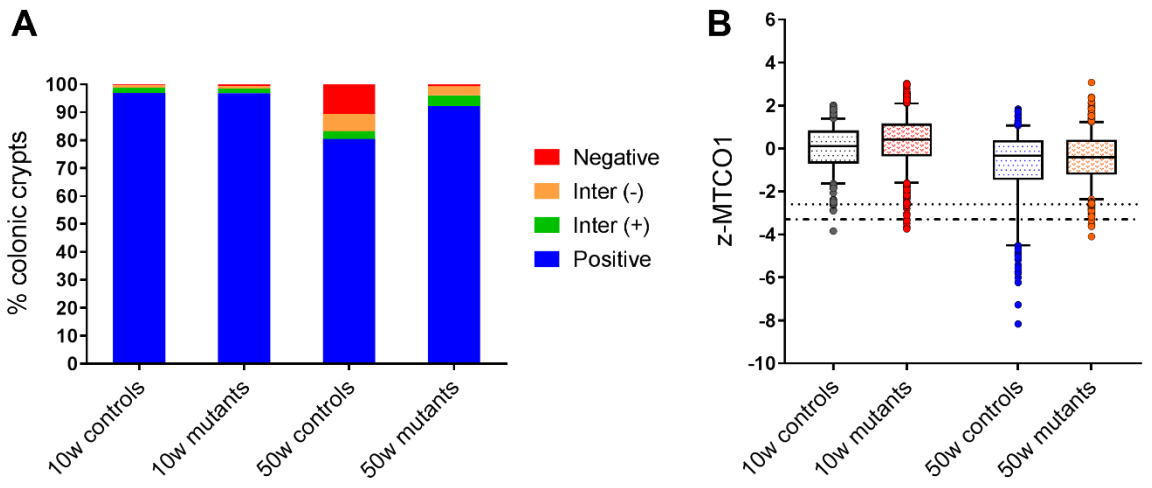

Figure 5.10 Quantification of the respiratory chain complex IV level in the colonic crypts of the $tRNA^{Ala}$ mutant mice. (A) Categorical z-scores of the complex IV level in the 10-week and 50-week $tRNA^{Ala}$ mutants compared with the age-matched wild-type controls. The complex IV level was classified as "positive", "intermediate positive", "intermediate negative" and "negative". The boundaries of the z-scores for each category are summarised in the Table 5.3. (B) Whisker-and-box plot of the z-MTCO1 showing the median and distribution of the complex IV level in the colonic crypts. Each point denotes a measurement of an individual crypt. The dotted lines are the limits for the "intermediate negative" and "negative" categories.

The modelling demonstrated a linear relationship between the absolute level of complex IV in the colonic crypts and the ear heteroplasmy of the 10-week mutants ($r = 0.164$, $p < 0.001$) but not in the 50-week mutants ($p > 0.05$), suggesting a loss of influence of initial mutation burden on the absolute complex IV level with age in the colonic epithelium. In addition, the modelling revealed a stronger correlation between the absolute complex IV level and crypt heteroplasmy in the 50-week mutants ($r = 0.142$, $p < 0.001$) compared with the 10-week mutants ($r = 0.081$, $p = 0.020$), suggesting an age-related increase in the association of heteroplasmy with absolute complex IV level in the crypts.

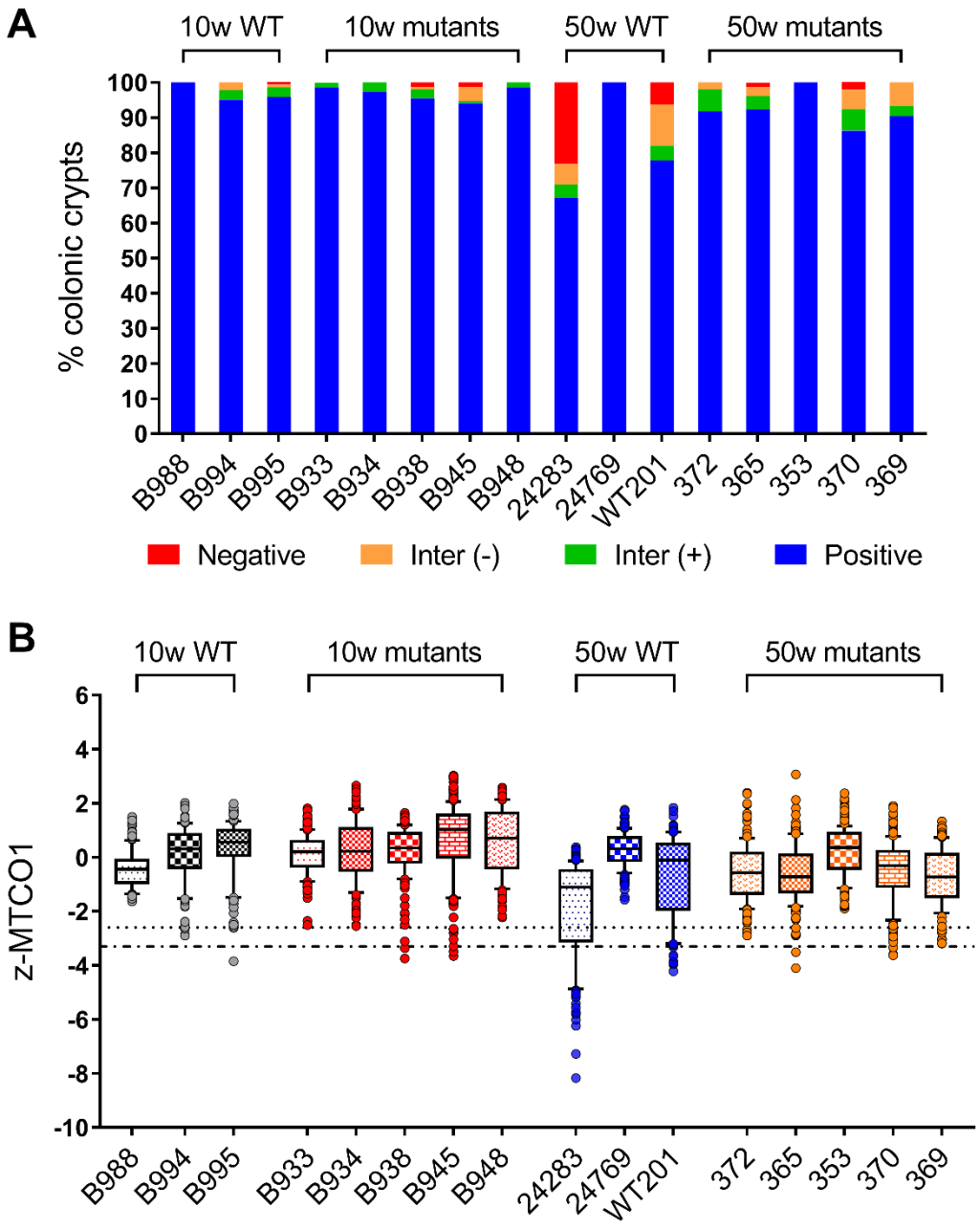

Figure 5.11 Quantification of the absolute complex IV protein level in the colonic epithelium of individual mice. (A) Categorical z-scores of the absolute complex IV level. Complex I level was classified as "positive", "intermediate positive", "intermediate negative" and "negative". The limits of the z-scores for each category are summarised in the Table 5.3. (B) An overview of z-MTCO1 showing the median and the distribution of the absolute complex IV level in the colonic crypts. Each point represents a measurement of an individual crypt. The 10-week mutant mice, B933, B934, B938, B945 and B952 carried 79%, 77%, 77%, 74% and 71% m.5024C>T in the ear respectively. The 50-week mutants, 372, 365, 353, 370 and 369 carried 80%, 79%, 73%, 73% and 71% m.5024C>T in the ear respectively. The dotted lines are the boundaries for the classification of "intermediate negative" and "negative".

5.4.2.3 Absolute OXPHOS level

To investigate the total level of OXPHOS deficiency in the colonic epithelium of the $tRNA^{Ala}$ mutant mice, profiles of RC complexes were plotted in Figure 5.12, where z-scores of the absolute level of complex I were drawn against those of the complex IV with the colour of the dots denoting the mitochondrial mass (MM) level. These results showed that isolated complex I deficiency (dots in the top left section) was the primary type of OXPHOS deficiency in the mutant mice with inherited m.5024C>T mutation, whereas isolated complex IV deficiency (dots in the bottom right section) was evident in the ageing wild-type mice (Figure 5.12). Most of the crypts with high MM level (orange and red for high and very high Tom20 level respectively) had normal OXPHOS function (dots in the top right section), regardless of the genotype and age, whereas complex IV defective crypts in the ageing wild-type mice had normal to low level of MM (beige, light blue and blue for normal, low and very low Tom20 level) (Figure 5.12).

Quantification of the total level of OXPHOS defect involved sorting the crypts into four groups: "complex I and complex IV both positive", "isolated complex I defect", "isolated complex IV defect" and "joint complexes I and IV defect". The defective crypts were the pooled data of the crypts with intermediate-negative and negative RC complex level in the previous study of individual RC complexes. The proportion of OXPHOS defective crypts was the aggregative percentage of the crypts with isolated complex I or IV defect and joint defect. The analysis showed a slightly higher percentage of OXPHOS-defective colonic crypts in the 50-week (9.84%) compared with the 10-week $tRNA^{Ala}$ mutant mice (8.00%) (Figure 5.13A). In addition, the 50-week mutants had a small percentage of crypts with joint complex defects that was not observed in the 10-week mutants (Figure 5.13). Isolated complex I defect was the main type of OXPHOS defect in the $tRNA^{Ala}$ mutant mice, whereas isolated complex IV defect was the primary phenotype of the aged wild-type mice (Figure 5.13).

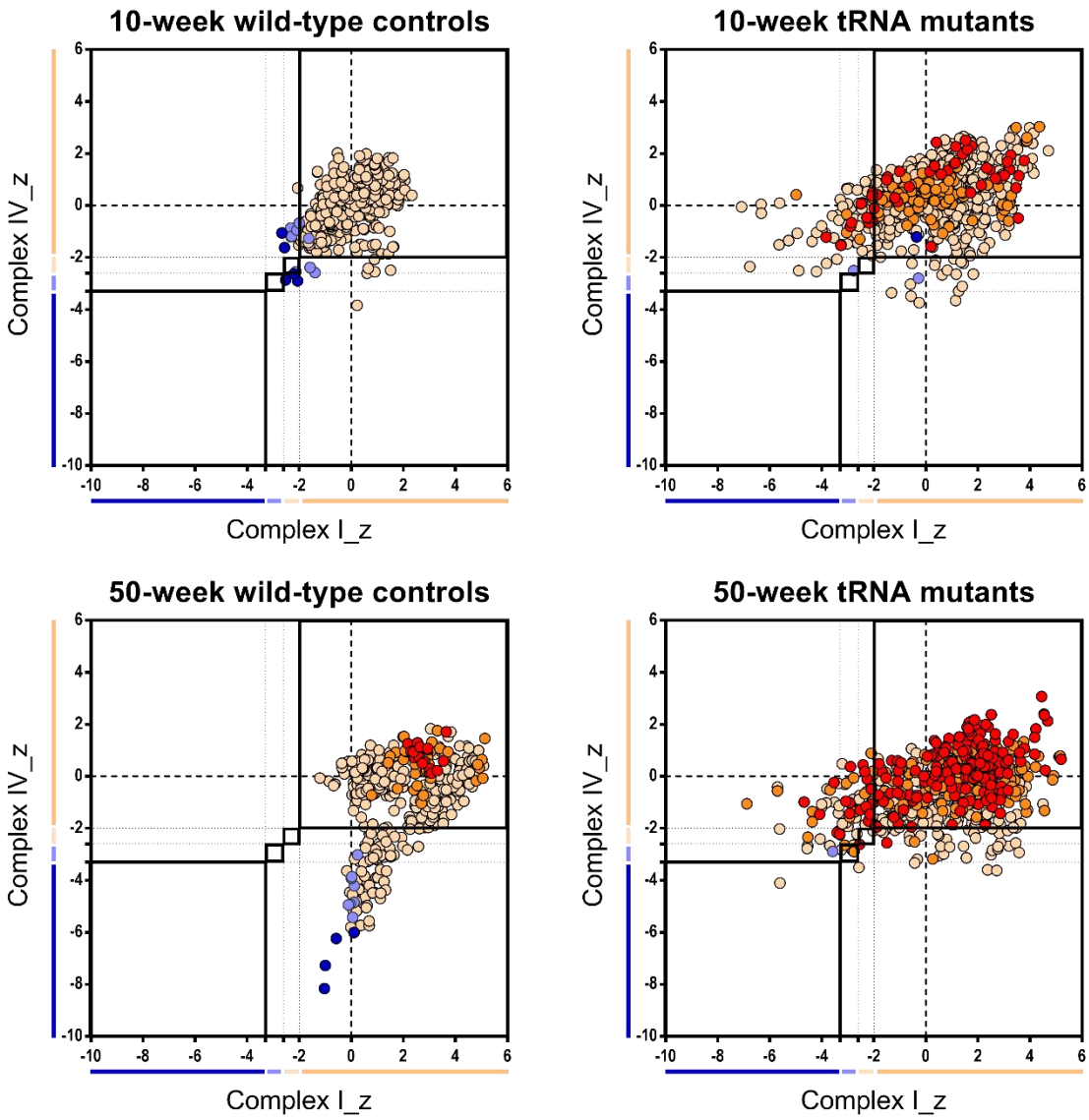

Figure 5.12 Profiles of the level of the RC complexes and mitochondrial mass in the colonic crypts of the wild-type and $tRNA^{Ala}$ mutant mice at 10 weeks and 50 weeks. Z-scores of NDUFB8 labelling complex I (horizontal axis) was drawn against the z-scores of MTCO1 labelling the RC complex IV (vertical axis). The colour indicates the classification of the Tom20 (marking MM) level: "very high" in red, "high" in orange, "normal" in beige, "low" in light blue and "very low" in blue. The boundaries for each class is summarised in Table 5.3. Each point signifies data of an individual crypt.

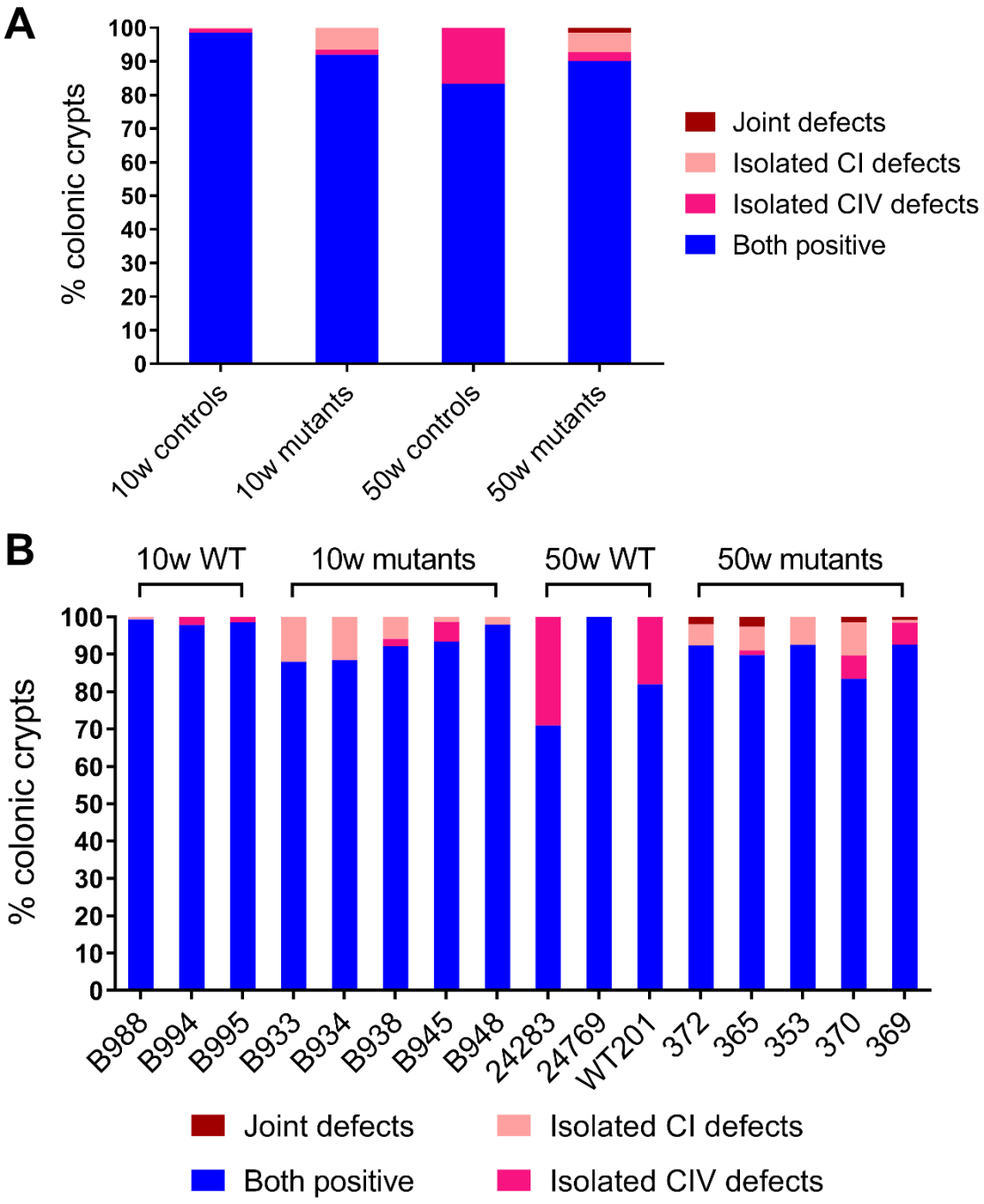

Figure 5.13 Absolute OXPHOS level in the colonic crypts of the (A) grouped and (B) individual 10-week and 50-week $tRNA^{Ala}$ mutant and wild-type mice. OXPHOS defect was classified into "both complex I and complex IV positive", "isolated complex I defective", "isolated complex IV defective" and "joint complex I and IV defective". Z-scores of the absolute complex I/IV level below "-2.6" was defined as defects in the complex I and IV. The 10-week mutant mice include B933, B934, B938, B945 and B952 with 79%, 77%, 77%, 74% and 71% m.5024C>T in the ear respectively. The 50-week mutants include 372, 365, 353, 370 and 369 with 80%, 79%, 73%, 73% and 71% m.5024C>T in the ear respectively.

The percentage of the OXPHOS-defective crypts in the 10-week mutants was correlated with the m.5024C>T heteroplasmy level in the three-week ear notch (presumed initial mutation load) ($p = 0.03$, $r_s = 0.975$, Spearman's rank correlation) (Figure 5.13B and Figure 5.14A). However, such a correlation was not found in the 50-week mutants ($p = 0.43$, Spearman's rank correlation) (Figure 5.13B and Figure 5.14B). Additionally, no correlation between the percentage of the OXPHOS-deficient crypts and the crypt heteroplasmy level was found in the 10-week, the 50-week mutants and the pooled mice of both age groups.

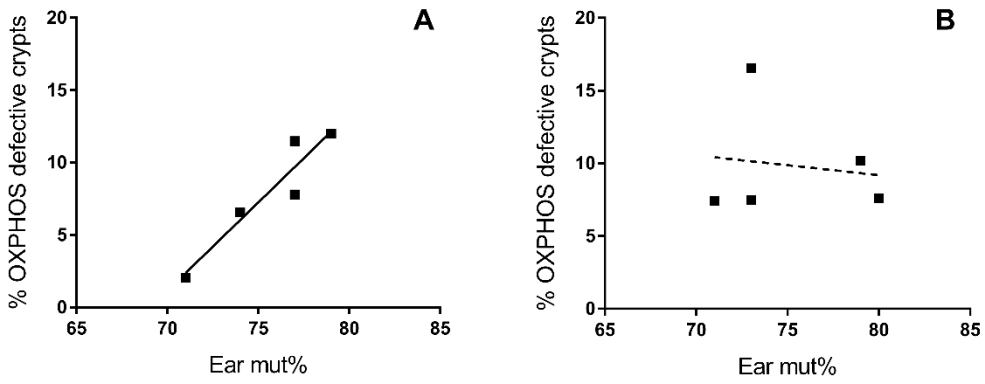

Figure 5.14 Correlation between the percentage of the OXPHOS-defective crypts and the m.5024C>T heteroplasmy level in the ear notch obtained at 3 weeks in the (A) 10-week and (B) 50-week $tRNA^{Ala}$ mutant mice. The percentage of the OXPHOS defective crypts was the pooled data of the "isolated complex I/IV defective" and the "joint complex I and IV defective". Each square represents an individual mutant mouse. Full line, $p = 0.03$; dotted line, $p = 0.43$, Spearman's rank correlation.

5.4.3 Quantification of relative levels of RC complexes to mitochondrial mass

5.4.3.1 Complex I level relative to mitochondrial mass

Defects in RC complexes caused by inherited mtDNA mutations are often associated with mitochondrial proliferation (Egger *et al.*, 1981; DiMauro *et al.*, 1985; Moraes *et al.*, 1992). To date, it is still unknown whether cellular function is affected by the total amount of RC complex proteins or the level relative to mitochondria mass in a cell. Thus, it is important to investigate the relative level of RC complexes against mitochondrial mass (MM). Tom20 is a nuclear-encoded peripheral subunit of the TOM (translocase of the outer mitochondrial membrane) complex for mediating the transportation of nuclear-encoded proteins into mitochondria (Yamano *et al.*, 2008; Yamamoto *et al.*, 2011), which is often used as a mitochondrial mass marker (Jourdain *et al.*, 2013; Contino *et al.*, 2017). Immunofluorescent co-labelling the RC complexes with the Tom20 antibody demonstrated a relative complex I deficiency in the colonic epithelium of the mutants in both age groups, and it was more pronounced in the 50-week mutants compared with the 10-week mutants (Figure 5.7 CI & Tom20 panel). Z-scores of the level of complex I/IV against Tom20 were calculated and categorised (specified in 5.3.3). Categorical data showed a slightly higher percentage of the crypts with relative complex I deficiency in the 50-week mutants (13.21% CI-negative and 4.99% CI intermediate-negative crypts) compared with the 10-week mutants (10.00% CI-negative and 6.27% CI-intermediate-negative) (Figure 5.15A). However, the median complex I level in the colonic epithelium of the 50-week mutants was slightly higher than that in the 10-week mutants (median difference = 0.26) (Figure 5.15A). These analyses revealed more crypts with relative complex I deficiency to MM (Figure 5.15) rather than the absolute deficiency (Figure 5.8) in the $tRNA^{Ala}$ mutant mice; however, they showed no pronounced difference in the relative complex I level between the 10-week and 50-week $tRNA^{Ala}$ mutant mice.

Data of the relative complex I level in individual mice is summarised in Figure 5.16. Modelling of the data showed a stronger linear relationship between the relative complex I level and the ear heteroplasmy in the colonic epithelium of the 10-week mutants ($r = 0.394$, $p < 0.001$) compared with the 50-week mutants ($r = 0.102$, $p = 0.003$). The relative complex I level also had a negative linear correlation with the crypt heteroplasmy in both 10-week ($r = 0.125$, $p<0.001$) and 50-week ($r = 0.105$, $p=0.002$) $tRNA^{Ala}$ mutant mice, though the relationships were weak.

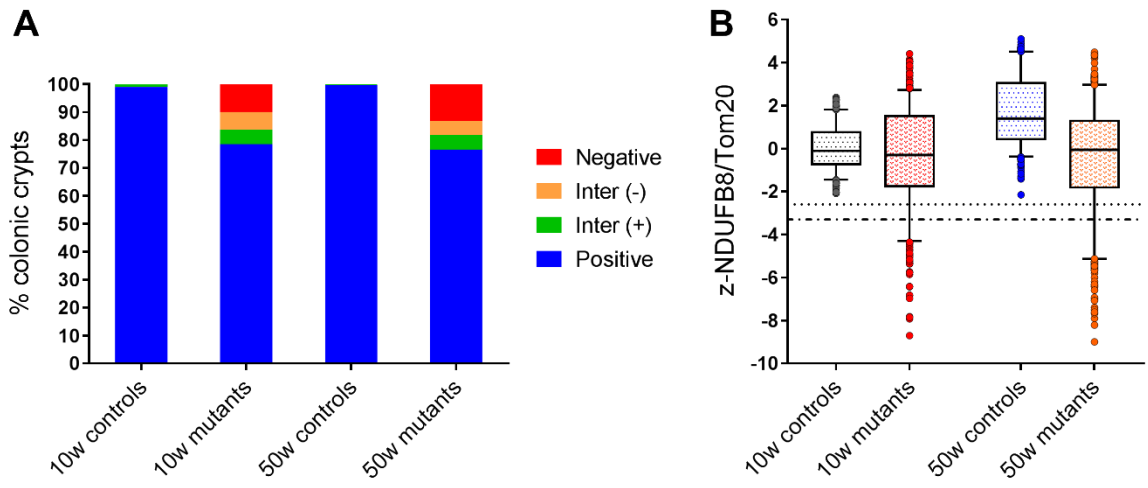

Figure 5.15 Respiratory chain complex I level (labelled by NDUFB8) relative to the mitochondrial mass (labelled by Tom20) in the colonic epithelium of the $tRNA^{Ala}$ mutant mice. (A) Categorical z-scores of the relative complex I level in the 10-week and 50-week $tRNA^{Ala}$ mutants compared with the age-matched wild-type controls. The relative complex I level was classified as "positive", "intermediate positive", "intermediate negative" and "negative". The borders of the z-scores for each group is summarised in the Table 5.3. (B) Whisker-and-box plot of the z-NDUFB8/Tom20 showing the median and distribution of the relative complex I level in the colonic crypts in the mutants and controls. Each point signifies a measurement of a single crypt. The dotted lines are the boundaries for the categorisation of "intermediate negative" and "negative".

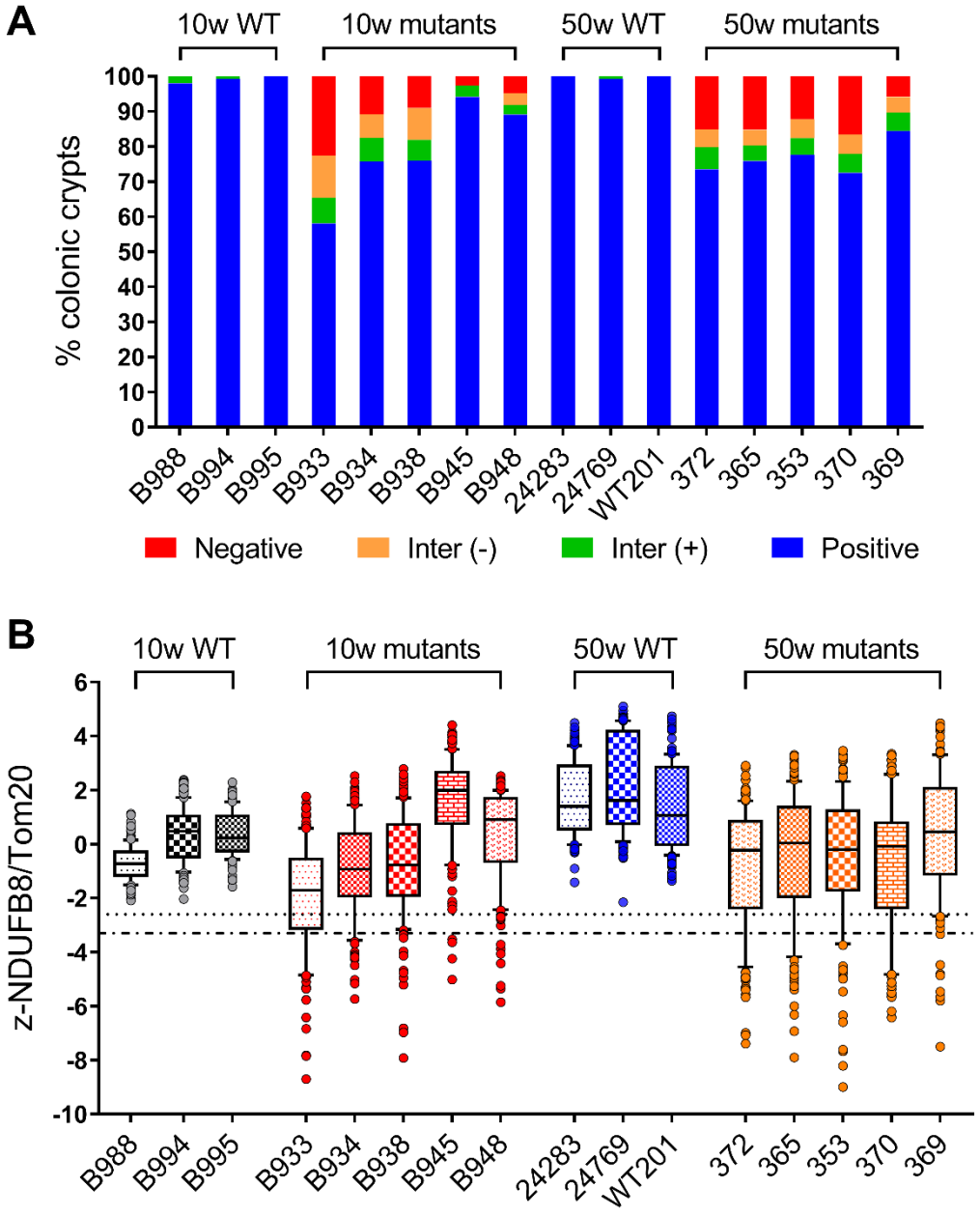

Figure 5.16 Relative complex I level to the mitochondrial mass in the intestinal crypts of individual tRNA^{Ala} mutant mice. (A) Categorical z-scores of the complex I level (marked by NDUFB8) relative to MM (marked by Tom20). Relative complex I level was categorised as "positive", "intermediate positive", "intermediate negative" and "negative". The borders for each category are summarised in the Table 5.3. (B) An overview of the continuous data showing the median and the distribution of the relative complex I level in the colonic epithelium. Each point is a read-out of a single crypt. The 10-week mutant mice include B933, B934, B938, B945 and B952 (79%, 77%, 77%, 74% and 71% m.5024C>T in the ear respectively). The 50-week mutants include 372, 365, 353, 370 and 369 (80%, 79%, 73%, 73% and 71% m.5024C>T in the ear respectively).

5.4.3.2 Complex IV level relative to mitochondrial mass

Although the absolute complex IV level (labelled by MTCO1 antibody) seemed not affected in the colonic epithelium of the $tRNA^{Ala}$ mutant mice on the image (Figure 5.7 complex IV panel), co-labelling with the mitochondrial mass marker Tom20 showed severe relative complex IV deficiency (crypts in orange) in the 50-week wild-type and mutant mice (Figure 5.7 CIV & Tom20 panel). Quantification of the z-MTCO1 against the Tom20 level revealed a decrease in the relative complex IV level with age, regardless of the genotype (Figure 5.17). Although the relative complex IV level was significantly reduced in the 50-week mutants (52.83% CIV-negative crypts) compared with the 10-week mutants (6.67% "negative") and even 50-week wild-type mice (18.35% "negative") (Figure 5.17A), the rate of the decrease with age was very similar between the wild-type and the $tRNA^{Ala}$ mutant mice (median difference (10 and 50 weeks) = 2.570 and 2.575 in the wild-type and mutant mice respectively).

Data from individual mice confirmed the findings of the grouped data (Figure 5.18). Modelling revealed that the relative complex IV level was inversely correlated with the ear heteroplasmy in the 10-week ($r = 0.152$, $p < 0.001$) but not the 50-week mutants. As with the relative complex I level, the relative complex IV level had similar weak linear relationships with the crypt heteroplasmy in the 10-week ($r = 0.131$, $p < 0.001$) and 50-week ($r = 0.126$, $p < 0.001$) $tRNA^{Ala}$ mutant mice.

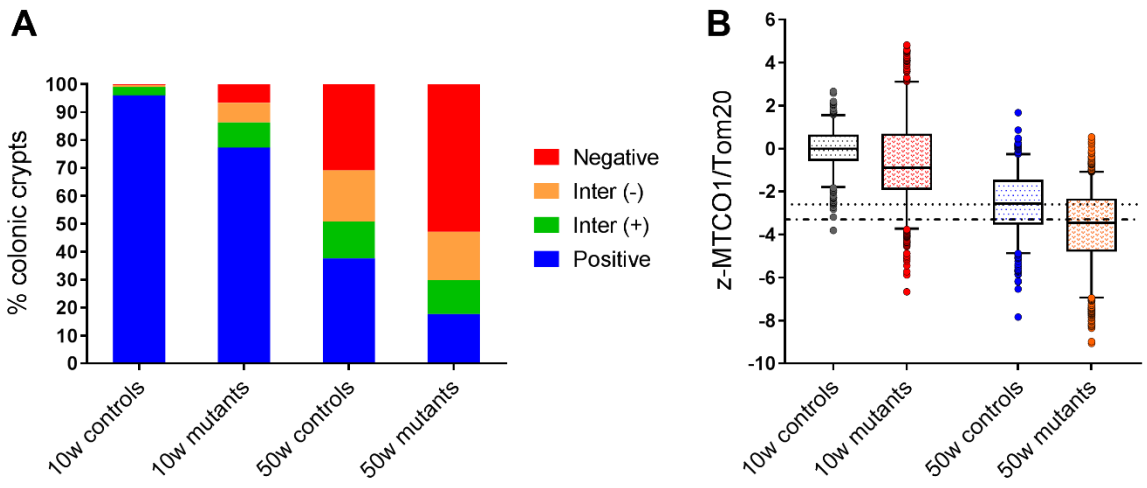

Figure 5.17 Respiratory chain complex IV level (labelled by MTCO-1) relative to the mitochondrial mass (labelled by Tom20) in the colonic crypts of the 10-week and 50-week $tRNA^{Ala}$ mutant and control mice. (A) Categorical z-scores of the relative complex IV level in the $tRNA^{Ala}$ mutants and the age-matched wild-type controls. The relative complex IV level was categorised as "positive", "intermediate positive", "intermediate negative" and "negative". The borders of the z-scores for each category are summarised in the Table 5.3. (B) Whisker-and-box plot of the z-MTCO1 against Tom20 level showing the median and distribution of the relative complex IV level in the colonic crypts in the mutants and controls. Each point signifies a measurement of a single crypt. The dotted lines are the boundaries for the categorisation of "intermediate negative" and "negative".

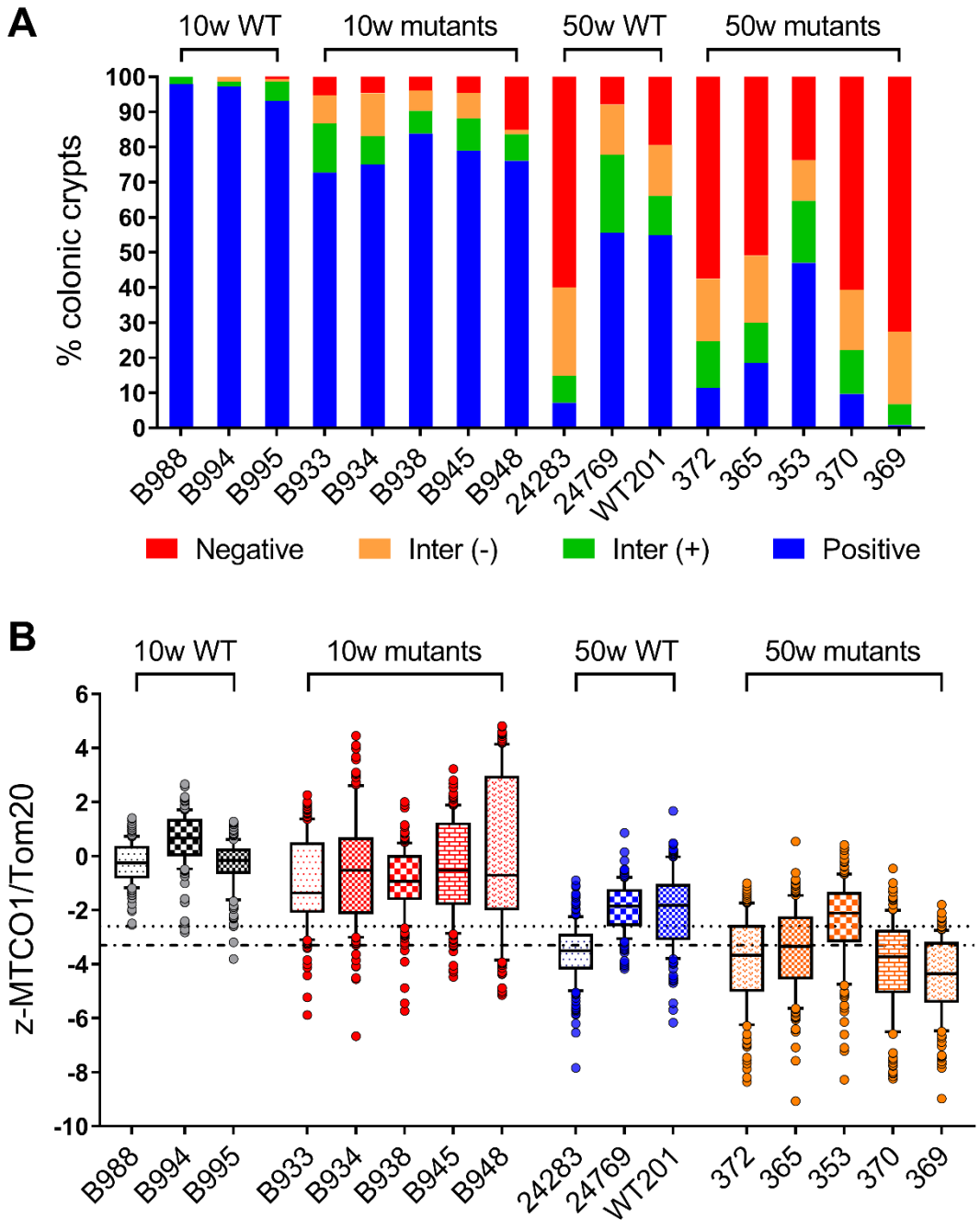

Figure 5.18 Relative complex IV level (labelled by MTCO1) to MM (labelled by Tom20) in the colonic epithelium of individual mouse. (A) Categorical data of z-MTCO1/Tom20. Relative complex IV level was classified as "positive", "intermediate positive", "intermediate negative" and "negative". The limits for each category are summarised in the Table 5.3. (B) An overview of the continuous z-MTCO1/Tom20 showing the median and the distribution of the relative complex IV level in the colonic crypts. Each point is a measurement of a single crypt. The 10-week mutant mice include B933, B934, B938, B945 and B952 (79%, 77%, 77%, 74% and 71% m.5024C>T in the ear respectively). The 50-week mutants include 372, 365, 353, 370 and 369 (80%, 79%, 73%, 73% and 71% m.5024C>T in the ear respectively).

5.4.3.3 OXPHOS level relative to mitochondrial mass

The immunofluorescent images revealed some crypts with normal complex IV level (Figure 5.7 complex IV panel) having a joint complex I and complex IV deficiency relative to mitochondrial mass in the 50-week mutants (yellow circles in Figure 5.7). Therefore, I further extensively investigated the OXPHOS level relative to the MM in the colonic epithelium of the $tRNA^{Ala}$ mutant mice. Z-scores of the relative complex I and CIV level against Tom20 were plotted in Figure 5.19. The crypts in the 10-week mutants mostly had relative complex I deficiency (top left sector), whereas crypts in the 50-week mutants were dominated by relatively isolated complex IV deficiency (bottom right sector) and joint defects in complex I and IV (bottom left sector) (Figure 5.19). The aged wild-type mice only had crypts with isolated complex IV deficiency (bottom right sector) (Figure 5.19). Quantification of the relative OXPHOS level to MM revealed an increase in the isolated complex IV defect with age in the colonic crypts of both wild-type and mutant mice (Figure 5.20). Isolated complex I defect was the main type of OXPHOS defect in the 10-week mutants, whereas the isolated complex IV defect prevailed in the crypts in the 50-week mutants (Figure 5.20). A decrease in the proportion of isolated complex I defective crypts was observed in the mutant mice with age, which was concomitant with an increase in the proportion of crypts with joint defects in the RC complexes (Figure 5.20). The relative OXPHOS deficiency was not correlated with the ear and the crypt heteroplasmy in either 10-week or 50-week $tRNA^{Ala}$ mutants, possibly because of the small sample size for this specific analysis method without modelling.

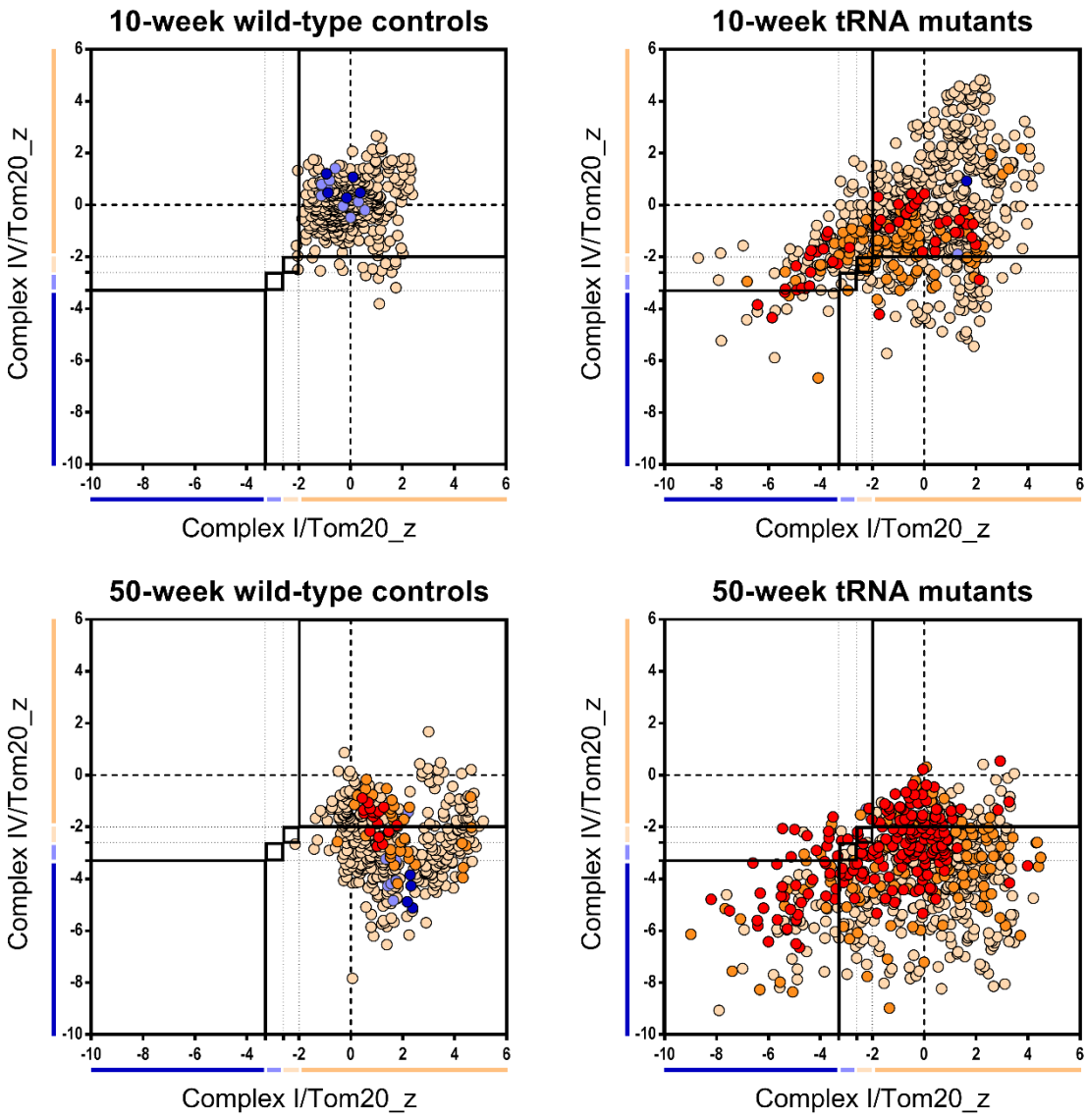

Figure 5.19 Profiles of the OXPHOS level relative to mitochondrial mass (marked by Tom20) in colonic epithelium of the 10-week and 50-week $tRNA^{Ala}$ mutant and wild-type mice. Z-scores of the relative complex I level to Tom20 (horizontal axis) was drawn against the z-scores of the relative complex IV level (vertical axis). The colour indicates the categorisation of the MM level: “very high” in red, “high” in orange, “normal” in beige, “low” in light blue and “very low” in blue. The borders for grouping is summarised in Table 5.3. Each dot is data of an individual crypt.

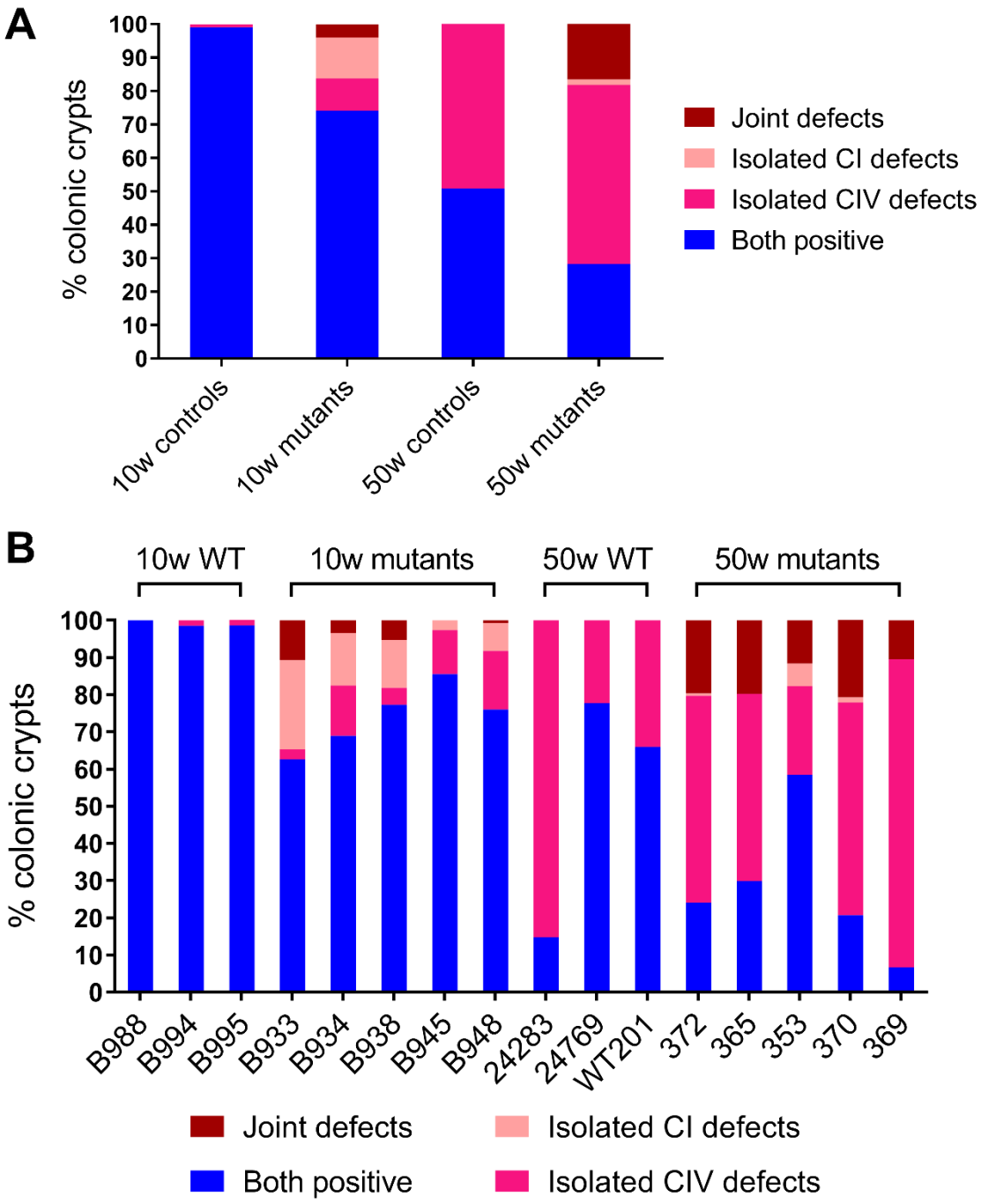

Figure 5.20 Relative OXPHOS deficiency in the colonic epithelium of the (A) grouped and (B) individual 10-week and 50-week $tRNA^{Ala}$ mutant and wild-type mice. Relative OXPHOS defect was categorised into "both complex I and IV positive", "isolated complex I defective", "isolated complex IV defective" and "joint complex I and IV defective". The z-scores of the complex I/IV relative to MM below "-2.6" was defined as defects in the RC complex I/IV. The 10-week mutant mice included in this study were B933, B934, B938, B945 and B952 with 79%, 77%, 77%, 74% and 71% m.5024C>T in the ear notch obtained at 3 weeks respectively. The 50-week mutants were 372, 365, 353, 370 and 369 with 80%, 79%, 73%, 73% and 71% m.5024C>T in the ear notch respectively.

5.4.4 Level of mitochondrial mass in colonic crypts

The immunofluorescence images and the OXPHOS profiles have shown a significant increase in the mitochondrial mass (marked by Tom20) in the colonic epithelium of the 50-week $tRNA^{Ala}$ mutants and a mild increase in the 10-week mutants and 50-week wild-type mice (Figure 5.7 Tom20 panel and Figure 5.12). Pixel intensity of the Tom20 channel was quantified and transformed into z-scores, which were grouped into "very low", "low", "normal", "high" and "very high" based on the approximate 95% and 99% confidence level (detailed in 5.3.3). Further quantification of the Tom20 z-scores demonstrated an increase in the percentage of the crypts with a high level of mitochondrial mass with age in both $tRNA^{Ala}$ mutant and wild-type mice (Figure 5.21A). The $tRNA^{Ala}$ mutants had a larger proportion of crypts with high mitochondrial mass than the age-matched wild-type controls at both 10 weeks and 50 weeks (Figure 5.21A). The categorical results were then confirmed by the distribution data (Figure 5.21B). A significant interaction was found between the mouse genotype and age, showing a more rapid increase in the Tom20 level in the $tRNA^{Ala}$ mutants compared with wild-types with age ($p < 0.001$, two-way ANOVA).

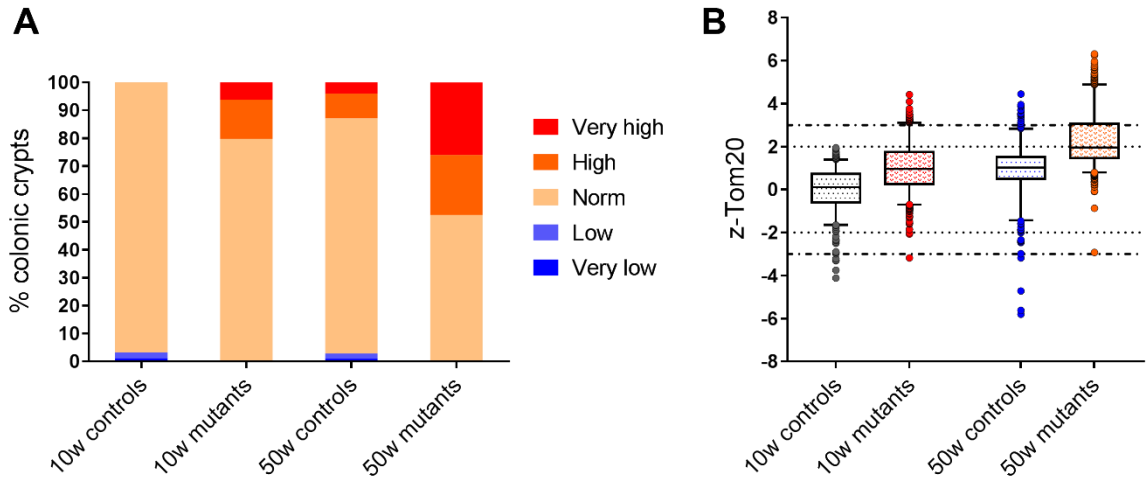

Figure 5.21 Level of the mitochondrial mass (labelled by Tom20) in the colonic crypts of the grouped 10-week and 50-week $tRNA^{Ala}$ mutant and wild-type mice. (A) Categorical z-scores of the Tom20 level in the 10-week and 50-week $tRNA^{Ala}$ mutants compared with the age-matched wild-type controls. The tom20 level was classified as "very high", "high", "normal", "low" and "very low". The boundaries of the z-scores for each group is summarised in the Table 5.3. (B) Whisker-and-box plot of the Tom20 z-scores showing the median and distribution of the MM level in the colonic crypts. Each point denotes a measurement of an individual crypt. The dotted lines are the boundaries of the categories.

Individual mouse analysis showed a consistent and pronounced increase in the Tom20 level in all 50-week mutants with approximately a half of the crypts having elevated mitochondrial mass (Figure 5.22A), which was significantly higher compared with the 10-week tRNA mutants (Figure 5.22). Of note, one aged wild-type mouse (24769) showed a marked mitochondrial proliferation (Figure 5.22), and it was the only mouse with no absolute complex IV deficiency in the aged wild-type group, suggesting a protective effect of mitochondrial proliferation during ageing (Figure 5.11).

Modelling of the data showed that Tom20 had a positive correlation with the crypt heteroplasmy in the 10-week mutants ($r = 0.130$, $p < 0.001$) but a negative correlation in the 50-week mutants ($r = 0.049$, $p = 0.018$). No correlation was found between the level of Tom20 in the colonic epithelium with the ear heteroplasmy in the 10-week mutants ($p = 0.933$). Whereas in 50-week mutants, Tom20 was negatively correlated with the heteroplasmy level in the ear ($r = 0.126$, $p < 0.001$). However, all these correlations were very weak as shown by the small r values, possibly due to the small sample size or due to the closeness of the heteroplasmy level between the examined mice.

The level of Tom20 was positively correlated with the absolute level of complex I in the colonic epithelium of all examined mice ($p < 0.0001$ in wild-type controls; $p = 0.028$ and 0.021 in 10-week and 50-week mutants respectively, Pearson correlation) (Figure 5.23A). The correlation was stronger in the wild-type mice compared with the mutants at both 10 weeks and 50 weeks but was similar within the same genotype ($r = 0.569$ and 0.479 in 10-week and 50-week wild-type mice; $r = 0.080$ and 0.084 in the mutants at 10 weeks and 50 weeks) (Figure 5.23A). The level of Tom20 was also positively correlated with the absolute level of complex IV in all mice ($p < 0.0001$ in all mouse groups, Pearson correlation), which was overall stronger than its correlation with complex I level (Figure 5.23). The correlation in the wild-type mice was stronger than the mutants in both age groups, and was slightly stronger at 50 weeks than 10 weeks within the same genotype ($r = 0.790$ and 0.827 in 10-week and 50-week wild-types; $r = 0.268$ and 0.438 in mutants at 10 weeks and 50 weeks) (Figure 5.23B).

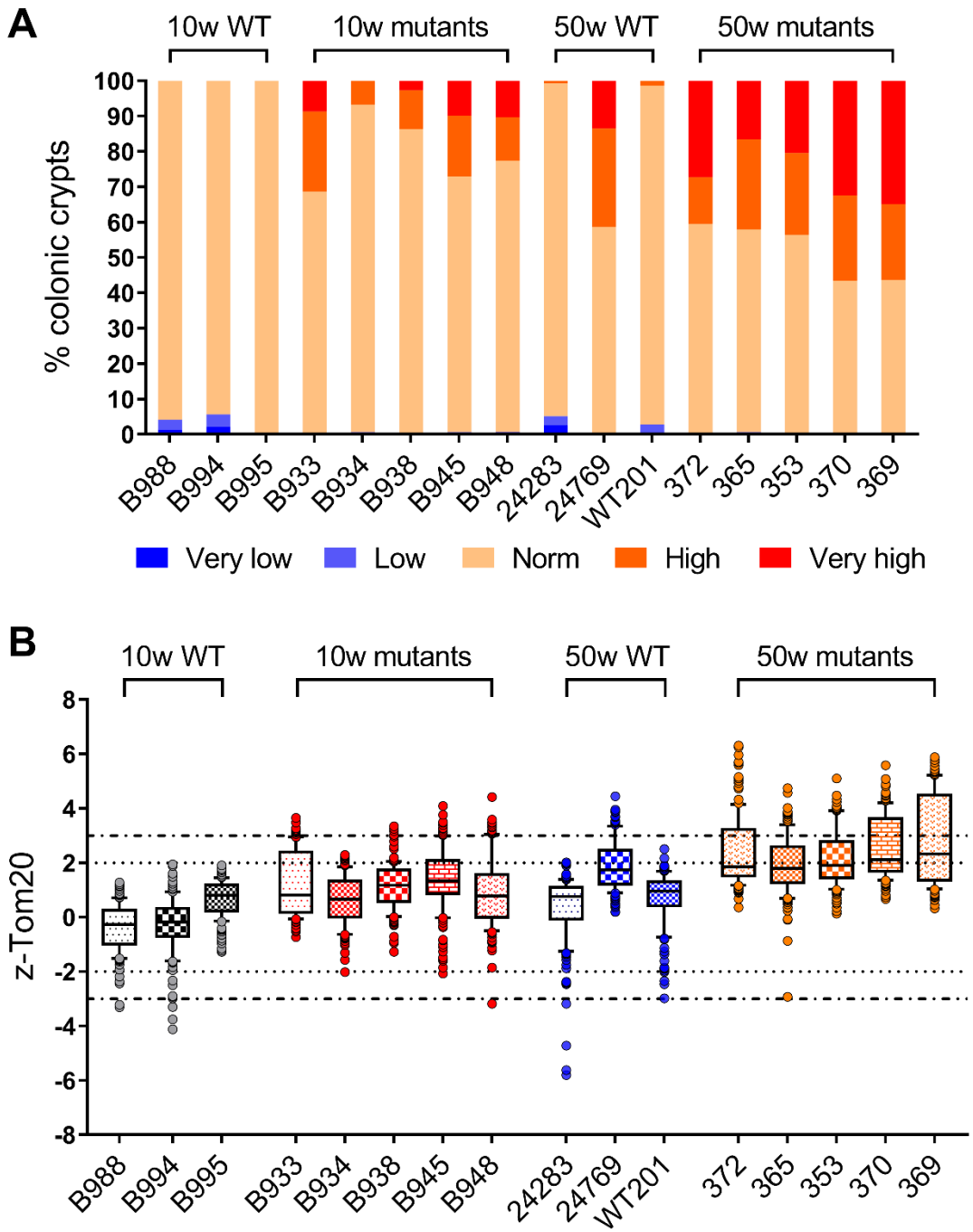

Figure 5.22 Mitochondrial mass level (labelled by Tom20) in the colonic epithelium in individual 10-week and 50-week $tRNA^{Ala}$ mutant and wild-type mice. (A) Categorical z-scores of Tom20 level. Tom20 level was categorised as “very high”, “high”, “normal”, “low” and “very low”. The limits for each category is summarised in the Table 5.3. (B) An overview of z-Tom20 showing the median and the distribution of the MM level. Each point represents a measurement of an individual crypt. The 10-week mutants, B933, B934, B938, B945 and B952 (79%, 77%, 77%, 74% and 71% m.5024C>T in the ear respectively) and the 50-week mutants, 372, 365, 353, 370 and 369 (80%, 79%, 73%, 73% and 71% m.5024C>T in the ear respectively) were included in this study. The dotted lines are the boundaries for the classification of the z-Tom20.

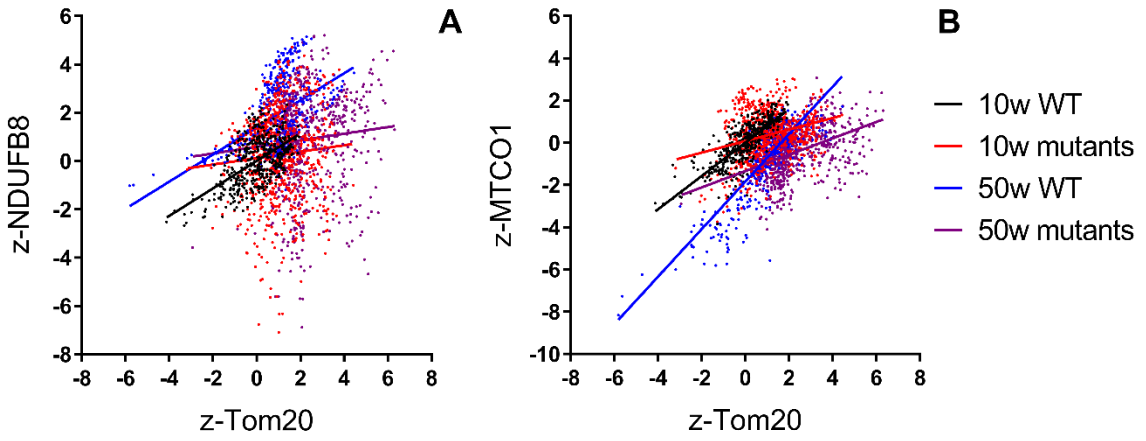

Figure 5.23 Linear relationships between the level of Tom20 and absolute (A) complexes I and (B) IV in the colonic crypts of the 10-week and 50-week wild-type and $tRNA^{Ala}$ mutant mice. (A) Equations for the linear relationship: 10-week wild-types, Y = 0.5685*X - 7.164e-00, R^2 = 0.323; 10-week mutants, Y = 0.1328*X + 0.1172, R^2 = 0.006; 50-week wild-types, Y = 0.5611*X + 1.387, R^2 = 0.230; 50-week mutants, Y = 0.1367*X + 0.5841, R^2 = 0.007. (B) 10-week wild-types, Y = 0.7901*X + 3.437e-008, R^2 = 0.624; 10-week mutants, Y = 0.2733*X + 0.07519, R^2 = 0.072; 50-week wild-types, Y = 1.125*X - 1.849, R^2 = 0.683; 50-week mutants, Y = 0.3877*X - 1.343, R^2 = 0.192; Pearson correlation analysis. WT, wild-type.

5.5 Discussion

Mitochondrial DNA disease is characterised by tissue-specific heterogeneous phenotypes (Taylor and Turnbull, 2005). Investigating the effect of dynamics of mtDNA mutations on biochemical phenotypes of tissue is vital to the understanding of the progression of mtDNA disease. I have found a normal OXPHOS function correlating with a decreased mutation load in mitotic GI epithelium in comparison to the post-mitotic smooth muscle of patients with inherited m.3243A>G mutation (Chapter 3). However, this study is cross-sectional, due to limitations in obtaining human samples at multiple stages of lifespan. Consequently, it is unable to show the age-related change in heteroplasmy level and its outcome in mitotic tissue. The establishment of the $tRNA^{Ala}$ mutant mice with inherited m.5024C>T mutations allows me to screen tissue in animals at different ages. I have demonstrated a significant reduction in the mutation load in the mitotic intestinal epithelium of the old mutant mice compared with the young mutants (Chapter 4). To understand the biochemical effect of this decrease at the genetic level with age, in this study, I have characterised the OXPHOS function of the mitotic GI epithelium in the 10-week and 50-week mutant mice using sequential COX/SDH histochemistry and quantitative immunofluorescence assay. For the latter study, I have investigated the absolute level of RC complexes I and IV and relative level to a mitochondrial mass marker, Tom20, in the colonic epithelium of the mutant mice.

OXPHOS function is affected by the inherited m.5024C>T mutation in the intestinal epithelium of the mutant mice. This is indicated by a proportion of small intestinal crypts (< 30%) with defects in COX activity in the mutants with high ear mutation load. The immunofluorescence study of the absolute protein level of RC complexes then confirms that a maximum of 16.55% colonic crypts are OXPHOS-defective, with complex I deficiency predominating over complex IV deficiency. In comparison, no obvious OXPHOS deficiency has been found in the young wild-type controls, suggesting that the OXPHOS deficiency in the mutants is caused by inherited m.5024C>T mutation. Isolated complex I defect is the main biochemical phenotype in the young mutants, in which I detect no crypts with joint defects in complexes I and IV, but the latter becomes evident with age. I have also detected a complex IV defect with no complex I deficiency in the old wild-type mice, suggesting that complex IV is more sensitive to ageing than complex I in the colonic crypts. This is in accordance with human studies showing that a vast majority of colonic crypts have isolated complex IV deficiency and joint defects in complex IV and other complexes in ageing humans, whereas only a small proportion of colonic crypts have isolated complex I deficiency (Greaves *et al.*, 2010).

In the young mutants, the level of OXPHOS defect is correlated with mutation load in the ear sampled at 3 weeks, a reference of initial mutation level, where mice with high ear heteroplasmy have a high level of OXPHOS deficiency in the colonic epithelium, indicating the pathogenicity of the m.5024C>T mutation. Such correlation is substantially weakened in the old mutants, suggesting a loss of influence of the initial mutation load on OXPHOS function in the colonic epithelium with age. On the contrary, I found a stronger correlation between the crypt heteroplasmy and the absolute level of RC complexes I and IV in the old mutants than that in the young mutants, suggesting an increase in the correlation between the expression of RC complexes and in situ tissue heteroplasmy with age. The results discussed above suggest that the OXPHOS level is closely correlated with inherited m.5024C>T mutation and is a good reflection of the variation in the heteroplasmy level in this mouse model.

OXPHOS defects, in particular, defects in complexes I and IV, increase in tissue with age due to accumulated somatic mtDNA mutations (Taylor *et al.*, 2003; Greaves *et al.*, 2010). In contrast, I found no difference in the COX activity between the young and old mutants in the small intestinal epithelium, which is consistent with the previous finding of COX function in the colonic epithelium (Baines, 2014). In addition, the absolute protein level of RC complexes did not decrease with age in the colonic epithelium of the $tRNA^{Ala}$ mutant mice. On the contrary, the absolute complex I level slightly increased in the old mutants compared with the young mutants. This is consistent with the decrease in the mutation load of inherited m.5024C>T mutation in the intestinal epithelium (Chapter 4). In addition, in comparison to the pronounced complex IV deficiency in the colonic crypts of the ageing wild-type mice, the $tRNA^{Ala}$ mutant mice barely had any crypts with absolute complex IV deficiency, suggesting that the $tRNA^{Ala}$ mutant mice might have a response to the inherited m.5024C>T mutation that has a protective effect which maintains OXPHOS function during ageing. This is in contrast to some studies where different breeding strategies of mtDNA-mutator mice were used to show that maternally transmitted mtDNA mutations play a synergistic role with the accumulation of somatic mtDNA mutations during ageing, which aggravate the deterioration of the phenotypes of the mitotic (colon and testis) and post-mitotic (heart and brain) tissue (Ross *et al.*, 2013). However, these maternally transmitted mtDNA mutations were low levels of miscellaneous pathogenic and non-pathogenic mtDNA variants due to mtDNA mutagenesis of the mother mice (Ross *et al.*, 2013). Whereas inherited mtDNA mutations that cause mtDNA diseases are specific mutations that are at a high level in symptomatic patients

(Craven *et al.*, 2017). It is possible that a high mutation load is needed at the beginning to trigger the protective mechanism.

Furthermore, I found a significantly elevated level of mitochondrial mass (labelled by Tom20) in the $tRNA^{Ala}$ mutant mice compared with the wild-type controls. Although age has an effect on upregulating MM in both mutant and wild-type mice, it interacts with the mouse genotype. As a result, the protein level of Tom20 increased faster with age in the $tRNA^{Ala}$ mutants than in the wild-type mice. Tom20 is a common mitochondrial mass marker encoded by nuclear DNA, which is not directly affected by defects in mtDNA (Yamano *et al.*, 2008; Jourdain *et al.*, 2013). The level of MM reflects the dynamics of mitochondrial biogenesis and mitophagy. The increase in the MM in the colonic epithelium of the $tRNA^{Ala}$ mutant mice could be a compensatory response to the OXPHOS deficiency caused by inherited mtDNA mutations, but also could be a reflection of machinery that actively removes the inherited mtDNA mutations by regulating mitochondrial biogenesis and mitophagy. In addition, despite less OXPHOS defects in the old mutants compared with the wild-type mice, the level of MM is still markedly higher in the mutants compared with the wild-types, suggesting a role of mitochondrial proliferation relevant to inherited mtDNA mutations rather than a simple compensatory response to OXPHOS deficiency. The findings of MM here are consistent with the increased level of nuclear-encoded mitochondrial markers, COX4 and SDHA, in the gastrointestinal epithelium from patients with m.3243A>G mutation (Chapter 3).

The modelling has provided information about the correlations between the MM and different factors, such as the level of complexes I and IV and the heteroplasmy of ears and crypts in the young and old mice. Complex IV level is positively correlated with Tom20 in the mutants, accounting for the preserved absolute complex IV protein level in the mutants with the elevated MM. The correlation of the MM with the level of complex IV is much stronger than its correlation with the level of complex I, which explains why the level of complex IV rather than the complex I relative to the MM is significantly dropped with the elevation in the MM. The linear relationship between the level of RC complex expression is stronger in wild-type mice compared with the $tRNA^{Ala}$ mutants, indicated by the higher correlation coefficient and steeper gradient of the regression equation. This might be a reason why the MM significantly increased in the mutants if it is a compensatory response to defective RC complexes. As a smaller increase in the level of RC complexes is concomitant with an increase in the MM in the mutants compared with the wild-type mice, the mutant mice may have to produce more mitochondria to elevate the OXPHOS level compared with wild-type mice. With reference to complex IV, its correlation with MM is slightly stronger in the old mice compared with the

young mice, suggesting an increment in the influence of MM on complex IV with age. The correlation between MM and ear or crypt heteroplasmy is very weak, even if the modelling tremendously reduces the loss of information from the data. This may be because the MM is a secondary parameter, regardless of whether it is a compensatory response or operating machinery. There is no correlation between ear heteroplasmy and the level of Tom20 in the colonic epithelium of the young mice but a weak negative correlation in the old mutants. The level of MM is positively correlated with crypt heteroplasmy in the young mutants, suggesting that mitochondrial proliferation might increase in response to high in situ mutation load. Their correlation turns to negative, which might be a consequence of the above hypothesis. With age, crypts in which mitochondrial proliferation fails to elevate to contribute to removing the mutation will have higher mutation load. However, as correlations cannot reflex any causal relationship, there could be various interpretations of these results, and it should be careful to draw any conclusions.

5.5.1 Future work

One limitation of this study is that the GI samples are obtained via resection from different mice in the two age groups, making it a multiple cross-sectional study rather than a longitudinal study. In this case, measurements at different ages cannot be compared within each mouse directly, increasing the complexity of data analysis to reduce the variation between individual mice. Colonoscopy technique in live mice could be used in the future to acquire biopsies within individual mouse at different time points (Becker *et al.*, 2007), which would facilitate the dynamic screening of samples in all aspects.

Crypts with OXPHOS deficiency caused by accumulated somatic mtDNA mutation only occupy a few percents of the whole crypt population in middle-aged individuals, which become obvious at a very late stage of lifespan (Taylor *et al.*, 2003). In this study, I have only examined the 10-week and the 50-week mice. However, a minimum age of 18 months (~ 70 weeks) is considered senescence for mice (Dutta and Sengupta, 2016). Including old mice in further studies could possibly reveal a more obvious age-related change in the biochemical phenotype in the $tRNA^{Ala}$ mutants and a larger difference between the wild-type and mutant mice during ageing to benefit the understanding of the process of ageing and mtDNA disease.

In this study, I have correlated the m.5024C>T heteroplasmy in the intestinal epithelial homogenate with the overall biochemical defect in the colonic epithelium. It would be worthwhile to determine the heteroplasmy in individual crypts and correlate it with the protein level of RC complexes in the crypt to gain in-depth knowledge of the association between the mutation load and OXPHOS function and validate the biochemical threshold previously determined via sequential COX/SDH histochemistry. In addition, as I have only studied the heteroplasmy of the m.5024C>T mutation, there is still possibility that the biochemical defect in the 50-week $tRNA^{Ala}$ mutant mice is caused by the age-related accumulation of somatic mtDNA mutations. Thus, next-generation sequencing to screen the whole mtDNA genome would be necessary in the future work.

Although sequential COX/SDH histochemistry is irreplaceable for examining the enzyme activity of COX on tissue specimens, semi-quantification based on label colours is more subjective compared with quantitative immunofluorescence assay, especially for tissue with partial OXPHOS deficiency. In this study, the COX/SDH histochemical assay reveals numerous COX-defective cells in the fundic and pyloric epithelium of the stomach in the $tRNA^{Ala}$ mutant mice. The semi-quantification methodology for comparatively homogenous intestinal crypts would not be applicable to gastric units with heterogeneous cell components that naturally have distinct COX activity. In addition, for investigating whether the difference

in the mutation load between the fundic and pyloric epithelium can cause any difference in the OXPHOS function, due to the cell components and structure of the two types of gastric units, it would be inappropriate to compare the number of COX-deficient cells directly. As discussed above, quantitative immunofluorescence or western blot would be a more stringent technique for determination of the OXPHOS function in the gastric epithelium and should be employed in the further study.

This study has shown elevated mitochondrial proliferation in the colonic epithelium of the $tRNA^{Ala}$ mutant, which is correlated with the OXPHOS level in crypts, suggesting a change in mitochondrial biogenesis and quality control. mtDNA copy number is also an index of these processes (Lee and Wei, 2005). It is worthy of investigating the level of mtDNA copy number and its association with OXPHOS level in intestinal crypts of the mutants. Fluorophore labelled individual crypts whose OXPHOS level are determined could be laser-microdissected for the further determination of mtDNA copy number by real-time PCR (Phillips *et al.*, 2014). In addition, it is also important to investigate mitochondrial biogenesis and mitophagy individually and their relationship with OXPHOS level by co-labelling immunofluorescence markers for mitochondrial biogenesis, e.g. PCG-1 alpha (Fernandez-Marcos and Auwerx, 2011), and mitophagy, e.g. Parkin and PINK1 (McWilliams and Muqit, 2017), with markers for RC complexes.

This study reveals a difference in the absolute protein level of RC complexes and relative level of RC complexes to mitochondrial mass in the colonic crypts of the $tRNA^{Ala}$ mutant particularly when the mice age. However, their effect on cellular function is unknown. It would be intriguing to investigate this by comparing the functionality of cells in intestinal crypts with normal absolute and relative OXPHOS level, those with normal absolute OXPHOS level but low relative level and those with low absolute and relative level.

5.6 Conclusions

In this study, I have characterised the OXPHOS function in the gastrointestinal epithelium of the $tRNA^{Ala}$ mutant mice. I have found an OXPHOS deficiency in the intestinal crypts of the mutants caused by the inherited m.5024C>T mutation, which maintains or slightly improves with age. This is in accordance with the age-related decrease in the mutation load in the intestinal crypts of the $tRNA^{Ala}$ mutants with age but in contrast to the deterioration of OXPHOS deficiency in wild-type controls. In addition, I have found an increase in mitochondrial proliferation in the mutants compared with the wild-type controls, which interacts with age and correlates with the protein level of RC complexes I and IV. These findings prove that the $tRNA^{Ala}$ mutant mice can be a good animal model for investigating the mechanism underpinning the age-related selective loss of inherited mtDNA mutations and suggest that this process might be associated with mitochondrial biogenesis and quality control.

Chapter 6 Investigating the cellular mechanism underlying the selective loss of inherited mtDNA mutations in the intestinal epithelium

6.1 Introduction

I have previously shown in Chapter 2 that the turnover of stem cell progenies may affect the rate of age-related selective loss of the inherited m.5024C>T mutation in the gastrointestinal epithelium of $tRNA^{Ala}$ mutant mice. Cell turnover is determined by cell proliferation and cell death, particularly apoptosis, the delicately programmed suicide of cells (Pellettieri and Alvarado, 2007). Mitochondria contribute to a variety of cellular and metabolic events in addition to the generation of ATP, which is intimately involved in the regulation of cell proliferation and apoptosis (Tait and Green, 2010; Antico Arciuch *et al.*, 2012; Lopez and Tait, 2015; Salazar-Roa and Malumbres, 2017). Mutations in mtDNA can cause mitochondrial malformation and dysfunction, which can lead to dysregulated renewal of mitotic tissue. The age-related somatic mtDNA mutations can affect the turnover of stem cell progenies by indirectly affecting somatic stem cell function (Su *et al.*, 2018) or directly affecting the proliferation and apoptosis of the daughter cells (Nooteboom *et al.*, 2010; Fox *et al.*, 2012). In ageing humans, downregulated cell proliferation and upregulated apoptosis have been found in colonic crypts with OXPHOS deficiency caused by the accumulation of somatic mtDNA mutations, resulting in a loss of cell population in these crypts (Nooteboom *et al.*, 2010). The establishment of the progeroid mtDNA-mutator mouse model further confirms the effect of somatic mtDNA mutations on cell cycle and apoptosis in mitotic tissue (Kujoth *et al.*, 2005; Fox *et al.*, 2012). Studies have shown an elevated level of apoptosis in the small intestinal villi of mtDNA-mutator mice compared with wild-type mice (Kujoth *et al.*, 2005). In addition, abundant apoptotic cells are observed in crypts of the small intestine from mtDNA-mutator mice, where intestinal stem cells and transit-amplifying cells are located, which is rarely seen in wild-type mice (Fox *et al.*, 2012). Furthermore, studies report reduced DNA synthesis that compromises cell proliferation, and an altered cell cycle in the small intestinal crypts, concomitant with a compromised regeneration ability of isolated crypts in vitro and a deceleration of cell migration toward the tip of the villus (Fox *et al.*, 2012). These studies demonstrate that somatic mtDNA mutations can affect the proliferation and apoptosis of intestinal epithelial cells, resulting in abnormal cell turnover of the tissue.

Despite a body of research on the association between the somatic mtDNA mutations and apoptosis (Lin and Beal, 2006; Liu *et al.*, 2009), the study of the effect of disease-causing mitochondrial DNA mutations on apoptosis is still in its infancy. Relevant studies are chiefly concerned with and limited to post-mitotic muscles of patients harbouring large-scale

deletions and common mt-tRNA mutations, such as m.3243A>G and m.8344A>G mutations, and the findings are in conflicts (Mirabella *et al.*, 2000; Ikezoe *et al.*, 2002; Umaki *et al.*, 2002; Auré *et al.*, 2006). Some reports show no sign of apoptosis in the muscle of the patients (Sciacco *et al.*, 2001), whereas others show enhanced apoptosis in the patients (Mirabella *et al.*, 2000; Ikezoe *et al.*, 2002; Umaki *et al.*, 2002; Auré *et al.*, 2006). In addition, the level of apoptosis seems to be mutation-specific, as in patients carrying point mutations in protein-encoding genes causing NARP and LHON, little to no apoptosis is found (Mirabella *et al.*, 2000). Some studies report that apoptosis primarily occurs in muscle fibres with RC deficiency and no difference in apoptosis is found between RRF and non-RRFs. In contrast, other studies report that apoptosis mainly occurs in muscle fibres with mitochondrial proliferation (Ikezoe *et al.*, 2002; Umaki *et al.*, 2002), irrespective of RC function (Auré *et al.*, 2006). One consistent finding is that the presence of apoptosis is associated with a high mutation load (Mirabella *et al.*, 2000; Auré *et al.*, 2006). Although these investigations were carried out on post-mitotic tissues, they suggest an association between apoptosis and disease-causing mtDNA mutations, and possible effects of the genetic and biochemical features of mtDNA diseases, including mutation load, OXPHOS defects and mitochondrial proliferation, on the level of apoptosis in tissue.

For mitotic cells, the studies on the impact of disease-causing mtDNA mutations on apoptosis are primarily in vitro, in either cybrid or patient fibroblasts (Geromel *et al.*, 2001; Liu *et al.*, 2009). Studies have shown that large-scale deletions (Liu *et al.*, 2004; Schoeler *et al.*, 2005; Lee *et al.*, 2006; Liu *et al.*, 2007), m.3243A>G (Liu *et al.*, 2004), m.8344A>G (Liu *et al.*, 2004) and point mutations in mtDNA protein-encoding genes (Geromel *et al.*, 2001; Danielson *et al.*, 2002; Carrozzo *et al.*, 2004; Ghelli *et al.*, 2008) cause oxidative stress in cells and predispose them to apoptosis. Despite no reports on apoptosis in fast-renewing mitotic tissue of patients with mtDNA disease, one study shows that in mice with high levels of large-scale deletions (Inoue *et al.*, 2000), enhanced apoptosis of dysfunctional spermatogenetic cells with RC defects leads to oligospermia and asthenozoospermia, resulting in male infertility of these mice (Nakada *et al.*, 2006). These studies have provided preliminary evidence that disease-causing mtDNA mutations can affect apoptosis of mitotic cells, which might lead to a reduced number and defective function of stem cell progenies.

As discussed above, the cell proliferation and apoptosis that regulate the turnover of mitotic tissue are closely associated with mitochondrial function and mtDNA mutations and might play a role in the selective loss of disease-causing mtDNA mutations.

6.2 Aims

This study aimed to determine whether cell proliferation and apoptosis of stem cell progenies are associated with the selective loss of inherited mtDNA mutations in mitotic tissue using the $tRNA^{Ala}$ mouse model. Specifically, this study aims to:

1. Determine whether there is any difference in the overall level of cell proliferation in the colonic crypts of 10-week and 50-week wild-type and $tRNA^{Ala}$ mutant mice, and ascertain whether there is any difference in cell proliferation within the crypts with different OXPHOS functions and levels of mitochondrial mass.
2. Determine the apoptosis level in the 10-week and 50-week colonic crypts of the $tRNA^{Ala}$ mutant mice in comparison to that in the wild-type controls.

6.3 Methods

6.3.1 Immunofluorescence and imaging

FFPE colon tissue of the $tRNA^{Ala}$ mutant mice was sectioned at a thickness of 4µm by myself for assay optimisation and by Anna Smith for the final experiments. Sections were deparaffinised, subjected to antigen retrieval and incubated in antibody cocktails (detailed in 2.8.2). Dewaxing timespan, antigen retrieval buffer and methodology, and antibody concentrations in the immunofluorescence assay were optimised for the formal experiment. Antibody combinations used in this study are shown in Table 6.1. Information about the antibodies and the optimised concentration thereof is summarised in Table 2.7 and Table 2.8. Five $tRNA^{Ala}$ mutant mice with high ear heteroplasmy (71% - 80%) and three wild-type controls at 10 weeks and 50 weeks were employed in this study, which is the same group of mice described in Chapter 5. For the study of cell proliferation, sections were counterstained using Hoechst to label the nuclei of cells in colonic crypts (described in 2.8.3). For the study of the apoptosis level, sections were counterstained with β-catenin, a cell surface marker, to facilitate the cell counting. For both studies, sections were co-labelled with the markers for the RC complex I (NDUFB8) and mitochondrial mass (Porin) to determine OXPHOS function in colonic epithelial cells. Sections were imaged using the Confocal Laser Microscope System in a z-stack fashion (detailed in 2.9.3).

Antibody combination for cell proliferation study		
Primary antibody	**Secondary antibody**	**Tertiary antibody**
Anti-NDUFB8 (ab110242)	Biotin-XX (A10519)	Streptavidin, Alexa Fluor 647 conjugate (S21374)
Anti-VDAC1 (ab14734)	Alexa Fluor 488 (A21141)	N/A
Anti-Ki-67 (#12202)	Alexa Fluor 546 (A11010)	N/A
Antibody combination for apoptosis study		
Primary antibody	**Secondary antibody**	**Tertiary antibody**
Anti-NDUFB8 (ab110242)	Biotin-XX (A10519)	Streptavidin, Alexa Fluor 405 conjugate S32351
Anti-TOM22 (ab57523)	Alexa Fluor 488 (A21131)	N/A
Anti-Caspase 3, active (cleaved) form (AB3623)	Alexa Fluor 546 (A11010)	N/A
Anti-β-catenin (sc-393501)	Alexa Fluor 647 (A21242)	N/A

Table 6.1 Antibody cocktails for the immunofluorescence assay in the studies of cell proliferation and apoptosis. EDTA was used as antigen retrieval buffer to obtain the optimal labelling effect of these antibodies. Details of the antibodies and their optimised concentrations are summarised in Table 2.7 and Table 2.8.

6.3.2 Image analysis

Z-stack images were incorporated for maximum intensity projection and pixel intensity of the markers for complex I and mitochondrial mass in each colonic crypt was measured as described in 2.9.3. Absolute and relative level of complex I is determined as z-scores (detailed in 5.3.3).

In the study of cell proliferation, the number of Ki-67 signals and nuclei (labelled by Hoechst) in each colonic crypt was manually counted. Non-specific binding of antibodies in the Ki-67 channel that were not overlapping with the signals of the nuclei were excluded (Figure 6.1). The level of cell proliferation in each crypt was defined as the percentage of proliferating cells, which is the number of Ki-67 positive nuclei over the number of Hoechst positive nuclei. In this situation, the integrity of the crypt structure is important. Therefore, counting was only performed on longitudinal crypts whose base and apex could be defined.

For quantifying the level of apoptosis, cells containing the signals of active caspase-3 were counted. The level of apoptosis was described by the number of signal-positive cells per hundred crypts. As apoptosis primarily occurs at the apex of a crypt, only longitudinal crypts with intact apical epithelium and apoptotic cells in these crypts were counted. Cells in the lumen were excluded.

6.4 Results

6.4.1 Cell proliferation and mouse genotype

Ki-67 is a common marker for proliferating cells for the reason that it is present in the nuclei of cells during all active phases of a cell cycle (G1, S, G2 and mitosis) but not in resting cells (G0) (Gerdes *et al.*, 1984; Scholzen and Gerdes, 2000). To determine whether the inherited m.5024C>T mutation combined with age has any effect on cell proliferation in the mitotic epithelium, I performed immunofluorescence on sections of colonic epithelium from the 10-week and 50-week wild-type and $tRNA^{Ala}$ mutant mice using markers for Ki-67 and DNA to label the proliferating cells and the nuclei respectively (Figure 6.1). In addition, I co-labelled the RC complex I and mitochondrial mass using antibodies against NDUFB8 and Porin to further study the association between the OXPHOS level, mitochondrial proliferation and cell proliferation (described in 6.4.2) (Figure 6.1). I then quantified the proportion of proliferating cells in individual colonic crypts of each mutant and compared it with that in the wild-type mice (6.3.2). Crypts were randomly selected regardless of the complex I level for the quantification to obtain an objective overall measure of the level of cell proliferation in each group. A total number of ~30 crypts in each group was examined with an approximately equal number of crypts selected in each mouse of each group. The overall percentage of the proliferating cells in individual crypts increased with age, irrespective of the genotype ($p = 0.022$, two-way ANOVA) (Figure 6.2A). However, no statistically significant difference in cell proliferation was found between the $tRNA^{Ala}$ and the wild-type genotype (Figure 6.2). The analysis of individual mice showed no difference in the percentage of proliferating cells in crypts of different mice within the same group based on the genotype and age, indicating consistency in counting (one-way ANOVA) (Figure 6.2B).

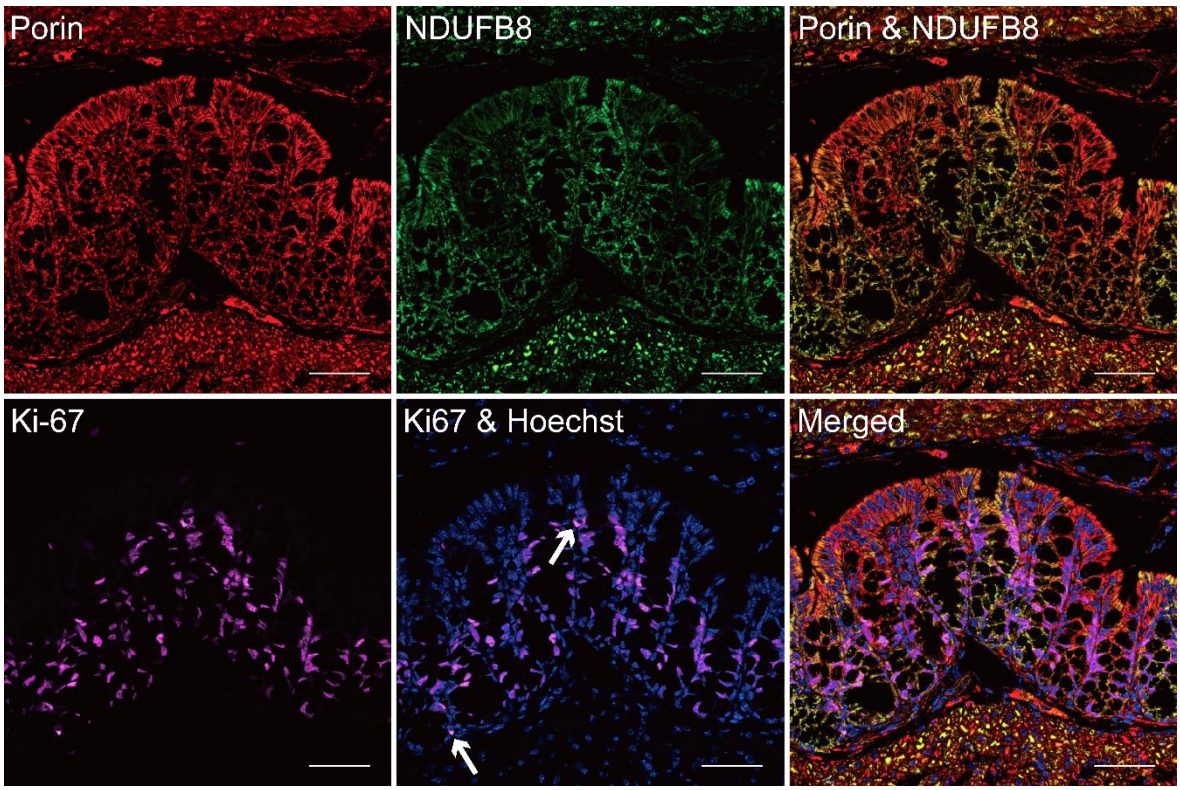

Figure 6.1 Representative immunofluorescence images for proliferating cells (Ki-67), RC complex I (NDUFB8), mitochondrial mass (Porin) and nuclei (Hoechst). Signals due to non-specific binding of the antibody at the Ki-67 channel that are not superimposed with nuclear labels were excluded from counting (white arrows). Scale bar = 50μm.

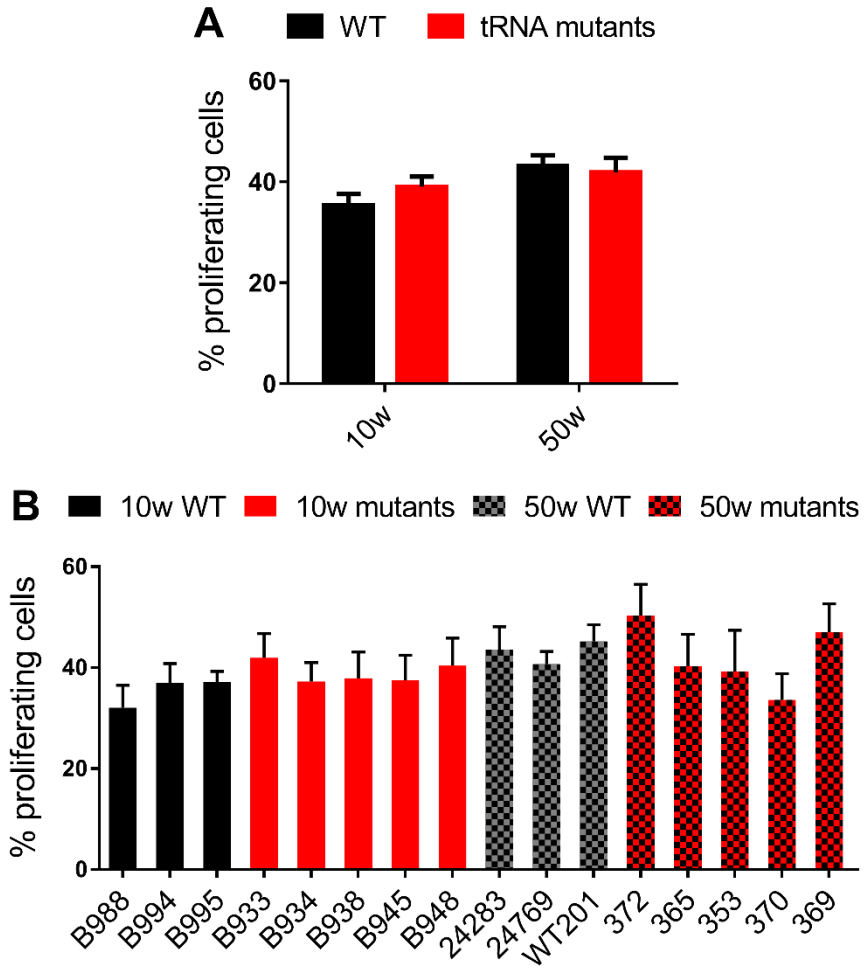

Figure 6.2 Cell proliferation level in the colonic crypts of (A) the grouped and (B) the individual 10-week and 50-week wild-type and $tRNA^{Ala}$ mutant mice. Five $tRNA^{Ala}$ mutant mice and three wild-type controls in each age group were examined. The level of cell proliferation is presented as the percentage of proliferating cells (the number of the Ki-67 immunofluorescence signals / the number of the nucleus signals). (A) n (10-week wildtypes) = 30, n (10-week mutants) = 31, n (50-week wildtypes) = 30, n (50-week mutants) = 25. (B) The 10-week mutant mice, B933, B934, B938, B945 and B952 carried 79%, 77%, 77%, 74% and 71% m.5024C>T in the ear respectively. The 50-week mutants, 372, 365, 353, 370 and 369 carried 80%, 79%, 73%, 73% and 71% m.5024C>T in the ear respectively. The number of crypts analysed: n (B988) = 10, n (B994) = 10, n (B995) = 10, n (B933) = 7, n (B934) = 7, n (B938) = 6, n (B945) = 6, n (B948) = 5, n (24283) = 10, n (24769) = 10, n (WT201) = 10, n (372) = 5, n (365) = 7, n (353) = 4, n (370) = 5 and n (369) = 4.

6.4.2 Cell proliferation, OXPHOS level and mitochondrial mass

6.4.2.1 Cell proliferation and absolute complex I

In colonic crypts of ageing humans, OXPHOS deficiency caused by the accumulation of somatic mtDNA mutations is associated with decreased cell proliferation and increased apoptosis (Nooteboom *et al.*, 2010). To investigate the effect of OXPHOS deficiency caused by the inherited m.5024C>T mutation with age on cell proliferation in colonic crypts, I measured the absolute protein level of complex I (CI) in individual colonic crypts of the $tRNA^{Ala}$ mutant mice and investigated the cell proliferation level in crypts with different absolute CI levels. The raw data of the measurement was transformed into z-scores using the data of the 10-week wild-type mice as the control group, and categorised into "positive", "intermediate positive", "intermediate negative" and "negative" according to the 95%, 99% and 99.9% confidence levels (detailed in Chapter 5). In line with the data in Chapter 5, quantification of the CI level showed CI defects in mutants but not in wild-type controls; and that the proportion of colonic crypts with CI deficiency slightly decreased in the 50-week mutants compared with the 10-week mutants, suggesting an improvement of the OXPHOS phenotype. In this study, only the "positive" and "negative" groups were included to increase the power of comparison. The percentage of proliferating cells in approximately 60 CI-positive crypts and 15 CI-negative crypts in each age group were analysed. No significant difference in the level of cell proliferation was found between the crypts with different OXPHOS classifications at either 10 weeks or 50 weeks (two-way ANOVA) (Figure 6.3A). The CI-positive crypts appeared to have a higher level of cell proliferation than the CI-negative crypts in the 50-week $tRNA^{Ala}$ mutant mice, but it is not statistically significant (Figure 6.3A). No correlation was found between the proportion of proliferating cells and the absolute complex I level in either wild-type or mutant mice at 10 nor 50 weeks ($p > 0.05$, Pearson correlation test). However, the analysis revealed a markedly increased cell proliferation in the CI-positive crypts at 50 weeks compared with that at 10 weeks ($p = 0.006$, two-way ANOVA) (Figure 6.3A). Due to the mild OXPHOS phenotype of the $tRNA^{Ala}$ mutant mice, there were only a limited number of crypts with absolute complex I deficiency in the images taken. For individual analysis, the data of one 10-week mutant and one 50-week mutant that contain ≥ five CI-negative crypts in each were analysed. Despite a trend showing a higher level of cell proliferation in the CI-positive crypts compared with the CI-negative crypts in each mouse, it was not statistically significant ($p > 0.05$, unpaired t-test) (Figure 6.3B).

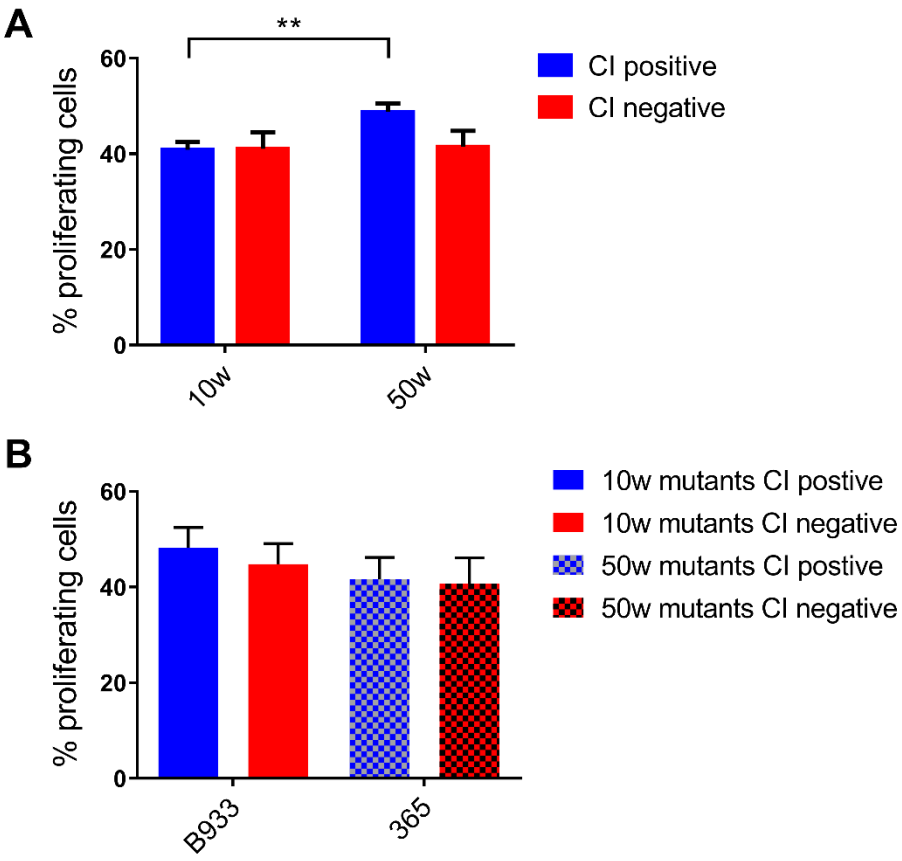

Figure 6.3 Cell proliferation in colonic crypts of $tRNA^{Ala}$ mutant mice with absolute positive and negative complex I function. (A) Percentages of proliferating cells in the CI-positive and CI-negative crypts of the 10-week and 50-week mutants. n (CI-positive crypts at 10 weeks) = 61, n (CI-negative crypts at 10 weeks) = 15, n (CI-positive crypts at 50 weeks) = 59, n (CI-negative crypts at 50 weeks) = 14. **, $p < 0.01$, Sidak's multiple comparison, two-way ANOVA. (B) The proportion of proliferating cells in colonic crypts of B933 (10 weeks, ear heteroplasmy = 79%) and 365 (50 weeks, ear heteroplasmy = 79%). n (CI-positive crypts of B933) = 11, n (CI-negative crypts of B933) = 10, n (CI-positive crypts of 365) = 11, n (CI-negative crypts of 365) = 6.

6.4.2.2 Cell proliferation and relative complex I level

In Chapter 5, I have shown a higher percentage of colonic crypts with OXPHOS deficiency relative to mitochondrial mass compared with those with absolute OXPHOS deficiency, and a distinct change in the absolute and relative complex IV level with age in crypts of $tRNA^{Ala}$ mutant mice. Thus, I also investigated the association between cell proliferation and the relative complex I level. Z-scores of the relative complex I level was calculated as absolute NDUFB8 level normalised by Porin level and categorised (detailed in Chapter 5). The data showed a decrease in the percentage of crypts with relative CI defects in the 50-week mutants compared with the 10-week mutants. The analysis of cell proliferation showed an overall higher level of cell proliferation in colonic crypts at 50 weeks compared with 10 weeks, irrespective of the OXPHOS level ($p = 0.005$, two-way ANOVA) (Figure 6.4A). In accordance with the results regarding the absolute complex I level, the percentage of proliferating cells was higher at 50 weeks compared with 10 weeks in colonic crypts with relatively normal CI level ($p = 0.006$, two-way ANOVA), whereas no change in cell proliferation was observed in crypts with relative CI deficiency with age (Figure 6.4A). In addition, no correlation was found between the cell proliferation level and the relative CI level in either wild-type or $tRNA^{Ala}$ mutant mice at 10 weeks or 50 weeks, which is in accordance with the data of absolute CI level ($p > 0.05$, Pearson correlation test). The analysis of individual mice revealed a higher level of cell proliferation in the CI-positive crypts compared with the CI-negative crypts in one 10-week mouse B938 and one 50-week mouse 372 ($p = 0.034$ and 0.012 respectively, unpaired t-test) (Figure 6.4B). However, no significant difference in cell proliferation was found between the crypts with different CI levels in the rest of the mice (Figure 6.4B).

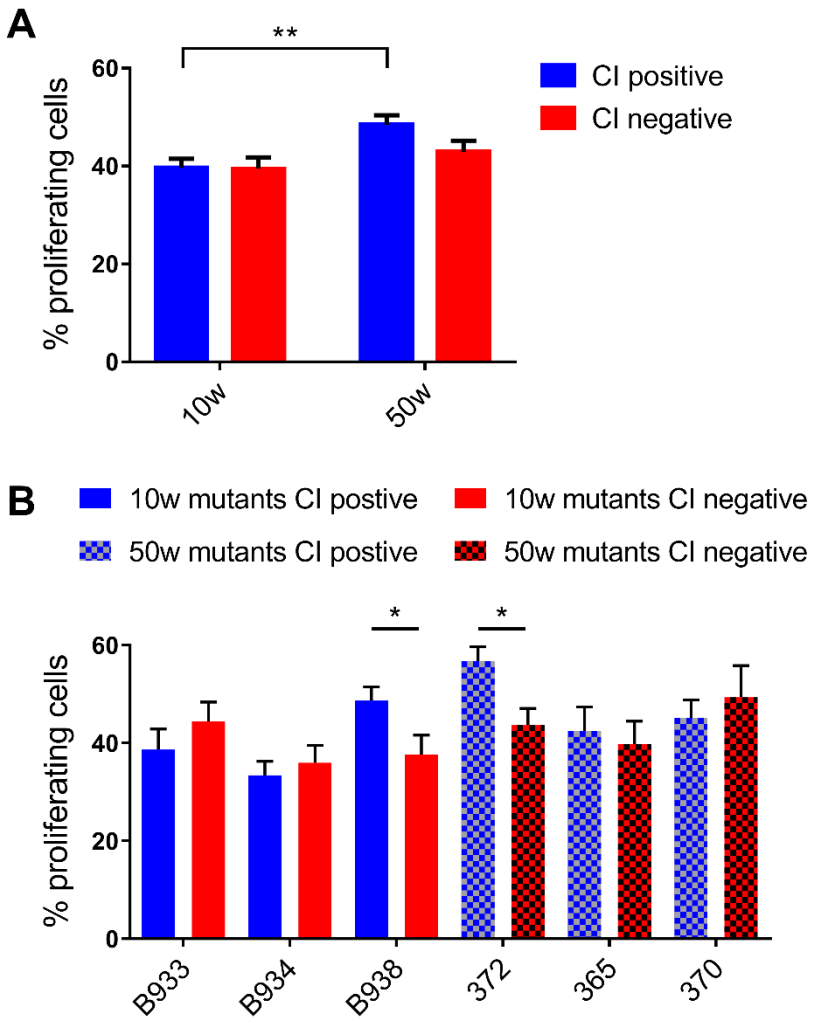

Figure 6.4 Cell proliferation in colonic crypts of $tRNA^{Ala}$ mutant mice with positive and negative complex I functions relative to mitochondrial mass (Porin). (A) Percentages of proliferating cells in relative CI-positive and CI-negative crypts of the 10-week and 50-week mutants. n (CI-positive crypts at 10 weeks) = 45, n (CI-negative crypts at 10 weeks) = 31, n (CI-positive crypts at 50 weeks) = 49, n (CI-negative crypts at 50 weeks) = 27. **, $p < 0.01$, Sidak's multiple comparisons, two-way ANOVA. (B) The proportion of proliferating cells in colonic crypts in individual mice at 10 weeks and 50 weeks. 10-week mutants: B933 (ear heteroplasmy = 79%), n (CI-positive crypts) = 5, n (CI-negative crypts) = 14; B934 (ear heteroplasmy = 77%), n (CI-positive crypts) = 10, n (CI-negative crypts) = 7; B938 (ear heteroplasmy = 77%), n (CI-positive crypts) = 10, n (CI-negative crypts) = 7; and 50-week 372 (ear heteroplasmy = 80%), n (CI-positive crypts) = 10, n (CI-negative crypts) = 7; 365 (ear heteroplasmy = 79%), n (CI-positive crypts) = 10, n (CI-negative crypts) = 7; and 370 (ear heteroplasmy = 73). n (CI-positive crypts) = 9, n (CI-negative crypts) = 6. *, $p < 0.05$, unpaired t-test.

6.4.2.3 Cell proliferation and porin level

Due to conflicts between the isotypes of the antibodies against Tom20 and Ki-67, I used porin as the mitochondrial mass marker for immunofluorescence in this study. I quantified the porin level in the colonic crypts of the 10-week and 50-week mutant and wild-type mice for marker verification (~20 crypts for each mouse). As with Tom20, porin was significantly upregulated in the $tRNA^{Ala}$ mutants compared with the wildtype mice at 10 weeks (Figure 6.5). The 50-week mutant mice also showed a larger percentage of colonic crypts with enhanced expression of porin compared with the aged wildtype mice (Figure 6.5A), despite no statistical significance in the continuous data (Figure 6.5B). As with Tom20, the protein level of porin increased with age in wild-type controls (Figure 6.5). However, this did not happen in the $tRNA^{Ala}$ mutant mice. Categorical data indicated a declined proportion of crypts with "very high" porin level in the 50-week mutants compared with the 10-week mutants (Figure 6.5A), whereas continuous data showed no difference in porin expression between the young and old mutants (Figure 6.5B), both of which contradict the findings of Tom20 in Chapter 5.

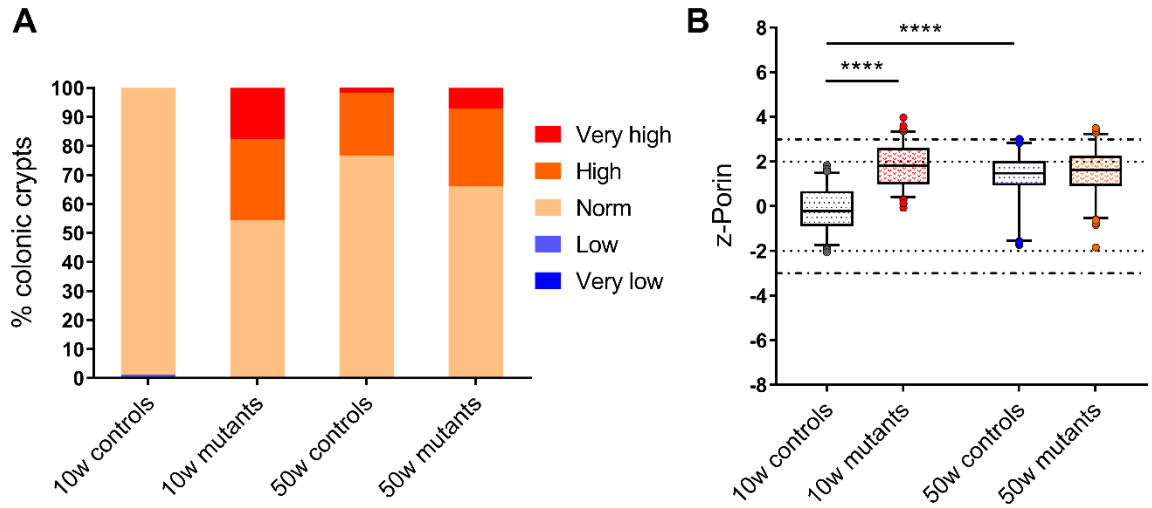

Figure 6.5 Protein levels of porin in wild-type and $tRNA^{Ala}$ mutant mice at 10 weeks and 50 weeks. (A) Categorical z-scores of the porin protein level. Data were classified into "very high", "high", "normal", "low" and "very low". The boundaries of the z-scores for each group were set according to the 95% and 99% confidence level (Table 5.3). (B) Whisker-and-box plot of the porin z-scores showing the median and distribution of the mitochondrial mass in the colonic crypts. Each point denotes a measurement of an individual crypt. The dotted lines are the boundaries of the categories. The number of examined crypts: n (10-week wild-type) = 77, n (10-week mutants) = 114, n (50-week wild-type) = 60, n (50-week mutants) =112; ~20 crypts in each mouse. ****, $p < 0.0001$, Kruskal-Wallis test.

To determine whether porin has any age-related effect on cell proliferation in colonic crypts, I compared the level of cell proliferation between the crypts with normal and high porin levels in 10-week and 50-week $tRNA^{Ala}$ mutant mice. The "high porin" group was the pooled group of crypts with "high" and "very high" porin level from Figure 6.5. The overall level of cell proliferation increased with age, irrespective of the porin level ($p < 0.001$, two-way ANOVA); however, no difference in the percentage of proliferating cells was found between the two porin categories in each age group (Figure 6.6A). Multiple comparisons revealed a significant increase in cell proliferation in the crypts with a high porin level in the 50-week mutants compared with the 10-week mutants ($p = 0.007$, two-way ANOVA) (Figure 6.6A).

To uncover whether the inherited m.5024C>T mutation has any impact on the age-related increase in cell proliferation with the high porin level, I compared the percentage of dividing cells in the colonic crypts with normal and high levels of porin in 50-week wild-type and $tRNA^{Ala}$ mutant mice. No difference in the level of cell proliferation was found between the genotypes or between the crypts with different porin classifications (two-way ANOVA) (Figure 6.6B). As the current data only includes a limited number of crypts with a high porin level in the aged wild-type mice, which may bias the result, the cell proliferation level of crypts with high porin levels should be examined in greater numbers in future analysis.

Despite no difference in the response of cell proliferation to porin between the aged wild-type and the $tRNA^{Ala}$ mutant mice, the level of porin and cell proliferation had opposite linear relationships in controls and mutants at 10 weeks (Figure 6.7). The percentage of proliferating cells in crypts was positively correlated with the porin level in the 10-week wildtype mice ($r = 0.4553$, $p = 0.012$), whereas it was negatively correlated with porin in 10-week mutant mice ($r = -0.2645$, $p = 0.016$) (Pearson correlation analysis) (Figure 6.7). However, for 50-week mice, despite the same trend within the same genotype as the 10-week mice, the linear relationships between cell proliferation and porin was not statistically significant in either wild-type or $tRNA^{Ala}$ mutant mice (Pearson correlation analysis) (Figure 6.7).

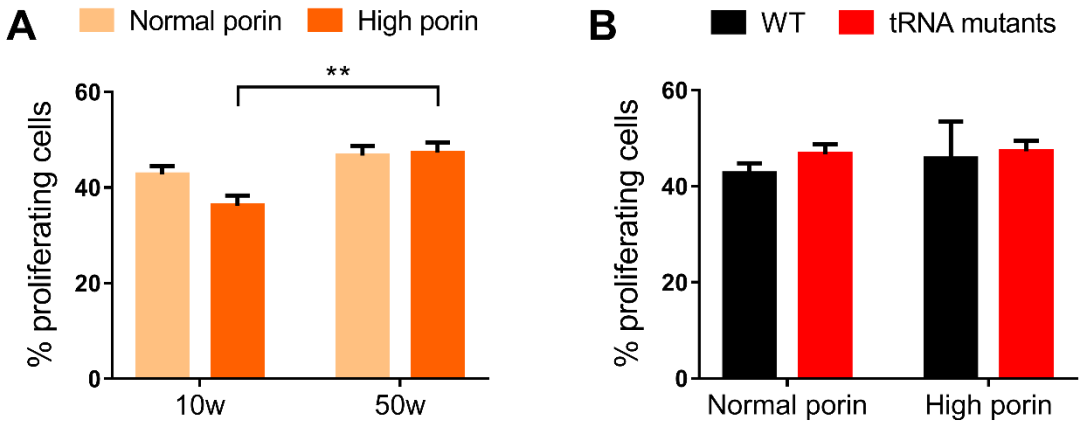

Figure 6.6 Associations between the level of cell proliferation and porin in colonic crypts. (A) The percentage of proliferating cells in the crypts of the 10-week and 50-week $tRNA^{Ala}$ mutants with normal and high porin levels. The number of crypts with normal and high porin level = 52 and 31 (10 weeks), 50 and 27 (50 weeks) respectively. **, p < 0,01, two-way ANOVA. (B) The fraction of proliferating cells in crypts with normal and high porin levels in the 50-week wild-type and $tRNA^{Ala}$ mutant mice. The "high porin" group in this figure include the crypts with "high" and "very high" porin level in Figure 6.5A. The number of crypts with normal and high porin = 25 and 5 (WT), 50 and 27 ($tRNA^{Ala}$ mutants) respectively.

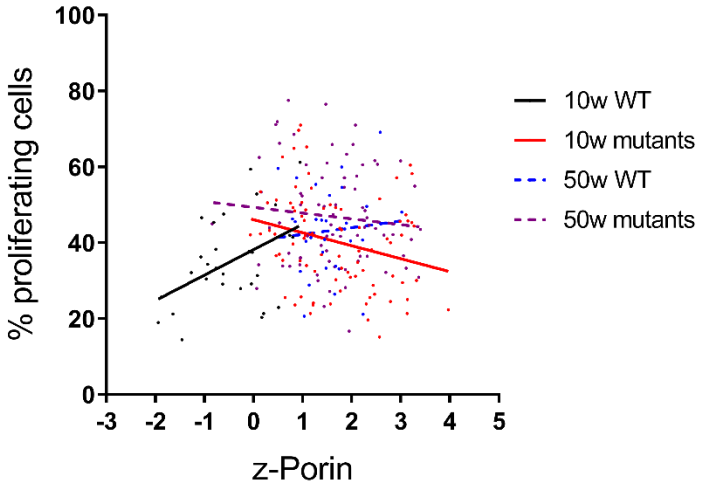

Figure 6.7 Linear relationships between the level of cell proliferation and porin in colonic crypts of the 10-week and 50-week wild-type and $tRNA^{Ala}$ mutant mice. Linear relationships between the percentages of proliferating cells and the z-scores of porin protein level in each crypt are shown as lines. Full and dotted lines indicate statistically significant and non-significant linear relationships (Pearson correlation analysis). Significant equations for linear regression are: 10-week wildtypes, $Y = 6.702*X + 38.19$, $R^2 = 0.207$ and 10-week mutants, $Y = -3.427*X + 46.08$, $R^2 = 0.070$. The number of crypts analysed: n (10-week wildtypes) = 30, n (10-week mutants) = 83, n (50-week wildtypes) = 30, n (50-week mutants) = 77.

6.4.3 Cell population in colonic crypts

Despite no significant difference in the frequency of proliferating cells in colonic crypts between the wild-type and the $tRNA^{Ala}$ mutant mice, a slight change in cell proliferation might result in massive alteration in the cell population. Therefore, I quantified the number of cells (labelled by Hoechst) in individual crypts in the $tRNA^{Ala}$ mutant mice and compared it with that in the wild-type mice at 10 and 50 weeks. The results showed a significantly lower number of cells in crypts of the $tRNA^{Ala}$ mutants compared with the wildtypes, regardless of age ($p = 0.001$, two-way ANOVA) (Figure 6.8A). Nevertheless, the difference between the genotypes within the same age group was not of statistical significance (two-way ANOVA) (Figure 6.8A). This is probably due to the small sample size. The individual analysis confirmed consistent counting between the individuals within the group of the 10-week wild-type and mutant mice and 50-week mutants; however, the cell population in mouse 24283 was markedly lower than that in the other two 50-week wild-type mice, leading to significant intra-group variations ($p < 0.001$, one-way ANOVA) (Figure 6.8B). In order to determine if this is a robust observation, a larger number of mice will be examined in the future study.

To determine whether CI is associated with increased colonic crypt cell populations, I compared the number of cells in crypts with different absolute and relative levels of CI in the $tRNA^{Ala}$ mutant mice at 10 and 50 weeks. However, I found no statistically significant difference in the cell population between crypts with different CI levels at any age (two-way ANOVA). In addition, I found no correlation between the absolute and relative CI level and the number of cells in crypts in any group of mice (Pearson correlation analysis). I also investigated whether the mitochondrial mass is associated with the crypt cell population. However, I found no statistically significant difference in the number of cells in crypts between the crypts with normal and high levels of porin in the $tRNA^{Ala}$ mutant mice (two-way ANOVA) nor any correlation between the porin level and the population of colonic epithelial cells in any groups of mice (Pearson correlation analysis).

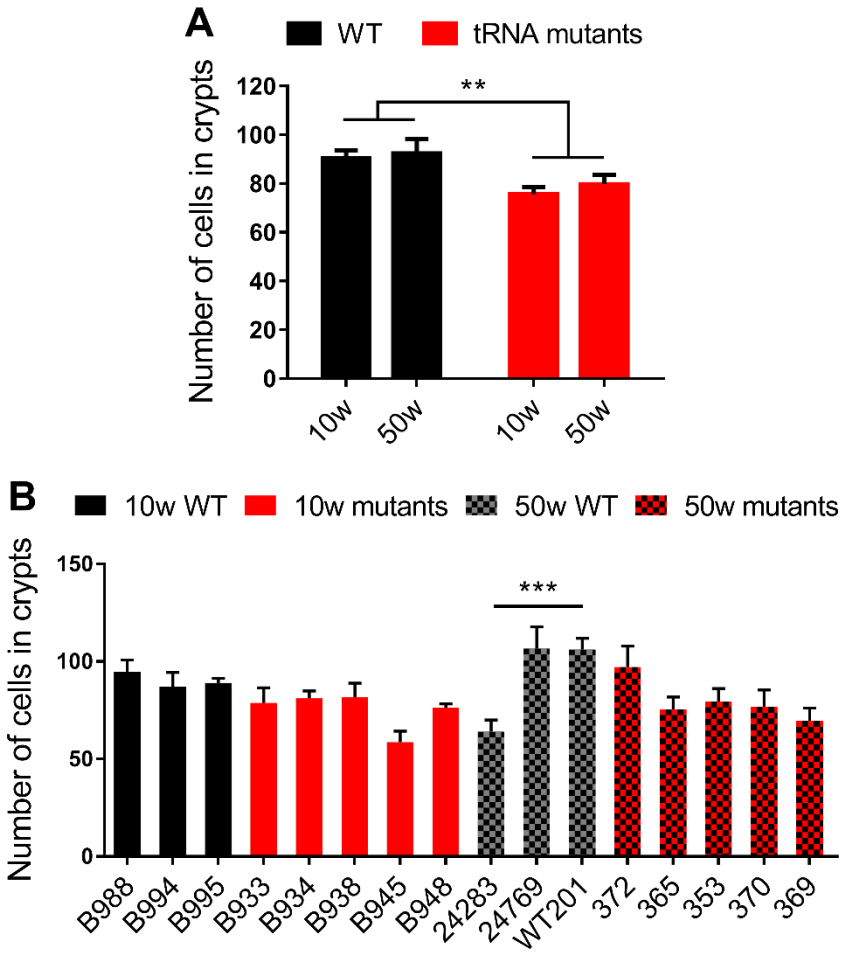

Figure 6.8 Colonic epithelial cell population in the (A) grouped and (B) individual wild-type and $tRNA^{Ala}$ mutant mice at 10 weeks and 50 weeks. The number of cells whose nuclei were labelled by Hoechst was counted in individual crypts. (A) The number of crypts examined: n (10-week wildtypes) = 30, n (10-week mutants) = 31, n (50-week wildtypes) = 30, n (50-week mutants) = 25. (B) The 10-week mutant mice, B933, B934, B938, B945 and B952 carried 79%, 77%, 77%, 74% and 71% m.5024C>T in the ear respectively. The 50-week mutants, 372, 365, 353, 370 and 369 carried 80%, 79%, 73%, 73% and 71% m.5024C>T in the ear respectively. The number of crypts investigated: n (B988) = 10, n (B994) = 10, n (B995) = 10, n (B933) = 7, n (B934) = 7, n (B938) = 6, n (B945) = 6, n (B948) = 5, n (24283) = 10, n (24769) = 10, n (WT201) = 10, n (372) = 5, n (365) = 7, n (353) = 4, n (370) = 5 and n (369) = 4.

6.4.4 Verification of mitochondrial mass markers

As shown in 6.4.2.3, though the porin level in the $tRNA^{Ala}$ mutant mice was higher than that in the wild-type controls, which was in line with the Tom20 level, it decreased with age in the mutants, unlike the Tom20. This might be due to the different sections that I examined or different attributes of mitochondrial mass markers. In addition, the porin antibody was unstable and presented unspecific bindings and uneven labelling on some sections in the presence of the apoptosis marker (cleaved caspase-3). Moreover, the isotype of the Tom20 antibody conflicted with that of the apoptosis marker. Thus, neither porin nor Tom20 was suitable for the apoptosis study. Therefore, it is necessary to assess different mitochondrial markers for ascertaining the difference between the findings of porin and Tom20 and for the investigation into the association between apoptosis and mitochondrial mass. I firstly tried COX4, which is a nuclear-encoded subunit used in the human studies (Chapter 3). I performed immunofluorescence to compare the protein levels of COX4 and Tom20, and their relationship with the level of CI (NDUFB8). However, I found crypts with COX defects often concomitant with CI deficiency in both 10-week and 50-week $tRNA^{Ala}$ mutant mice but not in age-matched wild-type controls, suggesting that COX4 expression was affected by the inherited m.5024C>T mutation and should not be used as a mitochondrial marker for this study (Figure 6.9).

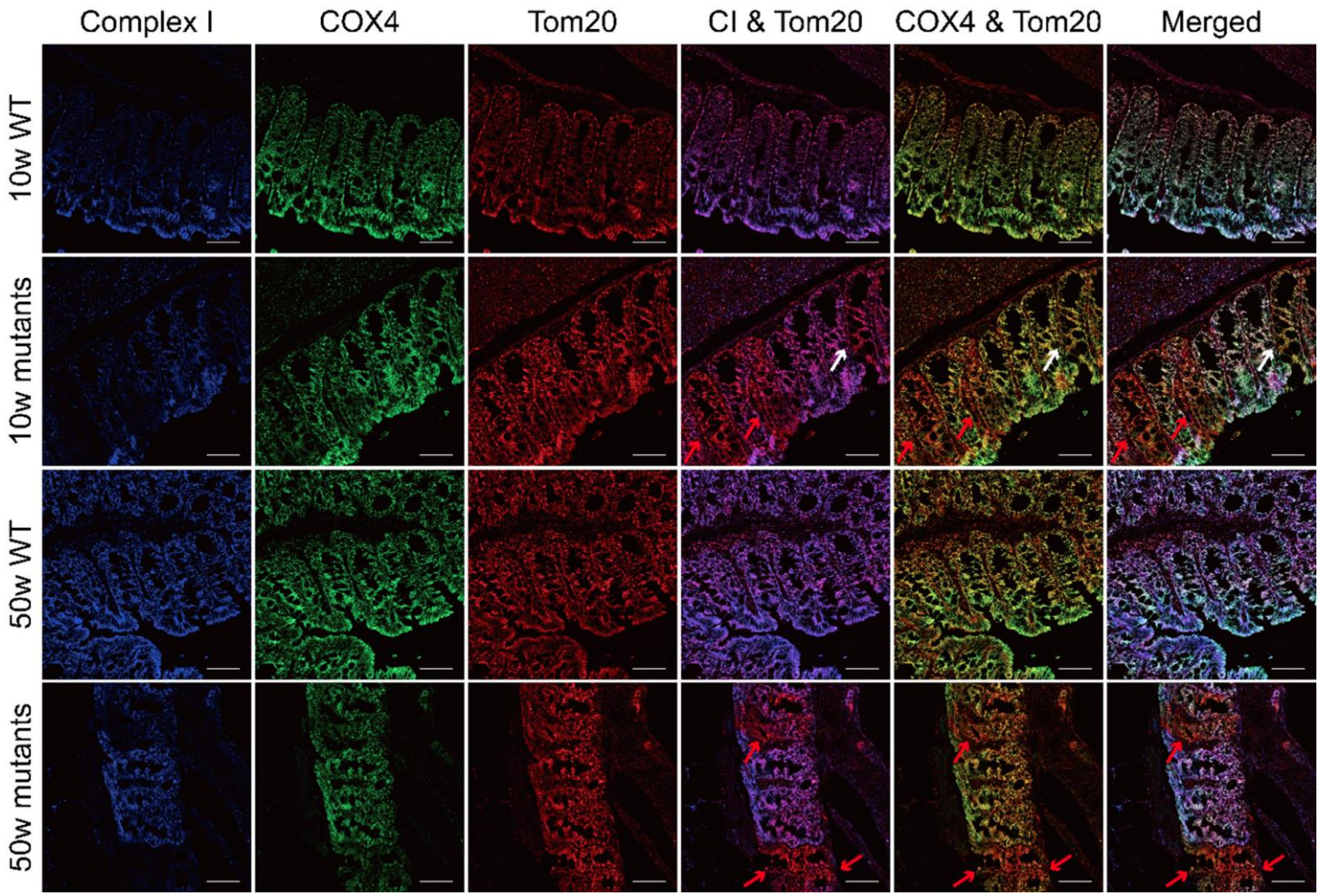

Figure 6.9 Representative immunofluorescence images showing the expression of complex I (NDUFB8) and mitochondrial markers (COX4 and Tom20) in colonic crypts of the wild-type and $tRNA^{Ala}$ mutant mice at 10 weeks and 50 weeks. White arrows show the crypts with isolated complex I deficiency. Red arrows indicate the crypts with both complex I and COX4 defect. Scale bar = 50μm.

Tom22 is a key subunit of the translocase of the outer mitochondrial membrane (TOM) complex mediating the import of cytosolic proteins into mitochondria with Tom20 and Tom40 subunits (Saeki *et al.*, 2000; Yano *et al.*, 2000; Yamano *et al.*, 2008; Wiedemann and Pfanner, 2017), which has been used as a mitochondrial mass marker in many studies (Latil *et al.*, 2012; Shi *et al.*, 2014). Tim23 is a crucial channel-forming protein of the presequence translocase of the inner mitochondrial membrane (TIM23 complex) that accepts proteins with presequence and manipulates their transportation into mitochondria (Truscott *et al.*, 2001; Wiedemann and Pfanner, 2017). Tim23 has also been used to label mitochondria and has proved to be consistent with other mitochondrial mass markers such as porin and Tom20 (Tang *et al.*, 2013). To verify different mitochondrial markers, I performed immunofluorescence to determine the expression of SDHA, Tom20, Tom22 and Tim23 on colon sections of the 10-week and 50-week wild-type and $tRNA^{Ala}$ mutant mice. The images show notably stronger signals of all four markers in the mutants compared with the wild-type controls, though the contrast at 50 weeks was not as obvious as that at 10 weeks (Figure 6.10).

The pixel intensity of approximately 105 crypts in each mouse was quantified and transformed into z-scores, allowing precise comparison of the protein levels of the four markers. For categorical analysis, z-scores were sorted into “very low”, “low, “normal”, “high” and “very high” as described in Chapter 5. The results of Tom20 was consistent with the findings in Chapter 5, showing that the mutants had a higher level of Tom20 in the colonic crypts than the wildtypes and that the expression of Tom20 increased with age in both wild-type and mutant mice (Figure 6.11). The expression of Tim23 showed the same trend with that of the Tom20 (Figure 6.11). A minor difference was that Tim23 expression elevated in more crypts of the 10-week mutants compared with Tom20 (Figure 6.11). The level of SDHA and Tom22 presented the same tendency as porin in the $tRNA^{Ala}$ mutant mice, where the 50-week mutants had lower levels of SDHA, Tom22 and porin in crypts compared with the 10-week mutants (Figure 6.11 and Figure 6.5). These results confirmed an increase in mitochondrial mass in the colonic crypts of the $tRNA^{Ala}$ mutants compared with the wild-type controls and revealed different trends in the expression of different mitochondrial markers with age in the $tRNA^{Ala}$ mutants.

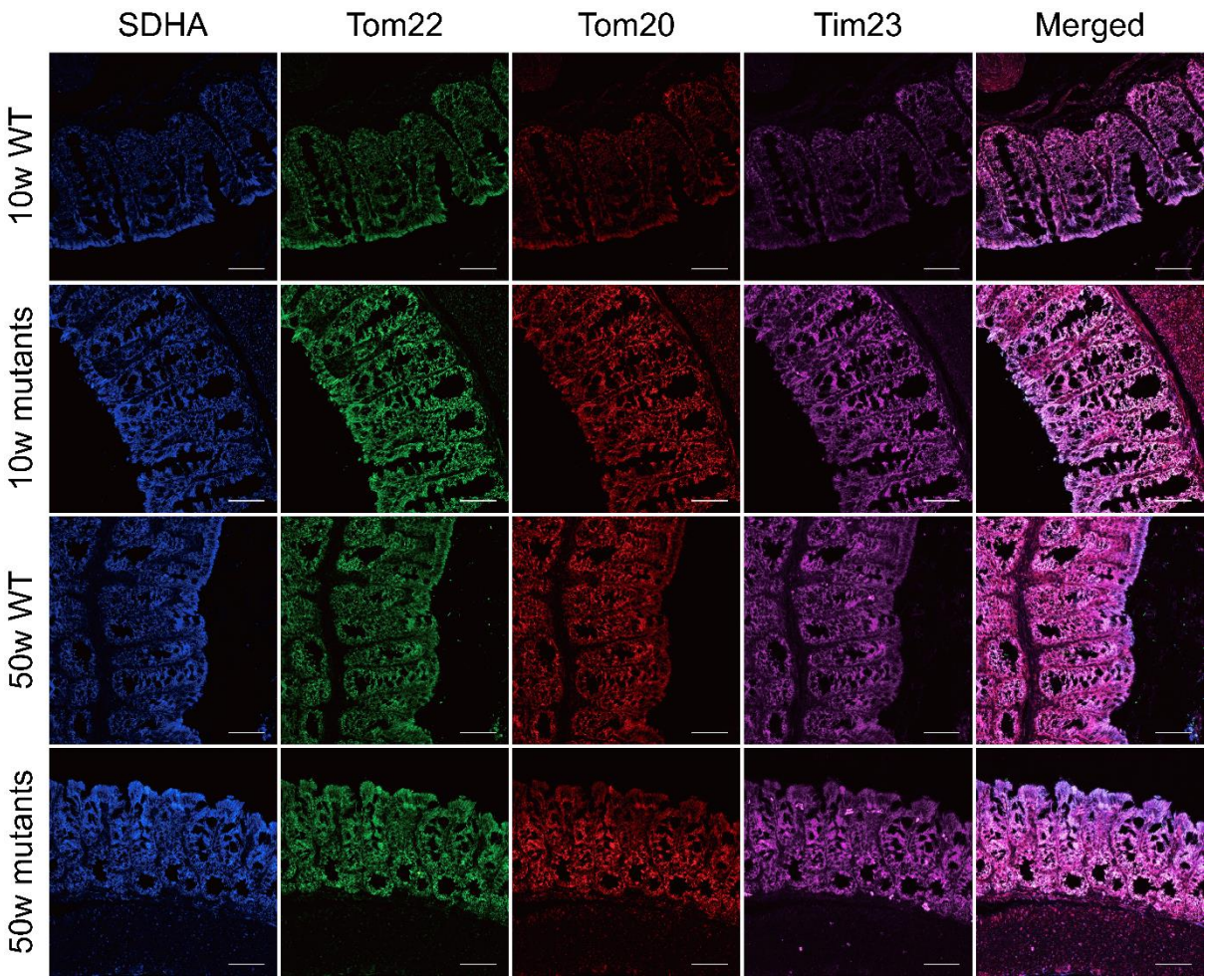

Figure 6.10 Example immunofluorescence images for four mitochondrial markers SDHA, Tom22, Tom20 and Tim23 in colonic crypts of the 10-week and 50-week wild-type and $tRNA^{Ala}$ mutant mice. Z-stack pictures covering the equal scanning thickness were taken using a confocal microscope and integrated as a single picture for each field of view. Scale bar = 50μm.

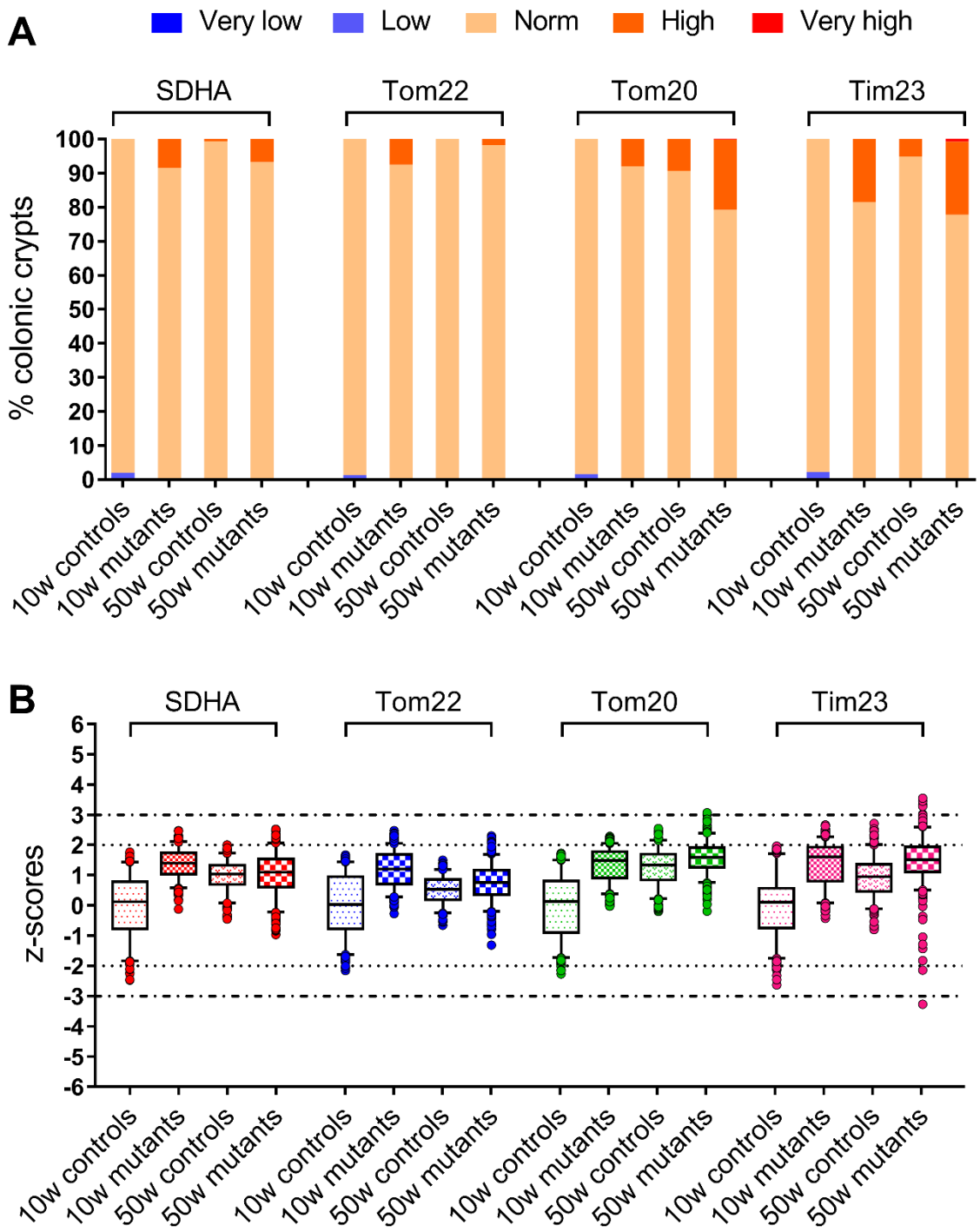

Figure 6.11 Protein levels of four mitochondrial markers SDHA, Tom22, Tom20 and Tim23 in the colonic crypts of the wild-type and $tRNA^{Ala}$ mutant mice at 10 weeks and 50 weeks. (A) Data were categorised into "very low", "low", "normal", "high" and "very high" with boundaries "-3, -2, 2 and 3" corresponding to the 95% and 99% confidence level. (B) An overview of the median and the distribution of the level of mitochondrial markers. Each point signifies a single crypt. The dotted lines are the borders of categories in the categorical data. The number of crypts examined: n (10-week wildtypes) = 313, n (10-week mutants) = 544, n (50-week wildtypes) = 307 and n (50-week mutants) = 557.

6.4.5 Apoptosis and mouse genotype

Mitochondria are intimately associated with the intrinsic pathway of apoptosis (Tait and Green, 2010). Dysregulated apoptosis has been found related to somatic mtDNA mutations and OXPHOS deficiency in mitotic colonic epithelium (Nooteboom *et al.*, 2010). Apoptosis is conducted through cleaving and activating caspase-3, and antibodies against cleaved caspase-3 (active form) are commonly used as an apoptosis marker (Kujoth *et al.*, 2005; Tait and Green, 2010). To determine whether apoptosis is affected in the colonic crypts of the $tRNA^{Ala}$ mutant mice and whether it is involved in the selective loss of the m.5024C>T mutation in mitotic intestinal epithelium, I performed immunofluorescence labelling complex I, mitochondrial mass and apoptotic epithelial cells with antibodies against NDUFB8, Tom22 and cleaved caspase-3 respectively (Figure 6.12). Tom22 was selected as the mitochondrial marker in this section because its isotype was compatible with the other antibodies. Confocal images were taken and processed as described in 2.9.3. Diffuse or punctate signals of cleaved caspase-3 were observed mainly in the cytoplasm of the colonic epithelial cells (Figure 6.12) (Bressenot *et al.*, 2009). Signals that partially overlapped the nuclear area (the region with no Tom22 labelling in a cell) were occasionally observed, indicating nuclear translocation of the active caspase-3 during apoptosis (Kamada *et al.*, 2005; Bressenot *et al.*, 2009). Beta-catenin (β-catenin) is a component of the cadherin-catenin adhesion complex that is predominantly expressed at the cell membrane in normal colonic epithelium (Iwamoto *et al.*, 2000; Brembeck *et al.*, 2006). To facilitate the counting of apoptotic cells, I co-labelled the section using β-catenin as a cell surface marker (Figure 6.12). I counted the number of all longitudinal crypts with a definitive base and apex in a section and the number of apoptotic cells within them, and transformed the data to the number of apoptotic cells in a hundred crypts as an index of the apoptosis level.

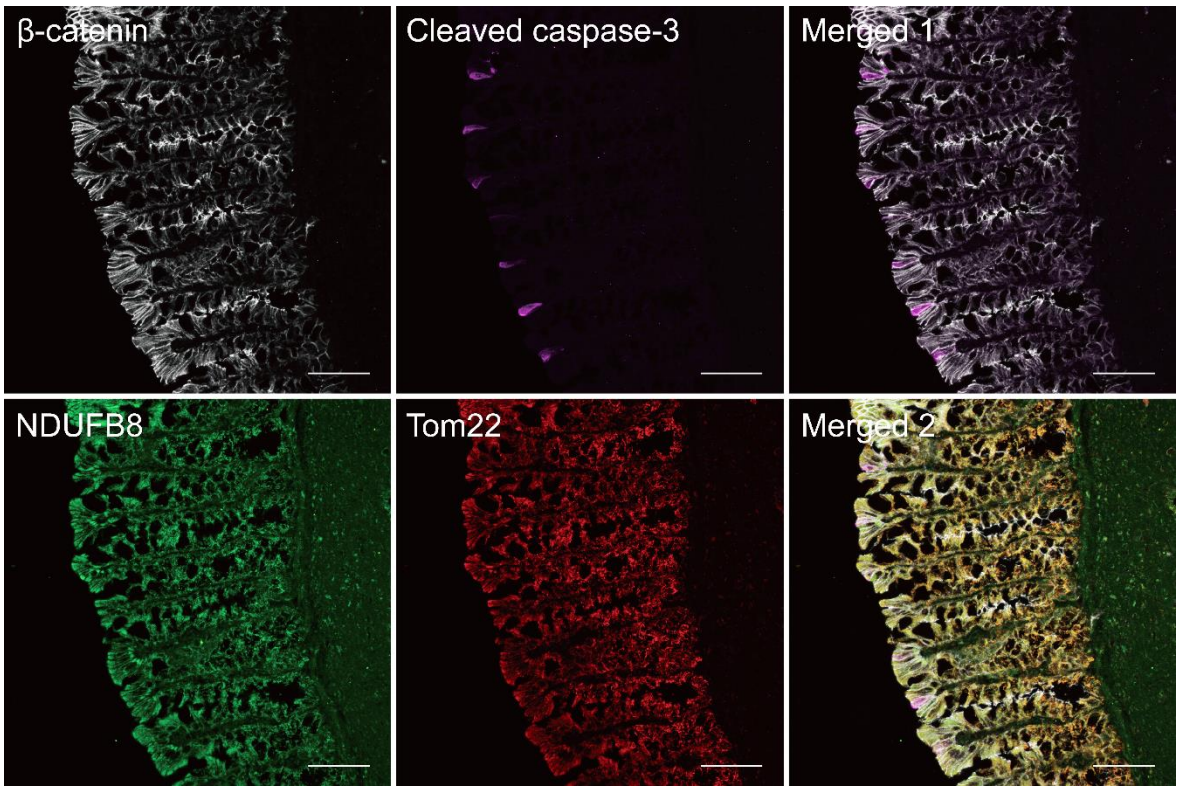

Figure 6.12 Representative immunofluorescence images for apoptotic cells (cleaved caspase-3), complex I (NDUFB8), mitochondria (Tom22) and epithelial cell membrane (β-catenin) in colonic crypts of a wild-type mouse. The merged view of the β-catenin and the cleaved caspase-3 channels facilitate the counting of the apoptotic cells. Scale bar = 50μm.

The apoptosis level in the crypts of the $tRNA^{Ala}$ mutant mice was lower at 10 weeks but slightly higher at 50 weeks compared with the wild-type mice, though no statistical significance was found (two-way ANOVA) (Figure 6.13A). The apoptosis level did not change in the wild-type mice with age, whereas it increased in the $tRNA^{Ala}$ mutant mice with age; however, the latter was not statistically significant (Figure 6.13A). Individual analysis showed notable variations between each mouse; nevertheless, it showed that most of the 10-week mutant mice had a lower level of apoptosis in the crypts compared with the 50-week mutant mice (Figure 6.13B). One limitation of this study was the small sample size, which weakened the power of statistical analysis. To strengthen the power of the experiment, a greater number of mice will need to be examined in future studies. Due to the restricted timespan of this PhD, I was not able to complete the quantification of the complex I and the Tom22 level to study their relationship with the apoptosis level in the colonic epithelium of the $tRNA^{Ala}$ mutant mice, but this will be carried out in future work.

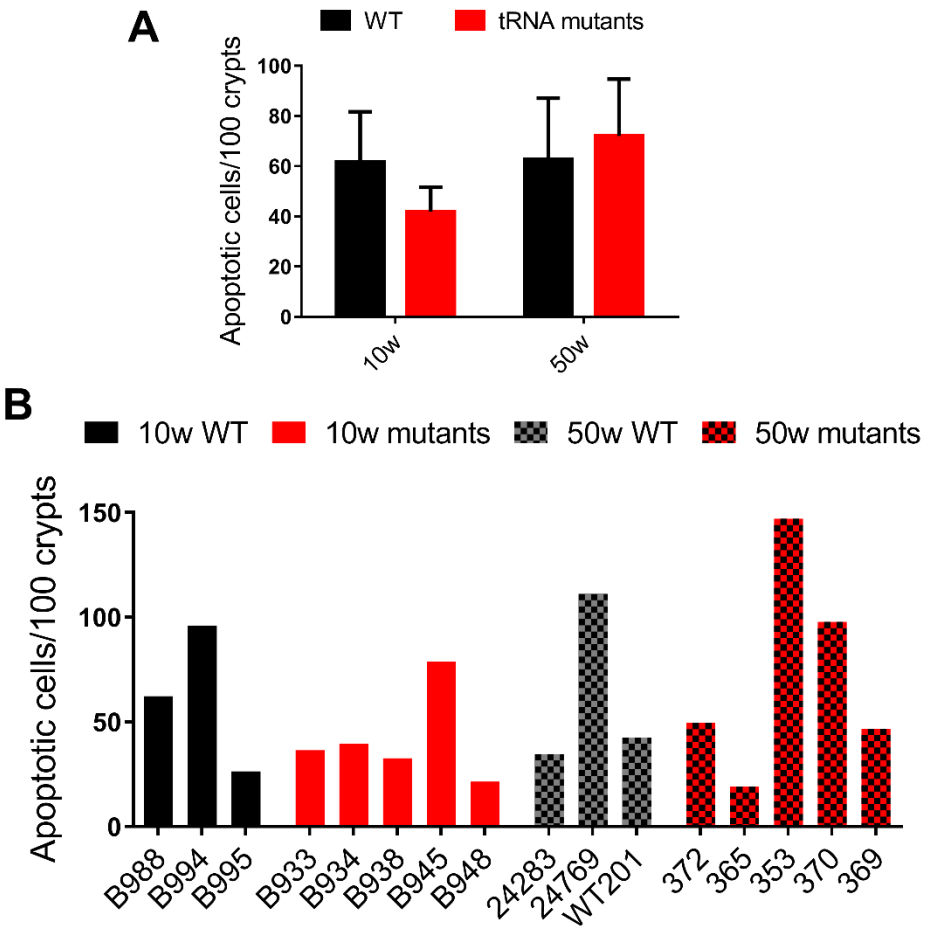

Figure 6.13 Apoptosis level in the colonic crypts of the (A) grouped and (B) individual wild-type and $tRNA^{Ala}$ mutant mice at 10 weeks and 50 weeks. The apoptosis level is denoted as the number of apoptotic cells in a hundred of crypts. The 10-week mutant mice, B933, B934, B938, B945 and B952 carried 79%, 77%, 77%, 74% and 71% m.5024C>T in the ear respectively. The 50-week mutants, 372, 365, 353, 370 and 369 carried 80%, 79%, 73%, 73% and 71% m.5024C>T in the ear respectively.

6.5 Discussion

The turnover rate of gastrointestinal epithelial cells may affect the rate of losing inherited mtDNA mutations (discussed in Chapter 4). Cell proliferation and apoptosis affect the cell turnover in mitotic tissue and are intimately associated with mitochondrial functionality (Tait and Green, 2010; Antico Arciuch *et al.*, 2012; Lopez and Tait, 2015; Salazar-Roa and Malumbres, 2017), making them potential candidates that contribute to the selective loss of inherited mtDNA mutations. Therefore, I have investigated the level of cell proliferation and apoptosis and their relationship to OXPHOS function and mitochondrial mass in the colonic crypts of 10-week and 50-week $tRNA^{Ala}$ mutant mice in comparison to wild-type controls.

I have demonstrated an increased level of cell proliferation in colonic crypts with age, regardless of the genotype and the OXPHOS function, which is in line with previous studies (Atillasoy and Holt, 1993; Nalapareddy *et al.*, 2017). However, I found no difference in the frequency of proliferating colonic epithelial cells between the $tRNA^{Ala}$ mutant and wild-type mice. This is in accordance with the findings in mice with accumulated somatic mtDNA mutations, where similar percentages of Ki-67 labelled proliferating cells in colonic crypts are found in ~ 50-week mtDNA-mutator mice and wild-type mice (Stamp, 2016), suggesting that the frequency of cells in the active cell cycle is unlikely to be affected by mtDNA mutations, regardless of whether they are inherited or somatic. Nonetheless, this does not rule out the possibility of changes in cell proliferation in the $tRNA^{Ala}$ mutant mice, as other facets of cell proliferation, such as the frequency of cells in each active phase of a cell cycle (e.g. G1, S, G2 and mitosis phase) and the rate of entering a cell cycle, have not been investigated to this point and are worth studying in the future. Of note, ageing is a systemic and perplex process with many factors changing continuously and dynamically. For example, mutations in nuclear oncogenes, such as *K-ras* and *c-myc*, might occur during ageing and affect cellular proliferation in intestines (Pappou and Ahuja, 2010; Liu *et al.*, 2011). The finding regarding the 50-week mice in this study is an integrated effect of mtDNA mutations with all the other age-related systemic changes.

The frequency of dividing cells in colonic crypts has no correlation with either the absolute CI level or the relative CI level to porin in either young or old wild-type or $tRNA^{Ala}$ mutant mice. In addition, I found no difference in the proportion of dividing cells between the CI-positive and CI-negative crypts in the young mutant mice. However, I found a significant increase in the frequency of proliferating cells in the CI-positive crypts with age, resulting in a higher level of cell proliferation in the CI-positive crypts compared with the CI-negative crypts in the 50-week $tRNA^{Ala}$ mutant mice. Although the latter is not statistically significant, possibly due

to the small sample size, it is in line with former studies on ageing human colon samples which shows a decreased cell proliferation in the crypts with COX defects compared with those with normal COX expression (Nooteboom *et al.*, 2010), suggesting that OXPHOS deficiency caused by inherited and somatic mtDNA mutations may have the same impact on cell proliferation in colonic crypts. In addition, this study illustrates that it is probably the enhanced cell proliferation in the OXPHOS-normal crypts rather than weakened proliferation in the OXPHOS-defective crypts with age that results in different levels of cell proliferation between the crypts with different OXPHOS functions in aged individuals. Overall, these results suggest that OXPHOS function may have an effect on cell proliferation in colonic crypts with age over time, but at a cross-sectional time point, it is not correlated with the level of cell proliferation within individuals.

I found no significant difference in the percentage of proliferating cells in crypts with a normal porin level compared with those with a high porin level in $tRNA^{Ala}$ mutant mice at 50 weeks, though in the 10-week mutants, the level of cell proliferation is slightly lower in crypts with high porin level compared with crypts with normal porin level. The frequency of dividing cells is significantly elevated in the crypts with a high porin level at 50 weeks compared with that at 10 weeks, whereas it is stable in crypts with a normal level of porin with age, suggesting an age-related influence of mitochondrial mass on cell proliferation. Despite an overlapping population of crypts with high porin level and normal CI function, this result is unlikely to be biased by the complex I level, since similar numbers of CI-positive and CI-negative crypts within the population of crypts with high porin level have been analysed. In addition, the majority of crypts with normal porin level are CI-positive, but they do not show increased cell proliferation with age as the crypts with normal CI expression do. Furthermore, I have found opposite linear relationships between the frequency of dividing cells and the level of porin in colonic crypts between the 10-week wild-type and $tRNA^{Ala}$ mutant mice. The cell proliferation level is positively correlated with mitochondrial mass in the young wild-type mice, whereas it is negatively correlated with mitochondrial mass in the young $tRNA^{Ala}$ mutant mice, which is consistent with the finding regarding the crypts with grouped porin level in the young mutants. This suggests a distinct response of colonic epithelial cell proliferation to mitochondrial mass or vice versa in mutant mice with inherited mtDNA mutations compared with wildtype mice. Although the regression line still shows an opposite trend between the wild-type and the $tRNA^{Ala}$ mutant mice, the correlation loses statistical significance in the old mice. This is in line with the finding that the cell proliferation level in the crypts with the same level of porin is not different between the 50-

week wild-type and $tRNA^{Ala}$ mutant mice, suggesting that age mitigates the effect of the inherited m.5024C>T mutation on the relationship between cell proliferation and mitochondrial mass.

Despite no significant difference in the proportion of proliferating cells between the wild-type and the $tRNA^{Ala}$ mutant mice, the crypt cell population is significantly smaller in the mutants compared with the wild-type controls, suggesting an effect of the inherited m.5024C>T mutation on colonic cell populations. This is in contrast to the findings in normal ageing mice and mtDNA-mutator mice with accumulated somatic mtDNA mutations, where the number of cells in crypts is higher than that in wild-type mice (Stamp, 2016; Nalapareddy *et al.*, 2017). In addition to cell proliferation, populations of cells can also be altered by changes in apoptosis. However, analysis of the apoptosis level revealed no significant difference in the number of apoptotic cells in colonic crypts between the wild-type and $tRNA^{Ala}$ mutant mice at either 10 weeks or 50 weeks. In fact, the apoptosis level seems lower in the mutants compared with controls at 10 weeks. Although cell proliferation and apoptosis are essential for maintaining cell populations, they do not regulate cell populations exclusively. Intestinal crypts in ageing animals have compromised cell proliferation and increased apoptosis, but they have more cells than those in young animals (Nalapareddy *et al.*, 2017), which is also the case in mtDNA-mutator mice (Fox *et al.*, 2012; Stamp, 2016). In this study, the shrinkage of the colonic epithelial cell population in the $tRNA^{Ala}$ mutant mice might be a consequence of the small change in the frequency of dividing cells in crypts and apoptosis, which is amplified with age. However, it may be associated with changes in cell cycles and/or crypt structure. The functions and number of stem cells, as well as the signals emitted from the stem cell niche, may also play a role. In addition, as I have only been able to investigate the apoptosis level in the whole crypt cell population at present using the available tissue, it is unknown whether intestinal stem cells undergo enhanced apoptosis, which could be selective and rapidly remove the mutation in the intestinal epithelium as well as change the whole crypt cell population. Further investigations are required to ascertain how inherited mtDNA mutations affect the cell population of intestinal crypts.

As expected, the porin level is higher in the colonic crypts of mutants compared with the wild-type mice in each age group. However, it is lower in the 50-week mutants than the 10-week mutants, contrary to Tom20. Hence, I have compared the levels of different mitochondrial markers, including SDHA, Tom22, Tom20 and Tim23, in the colonic epithelium in the wild-type and $tRNA^{Ala}$ mutant mice. All of them are upregulated in the mutants compared with the wildtypes in each age group, confirming that the $tRNA^{Ala}$ mutant

mice indeed have a higher mitochondrial mass in the colonic epithelium than the wild-type mice. The 50-week mutants have a lower level of porin, SDHA and Tom22 but a higher level of Tom20 and Tim23 in colonic crypts compared with the 10-week mutants, suggesting differential effects of age on the regulation of different mitochondrial markers in the $tRNA^{Ala}$ mutant mice. It is surprising that Tom22 and Tom20 change differently with age because they are both subunits of the TOM complex and they are functionally similar (Yamano *et al.*, 2008; Wiedemann and Pfanner, 2017). These findings suggest that inherited mtDNA mutations may have an indirect impact on the protein levels of the nuclear-encoded mitochondrial markers with age, which is highly protein-specific. It also reminds the researchers that the levels of mitochondrial markers have limits in reflecting the actual level of mitochondrial mass as it is dynamic and may have a specific age-related secondary response to mtDNA mutations.

6.5.1 Future work

One limitation of this study is the small sample size, especially the small number of the wild-type controls. This could reduce the power of statistical analyses. More mice will undoubtedly be examined for the study of the frequency of proliferating cells and apoptosis in the future. Due to the limited period of the PhD, I have not been able to investigate the relationship between the apoptosis level, the OXPHOS function and the mitochondrial mass at this stage. This will be carried out in future work.

Mitochondrial function and the regulation of cell cycles are mutually affected (Salazar-Roa and Malumbres, 2017). Key regulators of the cell cycle, for example, cyclin-Cdk complexes and cell cycle ubiquitin ligases, play an important role in the regulation of mitochondrial energy generation and biogenesis (Salazar-Roa and Malumbres, 2017). Future work will involve investigating the effect of inherited mtDNA mutations and OXPHOS defects on cell cycles using the $tRNA^{Ala}$ mutant mice, which will include the number of cells at different stages of the cell cycle, the rate of entering the cell cycle and the level of cell cycle regulators.

The shrinkage of the population of colonic epithelial cells might be associated with abnormalities of crypt morphology and stem cell regeneration. Wnt signalling pathway is crucial to the maintenance of intestinal mucosal homeostasis, crypt structure and function of stem cells (Fevr *et al.*, 2007; Nalapareddy *et al.*, 2017). Beta-catenin is a critical effector in Wnt signalling and is upregulated in colonic cancer (Korinek *et al.*, 1997; Morin *et al.*, 1997; Fevr *et al.*, 2007). β-catenin has been used in this study as a cell surface marker to facilitate

the counting of apoptotic cells, thus its protein level can be directly measured on the images in place to study whether Wnt/β catenin is affected by the m.5024C>T mutation. In addition to the reduced crypt cell population, it is also intriguing to know whether other aspects of epithelial proliferation, for example, the number of crypts is reduced in the $tRNA^{Ala}$ mutant mice.

Due to the lack of reliable stem cell markers for immunofluorescence, I have been unable to investigate the proportion of dividing intestinal stem cells or apoptosis level in stem cells on the tissue samples that I currently have. Ultimately, it would be vital to investigate the impact of inherited mtDNA mutations on the number and function of stem cells to ascertain the mechanism of the selective loss of inherited mtDNA mutations. This could be achieved by crossing the $tRNA^{Ala}$ mutant mice with Lgr5-EGFP-IRES-creERT2 mice (Barker *et al.*, 2007) or by isolating stem cells by fluorescence-activated cell sorting using combinations of cell surface markers (Wang *et al.*, 2013a; Nefzger C *et al.*, 2016).

6.6 Conclusion

In this study, I have investigated the frequency of proliferating cells and its association with the OXPHOS function and the mitochondrial mass in the colonic epithelium of the $tRNA^{Ala}$ mutant mice. I have confirmed the interaction between mitochondrial functions and cell proliferation in these mice. I have also shown that changes in the OXPHOS function and the mitochondrial mass caused by inherited and somatic mtDNA mutations might have the same impact on cell proliferation in aged individuals. In addition, I have demonstrated a possible effect of the inherited m.5024C>T mutation on cell populations and the interaction between the mitochondrial mass and cell proliferation in colonic crypts. Finally, I have verified different mitochondrial markers and confirmed mitochondrial proliferation in the $tRNA^{Ala}$ mutant mice compared with the wildtypes. These preliminary findings have provided ideas for investigating the mechanism of the selection against inherited mtDNA mutations in mitotic tissue and advanced the understanding of the mtDNA disease progression and phenotype development. However, the exact mechanism underlying the selective loss of inherited mtDNA mutations in dividing cells is still unknown and requires further studies.

Chapter 7 Final discussion

Mitochondrial DNA diseases are characterised by highly heterogeneous clinical manifestations with tissue-specific distribution and phenotypic expression of mtDNA mutations (Taylor and Turnbull, 2005). Mitotic segregation is believed to be amongst the factors that affect the dynamics of mtDNA mutations in mitotic tissue, contributing to the heterogeneity of mtDNA disorders (Taylor and Turnbull, 2005). However, different types of mtDNA mutations can have opposite outcomes over time in mitotic tissue. During ageing, a variety of mtDNA mutations occur somatically, and clonally expand to high levels in cells, with no evidence suggesting any selective pressures promoting or impeding their accumulation (Taylor *et al.*, 2003; Greaves *et al.*, 2012a). In mitotic tissue, such accumulation of somatic mtDNA mutations initiates in adult stem cells (Taylor *et al.*, 2003; Su *et al.*, 2018). In contrast, patients with mtDNA disease lose specific inherited mtDNA mutations in mitotic blood and certain epithelial cells, including buccal mucosa, urine and cervical smears, suggesting selective pressures against inherited mtDNA mutations in mitotic cell populations (Olsson *et al.*, 2001; Rahman *et al.*, 2001; de Laat *et al.*, 2012; Grady *et al.*, 2018). However, the loss of inherited mtDNA mutations is mostly unexplored. It is unknown whether such loss is a universal phenomenon occurring across all types of mitotic tissues, where it occurs in tissue, what effects it has on tissue phenotypes and the mechanisms underlying it. Understanding this process is critical not only to understanding the phenotype and progression of mtDNA disease but also to understanding the behaviour of somatic mtDNA mutations in ageing. Therefore, this work aims to further the understanding of the loss of inherited mtDNA mutations in mitotic tissue.

7.1 Gastrointestinal epithelial cells lose inherited m.3243A>G and m.8344A>G mutations

GI epithelium is a mitotic tissue that is rapidly renewed by somatic stem cells. The genetic assessment of different segments of the GI tracts from patients with the common inherited m.3243A>G and m.8344A>G mutations revealed a significantly lower mutation load in the epithelium of oesophagus, stomach, small intestine and colon compared with the post-mitotic smooth muscle in the same segment. However, in foetuses, the inherited m.3243A>G mutation is evenly distributed in mitotic and post-mitotic tissues (Matthews *et al.*, 1994; Cardaioli *et al.*, 2000; Monnot *et al.*, 2011). As there is no evidence suggesting any age-related increase in the mutation load in muscles, the finding suggests a loss of these mutations in mitotic GI epithelium. In addition, there is a substantial variation in heteroplasmy levels between intestinal crypts, where some crypts carry no mutations. A typical feature of

intestinal crypts is that they undergo monoclonal conversion, which allows a single stem cell to dominate the stem cell niche of a crypt and renew all cells in the crypt (Kim and Shibata, 2002; Snippert *et al.*, 2010; Kozar *et al.*, 2013). Therefore, these findings suggest that the loss of mutations occurs in intestinal stem cells, as the selection at any other level of the differentiation process could not result in crypts with no mutation. The selective loss of the inherited m.3243A>G mutation is correlated with an absence of OXPHOS deficiency in the GI epithelium, in contrast to the severe complex I defect in colonic smooth muscles. As previous studies have shown OXPHOS defects in both mitotic and post-mitotic tissues of teratomas that derive from iPSCs with high levels of m.3243A>G mutation (Hämäläinen *et al.*, 2013), it is reasonable to assume that patients may harbour OXPHOS defects in their GI epithelium in the first place and the loss of mutations may recover the OXPHOS function. However, the effect of the mutation loss on biochemical phenotypes needs to be confirmed by longitudinal studies or multiple cross-sectional studies. Due to the difficulties of obtaining human samples, it is necessary to use an animal model for further investigations.

7.2 $tRNA^{Ala}$ mutant mice: a good model to study selective loss of inherited mtDNA mutations

Previously, none of the mouse models with inherited mtDNA mutations have proven suitable for investigating the tissue-specific segregation of mtDNA mutations (reviewed in 1.6.3 of Chapter 1). In collaboration with Dr James Stewart and Prof Nils-Göran Larsson, Max Planck Institute for Biology of Ageing, Cologne, Germany, Dr Laura Greaves' team has developed a novel mouse model with an inherited m.5024C>T mutation in the mitochondrial $tRNA^{Ala}$ gene (Kauppila *et al.*, 2016). These mice are suggested to be a candidate to study the loss of inherited mtDNA mutations as mice with a high mutation load show an age-related decline in m.5024C>T heteroplasmy in blood (Kauppila *et al.*, 2016). Thorough genetic characterisation of these mice in two age groups reveals a loss of the m.5024C>T mutation in the mitotic spleen, pyloric epithelium of stomach and intestinal crypts. Such loss is absent in the post-mitotic heart, skeletal muscle, brain and GI smooth muscles of the mutants. The considerable variation in m.5024C>T mutation levels between individual intestinal crypts and the presence of some crypts harbouring extremely low levels of mutations recapitulate the findings in patients with mtDNA disease. Young mutant mice present different levels of OXPHOS deficiency in their colonic epithelium with the magnitude of deficiency closely correlated with their initial mutation loads. Despite no significant changes in COX activity with age, RC complex I defect is slightly recovered in the old mice, which is concomitant with the decrease in the level of inherited m.5024C>T mutations, suggesting a beneficial effect of the loss of

pathogenic m.5024C>T mutations on biochemical phenotypes. In addition, these mice display many features the same as the patients in the human study, such as the enhanced expression of mitochondrial markers and the upper limit of heteroplasmy levels in the intestinal epithelium, and tissue-specific loss rates of mutations, which are discussed in the next two sections. In brief, $tRNA^{Ala}$ mutant mice indeed have a loss of inherited m.5024C>T mutations in mitotic tissue. Their genetic and biochemical features recapitulate the findings in the human study, proving them a good model to investigate the mechanism underlying the loss of inherited mtDNA mutations. In addition, the examination of the mice in two age groups have provided useful information about the age-related genetic and biochemical changes in mitotic tissue.

7.3 Upper limits in mutation levels of inherited mtDNA mutations

In the human study, patients show an upper limit of inherited mtDNA mutations in the OXPHOS-normal GI epithelium, which varies between the epithelium of different GI segments and between the same types of epithelium in different individuals. This limit never exceeds the mutation level in the OXPHOS-defective smooth muscle of the same segment. Although the biochemical thresholds of mutations in GI epithelium and smooth muscles are likely to be slightly different, these results lead to an assumption that this upper limit might be associated with the biochemical threshold, where epithelial cells harbouring mutations beyond the limit may have OXPHOS defects and are eliminated by cellular quality control systems to decrease the mutation level in tissue. The upper limit of heteroplasmy is recapitulated in the intestinal and pyloric epithelium of the $tRNA^{Ala}$ mutant mice; however, it is higher than the biochemical threshold for m.5024C>T to cause COX deficiency in the mouse intestinal epithelium (Baines, 2014), suggesting that factors in addition to OXPHOS function contribute to the selective loss of inherited mutations. Moreover, the genetic examination of the young and old $tRNA^{Ala}$ mutant mice shows a dynamic change in m.5024C>T heteroplasmy in individual crypts and further confirms the existence of an upper limit. Heteroplasmy levels of the m.5024C>T mutation in all crypts are considerably similar in the young mice. The mutation levels of individual crypts drift symmetrically in both directions over time from the initial level until they reach the upper limit, leading to the considerable variation in crypt heteroplasmy in the old mutants. This results in a significant decline in the overall mutation level in the intestinal epithelium of the mutant mice with high initial mutation burdens, which is shown in this thesis, whereas in mutants with a low mutation burden from the start, such an effect may not be obvious. On the contrary, it might lead to an increase in the average mutation level of tissue. This might be able to account for the lack of mutation loss in blood

and increased numbers of COX-defective colonic crypts in the $tRNA^{Ala}$ mutants with low initial mutation levels (Baines, 2014; Kauppila *et al.*, 2016). It would be important to examine the mice with low mutation loads to advance the understanding of the dynamics of inherited mtDNA mutations in individual crypts with age. Upper limits of mutation heteroplasmy is a critical feature associated with the loss of inherited mtDNA mutations, which is absent for somatic mtDNA mutations as they accumulate to homoplasmy in the colonic epithelium of ageing humans. However, factors that determine the upper limit and mechanisms that prevent heteroplasmy from surpassing the limit is still unknown.

7.4 Tissue-specific rates of losing inherited mtDNA mutations

Another characteristic of the loss of inherited mtDNA mutations is the tissue-specific loss rate. In the human study, mutation levels of m.3243A>G in the epithelium of oesophagus, stomach and small intestine are different within the same patient, suggesting a different rate of losing the mutation. This is corroborated using the $tRNA^{Ala}$ mutant mice, which shows a lower loss rate of the m.5024C>T mutation in the epithelium of gastric pylorus compared with the epithelium of small intestine and no significant loss of the mutation in the epithelium of gastric fundus. This difference might be associated with different turnover rates of different types of epithelial cells, as the turnover of fundic epithelial cells is markedly slower than that of pyloric epithelial cells, which is both slower than the epithelial turnover of intestines (Hoffmann, 2008). However, the lower heteroplasmy in the oesophageal epithelium compared with the intestinal epithelium in patients suggests that the rate of losing inherited mtDNA mutations is unlikely to be determined exclusively by physiological turnover rates of mitotic tissue, as the regeneration of oesophageal epithelium is slower than that of intestinal epithelium (Creamer *et al.*, 1961; Squier and Kremer, 2001). It might also be associated with wound healing and repair of lesions in injured GI epithelium, considering oesophagal epithelium might have a higher risk of acute injuries compared with intestinal epithelium due to its frequent damage from food that may be of high temperature and hardness (Doupé *et al.*, 2012). However, the mechanism of the tissue-specific loss rate of inherited mtDNA mutations is still an enigma. It is also unknown whether the loss rate changes with age in tissue. Given that I only have the samples of mice in only two age groups in this project, it would be useful to examine $tRNA^{Ala}$ mutant mice at multiple stages of lifespan in the future.

7.5 Hypotheses for potential mechanisms underlying the selective loss of inherited mtDNA mutations in mitotic cells

The ultimate question of this project is how inherited mtDNA mutations are lost in mitotic tissue and why somatic mtDNA mutations lack such selective pressure and accumulate with age. Due to the limited time of this PhD, a number of questions remain unanswered. However, this work has provided important clues for the proposal of hypotheses and further investigations.

Regarding the distinct dynamics of inherited and somatic mtDNA mutations in mitotic tissue of patients with mtDNA disease and normal aged humans, one hypothesis is that mtDNA mutations are in essence under no selective pressures until they have reached a high level (Figure 7.1). Patients with mtDNA disease harbour high levels of mtDNA mutations from the start thus selection occurs earlier in patients compared with normal individuals who accumulate high levels of mutations only when they age (Figure 7.1). In this project, the old $tRNA^{Ala}$ mutant mice show no severe complex IV defects in colonic epithelium similar to the young mice whereas the age-matched wild-type mice present a significant complex IV deficiency in colonic crypts due to the aggregation of somatic mtDNA mutations. Previous studies show that low levels of inherited mtDNA mutations actually exacerbate OXPHOS defects caused by the amassing of somatic mutations (Ross *et al.*, 2013). These results suggest that high levels of m.5024C>T mutation might be required to trigger a protective effect that impedes the accumulation of somatic mtDNA mutations and maintains the OXPHOS function in mitotic tissue, which in part supports this hypothesis. However, a caveat to this hypothesis is that only specific inherited mtDNA mutations are lost in mitotic tissue of patients with age, suggesting that the selective pressures might only be induced by particular mutations, whereas normal individuals accumulate random mtDNA mutations during ageing.

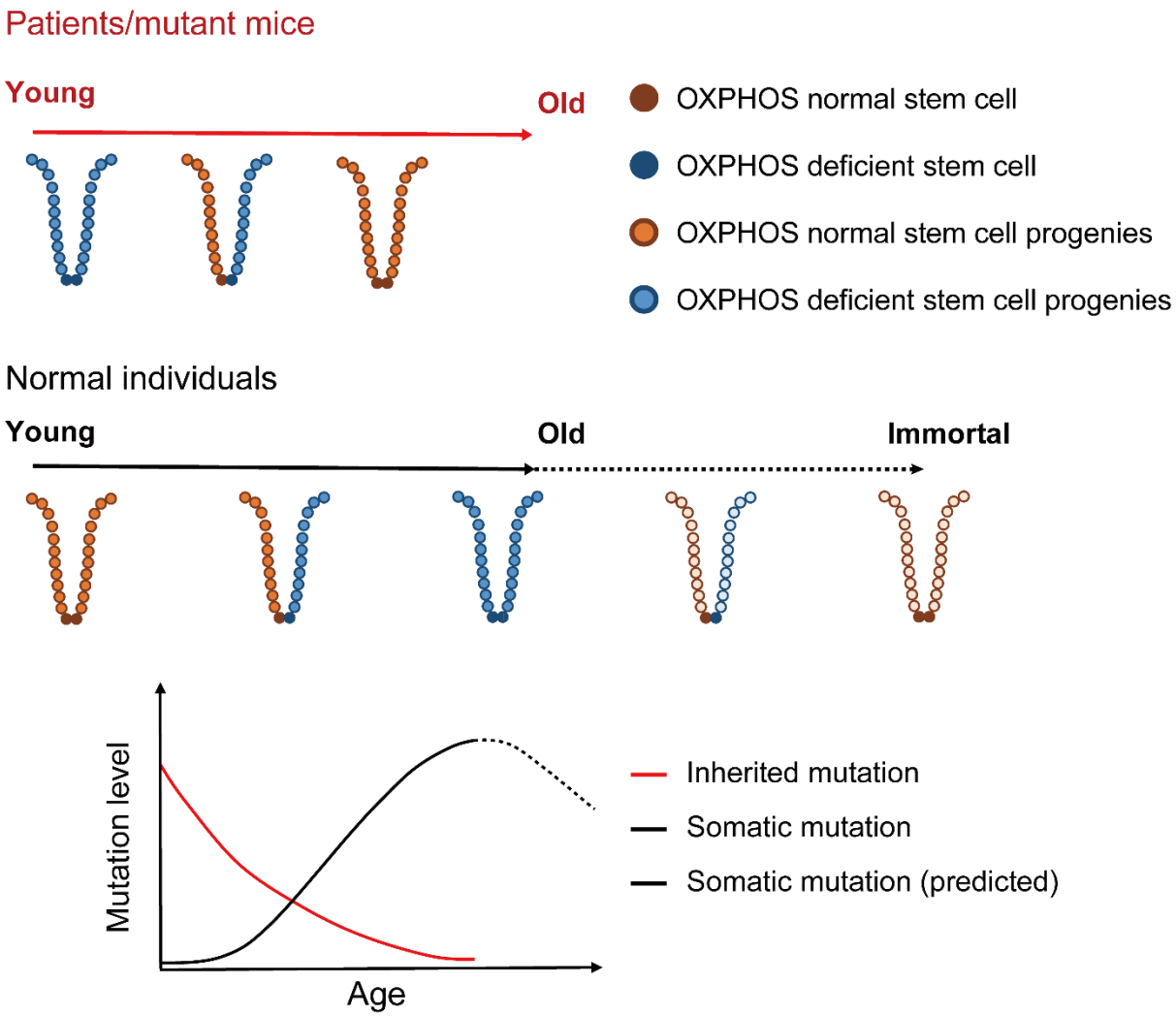

Figure 7.1 Mitochondrial DNA mutations are hypothesised under no selective pressures until they have reached a high level. By then, they trigger certain mechanisms to remove the mutations in the mitotic intestinal epithelium. Patients or $tRNA^{Ala}$ mutant mice harbour high levels of mutations from the start. Thus the selection occurs early. Whereas normal ageing individuals accumulate somatic mutations to a high level when they are aged, activating the selection late in life. If they live immortally, they might eventually lose somatic mutations as patients with mtDNA disease.

Both patients and mutant mice with inherited mtDNA mutations show an upregulated expression of different mitochondrial markers in GI epithelium. These markers include nuclear-encoded subunits of RC complexes and mitochondrial outer/inner membrane proteins. In $tRNA^{Ala}$ mutant mice, despite a different change in levels with age, all of these markers show enhanced expressions in mutants compared with controls. These findings suggest increased mitochondrial proliferation in individuals with inherited mtDNA mutations. The aged wild-type mice also have elevated mitochondrial content compared with the young wild-type mice, suggesting that mitochondrial proliferation might be a shared compensatory response to mtDNA mutations and/or OXPHOS dysfunction; however, mitochondrial proliferation in wild-type mice is not as strong as in the $tRNA^{Ala}$ mutant mice. It is as yet unknown what determines the magnitude of mitochondrial proliferation. Mitochondrial content is a combined result of mitochondrial biogenesis and degradation and is intimately associated with mitochondrial dynamics. Three possibilities can account for a net elevated mitochondrial level: (1) biogenesis and degradation both increase with a stronger effect of the former; (2) enhanced biogenesis with reduced degradation; (3) and both decrease with a larger magnitude of degradation. Mitophagy is a vital process in the mitochondrial quality control system, which mediates the selective degradation of dysfunctional mitochondria (Youle and Narendra, 2011). Mitochondrial biogenesis is generally thought to non-selectively increase mitochondrial content (Durham *et al.*, 2007). Based on current knowledge, the first and the last possibilities are more likely to facilitate the loss of inherited mtDNA mutations. Investigating mitochondrial biogenesis and mitophagy is crucial to the understanding of the mechanisms underlying the selective loss of inherited mtDNA mutations and should be included in future work.

Post-mitotic tissue does not lose inherited mtDNA mutations with age. The selective loss of inherited mtDNA mutations is undeniably associated with mitotic attributes of tissue and likely adult stem cells, which is supported by the presence of intestinal crypts with no detectable mutations. In addition, preliminary data in this project show a decreased crypt cell population in colonic crypts of $tRNA^{Ala}$ mutant mice and different age-related changes in cell proliferation between CI-positive and CI-negative crypts, suggesting mutation-related alteration in regeneration of colonic epithelial cells in $tRNA^{Ala}$ mutant mice, which might be associated with dysfunction of stem cells and dividing daughter cells. However, no conclusions can be drawn currently, and the role that stem cells play in the mutation loss needs to be further investigated.

Here I discuss a few hypotheses about how stem cells and progenitor cells are involved in the loss of inherited mtDNA mutations. First, mitochondria play an important role in the regulation of stem cell homeostasis, and mitochondrial dysfunction caused by mtDNA mutagenesis can enormously affect stem cell self-renewal and differentiation (Ahlqvist *et al.*, 2012). Therefore, intestinal stem cells with heavy mutation load might not be able to divide to renew themselves and produce progeny (Figure 7.2). In addition, high levels of mtDNA mutations cause mitochondrial dysfunction and predispose stem cells to apoptosis, depletion and senescence (Figure 7.2) (Su *et al.*, 2018). Together, these can lead to a loss of stem cells with high levels of mtDNA mutations in the stem cell pool, allowing stem cells with fewer mutations to dominate the stem cell niche and replenish the tissue, which entails a decline in the average mutation level of tissue.

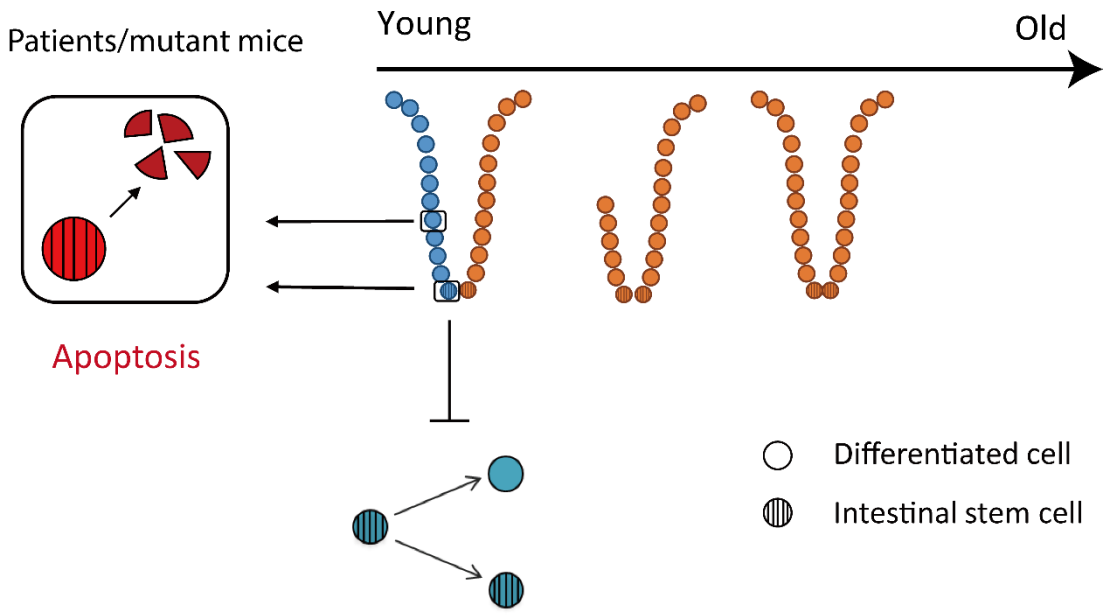

Figure 7.2 Hypothesis one: intestinal stem cells and progenitor cells with a high mtDNA mutation level undergo apoptosis; the function of stem cells with high mutation load might be compromised and unable to divide to renew themselves or generate daughter cells. As a result, stem cells with high mutation load will eventually be replaced by those with fewer mutations in the stem cell pool.

Second, some in vitro studies demonstrate that stem cells can asymmetrically segregate aged mitochondria into daughter cells and those with fewer aged mitochondria display more stem cell properties (Katajisto *et al.*, 2015). It is possible that stem cells also have a system to identify dysfunctional mitochondria with high levels of inherited mutations and segregate them during division for self-renewal or differentiation. The daughter cells (stem cells or progenitor cells) with fewer dysfunctional mitochondria regenerate the tissue, whilst those with more dysfunctional mitochondria undergo extinction (Figure 7.3).

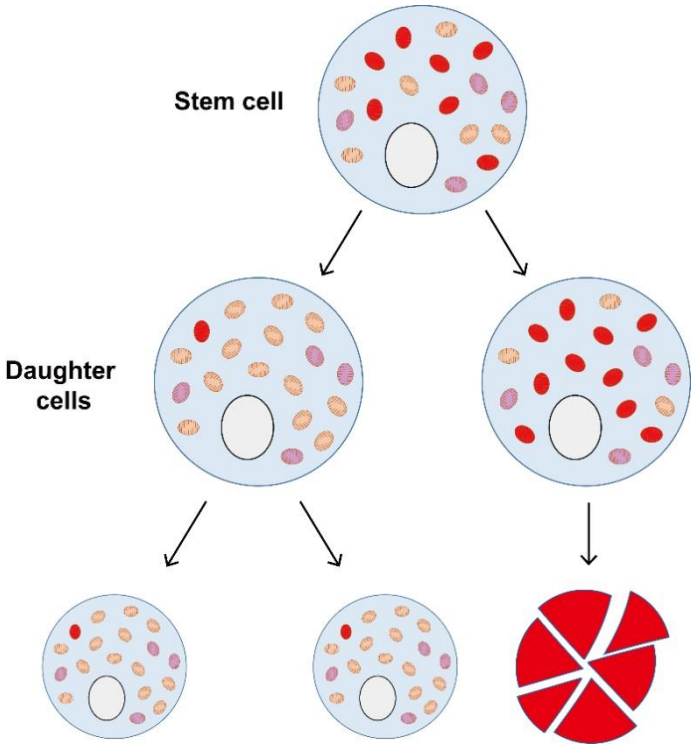

Figure 7.3 Hypothesis two: stem cells might have ability to identify and segregate dysfunctional mitochondria with high mutation load in one of their daughter cells in order to reduce the mutation load and maintain the cellular function of the other. The one that inherits most of the dysfunctional mitochondria from the mother cell will undergo cell death. Defective mitochondria are red. Normal mitochondria are beige. Mitochondria in the transitional status are pink.

Third, mitophagy is essential for stem cells to maintain their identity against senescence (García-Prat *et al.*, 2016). Stem cells might have a stringent quality control system to degrade dysfunctional mitochondria with high levels of inherited mtDNA mutations, enabling the biogenesis of normal mitochondria, which together decreases the mutation load in stem cells and their progenies (Figure 7.4). These hypothesised mechanisms might be impaired in normal ageing individuals, leading to the accumulation of somatic mtDNA mutations in stem cell populations. It would be critical to investigate the gene expression in isolated stem cells from $tRNA^{Ala}$ mutant mice and compare it with that in those isolated from young and aged wild-type mice to understand the mechanism whereby stem cells contribute to the loss of inherited mutations and whether it is associated with the presence of the upper heteroplasmy limit of inherited mtDNA mutations.

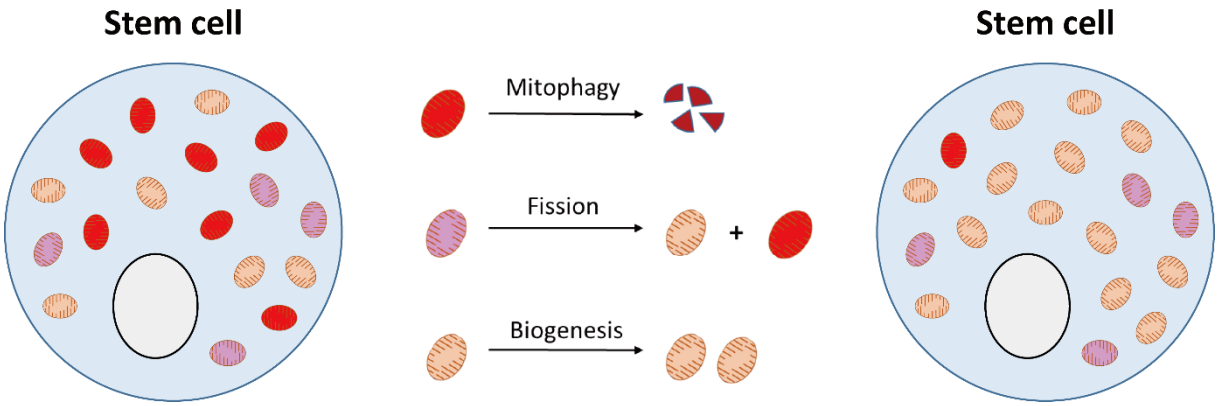

Figure 7.4 Hypothesis three: stem cells might be able to remove excessive mtDNA mutations by mitophagy and repopulate healthy mitochondria with enhanced mitochondrial biogenesis. Mitochondrial fission is required to isolate the impaired part of mitochondria for the subsequent mitophagy. Defective mitochondria are red. Normal mitochondria are beige. Sub-healthy mitochondria are pink.

7.6 Final conclusion

To summarise, this work has advanced the understanding of the loss of inherited mtDNA mutations and its effect on biochemical phenotypes in mitotic tissue, highlighting the contrasting selective pressures on inherited and somatic mtDNA mutations. The $tRNA^{Ala}$ mouse model has proved to be a good model for investigating the selective pressures against inherited mutations. Characterisation of these mice has provided important information about the development of the non-random distribution of inherited mtDNA mutations in different types of tissues and have furthered the understanding of mtDNA disease progression. This work has revealed important features of the selective loss of inherited mtDNA mutations and has demonstrated the requirement for mechanistic investigations, which are critical to understanding the development of mtDNA disease and ageing as well as its association with stem cell biology.

Chapter 8 Appendices

8.1 Appendix 1 Case history of patients with mtDNA disease

Patient 1, harbouring the m.3243A>G mutation, is a 33-year-old female with deafness, ataxia and GI dysmotility. Patient 2, carrying the m.3243A>G mutation, had progressive mitochondrial disease with deafness, diabetes, stroke-like episodes, cognitive impairment, cardiac abnormality, epilepsy and GI dysmotility. She died at the age of 36. Patient 3 with the m.3243A>G mutation, was the aunt of patient 2. She progressively developed symptoms of mitochondrial disease, including cognitive impairment, deafness and GI dysmotility. She died at the age of 64. Patient 4 harboured the m.8344A>G mutation with progressive development of mitochondrial disorders involving myoclonus, epilepsy, cognitive impairment and cardiac abnormalities. He died at age 56 years.

8.2 Appendix 2 Histochemical assays on colonic epithelium of the patient 4

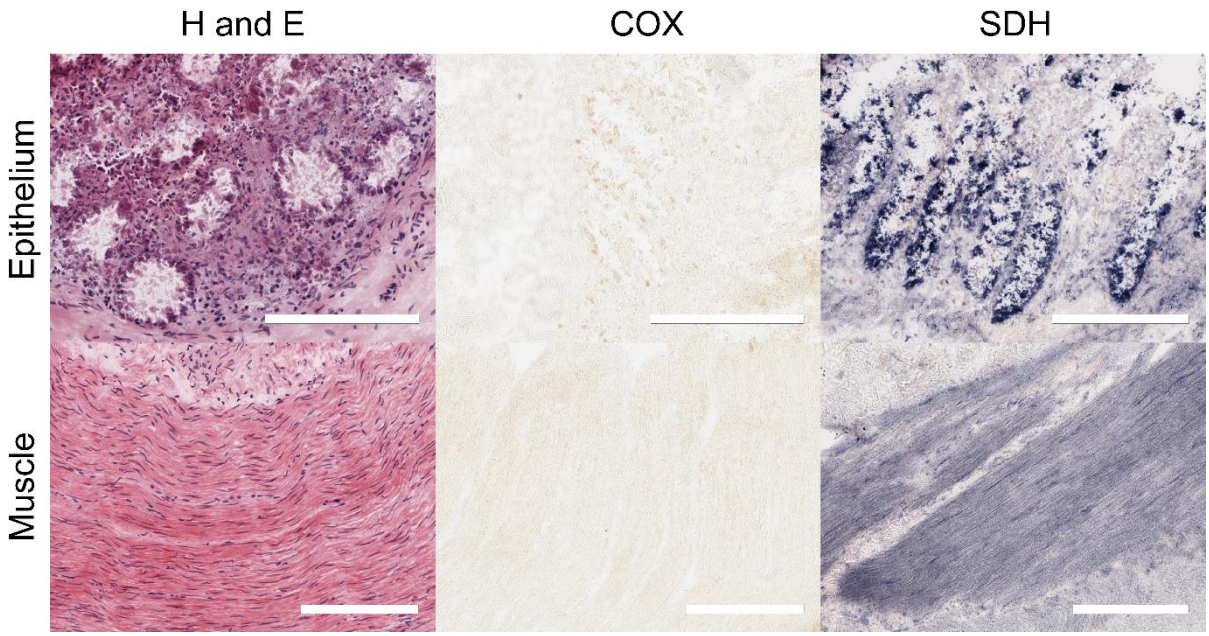

Figure 8.1 Haematoxylin and eosin staining, COX and SDH histochemical assays on colonic epithelium of the patient 4. Colonic crypts are severely degraded as is shown by the H and E staining. The morphology of cells is unidentifiable within the crypts. No tissue is labelled with the COX histochemical assay, which is likely due to tissue degradation. SDH assay reveals the presence of SDH activity in the smooth muscle; however, the labelling in the colonic crypts is possibly unspecific chemical precipitates on cell debris.

8.3 Appendix 3 “Inherited pathogenic mitochondrial DNA mutations and gastrointestinal stem cell populations.”

Su, Tianhong, Grady, John P., Afshar, Sorena, McDonald, Stuart A. C., Taylor, Robert W., Turnbull, Doug M., & Greaves, Laura C. (2018). Inherited pathogenic mitochondrial DNA mutations and gastrointestinal stem cell populations. *The Journal of Pathology*, 246(4), 427-432.

Journal of Pathology
J Pathol 2018; **246:** 427–432
Published online 5 November 2018 in Wiley Online Library (wileyonlinelibrary.com) DOI: 10.1002/path.5156

BRIEF DEFINITIVE REPORT

Inherited pathogenic mitochondrial DNA mutations and gastrointestinal stem cell populations

Tianhong Su[1], John P Grady[1], Sorena Afshar[2], Stuart AC McDonald[3], Robert W Taylor[1], Doug M Turnbull[1,4] and Laura C Greaves[1,4]*

[1] *Wellcome Centre for Mitochondrial Research, Institute of Neuroscience, Newcastle University, Newcastle upon Tyne, UK*
[2] *Human Nutrition Research Centre, Institute of Cellular Medicine, Newcastle University, Campus for Ageing and Vitality, Newcastle upon Tyne, UK*
[3] *Centre for Tumour Biology, Barts Cancer Institute, Queen Mary University of London, London, UK*
[4] *LLHW Centre for Ageing and Vitality, Newcastle University Institute for Ageing, The Medical School, Newcastle upon Tyne, UK*

**Correspondence to: LC Greaves, LLHW Centre for Ageing and Vitality, Institute of Neuroscience, The Medical School, Newcastle University, Newcastle upon Tyne, NE2 4HH, UK. E-mail: laura.greaves@ncl.ac.uk*

Abstract

Inherited mitochondrial DNA (mtDNA) mutations cause mitochondrial disease, but mtDNA mutations also occur somatically and accumulate during ageing. Studies have shown that the mutation load of some inherited mtDNA mutations decreases over time in blood, suggesting selection against the mutation. However, it is unknown whether such selection occurs in other mitotic tissues, and where it occurs within the tissue. Gastrointestinal epithelium is a canonical mitotic tissue rapidly renewed by stem cells. Intestinal crypts (epithelium) undergo monoclonal conversion with a single stem cell taking over the niche and producing progeny. We show: (1) that there is a significantly lower mtDNA mutation load in the mitotic epithelium of the gastrointestinal tract when compared to the smooth muscle in the same tissue in patients with the pathogenic m.3243A>G and m.8344A>G mutations; (2) that there is considerable variation seen in individual crypts, suggesting changes in the stem cell population; (3) that this lower mutation load is reflected in the absence of a defect in oxidative phosphorylation in the epithelium. This suggests that there is selection against inherited mtDNA mutations in the gastrointestinal stem cells that is in marked contrast to the somatic mtDNA mutations that accumulate with age in epithelial stem cells leading to a biochemical defect.

Keywords: mitochondrial DNA mutation; selection; segregation; mitochondrial disease; intestinal stem cell; gastrointestinal epithelium; MELAS; MERRF; m.3243A>G; alimentary canal

Received 27 June 2018; Revised 2 August 2018; Accepted 12 August 2018

No conflicts of interest were declared.

Introduction

Mitochondria are ubiquitous organelles present in eukaryotic cells, a major function of which is to generate ATP via the process of oxidative phosphorylation (OXPHOS). Mitochondria contain their own DNA (mtDNA), which encodes 13 essential protein subunits of the OXPHOS system, 22 tRNAs and 2 rRNAs. Each cell contains multiple copies of mtDNA. Cells may be homoplasmic, where all the copies of mitochondrial DNA are identical, or heteroplasmic, with a mixture of mutated and wild-type mtDNA molecules. The vast majority of mtDNA mutations are functionally recessive and an OXPHOS defect only occurs when the mutation load exceeds a critical threshold [1].

Mutations of mtDNA are a common cause of human inherited disease [2], but they also accumulate somatically in tissues such as skeletal muscle, intestinal epithelium, and blood with age [3–5]. In patients with primary heteroplasmic mtDNA disease, despite uniform mutation load across all tissues during foetal development [6–8], some mtDNA mutations show a decrease in the mutation load with age in blood and a few epithelial tissues [9–11]. This suggests that mitotic tissue may selectively lose inherited mtDNA mutations over time. This is in marked contrast to somatic mtDNA mutations that accumulate in such tissues with age [4,5,12]. In addition, it is unknown whether the loss of inherited mtDNA mutations is a common feature for all mitotic tissues and where it happens in the tissue. To address some of these questions, we have investigated germline pathogenic heteroplasmic mtDNA mutations in gastrointestinal stem cell populations. We compared OXPHOS activity, mitochondrial protein expression, and mutation load in the epithelium and smooth muscle of the oesophagus, stomach,

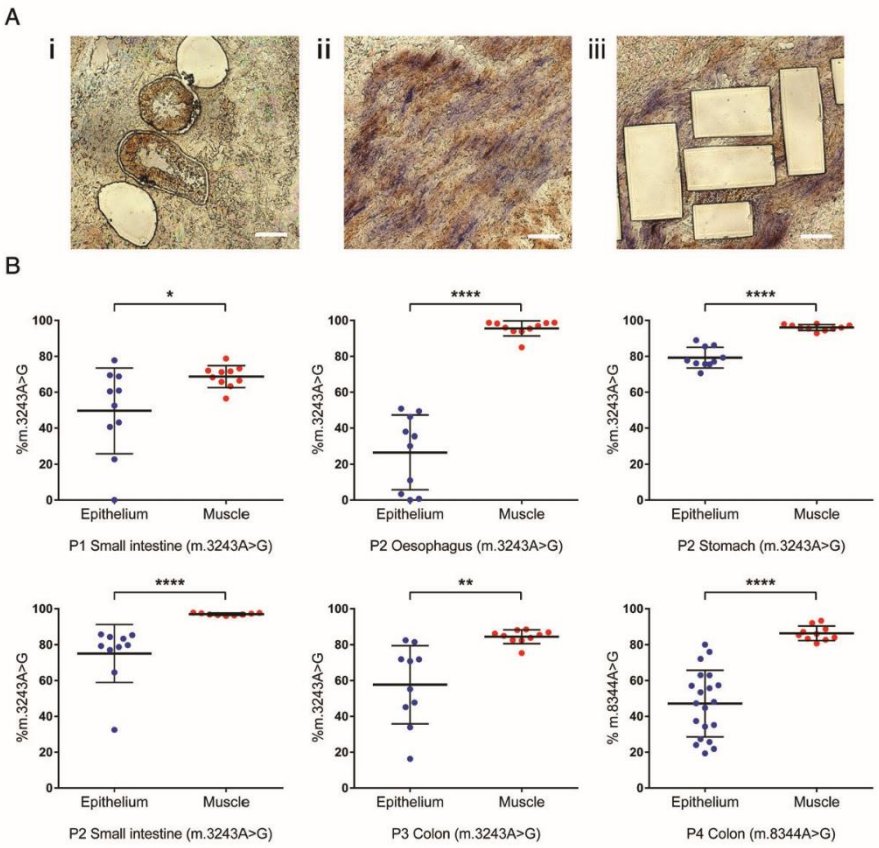

Figure 1. Lower levels of m.3243A>G and m.8344A>G detected in the mitotic epithelium compared with the post-mitotic smooth muscle of GI tract tissues. (A) Representative images of laser-microdissected (i) intestinal crypts and smooth muscles before (ii) and after (iii) laser microdissection. (B) Quantitative pyrosequencing showing the mutation levels of inherited m.3243A>G in the epithelium and the smooth muscle of the oesophagus, the stomach, the small intestine (SI), and the colon from three patients, and inherited m.8344A>G in the colonic epithelium and smooth muscle of one patient. Each replicate represents DNA extracted from five pooled crypts of the intestines, five gastric pits of the stomach or five small areas of smooth muscle. Oesophageal DNA was obtained from the tissue laser cut as an intact area in a field of view. P1 SI ($n_e = 10$, $n_m = 10$), P2 oesophagus ($n_e = 10$, $n_m = 10$), P2 stomach ($n_e = 10$, $n_m = 10$), P2 SI ($n_e = 10$, $n_m = 9$), P3 colon ($n_e = 10$, $n_m = 10$), P4 colon ($n_e = 20$, $n_m = 10$). $^{*}p < 0.05$, $^{**}p < 0.005$, and $^{****}p < 0.0001$ by unpaired t-test or Mann–Whitney U-test based on the normality of the data.

and the small and large intestines of patients with the common inherited m.3243A>G mtDNA variant within MT-TL1 (encoding mitochondrial $tRNA^{Leu(UUR)}$) and m.8344A>G mtDNA variant within MT-TK (encoding mitochondrial $tRNA^{Lys}$).

Materials and methods

Patients

Gastrointestinal tissue samples were collected from three patients with m.3243A>G (patient 1 following ileum resection at the age of 30; patients 2 and 3, aged 36 and 64, respectively at post-mortem) and from one patient with m.8344A>G aged 56. Control tissue was either taken during endoscopy from patients in whom no pathology was found or at resection for colon cancer at a distance of > 20 cm from the neoplasm. Details of the subjects may be found in the supplementary material, Supplementary materials and methods and Tables S1 and S2. Ethical approval was obtained from Newcastle and North Tyneside LREC.

Pyrosequencing

Epithelial crypts and smooth muscle fibres were randomly selected and laser-microdissected using a PALM Laser microdissection system (Zeiss, Jena, Germany) (Figure 1A). Total DNA was extracted by cell lysis

as previously described [13]. PyroMark Assay design software v2.0 (QIAGEN, Hilden, Germany) was used to design the primer trio for pyrosequencing (supplementary material, Table S3). Heteroplasmy levels were quantified using the PyroMark Q96 software according to the manufacturer's instructions.

Sequential Cytochrome c Oxidase/Succinate Dehydrogenase (COX/SDH) histochemistry

Sequential COX/SDH histochemistry was carried out as previously described [4]. Quantification of COX deficiency was calculated as the proportion of COX-deficient crypts by all the crypts counted on two sections.

Immunofluorescence

Quadruple immunofluorescence was performed as previously described [14]. Details of the antibodies used may be found in the supplementary material, Table S4. The optical density of the fluorescent images was measured by ImageJ. Background correction and the method to determine the parameters (mean and standard deviation, SD) of the control population have been described formerly [14]. The Z-score of each respiratory chain subunit for the disease case was calculated and categorised based on the normal population. For NDUFB8, the level was classified as 'negative' (< −3 SD), 'intermediate' (−3 to −2 SD) or 'positive' (> −2 SD). For the non-mtDNA encoded proteins COX4 and SDHA, the levels were categorised as 'low' (< −2 SD), 'normal' (−2 to 2 SD) or 'high' (> 2 SD).

Results

MtDNA mutation load in epithelial crypts compared with smooth muscle fibres

The load of the m.3243A>G mutation was lower in crypts laser-microdissected from the mucosa compared with fibres from the smooth muscle in oesophagus ($p < 0.0001$, Mann–Whitney U-test), stomach ($p < 0.0001$, unpaired t-test), the small intestines (SI) ($p < 0.05$ for patient 1 and $p < 0.0001$ for patient 2, unpaired t-test and Mann–Whitney U-test respectively), and colon ($p < 0.005$, unpaired t-test) (Figure 1B). In addition, our studies showed a markedly lower heteroplasmy in the mitotic epithelium than in the smooth muscle of colon from the patient with the m.8344A>G mutation ($p < 0.0001$, unpaired t-test) (Figure 1B). The mutation load in the epithelium was notably variable, with no detectable mutation in some of the intestinal crypts and oesophageal epithelium. We did not observe any crypts with m.3243A>G higher than 86% or any oesophageal epithelium with m.3243A>G higher than 51%. The colonic epithelium also showed an upper threshold for m.8344A>G of approximately 80%. In most cases, the level in the mucosal epithelium was also lower than other post-mitotic tissues such as skeletal and cardiac muscle, suggesting a loss of mutation overall (supplementary material, Table S2).

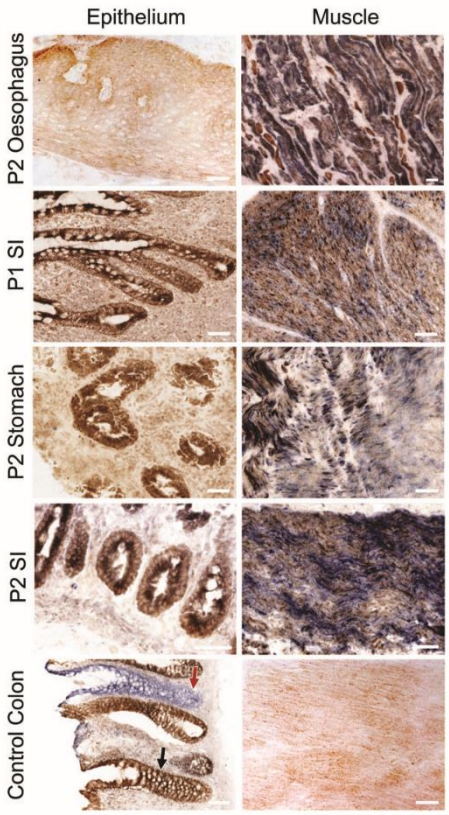

Figure 2. Deficient COX activity in post-mitotic smooth muscle but normal COX activity in mitotic epithelium of the alimentary canal in patients with inherited m.3243A>G. The left panel shows the COX-normal epithelium that is labelled brown in the SI of patient 1, and the oesophagus, the stomach, and the SI of patient 2, while the right panel manifests the blue COX-deficient muscle fibres in these tissues. The control panel shows the COX-normal epithelium (black arrow) and smooth muscle from a normal individual who also has crypts with defective COX activity (red arrow), due to accumulated somatic mtDNA mutations during ageing. Scale bar = 50 µm.

Enzyme activity and protein level of OXPHOS complexes

The m.3243A>G mutation in the $tRNA^{Leu(UUR)}$ gene impairs mitochondrial protein synthesis, causing defects in single or multiple respiratory chain complexes, including complex I and complex IV (COX) enzyme activity [15]. We hypothesised that if the inherited pathogenic mutation was lost in the epithelium, this would alleviate the mitochondrial biochemical defect within the tissue [15]. Sequential COX/SDH histochemistry showed very little COX activity in the post-mitotic

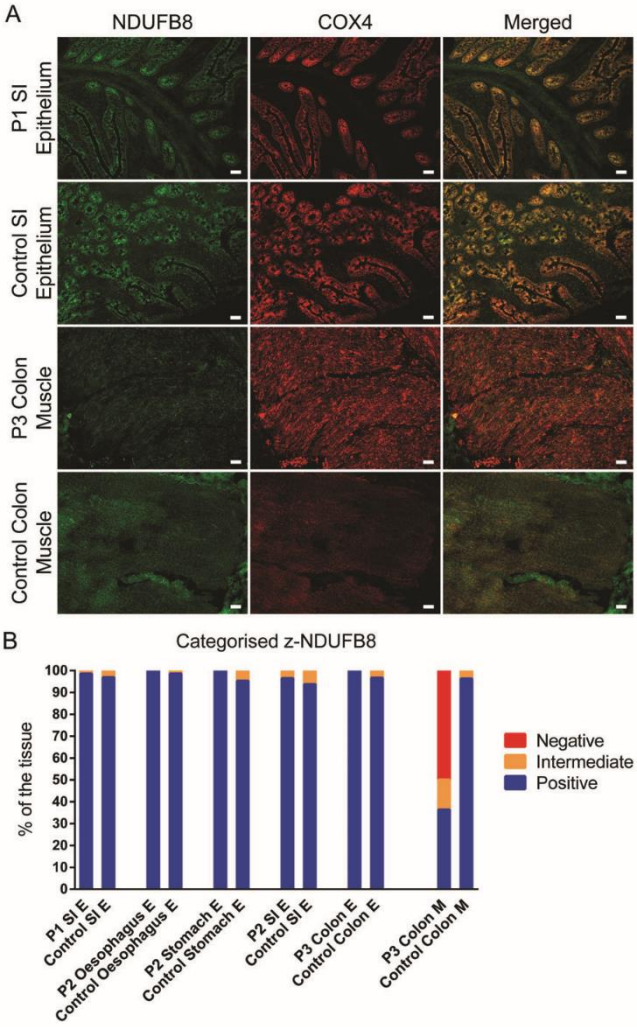

Figure 3. Protein levels of complex I were normal in the mitotic epithelium along the gastrointestinal tract but deficient in the post-mitotic smooth muscles. (A) Example of immunofluorescence images showing the levels of NDUFB8 (complex I) (green) and COX4 (red), a nuclear encoded subunit that is not compromised by the m.3243A>G mutation. (B) Quantative measurement of the protein level of NDUFB8. *Z*-scores of NDUFB8 for each patient were calculated and categorised based on the age-matched control population. The numbers of crypts for quantification were as follows: *n* (P1 SI) = 70; *n* (control) =128; *n* (P2 SI) = 28; *n* (control) = 48; *n* (P2 stomach) = 6; *n* (control) = 36; *n* (P3 colon) = 20; *n* (control) = 91. Oesophageal epithelium and colonic smooth muscle from the whole section were selected for quantification. Patient data were compared with data from two controls for the stomach; three controls for the colon, the oesophagus, and the SI of patient 2; and four controls for the SI of patient 1. E = epithelium. M = muscle. Scale bar = 50 μm

smooth muscle of all three regions of the gastrointestinal tract. However, COX activity was largely preserved in the epithelial cells (Figure 2). We detected no COX deficiency in the oesophagus and SI of patient 2, and only 1.25% COX deficiency in the SI epithelium of patient 1, 2.67% in the stomach epithelium of patient 2, and 2.59% in the large intestinal epithelium of patient 3.

Since there is no reliable histochemical assay for complex I, we used immunofluorescence to quantify the levels of NDUFB8, a subunit of respiratory chain complex I critical to the complex assembly and often lost in OXPHOS deficiency [14]. NDUFB8 showed normal expression in the epithelium of the colon, oesophagus, stomach, and SI of the patients (Figure 3) compared with age-matched controls. In contrast, NDUFB8 was

low with 50% deficiency in the post-mitotic smooth muscle of the colon from patients compared with age-matched controls (Figure 3). We found higher levels of nuclear encoded mitochondrial proteins, SDHA and COX4, both of which are reported to be preserved in tissues with mtDNA defects [16], in the epithelium of the patients' oesophagus (47.62% and 40.91%, respectively), stomach (14.29% for SDHA), and SI (10% in patient 2 for SDHA; 8.57% in patient 1 and 14.29% in patient 2 for COX4) (supplementary material, Figure S1). SDHA also increased in the colonic muscle of the patient (27.27% (supplementary material, Figure S1)). This is likely a compensatory response.

Discussion

Understanding the behaviour of mtDNA mutations in different tissues is critical not only to understanding the phenotype of inherited mtDNA disease but also in our understanding of the impact of acquired mtDNA mutations seen in human ageing. Here, we have investigated multiple epithelial tissues from patients with inherited mtDNA mutations and have shown a significantly lower mtDNA mutation level in epithelial cells compared with the post-mitotic smooth muscle fibres of the oesophagus, the stomach, and the small and the large intestine. We show that the mutation level is correlated with the finding of normal COX activity and complex I protein levels in epithelial cells, but deficient COX activity and low complex I protein expression in the post-mitotic smooth muscle from the same patients. The finding of respiratory chain deficiency in the gastrointestinal smooth muscle is similar to previous reports [17] and entirely consistent with the severe symptoms of bowel dysmotility in many patients with mitochondrial disease.

Previous reports in foetal tissues show that the level of mtDNA mutation was largely uniform in all tissues [6–8]. Given that there is little evidence that the mutation burden changes with age in muscle [10], our results suggest a loss of inherited mtDNA mutation in the mitotic gastrointestinal epithelium with age. This is consistent with previous reports showing a loss of the m.3243A>G mutation in patients' blood over time [9,10]. However, as all of our patients are adults, the exact time of the loss remains unknown. It is known that m.3243A>G mutation load is the same in all tissues during embryo development and fetal growth [6–8] and the studies in blood (where serial measurements are possible) show loss of mutation throughout life but most markedly in the early years [9,10]. Whilst we have a very small patient cohort, we did determine if there was a trend for more mutation loss in epithelial cells in the older patient (64 years) when compared with the same type of epithelial tissue from the younger patient (30 years). We did not detect a difference but previous studies in blood have shown considerable individual variation and a slowing down of selection after early adult life [10].

The site of the loss of mutation in mitotic tissues is unknown but previous *in silico* modelling suggests that the selective loss occurs in haematopoietic stem cells [18]. Intestinal crypts have stem cells at the base with amplifying cells and differentiated progenies present in the crypt. Crypts also undergo monoclonal conversion until a whole crypt derives from a single stem cell [19]. In this context, the pattern of mtDNA mutation load seen in crypts is interesting since it shows marked variation in the level, with some crypts carrying no detectable mutation. This strongly indicates that selection against the mutation is occurring at the stem cell level since selection at any other stage is unlikely to result in no detectable mutation. The overall marked decrease in the mutation level and the upper cut-off threshold in the intestinal crypts imply a negative selection against the mutations, not a bidirectional random genetic drift.

These observations in intestinal crypts in patients with mtDNA disease are in marked contrast to the observation in normal ageing of human gastrointestinal stem cells, where mitochondrial DNA mutations accumulate somatically up to homoplasmy, resulting in OXPHOS deficiency [4,12,20]. In contrast to our data for inherited mtDNA mutations, there is no evidence of any selective pressures on these somatic mtDNA mutations [21]. The difference in the selective pressures on somatic and inherited mtDNA mutations remains unknown but indicates significant changes in stem cell biology in the normal ageing process.

Acknowledgements

This study was funded by the Newcastle University Centre for Ageing and Vitality supported by the BBSRC, EPSRC, ESRC, and MRC as part of the cross-council Lifelong Health and Wellbeing Initiative (DMT, LCG); the Wellcome Centre for Mitochondrial Research (203105/Z/16/Z; LCG, RWT, DMT); UK NIHR Biomedical Research Centre in Age and Age Related Diseases award to the Newcastle upon Tyne Hospitals NHS Foundation (DMT); and the UK NHS Highly Specialised Service for Rare Mitochondrial Disorders of Adults and Children (DMT, RWT).

Author contributions statement

LCG and DMT conceived and designed the study. SA, SACM, and RWT provided study material. TS collected and/or assembled data. TS and JPG analysed and interpreted data. TS, LCG, and DMT wrote the manuscript. TS, JPG, SA, SACM, RWT, DMT, and LCG had final approval of the manuscript.

References

1. Taylor RW, Turnbull DM. Mitochondrial DNA mutations in human disease. *Nat Rev Genet* 2005; **6**: 389–402.

2. Gorman GS, Schaefer AM, Ng Y, *et al.* Prevalence of nuclear and mitochondrial DNA mutations related to adult mitochondrial disease. *Ann Neurol* 2015; **77:** 753–759.
3. Bua E, Johnson J, Herbst A, *et al.* Mitochondrial DNA-deletion mutations accumulate intracellularly to detrimental levels in aged human skeletal muscle fibers. *Am J Hum Genet* 2006; **79:** 469–480.
4. Taylor RW, Barron MJ, Borthwick GM, *et al.* Mitochondrial DNA mutations in human colonic crypt stem cells. *J Clin Invest* 2003; **112:** 1351–1360.
5. Shin MG, Kajigaya S, Tarnowka M, *et al.* Mitochondrial DNA sequence heterogeneity in circulating normal human CD34 cells and granulocytes. *Blood* 2004; **103:** 4466–4477.
6. Matthews PM, Hopkin J, Brown RM, *et al.* Comparison of the relative levels of the 3243 (A→G) mtDNA mutation in heteroplasmic adult and fetal tissues. *J Med Genet* 1994; **31:** 41–44.
7. Cardaioli E, Fabrizi GM, Grieco GS, *et al.* Heteroplasmy of the A3243G transition of mitochondrial tRNA$^{Leu(UUR)}$ in a MELAS case and in a 25-week-old miscarried fetus. *J Neurol* 2000; **247:** 885–887.
8. Monnot S, Gigarel N, Samuels DC, *et al.* Segregation of mtDNA throughout human embryofetal development: m. 3243A> G as a model system. *Hum Mutat* 2011; **32:** 116–125.
9. Rahman S, Poulton J, Marchington D, *et al.* Decrease of 3243 A→ G mtDNA mutation from blood in MELAS syndrome: a longitudinal study. *Am J Hum Genet* 2001; **68:** 238–240.
10. Grady JP, Pickett SJ, Ng YS, *et al.* mtDNA heteroplasmy level and copy number indicate disease burden in m.3243A>G mitochondrial disease. *EMBO Mol Med* 2018; **10:** e8262.
11. Olsson C, Johnsen E, Nilsson M, *et al.* The level of the mitochondrial mutation A3243G decreases upon ageing in epithelial cells from individuals with diabetes and deafness. *Eur J Hum Genet* 2001; **9:** 917–921.
12. Greaves LC, Barron MJ, Plusa S, *et al.* Defects in multiple complexes of the respiratory chain are present in ageing human colonic crypts. *Exp Gerontol* 2010; **45:** 573–579.
13. Rygiel KA, Grady JP, Taylor RW, *et al.* Triplex real-time PCR – an improved method to detect a wide spectrum of mitochondrial DNA deletions in single cells. *Sci Rep* 2015; **5:** 9906.
14. Rocha MC, Grady JP, Grünewald A, *et al.* A novel immunofluorescent assay to investigate oxidative phosphorylation deficiency in mitochondrial myopathy: understanding mechanisms and improving diagnosis. *Sci Rep* 2015; **5:** 15037.
15. Hämäläinen RH, Manninen T, Koivumäki H, *et al.* Tissue- and cell-type-specific manifestations of heteroplasmic mtDNA 3243A>G mutation in human induced pluripotent stem cell-derived disease model. *Proc Natl Acad Sci U S A* 2013; **110:** E3622–E3630.
16. Chrysostomou A, Grady JP, Laude A, *et al.* Investigating complex I deficiency in Purkinje cells and synapses in patients with mitochondrial disease. *Neuropathol Appl Neurobiol* 2016; **42:** 477–492.
17. Betts J, Barron MJ, Needham SJ, *et al.* Gastrointestinal tract involvement associated with the 3243A> G mitochondrial DNA mutation. *Neurology* 2008; **70:** 1290–1292.
18. Rajasimha HK, Chinnery PF, Samuels DC. Selection against pathogenic mtDNA mutations in a stem cell population leads to the loss of the 3243A→G mutation in blood. *Am J Hum Genet* 2008; **82:** 333–343.
19. Snippert HJ, van der Flier LG, Sato T, *et al.* Intestinal crypt homeostasis results from neutral competition between symmetrically dividing Lgr5 stem cells. *Cell* 2010; **143:** 134–144.
20. McDonald SAC, Greaves LC, Gutierrez-Gonzalez L, *et al.* Mechanisms of field cancerization in the human stomach: the expansion and spread of mutated gastric stem cells. *Gastroenterology* 2008; **134:** 500–510.
21. Greaves LC, Elson JL, Nooteboom M, *et al.* Comparison of mitochondrial mutation spectra in ageing human colonic epithelium and disease: absence of evidence for purifying selection in somatic mitochondrial DNA point mutations. *PLoS Genet* 2012; **8:** e1003082.

SUPPLEMENTARY MATERIAL ONLINE

Supplementary materials and methods

Supplementary figure legends

Figure S1. Quantitative measurement of COX4 and SDHA level in the gastrointestinal epithelium and smooth muscle

Table S1. Information of the subjects and the obtained tissue

Table S2. Heteroplasmic levels of pathogenic mtDNA mutations measured in various tissues of the four patients

Table S3. Primer sequences used for pyrosequencing to quantify m.3243A>G and m.8344A>G mutation levels

Table S4. Antibodies and concentrations used in the immunofluorescence assay

8.4 Appendix 4 “Roles of Mitochondrial DNA Mutations in Stem Cell Ageing.”

Su, Tianhong, Turnbull, Doug, & Greaves, Laura. (2018). Roles of Mitochondrial DNA Mutations in Stem Cell Ageing. *Genes, 9*(4), 182.

genes

MDPI

Review

Roles of Mitochondrial DNA Mutations in Stem Cell Ageing

Tianhong Su [1], Doug M. Turnbull [1,2] and Laura C. Greaves [1,2,*]

[1] Wellcome Centre for Mitochondrial Research, Institute of Neuroscience, Newcastle University, Newcastle upon Tyne NE2 4HH, UK; t.su2@newcastle.ac.uk (T.S.); doug.turnbull@newcastle.ac.uk (D.M.T.)

[2] LLHW Centre for Aging and Vitality, Newcastle University Institute for Aging, The Medical School, Newcastle upon Tyne NE2 4HH, UK

* Correspondence: laura.greaves@newcastle.ac.uk; Tel.: +44-(0)-191-208-6291

Received: 26 February 2018; Accepted: 26 March 2018; Published: 27 March 2018

Abstract: Mitochondrial DNA (mtDNA) mutations accumulate in somatic stem cells during ageing and cause mitochondrial dysfunction. In this review, we summarize the studies that link mtDNA mutations to stem cell ageing. We discuss the age-related behaviours of the somatic mtDNA mutations in stem cell populations and how they potentially contribute to stem cell ageing by altering mitochondrial properties in humans and in mtDNA-mutator mice. We also draw attention to the diverse fates of the mtDNA mutations with different origins during ageing, with potential selective pressures on the germline inherited but not the somatic mtDNA mutations.

Keywords: stem cell; mitochondrial DNA mutation; ageing; purifying selection; mitochondrial mutagenesis; progenitor; mitochondrial disease; ageing mouse model; mitochondrial DNA-mutator mouse; mitochondria

1. Introduction

Ageing is a process where tissue gradually loses homeostasis and regeneration [1]. This process is systemic and closely associated to age-related changes in somatic stem cells [2]. These cells renew themselves and differentiate into tissue-specific daughter cells for tissue maintenance and regeneration. The age-related alterations in somatic stem cell properties include failure to generate functional progenies, depletion of the stem cell pool and cancerous transformation [3]. These changes largely affect mitotic tissue, such as blood, intestine and skin, where the stem cells actively produce progenies to maintain the high turnover of the tissue [4,5]. However, they also contribute to ageing post-mitotic tissue, such as brain and muscle, though stem cells in these tissues are considered quiescent under normal physiological conditions and activated in response to damage for repairing the tissue [6,7].

Mitochondria synthesize ATP via oxidative phosphorylation (OXPHOS) through five multi-subunit complexes. Mitochondria contain their own DNA (mtDNA), which encodes key subunits of these complexes. Replication of the mitochondrial genome is independent of the cell cycle [8]. In addition, mtDNA is susceptible to damage due to lack of histone protection and proximity to oxidative stress [9]. Due to these reasons, compared with the nuclear DNA, mtDNA is more prone to mutations. Multiple copies of mtDNA reside in a cell. Mutations of mtDNA usually occur as a proportion of the total copies and once they reach a threshold, mitochondria will display respiratory chain deficiency, a consequence of which is potentially excessive production of reactive oxygen species (ROS) [10]. mtDNA is maternally transmitted through germline with a bottleneck effect, where only a small portion of mtDNA molecules are distributed into each primordial germ cell,

which are amplified in later oogenesis. As a result, mature oocytes may have very different levels of mtDNA mutations [11].

Ageing is accompanied by a reduction of mitochondrial function, resulting in respiratory chain defects which are thought to be associated with the accumulation of somatic mtDNA mutations [12]. The age-related change in mitochondria may in turn accelerate the ageing process [13]. Although the significance of mtDNA mutations in various parenchymal cells in normal ageing and age-related degenerative diseases has been broadly studied [14], the findings might not be able to be extrapolated to stem cells, as they are distinct from somatic cells in terms of biological and metabolic characteristics. With an increasing amount of research linking mtDNA mutations to stem cell ageing in the last decade, we discuss how the somatic mtDNA mutations behave during ageing in stem cell populations and how they potentially influence phenotypes of the stem cells with the evidence from the recent studies. Specifically, we want to draw attention to an intriguing age-related phenomenon of the germline inherited mtDNA mutations in patients with mitochondrial disorders, as opposed to the accumulated somatic mtDNA mutations in normal individuals, as mtDNA mutations from different origins seem to have diverse fates with age.

2. Somatic mtDNA Mutations in Normal Ageing Humans

Respiratory chain defects have been observed in a variety of tissues in normal ageing humans, including the tissue traditionally considered post-mitotic, such as skeletal muscle [15], heart [16] and brain [17]; tissue with substantial mitotic potential after injury, for example, the liver [18]; as well as the typical mitotic tissue such as the epithelium of the stomach [19], small intestine [20] and colon (Figure 1) [21,22]. Various somatic mtDNA mutations were found to clonally expand and accumulate to high levels with age in the respiratory chain deficient areas of the tissue, regardless of their pathogenicity [21,23–27]. In addition, Shin et al. found increased mtDNA heterogeneity in CD34+ marked haematopoietic stem cell (HSC) and the progenitor cells both in the bone marrow and the peripheral blood from the adult donors compared to the homogenous umbilical cord blood [26,28]. In the intestinal crypt where all the cells derive from the stem cells located at the base of the crypt, the same somatic mtDNA mutation was determined at different regions along the OXPHOS defective crypt, indicating that they originated from a communal stem cell that harboured the mutation [20]. Monoclonal conversion where a single stem cell with the accumulated somatic mtDNA mutation passes the mutation to its progenies to occupy the entire crypt has also been observed in the stomach [19]. These studies provide robust evidence that in mitotic tissue, the accumulation of the somatic mtDNA mutation during ageing initiates in stem cells. However, whether the mutations aggregate in the stem cell of post-mitotic tissue, such as neural stem cells and satellite cells (muscle stem cell) and how they influence the fate of their progenies in aged humans remains unclear.

The accumulation of the somatic mtDNA mutation during ageing can be entirely achieved by random genetic drift, which takes place early in life in contrast to the damage to mtDNA by excessive ROS production from the respiratory chain defect [29]. The pathogenicity of the acquired mtDNA mutations is markedly higher than in germline variants, suggesting that the purifying selective mechanism against germline mtDNA mutations is absent from the somatic mtDNA mutations [30].

The occurrence and the spread of the somatic mtDNA mutations during ageing are notably tissue-specific, potentially influenced by the mitotic capability of the tissue. In contrast to miscellaneous mtDNA point mutations found in the colonic stem cell populations, no large-scale deletions have been detected in any OXPHOS deficient crypts [21]. Post-mitotic brain and muscle preferentially accumulate mtDNA deletions instead of point mutations with age [31,32]. It has been proposed that neurons, which are highly energy consuming and sensitive to ROS, tend to acquire mtDNA deletions during the process of repairing the mtDNA that are injured by ROS [33]. Whereas in mitotic tissue, mtDNA mutations are likely to arise from errors during replication [31]. Furthermore, the stem cell niche is involved in dispersing the somatic mtDNA mutations specifically in mitotic tissue during ageing. Gland and crypt fission from the stem cell niche in the stomach and colon, respectively, have been shown to spread the mutation from a single unit to form a patch [19,34].

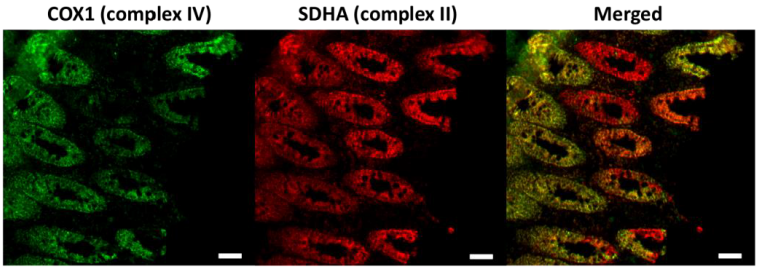

Figure 1. Immunofluorescence images of the respiratory chain deficiency caused by the age-dependent accumulation of somatic mitochondrial DNA (mtDNA) mutations in the colon. Respiratory chain complex IV (marked by the COX1 antibody) is encoded by both mtDNA and nuclear DNA (nDNA), which is affected by the increased burden of mtDNA mutations. Complex II (labelled by the SDHA antibody) is entirely encoded by nDNA. The complex IV deficient colonic cells are indicated red in the merged picture. COX1, a key subunit of complex IV encoded by mtDNA. SDHA, one of the four nuclear encoded subunits of complex II. Scale bar: 50 μm.

However, limited numbers of human studies delve into how somatic mtDNA mutations affect the function of stem cells and their progenies to contribute to the ageing phenotype of the tissue, and the findings are controversial. Respiratory chain deficiency due to accumulated somatic mtDNA mutations in colonic stem cells diminished the cell population of the crypt by weakening the cell proliferation and enhancing the apoptosis of the stem cell progenies [35]. In contrast, the level of the lineage markers labelling all the differentiated daughter cells derived from the OXPHOS deficient stem cell were shown to be normal when compared to OXPHOS normal epithelium of the gastric unit and the small intestinal crypt, indicating that the functionality of the progenies were not affected [19,20]. Additionally, the patch of hepatic progenitor cells and their descendants with OXPHOS defects did not show any synthetic, metabolic or proliferative impairment [18]. Due to restricted sources of human tissue samples, difficulties in tracing the stem cell dynamic condition in humans, and shortage of the stem cell markers, the mechanism by which somatic mtDNA mutations influence stem cell ageing still remains unknown in humans, and scientists have pursued animal models for investigation.

3. Ageing of Somatic Stem Cell Populations in mtDNA-Mutator Mice

The development of an mtDNA-mutator mouse model highlights the potentially important role of somatic mtDNA mutations in ageing. These mice carry a knock-in mutation in the exonuclease domain of the mtDNA polymerase γ (*Polg*), compromising the proofreading ability of *Polg*, which results in an accumulation of mtDNA mutations with age [36,37]. The mutant mice have a shortened lifespan and display a series of progeroid phenotypes, such as weight loss, kyphosis, hair greying and loss, impaired hearing, thin subcutaneous fat, osteoporosis, sarcopenia and sterility, which mimics the signs of normal human ageing [36,37]. In addition, the development of mitotic tissue including intestine, thymus and testicle, is largely affected in the mutant mice [37]. Mutator mice suffer progressive anaemia due to defective haematopoiesis, which is the main cause of death [36–38]. These findings provide evidence that links the accumulation of somatic mtDNA mutations to stem cell ageing.

3.1. Age-Dependent Dysfunction of Stem Cells and Their Progenitors in Mitotic Tissue

The age-dependent accumulation of the somatic mtDNA mutations in the mtDNA-mutator mice either alters the properties of stem cells per se or the downstream progenitors. Studies initially focused on the haematopoietic system, which is a well-established model for stem cell research. Reports show that the mice suffer from abnormal haematopoiesis for both erythroid and lymphoid lineage [38–40] and that this consequence caused by the mtDNA mutation in the haematopoietic

component is intrinsic, as transplanting the bone marrow from the homozygous mutants to the wildtype mice recapitulates the mutant phenotype [38]. Different stages of the progenitor cells through haematopoiesis have been shown to be more perturbed than the HSCs. However, HSCs themselves show notably compromised ability for repopulation and self-renewal after serial transplantation [39]. In addition, studies show that the development of the haematopoietic system is dysregulated during embryogenesis in the mtDNA mutator mice [40]. Intestinal epithelium is another beneficial model for somatic stem cell research as it allows us to visualise the gradual cradle-to-grave manifestations of the stem cell progenies in a straightforward fashion. Research on the small intestinal epithelium of the mutant mice reveals abnormal cell proliferation and increased apoptosis in the Lieberkühn crypt, where intestinal stem cells (ISC) and transit-amplifying cells are located [41]. Furthermore, the organoids consisting of ISCs and Paneth cells derived from the isolated crypts of the mutants did not grow efficiently in vitro [41]. These alterations resulted in prolonged cell migration and swollen morphology of the intestinal epithelium, leading to impaired fat absorption of the mtDNA mutator mice [41]. Studies have shown that, as with humans, the mtDNA mutations accumulating in the colonic crypts of the heterozygous mutator mice randomly distribute through the mitochondrial genome with no advantageous selection towards pathogenic mutations [42]. The clonal expansion of the mutations can be simulated by the model of random genetic drift [42]. In contrast, there is a strong rapid negative selection against nonsynonymous mtDNA mutations in the protein-coding regions through germline transmission [11,43], underlining the difference in the mechanisms of the selection during ageing and germline transmission.

3.2. Ageing of Progenitor Cells in Post-Mitotic Tissue

Compared to the severe symptoms due to mtDNA mutations in blood and other mitotic tissue, post-mitotic tissue seems less affected by mtDNA mutagenesis in the mtDNA mutator mice. Although respiratory chain function is preserved in the cerebrum, cerebellum and skeletal muscles, studies have shown direct alterations in the homeostasis of neural stem cells and muscle progenitors [40,44]. The number of the nestin-positive neuronal stem cells was decreased in the OXPHOS deficient subventricular zone of the adult mtDNA mutator mice, although the number of neurons was normal [40]. Neural stem cells (NSC) isolated from the embryos of the mutator mice showed strikingly reduced self-renewal ability, primarily because of the mtDNA mutagenesis, but not the secondary ROS, as these cells accumulated high levels of mtDNA point mutations, while barely showing respiratory chain deficiency [40]. Cardiac progenitor cells (CPC) isolated from the mtDNA mutator mice displayed attenuated proliferation and higher inclination to death [44]. Mutagenesis of mtDNA also blocked the metabolic transition of the mutant CPCs from glycolysis to OXPHOS as they differentiated, resulting in a massive cell death through differentiation [44]. Furthermore, myoblasts extracted from the mtDNA mutator mice were found to generate thinner myotubes in skeletal muscles [44]. These findings have underlined the functional change in somatic stem cells and precursors in the post-mitotic tissue due to age-related mtDNA mutagenesis.

4. Potential Mechanism Whereby Age-Related mtDNA Mutagenesis Affects Somatic Stem Cells

ROS is crucial for stem cell maintenance and is involved in manipulating stem cell differentiation, though too much ROS may be detrimental [45,46]. Mitochondrial DNA mutations are traditionally thought to affect the respiratory chain function of mitochondria, the main endogenous source of ROS, and interfere stem cell homeostasis [47]. The free radical theory of ageing based on mitochondria was initially proposed by Harman, where defective respiratory chain generates excessive ROS, damaging mtDNA and engendering somatic mtDNA mutagenesis with age, which further causes increased oxidative stress, forming a vicious cycle [48]. This theory was challenged when no obvious ROS elevation was found in different tissues of the mtDNA-mutator mice [37,49]. Analogous findings have been reported also in somatic stem cells [39]. However, treatment of antioxidant *N*-acetyl-L-cysteine (NAC) could rescue the impaired self-renewal ability of NSCs and abnormal haematopoiesis in the mutator mice [40]. The exact mechanism underlying these contradictory findings is as yet unknown. Despite an off-target possibility of NAC [50], these findings

suggest that mtDNA mutagenesis may slightly alter the ROS/redox level (Figure 2), which is able to imbalance the quiescence and regeneration of the somatic stem cells [40]. This tiny change in the ROS/redox level might be insufficient to be detected, but it can be neutralized by NAC. However, the effect of the NAC on the stem cell population only seems to be effective if given during embryogenesis [40]. Of note, whether the effect of the antioxidant on the somatic stem cell benefits alleviating the ageing phenotype of either the stem cell or the tissue of the mutator mice remains controversial, as long-term treatment of NAC from embryogenesis did not rescue the aberrant erythropoiesis in the adult mutator mice [51]. In addition, calorie restriction, which reduces ROS and enhances antioxidative defence shows no effect on ameliorating the ageing phenotype of the mutator mice [52].

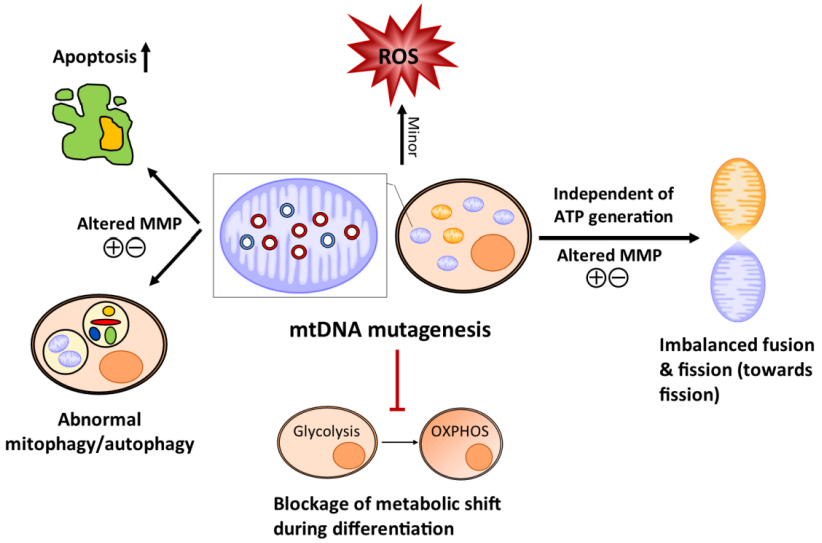

Figure 2. Schematic diagram of how the mitochondrial abnormalities caused by the age-dependent accumulation of somatic mtDNA mutations affect stem cell homeostasis in the mtDNA mutator mice. Mitochondrial DNA mutagenesis causes minor changes in reactive oxygen species (ROS)/redox level, which may alter stem cell identity (quiescence and regeneration). The somatic mtDNA mutation increases apoptosis and also shifts the level of mitophagy/autophagy in the stem cell population possibly through the loss of the mitochondrial membrane potential (MMP), which may eventually engender stem cell/progenitor depletion and accelerate stem cell senescence. Mitochondrial DNA mutagenesis imbalances mitochondrial dynamics towards fission independent of ATP production, which can affect stem cell self-renewal and differentiation. The amassing of somatic mtDNA mutations prevents stem cells from converting glycolysis to oxidative phosphorylation (OXPHOS) as they differentiate, resulting in cell death and failure to produce progenies. Normal mitochondria are coloured orange and dysfunctional mitochondria are in blue. Mutated mtDNA are red and the normal mtDNA are blue.

Recently, studies have reported another pre-ageing mouse model established by induced expression of mitochondrial-targeted endonuclease (Mito-PstI) [53,54]. The main consequence of the double strand breaks of the mtDNA caused by the induction in these mice was mtDNA depletion [53,54]. In addition, mtDNA deletions accumulated in the post-mitotic brain and heart, but not in the lung and liver of these mice, though the expression of endonuclease was low in the brain and muscle but very high in the liver and lung [54]. Mitotic tissue was preferentially affected, with effects on the function of stem cells and progenitor cells. The differentiation of thymic progenitor cells was blocked

at an early stage, leading to thymus shrinkage in these mice [54]. Satellite cells were lost in skeletal muscles of these mice, causing muscle wasting, but no change in the oxidative stress was detected in the muscle [53]. In addition, in the mitotic tissue that mainly displayed the ageing phenotype, no mtDNA depletion was found, implying that there might be another pathway that causes ageing rather than the secondary ROS generation caused by mtDNA depletion [54]. Together with the findings of the mtDNA-mutator mice, these observations suggest multi-factorial causes of ageing due to mtDNA mutagenesis or damage. In the cell model with the induction of the mtDNA endonuclease, elevated levels of ROS were detected, and this upregulated the ageing-related cell cycle arrest nuclear signalling pathway. This can be corrected by antioxidant NAC [54]. The absence of detectable changes in oxidative stress in either mtDNA-mutator mice or the Mito-PstI mice is interesting, especially since many of the effects are reversed by NAC.

Accumulation of somatic mtDNA mutations can also cause dramatic alterations in mitochondrial dynamics, which is further able to perturb stem cell self-renewal and differentiation. During differentiation of the CPCs from the mtDNA mutator mouse, mitochondria displayed a series of abnormalities when compared to the WT mice, including imbalanced fusion and fission, reduced membrane potential, and poor development of the mitochondrial microstructure [44]. Mitochondrial dynamics can change mitochondrial morphology and regulate stem cell destiny by ROS signalling independent of generating ATP by OXPHOS [55]. Hence, though no change has been found in the ATP level in the stem cells from the mtDNA-mutator mice [39,41,44], the age-dependent accumulation of mtDNA mutations may still be able to alter the fate of stem cells secondarily through anomalous mitochondrial dynamics (Figure 2).

In addition, the age-related mutagenesis of somatic mtDNA may hamper stem cell metabolism as they differentiate (Figure 2). Stem cells are naturally glycolytic, and actively suppress OXPHOS to maintain quiescence. Differentiation of stem cells requires a metabolic transition from glycolysis to OXPHOS to increase ATP production [45]. Somatic mtDNA mutations prohibited this metabolic shift as CPCs differentiate, leading to substantial cell death [44]. This could also be the reason for the blockage of the differentiation at different stages through the early erythropoiesis [39].

Furthermore, the quality control of mitochondria is perturbed in the stem cell population of the mtDNA-mutator mice, which may contribute to stem cell senescence. Autophagy is crucial for maintaining stem cell quiescence and stemness against ageing [56,57]. Studies have reported upregulated mitophagy rates in the CPCs [44] and inhibited autophagy in the early erythroid precursors of the mtDNA-mutator mice, the latter of which contributed to the malfunction of erythropoiesis [58]. Moreover, a lowered mitochondrial membrane potential (MMP) has been found in the HSCs, various haematopoietic progenitors, and the CPCs in the mtDNA-mutator mice [39,44], which is associated with mitophagy activation [59]. These observations indicate that mtDNA mutagenesis may affect stem cell function by interfering with the level of mitophagy/autophagy (Figure 2). However, how exactly mitophagy/autophagy responds to mtDNA mutagenesis in stem cells is uncertain, as the findings seem to be contradictory in different stem cell/progenitor populations. Of note, the loss of the MMP also occurs during apoptosis [60]. Consistently, strikingly increased apoptosis levels were found in the erythroid precursors and the ISC population (Figure 2) [39,41], which may subsequently lead to the depletion of the stem cell/progenitors. Surprisingly, no change in the apoptosis was observed in the HSC [39].

The effect of age-related mtDNA mutagenesis on somatic stem cell ageing seems highly tissue-specific. For haematopoiesis, it primarily affects the differentiation of downstream progenitor cells rather than HSCs themselves [39]. In contrast, it markedly affects NSCs but its impact fades during differentiation [40].

5. Behaviour of mtDNA Mutations Inherited through Germline with Age

mtDNA mutations from different origins seem to act differently with age, despite causing the same biochemical defect [14]. Mitochondrial disorders are caused by mtDNA mutations inherited through the germline or occurring during embryogenesis. As opposed to the acquired somatic mtDNA mutations that accumulate in stem cell populations with age, some of the inherited mtDNA

mutations are lost in mitotic tissue over time. Pearson syndrome is a severe medical condition caused by a single, large-scale mtDNA deletion affecting the bone marrow haematopoietic compartment and causing pancytopenia in patients [61]. However, the anaemia and the vacuolated haematopoietic precursors in the bone marrow can be rescued by an age-related loss of the deletion and patients may subsequently develop Kearns-Sayer syndrome, which primarily affects post-mitotic tissue [62–64]. It has also been reported that the mutation level of the inherited m.3243A>G, the most common mtDNA point mutation that causes mitochondrial disease, decreased in blood and various epithelial tissues with age in patients and asymptomatic carriers [65–68]. The in silico simulation suggests that the loss of the mutation occurs in HSCs [69]. In addition, in a recently-developed mouse model of mitochondrial disease, the inherited m.5024C>T was lost in the blood of the mice with high mutation levels with age [70]. These studies imply that these inherited mtDNA mutations seem to be selected against in the stem cell population in contrast to the somatic mtDNA mutations, which are under no selective pressures [30]. However, no observations of the negative selection have been reported directly in stem cells in vivo, and the mechanism is as yet unexplored. Investigating the underlying mechanism of the mtDNA mutation with different origins reacting differentially to age is crucial for understanding both the process of normal ageing and development of the mitochondrial disease.

6. Conclusions

We have provided evidence of the somatic mtDNA mutations accumulating in stem cell populations in normal humans and discussed their tissue-specific ability to expand clonally during ageing. The premature ageing mtDNA-mutator mouse model gives insight into how acquired mtDNA mutations affect the function of the stem cells and progenitors in both the mitotic and post-mitotic tissue, as well as the potential mechanisms by which age-related mtDNA mutagenesis affects stem cell homeostasis. We also highlight the intriguing contrast in the selective pressures against the mtDNA mutation with different origins in the fast-renewing mitotic tissue. Stem cells, which are responsible for tissue maintenance and regeneration, might be involved in the selective process against the inherited mtDNA mutation. Recently, studies have reported that stem cells might actively regulate their identity by manipulating the quality control of the mitochondria, for example, by removing the dysfunctional mitochondria [56] or by unevenly segregating young and aged mitochondria [71]. The quality control system might lose the function during ageing, leading to the absence of selective pressures on the somatic mtDNA mutations, which in turn accelerates ageing. We believe that investigating the mechanism of the difference in the selective pressure on the somatic and the inherited mtDNA mutations has a profound influence on understanding the progress of normal ageing, ageing-related degenerative diseases and cancer formation [72,73]. Studies have now provided several methods for preventing the germline transmission of the inherited mtDNA mutations to enable producing healthy children from affected mothers [74–76]. However, no efficacious interventions have been found for diseases caused by mutations that occur during embryogenesis. Understanding the mechanism of the selective pressure on the inborn mtDNA mutation will also propel the development of the treatment for mitochondrial disorders, especially for those occurring during embryogenesis and those that are recessive with late-onset.

Acknowledgments: This work was supported by the Newcastle University Centre for Aging and Vitality supported by the Biotechnology and Biological Sciences Research Council (BBSRC), Engineering and Physical Sciences Research Council (EPSRC), Economic and Social Research Council (ESRC), and Medical Research Council (MRC) as part of the cross-council Lifelong Health and Wellbeing Initiative; the Wellcome Centre for Mitochondrial Research (203105/Z/16/Z); UK National Institute for Health Research (NIHR) Biomedical Research Centre in Age and Age Related Diseases award to the Newcastle upon Tyne Hospitals National Health Service (NHS) Foundation; the UK NHS Highly Specialized Service for Rare Mitochondrial Disorders of Adults and Children.

Author Contributions: T.S., L.C.G. and D.M.T. wrote the manuscript.

Conflicts of Interest: The authors declare no conflicts of interest.

References

1. Rando, T.A. Stem cells, ageing and the quest for immortality. *Nature* **2006**, *441*, 1080–1086.
2. Jones, D.L.; Rando, T.A. Emerging models and paradigms for stem cell ageing. *Nat. Cell Biol.* **2011**, *13*, 506–512.
3. Liu, L.; Rando, T.A. Manifestations and mechanisms of stem cell aging. *J. Cell Biol.* **2011**, *193*, 257–266.
4. Barker, N. Adult intestinal stem cells: Critical drivers of epithelial homeostasis and regeneration. *Nat. Rev. Mol. Cell Biol.* **2014**, *15*, 19–33.
5. Mendelson, A.; Frenette, P.S. Hematopoietic stem cell niche maintenance during homeostasis and regeneration. *Nat. Med.* **2014**, *20*, 833–846.
6. Seale, P.; Rudnicki, M.A. A new look at the origin, function, and "stem-cell" status of muscle satellite cells. *Dev. Biol.* **2000**, *218*, 115–124.
7. Bond, A.M.; Ming, G.-L.; Song, H. Adult mammalian neural stem cells and neurogenesis: Five decades later. *Cell Stem Cell* **2015**, *17*, 385–395.
8. Bogenhagen, D.; Clayton, D.A. Mouse L cell mitochondrial DNA molecules are selected randomly for replication throughout the cell cycle. *Cell* **1977**, *11*, 719–727.
9. Alexeyev, M.; Shokolenko, I.; Wilson, G.; LeDoux, S. The maintenance of mitochondrial DNA integrity—Critical analysis and update. *Cold Spring Harb. Perspect. Biol.* **2013**, *5*, a012641, doi:10.1101/cshperspect.a012641.
10. Murphy, M.P. How mitochondria produce reactive oxygen species. *Biochem. J.* **2009**, *417*, 1–13.
11. Stewart, J.B.; Freyer, C.; Elson, J.L.; Larsson, N.-G. Purifying selection of mtDNA and its implications for understanding evolution and mitochondrial disease. *Nat. Rev. Genet.* **2008**, *9*, 657–662.
12. Linnane, A.; Ozawa, T.; Marzuki, S.; Tanaka, M. Mitochondrial DNA mutations as an important contributor to ageing and degenerative diseases. *Lancet* **1989**, *333*, 642–645.
13. Sun, N.; Youle, R.J.; Finkel, T. The mitochondrial basis of aging. *Mol. Cell* **2016**, *61*, 654–666.
14. Reeve, A.K.; Krishnan, K.J.; Turnbull, D. Mitochondrial DNA mutations in disease, aging, and neurodegeneration. *Ann. N. Y. Acad. Sci.* **2008**, *1147*, 21–29.
15. Müller-Höcker, J. Cytochrome *c* oxidase deficient fibres in the limb muscle and diaphragm of man without muscular disease: An age-related alteration. *J. Neurol. Sci.* **1990**, *100*, 14–21.
16. Müller-Höcker, J. Cytochrome *c* oxidase deficient cardiomyocytes in the human heart—an age-related phenomenon. A histochemical ultracytochemical study. *Am. J. Pathol.* **1989**, *134*, 1167–1173.
17. Cottrell, D.A.; Blakely, E.L.; Johnson, M.A.; Ince, P.G.; Borthwick, G.M.; Turnbull, D.M. Cytochrome *c* oxidase deficient cells accumulate in the hippocampus and choroid plexus with age. *Neurobiol. Aging* **2001**, *22*, 265–272.
18. Fellous, T.G.; Islam, S.; Tadrous, P.J.; Elia, G.; Kocher, H.M.; Bhattacharya, S.; Mears, L.; Turnbull, D.M.; Taylor, R.W.; Greaves, L.C.; et al. Locating the stem cell niche and tracing hepatocyte lineages in human liver. *Hepatology* **2009**, *49*, 1655–1663.
19. McDonald, S.A.C.; Greaves, L.C.; Gutierrez-Gonzalez, L.; Rodriguez-Justo, M.; Deheragoda, M.; Leedham, S.J.; Taylor, R.W.; Lee, C.Y.; Preston, S.L.; Lovell, M.; et al. Mechanisms of field cancerization in the human stomach: The expansion and spread of mutated gastric stem cells. *Gastroenterology* **2008**, *134*, 500–510.
20. Gutierrez-Gonzalez, L.; Deheragoda, M.; Elia, G.; Leedham, S.J.; Shankar, A.; Imber, C.; Jankowski, J.A.; Turnbull, D.M.; Novelli, M.; Wright, N.A.; et al. Analysis of the clonal architecture of the human small intestinal epithelium establishes a common stem cell for all lineages and reveals a mechanism for the fixation and spread of mutations. *J. Pathol.* **2009**, *217*, 489–496.
21. Taylor, R.W.; Barron, M.J.; Borthwick, G.M.; Gospel, A.; Chinnery, P.F.; Samuels, D.C.; Taylor, G.A.; Plusa, S.M.; Needham, S.J.; Greaves, L.C.; et al. Mitochondrial DNA mutations in human colonic crypt stem cells. *J. Clin. Investig.* **2003**, *112*, 1351–1360.
22. Greaves, L.C.; Barron, M.J.; Plusa, S.; Kirkwood, T.B.; Mathers, J.C.; Taylor, R.W.; Turnbull, D.M. Defects in multiple complexes of the respiratory chain are present in ageing human colonic crypts. *Exp. Gerontol.* **2010**, *45*, 573–579.
23. Bua, E.; Johnson, J.; Herbst, A.; Delong, B.; McKenzie, D.; Salamat, S.; Aiken, J.M. Mitochondrial DNA–deletion mutations accumulate intracellularly to detrimental levels in aged human skeletal muscle fibers. *Am. J. Hum. Genet.* **2006**, *79*, 469–480.

24. Kraytsberg, Y.; Kudryavtseva, E.; McKee, A.C.; Geula, C.; Kowall, N.W.; Khrapko, K. Mitochondrial DNA deletions are abundant and cause functional impairment in aged human substantia nigra neurons. *Nat. Genet.* **2006**, *38*, 518–520.
25. Meissner, C.; Bruse, P.; Mohamed, S.A.; Schulz, A.; Warnk, H.; Storm, T.; Oehmichen, M. The 4977bp deletion of mitochondrial DNA in human skeletal muscle, heart and different areas of the brain: A useful biomarker or more? *Exp. Gerontol.* **2008**, *43*, 645–652.
26. Shin, M.G.; Kajigaya, S.; Tarnowka, M.; McCoy, J.P.; Levin, B.C.; Young, N.S. Mitochondrial DNA sequence heterogeneity in circulating normal human CD34 cells and granulocytes. *Blood* **2004**, *103*, 4466–4477.
27. Zheng, Y.; Luo, X.; Zhu, J.; Zhang, X.; Zhu, Y.; Cheng, H.; Xia, Z.; Su, N.; Zhang, N.; Zhou, J. Mitochondrial DNA 4977 bp deletion is a common phenomenon in hair and increases with age. *Bosn. J. Basic Med. Sci.* **2012**, *12*, 187–192.
28. Shin, M.G.; Kajigaya, S.; McCoy, J.P.; Levin, B.C.; Young, N.S. Marked mitochondrial DNA sequence heterogeneity in single CD34+ cell clones from normal adult bone marrow. *Blood* **2004**, *103*, 553–561.
29. Elson, J.L.; Samuels, D.C.; Turnbull, D.M.; Chinnery, P.F. Random intracellular drift explains the clonal expansion of mitochondrial DNA mutations with age. *Am. J. Hum. Genet.* **2001**, *68*, 802–806.
30. Greaves, L.C.; Elson, J.L.; Nooteboom, M.; Grady, J.P.; Taylor, G.A.; Taylor, R.W.; Mathers, J.C.; Kirkwood, T.B.L.; Turnbull, D.M. Comparison of mitochondrial mutation spectra in ageing human colonic epithelium and disease: Absence of evidence for purifying selection in somatic mitochondrial DNA point mutations. *PLoS Genet.* **2012**, *8*, e1003082,doi:10.1371/journal.pgen.1003082.
31. Reeve, A.K.; Krishnan, K.J.; Taylor, G.; Elson, J.L.; Bender, A.; Taylor, R.W.; Morris, C.M.; Turnbull, D.M. The low abundance of clonally expanded mitochondrial DNA point mutations in aged substantia nigra neurons. *Aging Cell* **2009**, *8*, 496–498.
32. Pallotti, F.; Chen, X.; Bonilla, E.; Schon, E.A. Evidence that specific mtDNA point mutations may not accumulate in skeletal muscle during normal human aging. *Am. J. Hum. Genet.* **1996**, *59*, 591–602.
33. Krishnan, K.J.; Reeve, A.K.; Samuels, D.C.; Chinnery, P.F.; Blackwood, J.K.; Taylor, R.W.; Wanrooij, S.; Spelbrink, J.N.; Lightowlers, R.N.; Turnbull, D.M. What causes mitochondrial DNA deletions in human cells? *Nat. Genet.* **2008**, *40*, 275–279.
34. Greaves, L.C.; Preston, S.L.; Tadrous, P.J.; Taylor, R.W.; Barron, M.J.; Oukrif, D.; Leedham, S.J.; Deheragoda, M.; Sasieni, P.; Novelli, M.R.; et al. Mitochondrial DNA mutations are established in human colonic stem cells, and mutated clones expand by crypt fission. *Proc. Natl. Acad. Sci. USA* **2006**, *103*, 714–719.
35. Nooteboom, M.; Johnson, R.; Taylor, R.W.; Wright, N.A.; Lightowlers, R.N.; Kirkwood, T.B.L.; Mathers, J.C.; Turnbull, D.M.; Greaves, L.C. Age-associated mitochondrial DNA mutations lead to small but significant changes in cell proliferation and apoptosis in human colonic crypts. *Aging Cell* **2010**, *9*, 96–99.
36. Trifunovic, A.; Wredenberg, A.; Falkenberg, M.; Spelbrink, J.N.; Rovio, A.T.; Bruder, C.E.; Bohlooly-y, M.; Gidlöf, S.; Oldfors, A.; Wibom, R.; et al. Premature ageing in mice expressing defective mitochondrial DNA polymerase. *Nature* **2004**, *429*, 417–423.
37. Kujoth, G.C.; Hiona, A.; Pugh, T.D.; Someya, S.; Panzer, K.; Wohlgemuth, S.E.; Hofer, T.; Seo, A.Y.; Sullivan, R.; Jobling, W.A.; et al. Mitochondrial DNA mutations, oxidative stress, and apoptosis in mammalian aging. *Science* **2005**, *309*, 481–484.
38. Chen, M.L.; Logan, T.D.; Hochberg, M.L.; Shelat, S.G.; Yu, X.; Wilding, G.E.; Tan, W.; Kujoth, G.C.; Prolla, T.A.; Selak, M.A.; et al. Erythroid dysplasia, megaloblastic anemia, and impaired lymphopoiesis arising from mitochondrial dysfunction. *Blood* **2009**, *114*, 4045–4053.
39. Norddahl, G.L.; Pronk, C.J.; Wahlestedt, M.; Sten, G.; Nygren, J.M.; Ugale, A.; Sigvardsson, M.; Bryder, D. Accumulating mitochondrial DNA mutations drive premature hematopoietic aging phenotypes distinct from physiological stem cell aging. *Cell Stem Cell* **2011**, *8*, 499–510.
40. Ahlqvist, K.J.; Hämäläinen, R.H.; Yatsuga, S.; Uutela, M.; Terzioglu, M.; Götz, A.; Forsström, S.; Salven, P.; Angers-Loustau, A.; Kopra, O.H.; et al. Somatic progenitor cell vulnerability to mitochondrial DNA mutagenesis underlies progeroid phenotypes in POLG mutator mice. *Cell Metab.* **2012**, *15*, 100–109.
41. Fox, R.G.; Magness, S.; Kujoth, G.C.; Prolla, T.A.; Maeda, N. Mitochondrial DNA polymerase editing mutation, POLGD257A, disturbs stem-progenitor cell cycling in the small intestine and restricts excess fat absorption. *Am. J. Physiol. Gastrointest. Liver Physiol.* **2012**, *302*, G914–G924.
42. Baines, H.L.; Stewart, J.B.; Stamp, C.; Zupanic, A.; Kirkwood, T.B.L.; Larsson, N.-G.; Turnbull, D.M.; Greaves, L.C. Similar patterns of clonally expanded somatic mtDNA mutations in the colon of heterozygous mtDNA mutator mice and ageing humans. *Mech. Ageing Dev.* **2014**, *139*, 22–30.

43. Stewart, J.B.; Freyer, C.; Elson, J.L.; Wredenberg, A.; Cansu, Z.; Trifunovic, A.; Larsson, N.-G. Strong purifying selection in transmission of mammalian mitochondrial DNA. *PLoS Biol.* **2008**, *6*, e10, doi:10.1371/journal.pbio.0060010.
44. Orogo, A.M.; Gonzalez, E.R.; Kubli, D.A.; Baptista, I.L.; Ong, S.-B.; Prolla, T.A.; Sussman, M.A.; Murphy, A.N.; Gustafsson, Å.B. Accumulation of mitochondrial DNA mutations disrupts cardiac progenitor cell function and reduces survival. *J. Biol. Chem.* **2015**, *290*, 22061–22075.
45. Tan, D.Q.; Suda, T. Reactive oxygen species and mitochondrial homeostasis as regulators of stem cell fate and function. *Antioxid. Redox Signal.* **2017**, doi:10.1089/ars.2017.7273.
46. Sena, L.A.; Chandel, N.S. Physiological roles of mitochondrial reactive oxygen species. *Mol. Cell* **2012**, *48*, 158–167.
47. Hämäläinen, R.H. Mitochondria and mtDNA integrity in stem cell function and differentiation. *Curr. Opin. Gene. Dev.* **2016**, *38*, 83–89.
48. Harman, D. The biologic clock: The mitochondria? *J. Am. Geriatr. Soc.* **1972**, *20*, 145–147.
49. Trifunovic, A.; Hansson, A.; Wredenberg, A.; Rovio, A.T.; Dufour, E.; Khvorostov, I.; Spelbrink, J.N.; Wibom, R.; Jacobs, H.T.; Larsson, N.G. Somatic mtDNA mutations cause aging phenotypes without affecting reactive oxygen species production. *Proc. Natl. Acad. Sci. USA* **2005**, *102*, 17993–17998.
50. Baines, H.L.; Turnbull, D.M.; Greaves, L.C. Human stem cell aging: Do mitochondrial DNA mutations have a causal role? *Aging Cell* **2014**, *13*, 201–205.
51. Ahlqvist, K.J.; Leoncini, S.; Pecorelli, A.; Wortmann, S.B.; Ahola, S.; Forsström, S.; Guerranti, R.; De Felice, C.; Smeitink, J.; Ciccoli, L.; et al. mtDNA mutagenesis impairs elimination of mitochondria during erythroid maturation leading to enhanced erythrocyte destruction. *Nat. Commun.* **2015**, *6*, 6494, doi:10.1038/ncomms7494.
52. Someya, S.; Kujoth, G.C.; Kim, M.J.; Hacker, T.A.; Vermulst, M.; Weindruch, R.; Prolla, T.A. Effects of calorie restriction on the lifespan and healthspan of POLG mitochondrial mutator mice. *PLoS ONE* **2017**, *12*, e0171159, doi:10.1371/journal.pone.0171159.
53. Wang, X.; Pickrell, A.M.; Rossi, S.G.; Pinto, M.; Dillon, L.M.; Hida, A.; Rotundo, R.L.; Moraes, C.T. Transient systemic mtDNA damage leads to muscle wasting by reducing the satellite cell pool. *Hum. Mol. Genet.* **2013**, *22*, 3976–3986.
54. Pinto, M.; Pickrell, A.M.; Wang, X.; Bacman, S.R.; Yu, A.; Hida, A.; Dillon, L.M.; Morton, P.D.; Malek, T.R.; Williams, S.L.; et al. Transient mitochondrial DNA double strand breaks in mice cause accelerated aging phenotypes in a ROS-dependent but p53/p21-independent manner. *Cell Death Differ.* **2016**, *24*, 288–299.
55. Khacho, M.; Clark, A.; Svoboda, D.S.; Azzi, J.; MacLaurin, J.G.; Meghaizel, C.; Sesaki, H.; Lagace, D.C.; Germain, M.; Harper, M.E.; et al. Mitochondrial dynamics impacts stem cell identity and fate decisions by regulating a nuclear transcriptional program. *Cell Stem Cell* **2016**, *19*, 232–247.
56. García-Prat, L.; Martínez-Vicente, M.; Perdiguero, E.; Ortet, L.; Rodríguez-Ubreva, J.; Rebollo, E.; Ruiz-Bonilla, V.; Gutarra, S.; Ballestar, E.; Serrano, A.L.; et al. Autophagy maintains stemness by preventing senescence. *Nature* **2016**, *529*, 37–42.
57. Ho, T.T.; Warr, M.R.; Adelman, E.R.; Lansinger, O.M.; Flach, J.; Verovskaya, E.V.; Figueroa, M.E.; Passegue, E. Autophagy maintains the metabolism and function of young and old stem cells. *Nature* **2017**, *543*, 205–210.
58. Li-Harms, X.; Milasta, S.; Lynch, J.; Wright, C.; Joshi, A.; Iyengar, R.; Neale, G.; Wang, X.; Wang, Y.-D.; Prolla, T.A.; et al. Mito-protective autophagy is impaired in erythroid cells of aged mtDNA-mutator mice. *Blood* **2015**, *125*, 162–174.
59. Twig, G.; Elorza, A.; Molina, A.J.; Mohamed, H.; Wikstrom, J.D.; Walzer, G.; Stiles, L.; Haigh, S.E.; Katz, S.; Las, G.; et al. Fission and selective fusion govern mitochondrial segregation and elimination by autophagy. *EMBO J.* **2008**, *27*, 433–446.
60. Tait, S.W.G.; Green, D.R. Mitochondria and cell death: Outer membrane permeabilization and beyond. *Nat. Rev. Mol. Cell Biol.* **2010**, *11*, 621–632.
61. Pearson, H.A.; Lobel, J.S.; Kocoshis, S.A.; Naiman, J.L.; Windmiller, J.; Lammi, A.T.; Hoffman, R.; Marsh, J.C. A new syndrome of refractory sideroblastic anemia with vacuolization of marrow precursors and exocrine pancreatic dysfunction. *J. Pediatr.* **1979**, *95*, 976–984.
62. Larsson, N.-G.; Holme, E.; Kristiansson, B.; Oldfors, A.; Tulinius, M. Progressive increase of the mutated mitochondrial DNA fraction in Kearns-Sayre syndrome. *Pediatr. Res.* **1990**, *28*, 131–136.

63. McShane, M.A.; Hammans, S.R.; Sweeney, M.; Holt, I.J.; Beattie, T.J.; Brett, E.M.; Harding, A.E. Pearson syndrome and mitochondrial encephalomyopathy in a patient with a deletion of mtDNA. *Am. J. Hum. Genet.* **1991**, *48*, 39–42.
64. Nørby, S.; Lestienne, P.; Nelson, I.; Nielsen, I.M.; Schmalbruch, H.; Sjö, O.; Warburg, M. Juvenile Kearns-Sayre syndrome initially misdiagnosed as a psychosomatic disorder. *J. Med. Genet.* **1994**, *31*, 45–50.
65. 't Hart, L.M.; Jansen, J.J.; Lemkes, H.H.; de Knijff, P.; Maassen, J.A. Heteroplasmy levels of a mitochondrial gene mutation associated with diabetes mellitus decrease in leucocyte DNA upon aging. *Hum. Mutat.* **1996**, *7*, 193–197.
66. Olsson, C.; Johnsen, E.; Nilsson, M.; Wilander, E.; Syvanen, A.C.; Lagerstrom-Fermer, M. The level of the mitochondrial mutation A3243G decreases upon ageing in epithelial cells from individuals with diabetes and deafness. *Eur. J. Hum. Genet.* **2001**, *9*, 917–921.
67. Rahman, S.; Poulton, J.; Marchington, D.; Suomalainen, A. Decrease of 3243 A→G mtDNA mutation from blood in MELAS syndrome: A longitudinal study. *Am. J. Hum. Genet.* **2001**, *68*, 238–240.
68. Frederiksen, A.L.; Andersen, P.H.; Kyvik, K.O.; Jeppesen, T.D.; Vissing, J.; Schwartz, M. Tissue specific distribution of the 3243A→G mtDNA mutation. *J. Med. Genet.* **2006**, *43*, 671–677.
69. Rajasimha, H.K.; Chinnery, P.F.; Samuels, D.C. Selection against pathogenic mtDNA mutations in a stem cell population leads to the loss of the 3243A→G mutation in blood. *Am. J. Hum. Genet.* **2008**, *82*, 333–343.
70. Kauppila, J.H.; Baines, H.L.; Bratic, A.; Simard, M.-L.; Freyer, C.; Mourier, A.; Stamp, C.; Filograna, R.; Larsson, N.-G.; Greaves, L.C.; et al. A phenotype-driven approach to generate mouse models with pathogenic mtDNA mutations causing mitochondrial disease. *Cell Rep.* **2016**, *16*, 2980–2990.
71. Katajisto, P.; Döhla, J.; Chaffer, C.L.; Pentinmikko, N.; Marjanovic, N.; Iqbal, S.; Zoncu, R.; Chen, W.; Weinberg, R.A.; Sabatini, D.M. Asymmetric apportioning of aged mitochondria between daughter cells is required for stemness. *Science* **2015**, *348*, 340–343.
72. Khrapko, K.; Vijg, J. Mitochondrial DNA mutations and aging: Devils in the details? *Trends Genet.* **2009**, *25*, 91–98.
73. Popadin, K.; Gunbin, K.V.; Khrapko, K. Mitochondrial DNA mutations and cancer: Lessons from the parathyroid. *Am. J. Pathol.* **2014**, *184*, 2852–2854.
74. Craven, L.; Tuppen, H.A.; Greggains, G.D.; Harbottle, S.J.; Murphy, J.L.; Cree, L.M.; Murdoch, A.P.; Chinnery, P.F.; Taylor, R.W.; Lightowlers, R.N.; et al. Pronuclear transfer in human embryos to prevent transmission of mitochondrial DNA disease. *Nature* **2010**, *465*, 82–85.
75. Tachibana, M.; Amato, P.; Sparman, M.; Woodward, J.; Sanchis, D.M.; Ma, H.; Gutierrez, N.M.; Tippner-Hedges, R.; Kang, E.; Lee, H.-S.; et al. Towards germline gene therapy of inherited mitochondrial diseases. *Nature* **2012**, *493*, 627–631.
76. Wang, T.; Sha, H.; Ji, D.; Zhang, H.L.; Chen, D.; Cao, Y.; Zhu, J. Polar body genome transfer for preventing the transmission of inherited mitochondrial diseases. *Cell* **2014**, *157*, 1591–1604.

Chapter 9 References

Abramov, A.Y. and Duchen, M.R. (2010) 'Impaired mitochondrial bioenergetics determines glutamate-induced delayed calcium deregulation in neurons', *Biochim Biophys Acta*, 1800(3), pp. 297-304.

Acín-Pérez, R., Bayona-Bafaluy, M.a.P., Fernández-Silva, P., Moreno-Loshuertos, R., Pérez-Martos, A., Bruno, C., Moraes, C.T. and Enríquez, J.A. (2004) 'Respiratory Complex III Is Required to Maintain Complex I in Mammalian Mitochondria', *Molecular Cell*, 13(6), pp. 805-815.

Ahlqvist, K.J., Hämäläinen, R.H., Yatsuga, S., Uutela, M., Terzioglu, M., Götz, A., Forsström, S., Salven, P., Angers-Loustau, A. and Kopra, O.H. (2012) 'Somatic progenitor cell vulnerability to mitochondrial DNA mutagenesis underlies progeroid phenotypes in Polg mutator mice', *Cell metabolism*, 15(1), pp. 100-109.

Akman, G., Desai, R., Bailey, L.J., Yasukawa, T., Dalla Rosa, I., Durigon, R., Holmes, J.B., Moss, C.F., Mennuni, M., Houlden, H., Crouch, R.J., Hanna, M.G., Pitceathly, R.D.S., Spinazzola, A. and Holt, I.J. (2016) 'Pathological ribonuclease H1 causes R-loop depletion and aberrant DNA segregation in mitochondria', *Proceedings of the National Academy of Sciences of the United States of America*, 113(30), pp. E4276-E4285.

Alston, C.L., Rocha, M.C., Lax, N.Z., Turnbull, D.M. and Taylor, R.W. (2017) 'The genetics and pathology of mitochondrial disease', *J Pathol*, 241(2), pp. 236-250.

Anderson, S., Bankier, A.T., Barrell, B.G., De Bruijn, M.H.L., Coulson, A.R., Drouin, J., Eperon, I.C., Nierlich, D.P., Roe, B.A. and Sanger, F. (1981) 'Sequence and organization of the human mitochondrial genome'.

Andrews, R.M., Kubacka, I., Chinnery, P.F., Lightowlers, R.N., Turnbull, D.M. and Howell, N. (1999) 'Reanalysis and revision of the Cambridge reference sequence for human mitochondrial DNA', *Nature genetics*, 23(2), pp. 147-147.

Antico Arciuch, V.G., Elguero, M.E., Poderoso, J.J. and Carreras, M.C. (2012) 'Mitochondrial Regulation of Cell Cycle and Proliferation', *Antioxidants & Redox Signaling*, 16(10), pp. 1150-1180.

Aoki, R., Shoshkes-Carmel, M., Gao, N., Shin, S., May, C.L., Golson, M.L., Zahm, A.M., Ray, M., Wiser, C.L., Wright, C.V.E. and Kaestner, K.H. (2016) 'Foxl1-Expressing

Mesenchymal Cells Constitute the Intestinal Stem Cell Niche', *Cellular and Molecular Gastroenterology and Hepatology*, 2(2), pp. 175-188.

Ardail, D., Privat, J.P., Egret-Charlier, M., Levrat, C., Lerme, F. and Louisot, P. (1990) 'Mitochondrial contact sites. Lipid composition and dynamics', *Journal of Biological Chemistry*, 265(31), pp. 18797-802.

Atillasoy, E. and Holt, P.R. (1993) 'Gastrointestinal proliferation and aging', *J Gerontol*, 48(2), pp. B43-9.

Auré, K., Fayet, G., Leroy, J.P., Lacène, E., Romero, N.B. and Lombès, A. (2006) 'Apoptosis in mitochondrial myopathies is linked to mitochondrial proliferation', *Brain*, 129(5), pp. 1249-1259.

Baines, H. (2014) 'Using mouse models to learn about mitochondrial DNA point mutations in ageing and disease', *Thesis submitted for the degree of Doctor of Philosophy at Newcastle University*.

Baines, H.L., Stewart, J.B., Stamp, C., Zupanic, A., Kirkwood, T.B.L., Larsson, N.-G., Turnbull, D.M. and Greaves, L.C. (2014a) 'Similar patterns of clonally expanded somatic mtDNA mutations in the colon of heterozygous mtDNA mutator mice and ageing humans', *Mechanisms of ageing and development*, 139, pp. 22-30.

Baines, H.L., Turnbull, D.M. and Greaves, L.C. (2014b) 'Human stem cell aging: do mitochondrial DNA mutations have a causal role?', *Aging Cell*, 13(2), pp. 201-205.

Barker, N. (2014) 'Adult intestinal stem cells: critical drivers of epithelial homeostasis and regeneration', *Nat Rev Mol Cell Biol*, 15(1), pp. 19-33.

Barker, N. (2018) 'Digesting recent stem cell advances in the gut', *Nature Reviews Gastroenterology &Amp; Hepatology*, 15, p. 78.

Barker, N., Bartfeld, S. and Clevers, H. (2010a) 'Tissue-Resident Adult Stem Cell Populations of Rapidly Self-Renewing Organs', *Cell Stem Cell*, 7(6), pp. 656-670.

Barker, N., Huch, M., Kujala, P., van de Wetering, M., Snippert, H.J., van Es, J.H., Sato, T., Stange, D.E., Begthel, H. and van den Born, M. (2010b) 'Lgr5+ ve stem cells drive self-renewal in the stomach and build long-lived gastric units in vitro', *Cell stem cell*, 6(1), pp. 25-36.

Barker, N., Ridgway, R.A., van Es, J.H., van de Wetering, M., Begthel, H., van den Born, M., Danenberg, E., Clarke, A.R., Sansom, O.J. and Clevers, H. (2008) 'Crypt stem cells as the cells-of-origin of intestinal cancer', *Nature*, 457, p. 608.

Barker, N., van Es, J.H., Kuipers, J., Kujala, P., van den Born, M., Cozijnsen, M., Haegebarth, A., Korving, J., Begthel, H. and Peters, P.J. (2007) 'Identification of stem cells in small intestine and colon by marker gene Lgr5', *Nature*, 449(7165), pp. 1003-1007.

Barrell, B.G., Anderson, S., Bankier, A.T., de Bruijn, M.H., Chen, E., Coulson, A.R., Drouin, J., Eperon, I.C., Nierlich, D.P., Roe, B.A., Sanger, F., Schreier, P.H., Smith, A.J., Staden, R. and Young, I.G. (1980) 'Different pattern of codon recognition by mammalian mitochondrial tRNAs', *Proceedings of the National Academy of Sciences of the United States of America*, 77(6), pp. 3164-3166.

Bartfeld, S. and Koo, B.-K. (2017) 'Adult gastric stem cells and their niches', *Wiley Interdisciplinary Reviews: Developmental Biology*, 6(2), p. e261.

Bayrhuber, M., Meins, T., Habeck, M., Becker, S., Giller, K., Villinger, S., Vonrhein, C., Griesinger, C., Zweckstetter, M. and Zeth, K. (2008) 'Structure of the human voltage-dependent anion channel', *Proceedings of the National Academy of Sciences*, 105(40), p. 15370.

Becker, C., Fantini, M.C. and Neurath, M.F. (2007) 'High resolution colonoscopy in live mice', *Nature Protocols*, 1, p. 2900.

Benigni, A., Morigi, M. and Remuzzi, G. (2010) 'Kidney regeneration', *The Lancet*, 375(9722), pp. 1310-1317.

Berkovic, S.F., Carpenter, S., Evans, A., Karpati, G., Shoubridge, E.A., Andermann, F., Meyer, E., Tyler, J.L., Diksic, M. and Arnold, D. (1989) 'Myoclonus epilepsy and ragged-red fibres (MERRF) 1. A clinical, pathological, biochemical, magnetic resonance spectrographic and positron emission tomographic study', *Brain*, 112(5), pp. 1231-1260.

Betts, J., Barron, M.J., Needham, S.J., Schaefer, A.M., Taylor, R.W. and Turnbull, D.M. (2008) 'Gastrointestinal tract involvement associated with the 3243A> G mitochondrial DNA mutation', *Neurology*, 70(15), pp. 1290-1292.

Bibb, M.J., Van Etten, R.A., Wright, C.T., Walberg, M.W. and Clayton, D.A. (1981) 'Sequence and gene organization of mouse mitochondrial DNA', *Cell*, 26(2, Part 2), pp. 167-180.

Bindoff, L.A., Desnuelle, C., Birch-Machin, M.A., Pellissier, J.-F., Serratrice, G., Dravet, C., Bureau, M., Howell, N. and Turnbull, D.M. (1991) 'Multiple defects of the mitochondrial respiratory chain in a mitochondrial encephalopathy (MERRF): a clinical, biochemical and molecular study', *Journal of the neurological sciences*, 102(1), pp. 17-24.

Birket, M.J., Orr, A.L., Gerencser, A.A., Madden, D.T., Vitelli, C., Swistowski, A., Brand, M.D. and Zeng, X. (2011) 'A reduction in ATP demand and mitochondrial activity with neural differentiation of human embryonic stem cells', *Journal of Cell Science*, 124(3), p. 348.

Bjerknes, M. and Cheng, H. (2002) 'Multipotential stem cells in adult mouse gastric epithelium', *American Journal of Physiology-Gastrointestinal and Liver Physiology*, 283(3), pp. G767-G777.

Blakely, E.L., Swalwell, H., Petty, R.K.H., McFarland, R., Turnbull, D.M. and Taylor, R.W. (2007) 'Sporadic myopathy and exercise intolerance associated with the mitochondrial 8328G>A tRNALys mutation', *Journal of Neurology*, 254(9), p. 1283.

Bogenhagen, D. and Clayton, D.A. (1977) 'Mouse L cell mitochondrial DNA molecules are selected randomly for replication throughout the cell cycle', *Cell*, 11(4), pp. 719-727.

Bonekamp, N.A. and Larsson, N.-G. (2018) 'SnapShot: Mitochondrial Nucleoid', *Cell*, 172(1), pp. 388-388.e1.

Boos, F., Wollin, M. and Herrmann, J.M. (2016) 'Methionine on the rise: how mitochondria changed their codon usage', *The EMBO Journal*, 35(19), pp. 2066-2067.

Bowmaker, M., Yang, M.Y., Yasukawa, T., Reyes, A., Jacobs, H.T., Huberman, J.A. and Holt, I.J. (2003) 'Mammalian mitochondrial DNA replicates bidirectionally from an initiation zone', *Journal of Biological Chemistry*, 278(51), pp. 50961-50969.

Brand, M.D. (1990) 'The proton leak across the mitochondrial inner membrane', *Biochimica et Biophysica Acta (BBA)-Bioenergetics*, 1018(2), pp. 128-133.

Braymer, J.J. and Lill, R. (2017) 'Iron-Sulfur Cluster Biogenesis and Trafficking in Mitochondria', *Journal of Biological Chemistry*.

Brembeck, F.H., Rosário, M. and Birchmeier, W. (2006) 'Balancing cell adhesion and Wnt signaling, the key role of β-catenin', *Current Opinion in Genetics & Development*, 16(1), pp. 51-59.

Bressenot, A., Marchal, S., Bezdetnaya, L., Garrier, J., Guillemin, F. and Plénat, F. (2009) 'Assessment of Apoptosis by Immunohistochemistry to Active Caspase-3, Active Caspase-7, or Cleaved PARP in Monolayer Cells and Spheroid and Subcutaneous Xenografts of Human Carcinoma', *Journal of Histochemistry and Cytochemistry*, 57(4), pp. 289-300.

Brière, J.J., Favier, J., Ghouzzi, V.E., Djouadi, F., Benit, P., Gimenez, A.P. and Rustin, P. (2005) 'Succinate dehydrogenase deficiency in human', *Cellular and Molecular Life Sciences CMLS*, 62(19-20), pp. 2317-2324.

Brown, W.M., George, M. and Wilson, A.C. (1979) 'Rapid evolution of animal mitochondrial DNA', *Proceedings of the National Academy of Sciences of the United States of America*, 76(4), pp. 1967-1971.

Buczacki, S.J.A., Zecchini, H.I., Nicholson, A.M., Russell, R., Vermeulen, L., Kemp, R. and Winton, D.J. (2013) 'Intestinal label-retaining cells are secretory precursors expressing Lgr5', *Nature*, 495, p. 65.

Burr, S.P., Pezet, M. and Chinnery, P.F. (2018) 'Mitochondrial DNA Heteroplasmy and Purifying Selection in the Mammalian Female Germ Line', *Development, Growth & Differentiation*, 60(1), pp. 21-32.

Campisi, J. and di Fagagna, F.d.A. (2007) 'Cellular senescence: when bad things happen to good cells', *Nature reviews Molecular cell biology*, 8(9), pp. 729-740.

Cantó, C. and Auwerx, J. (2009) 'Caloric restriction, SIRT1 and longevity', *Trends in Endocrinology & Metabolism*, 20(7), pp. 325-331.

Cardaioli, E., Fabrizi, G.M., Grieco, G.S., Dotti, M.T. and Federico, A. (2000) 'Heteroplasmy of the A3243G transition of mitochondrial tRNA Leu (UUR) in a MELAS case and in a 25-week-old miscarried fetus', *Journal of neurology*, 247(11), pp. 885-887.

Carrozzo, R., Rizza, T., Stringaro, A., Pierini, R., Mormone, E., Santorelli, F.M., Malorni, W. and Matarrese, P. (2004) 'Maternally-inherited Leigh syndrome-related mutations bolster mitochondrial-mediated apoptosis', *Journal of Neurochemistry*, 90(2), pp. 490-501.

Cha, M.-Y., Kim, D.K. and Mook-Jung, I. (2015) 'The role of mitochondrial DNA mutation on neurodegenerative diseases', *Experimental &Amp; Molecular Medicine*, 47, p. e150.

Chan, D.C. (2012) 'Fusion and Fission: Interlinked Processes Critical for Mitochondrial Health', *Annual Review of Genetics*, 46(1), pp. 265-287.

Chang, D.D. and Clayton, D.A. (1985) 'Priming of human mitochondrial DNA replication occurs at the light-strand promoter', *Proceedings of the National Academy of Sciences*, 82(2), p. 351.

Chatterjee, A., Mambo, E. and Sidransky, D. (2006) 'Mitochondrial DNA mutations in human cancer', *Oncogene*, 25, p. 4663.

Chen, F., Liu, Y., Wong, N.-K., Xiao, J. and So, K.-F. (2017) 'Oxidative Stress in Stem Cell Aging', *Cell transplantation*, 26(9), pp. 1483-1495.

Chen, H. and Chan, D.C. (2006) 'Critical dependence of neurons on mitochondrial dynamics', *Current opinion in cell biology*, 18(4), pp. 453-459.

Chen, H. and Chan, D.C. (2017) 'Mitochondrial Dynamics in Regulating the Unique Phenotypes of Cancer and Stem Cells', *Cell Metabolism*, 26(1), pp. 39-48.

Chen, H., Detmer, S.A., Ewald, A.J., Griffin, E.E., Fraser, S.E. and Chan, D.C. (2003) 'Mitofusins Mfn1 and Mfn2 coordinately regulate mitochondrial fusion and are essential for embryonic development', *The Journal of Cell Biology*, 160(2), pp. 189-200.

Chen, M.L., Logan, T.D., Hochberg, M.L., Shelat, S.G., Yu, X., Wilding, G.E., Tan, W., Kujoth, G.C., Prolla, T.A. and Selak, M.A. (2009) 'Erythroid dysplasia, megaloblastic anemia, and impaired lymphopoiesis arising from mitochondrial dysfunction', *Blood*, 114(19), pp. 4045-4053.

Cheng, H. and Leblond, C.P. (1974) 'Origin, differentiation and renewal of the four main epithelial cell types in the mouse small intestine V. Unitarian theory of the origin of the four epithelial cell types', *American Journal of Anatomy*, 141(4), pp. 537-561.

Chinnery, P.F., DiMauro, S., Shanske, S., Schon, E.A., Zeviani, M., Mariotti, C., Carrara, F., Lombes, A., Laforet, P. and Ogier, H. (2004) 'Risk of developing a mitochondrial DNA deletion disorder', *The Lancet*, 364(9434), pp. 592-596.

Chinnery, P.F. and Samuels, D.C. (1999) 'Relaxed replication of mtDNA: A model with implications for the expression of disease', *American Journal of Human Genetics*, 64(4), pp. 1158-1165.

Chinnery, P.F., Thorburn, D.R., Samuels, D.C., White, S.L., Dahl, H.-H.M., Turnbull, D.M., Lightowlers, R.N. and Howell, N. (2000) 'The inheritance of mitochondrial DNA heteroplasmy: random drift, selection or both?', *Trends in Genetics*, 16(11), pp. 500-505.

Chinnery, P.F., Zwijnenburg, P.J.G., Walker, M., Howell, N., Taylor, R.W., Lightowlers, R.N., Bindoff, L. and Turnbull, D.M. (1999) 'Nonrandom tissue distribution of mutant mtDNA', *American journal of medical genetics*, 85(5), pp. 498-501.

Chomyn, A., Martinuzzi, A., Yoneda, M., Daga, A., Hurko, O., Johns, D., Lai, S.T., Nonaka, I., Angelini, C. and Attardi, G. (1992a) 'MELAS mutation in mtDNA binding site for transcription termination factor causes defects in protein synthesis and in respiration but no change in levels of upstream and downstream mature transcripts', *Proceedings of the National Academy of Sciences*, 89(10), pp. 4221-4225.

Chomyn, A., Martinuzzi, A., Yoneda, M., Daga, A., Hurko, O., Johns, D., Lai, S.T., Nonaka, I., Angelini, C. and Attardi, G. (1992b) 'MELAS mutation in mtDNA binding site for transcription termination factor causes defects in protein synthesis and in respiration but no change in levels of upstream and downstream mature transcripts', *Proceedings of the National Academy of Sciences of the United States of America*, 89(10), pp. 4221-4225.

Chrysostomou, A., Grady, J.P., Laude, A., Taylor, R.W., Turnbull, D.M. and Lax, N.Z. (2015) 'Investigating complex I deficiency in Purkinje cells and synapses in patients with mitochondrial disease', *Neuropathology and applied neurobiology*.

Cipolat, S., de Brito, O.M., Dal Zilio, B. and Scorrano, L. (2004) 'OPA1 requires mitofusin 1 to promote mitochondrial fusion', *Proceedings of the National Academy of Sciences of the United States of America*, 101(45), pp. 15927-15932.

Clason, T., Ruiz, T., Schägger, H., Peng, G., Zickermann, V., Brandt, U., Michel, H. and Radermacher, M. (2010) 'The structure of eukaryotic and prokaryotic complex I', *Journal of structural biology*, 169(1), pp. 81-88.

Clayton, D.A. (1982) 'Replication of animal mitochondrial DNA', *Cell*, 28(4), pp. 693-705.

Clayton, D.A. (2000) 'Transcription and replication of mitochondrial DNA', *Hum Reprod*, 15 Suppl 2, pp. 11-7.

Coller, H.A., Khrapko, K., Bodyak, N.D., Nekhaeva, E., Herrero-Jimenez, P. and Thilly, W.G. (2001) 'High frequency of homoplasmic mitochondrial DNA mutations in human tumors can be explained without selection', *Nature Genetics*, 28, p. 147.

Contino, S., Porporato, P.E., Bird, M., Marinangeli, C., Opsomer, R., Sonveaux, P., Bontemps, F., Dewachter, I., Octave, J.-N., Bertrand, L., Stanga, S. and Kienlen-Campard, P. (2017) 'Presenilin 2-Dependent Maintenance of Mitochondrial Oxidative Capacity and Morphology', *Frontiers in Physiology*, 8, p. 796.

Cory, S. and Adams, J.M. (2002) 'The Bcl2 family: regulators of the cellular life-or-death switch', *Nature Reviews Cancer*, 2, p. 647.

Cottrell, D.A., Blakely, E.L., Johnson, M.A., Ince, P.G., Borthwick, G.M. and Turnbull, D.M. (2001) 'Cytochrome c oxidase deficient cells accumulate in the hippocampus and choroid plexus with age', *Neurobiology of aging*, 22(2), pp. 265-272.

Craven, L., Alston, C.L., Taylor, R.W. and Turnbull, D.M. (2017) 'Recent Advances in Mitochondrial Disease', *Annu Rev Genomics Hum Genet*, 18, pp. 257-275.

Craven, L., Tuppen, H.A., Greggains, G.D., Harbottle, S.J., Murphy, J.L., Cree, L.M., Murdoch, A.P., Chinnery, P.F., Taylor, R.W. and Lightowlers, R.N. (2010) 'Pronuclear transfer in human embryos to prevent transmission of mitochondrial DNA disease', *Nature*, 465(7294), pp. 82-85.

Creamer, B., Shorter, R.G. and Bamforth, J. (1961) 'The turnover and shedding of epithelial cells: Part I The turnover in the gastro-intestinal tract', *Gut*, 2(2), pp. 110-116.

Crick, F.H.C. (1966) 'Codon—anticodon pairing: The wobble hypothesis', *Journal of Molecular Biology*, 19(2), pp. 548-555.

Cunningham, G.C. (1963) 'Rapid examination of muscle tissue', *An improved trichrome method for fresh-frozenbiopsy sections. Ibid*, 13, pp. 919-923.

Danielson, S.R., Wong, A., Carelli, V., Martinuzzi, A., Schapira, A.H.V. and Cortopassi, G.A. (2002) 'Cells Bearing Mutations Causing Leber's Hereditary Optic Neuropathy Are

Sensitized to Fas-induced Apoptosis', *Journal of Biological Chemistry*, 277(8), pp. 5810-5815.

De Grey, A.D.N.J. (2005) 'A proposed refinement of the mitochondrial free radical theory of aging', *BioEssays*, 19(2), pp. 161-166.

de Laat, P., Janssen, M.C.H., Alston, C.L., Taylor, R.W., Rodenburg, R.J.T. and Smeitink, J.A.M. (2016) 'Three families with 'de novo' m.3243A>G mutation', *BBA Clinical*, 6, pp. 19-24.

de Laat, P., Koene, S., van den Heuvel, L.P.W.J., Rodenburg, R.J.T., Janssen, M.C.H. and Smeitink, J.A.M. (2012) 'Clinical features and heteroplasmy in blood, urine and saliva in 34 Dutch families carrying the m.3243A > G mutation', *Journal of Inherited Metabolic Disease*, 35(6), pp. 1059-1069.

DeWard, A.D., Cramer, J. and Lagasse, E. (2014) 'Cellular heterogeneity in the mouse esophagus implicates the presence of a nonquiescent epithelial stem cell population', *Cell Rep*, 9(2), pp. 701-11.

Dikalov, S.I. and Harrison, D.G. (2012) 'Methods for Detection of Mitochondrial and Cellular Reactive Oxygen Species', *Antioxidants & Redox Signaling*, 20(2), pp. 372-382.

DiMauro, S., Bonilla, E., Zeviani, M., Nakagawa, M. and DeVivo, D.C. (1985) 'Mitochondrial myopathies', *Annals of Neurology*, 17(6), pp. 521-538.

DiMauro, S. and Schon, E.A. (2003) 'Mitochondrial respiratory-chain diseases', *New England Journal of Medicine*, 348(26), pp. 2656-2668.

Doupé, D.P., Alcolea, M.P., Roshan, A., Zhang, G., Klein, A.M., Simons, B.D. and Jones, P.H. (2012) 'A single progenitor population switches behavior to maintain and repair esophageal epithelium', *Science*, 337(6098), pp. 1091-1093.

Dudkina, N.V., Kouřil, R., Peters, K., Braun, H.-P. and Boekema, E.J. (2010) 'Structure and function of mitochondrial supercomplexes', *Biochimica et Biophysica Acta (BBA) - Bioenergetics*, 1797(6), pp. 664-670.

Dunbar, D.R., Moonie, P.A., Jacobs, H.T. and Holt, I.J. (1995) 'Different cellular backgrounds confer a marked advantage to either mutant or wild-type mitochondrial genomes', *Proceedings of the National Academy of Sciences*, 92(14), p. 6562.

Durham, S.E., Samuels, D.C., Cree, L.M. and Chinnery, P.F. (2007) 'Normal levels of wild-type mitochondrial DNA maintain cytochrome c oxidase activity for two pathogenic mitochondrial DNA mutations but not for m.3243A-->G', *Am J Hum Genet*, 81(1), pp. 189-95.

Dutta, S. and Sengupta, P. (2016) 'Men and mice: Relating their ages', *Life Sciences*, 152, pp. 244-248.

Eastwood, G.L. (1977) 'Gastrointestinal epithelial renewal', *Gastroenterology*, 72(5), pp. 962-975.

Eckelman, B.P., Salvesen, G.S. and Scott, F.L. (2006) 'Human inhibitor of apoptosis proteins: why XIAP is the black sheep of the family', *EMBO Reports*, 7(10), pp. 988-994.

Egger, J., Lake, B.D. and Wilson, J. (1981) 'Mitochondrial cytopathy. A multisystem disorder with ragged red fibres on muscle biopsy', *Archives of Disease in Childhood*, 56(10), pp. 741-752.

Elliott, H.R., Samuels, D.C., Eden, J.A., Relton, C.L. and Chinnery, P.F. (2008) 'Pathogenic Mitochondrial DNA Mutations Are Common in the General Population', *The American Journal of Human Genetics*, 83(2), pp. 254-260.

Elson, J.L., Samuels, D.C., Turnbull, D.M. and Chinnery, P.F. (2001) 'Random intracellular drift explains the clonal expansion of mitochondrial DNA mutations with age', *The American Journal of Human Genetics*, 68(3), pp. 802-806.

Elson, J.L., Turnbull, D.M. and Howell, N. (2004) 'Comparative Genomics and the Evolution of Human Mitochondrial DNA: Assessing the Effects of Selection', *The American Journal of Human Genetics*, 74(2), pp. 229-238.

Falkenberg, M. (2018) 'Mitochondrial DNA replication in mammalian cells: overview of the pathway', *Essays In Biochemistry*.

Falkenberg, M., Gaspari, M., Rantanen, A., Trifunovic, A., Larsson, N.-G. and Gustafsson, C.M. (2002) 'Mitochondrial transcription factors B1 and B2 activate transcription of human mtDNA', *Nature genetics*, 31(3), pp. 289-294.

Falkenberg, M., Larsson, N.-G. and Gustafsson, C.M. (2007) 'DNA replication and transcription in mammalian mitochondria', *Annu. Rev. Biochem.*, 76, pp. 679-699.

Fan, W., Waymire, K.G., Narula, N., Li, P., Rocher, C., Coskun, P.E., Vannan, M.A., Narula, J., MacGregor, G.R. and Wallace, D.C. (2008) 'A Mouse Model of Mitochondrial Disease Reveals Germline Selection Against Severe mtDNA Mutations', *Science*, 319(5865), p. 958.

Farr, C.L., Wang, Y. and Kaguni, L.S. (1999) 'Functional Interactions of Mitochondrial DNA Polymerase and Single-stranded DNA-binding Protein: TEMPLATE-PRIMER DNA BINDING AND INITIATION AND ELONGATION OF DNA STRAND SYNTHESIS', *Journal of Biological Chemistry*, 274(21), pp. 14779-14785.

Fernandez-Marcos, P.J. and Auwerx, J. (2011) 'Regulation of PGC-1α, a nodal regulator of mitochondrial biogenesis', *The American Journal of Clinical Nutrition*, 93(4), pp. 884S-890S.

Fevr, T., Robine, S., Louvard, D. and Huelsken, J. (2007) 'Wnt/β-catenin is essential for intestinal homeostasis and maintenance of intestinal stem cells', *Molecular and cellular biology*, 27(21), pp. 7551-7559.

Finnilä, S., Tuisku, S., Herva, R. and Majamaa, K. (2001) 'A novel mitochondrial DNA mutation and a mutation in the Notch3 gene in a patient with myopathy and CADASIL', *Journal of Molecular Medicine*, 79(11), pp. 641-647.

Fleischer, S., Klouwen, H. and Brierley, G. (1961) 'Studies of the electron transfer system. 38. Lipid composition of purified enzyme preparations derived from beef heart mitochondria', *J Biol Chem*, 236, pp. 2936-41.

Floros, V.I., Pyle, A., Dietmann, S., Wei, W., Tang, W.C.W., Irie, N., Payne, B., Capalbo, A., Noli, L., Coxhead, J., Hudson, G., Crosier, M., Strahl, H., Khalaf, Y., Saitou, M., Ilic, D., Surani, M.A. and Chinnery, P.F. (2018) 'Segregation of mitochondrial DNA heteroplasmy through a developmental genetic bottleneck in human embryos', *Nature Cell Biology*, 20(2), pp. 144-151.

Forbes, S.J. and Newsome, P.N. (2016) 'Liver regeneration — mechanisms and models to clinical application', *Nature Reviews Gastroenterology &Amp; Hepatology*, 13, p. 473.

Forkink, M., Smeitink, J.A.M., Brock, R., Willems, P.H.G.M. and Koopman, W.J.H. (2010) 'Detection and manipulation of mitochondrial reactive oxygen species in mammalian cells', *Biochimica et Biophysica Acta (BBA)-Bioenergetics*, 1797(6), pp. 1034-1044.

Fox, R.G., Magness, S., Kujoth, G.C., Prolla, T.A. and Maeda, N. (2012) 'Mitochondrial DNA polymerase editing mutation, PolgD257A, disturbs stem-progenitor cell cycling in the

small intestine and restricts excess fat absorption', *American Journal of Physiology-Gastrointestinal and Liver Physiology*, 302(9), pp. G914-G924.

Frederiksen, A.L., Andersen, P.H., Kyvik, K.O., Jeppesen, T.D., Vissing, J. and Schwartz, M. (2006) 'Tissue specific distribution of the 3243A→ G mtDNA mutation', *Journal of medical genetics*, 43(8), pp. 671-677.

Frey, T.G. and Mannella, C.A. (2000) 'The internal structure of mitochondria', *Trends in Biochemical Sciences*, 25(7), pp. 319-324.

Freyer, C., Cree, L.M., Mourier, A., Stewart, J.B., Koolmeister, C., Milenkovic, D., Wai, T., Floros, V.I., Hagstrom, E., Chatzidaki, E.E., Wiesner, R.J., Samuels, D.C., Larsson, N.G. and Chinnery, P.F. (2012) 'Variation in germline mtDNA heteroplasmy is determined prenatally but modified during subsequent transmission', *Nat Genet*, 44(11), pp. 1282-5.

Fukuhara, N., Tokiguchi, S., Shirakawa, K. and Tsubaki, T. (1980) 'Myoclonus epilepsy associated with ragged-red fibres (mitochondrial abnormalities): Disease entity or a syndrome?: Light- and electron-microscopic studies of two cases and review of literature', *Journal of the Neurological Sciences*, 47(1), pp. 117-133.

Fusté, J.M., Wanrooij, S., Jemt, E., Granycome, C.E., Cluett, T.J., Shi, Y., Atanassova, N., Holt, I.J., Gustafsson, C.M. and Falkenberg, M. (2010) 'Mitochondrial RNA Polymerase Is Needed for Activation of the Origin of Light-Strand DNA Replication', *Molecular Cell*, 37(1), pp. 67-78.

García-Prat, L., Martínez-Vicente, M., Perdiguero, E., Ortet, L., Rodríguez-Ubreva, J., Rebollo, E., Ruiz-Bonilla, V., Gutarra, S., Ballestar, E. and Serrano, A.L. (2016) 'Autophagy maintains stemness by preventing senescence', *Nature*, 529(7584), pp. 37-42.

Gehart, H. and Clevers, H. (2019) 'Tales from the crypt: new insights into intestinal stem cells', *Nature Reviews Gastroenterology & Hepatology*, 16(1), pp. 19-34.

Gehlert, S., Bloch, W. and Suhr, F. (2015) 'Ca(2+)-Dependent Regulations and Signaling in Skeletal Muscle: From Electro-Mechanical Coupling to Adaptation', *International Journal of Molecular Sciences*, 16(1), pp. 1066-1095.

Gerbe, F., Sidot, E., Smyth, D.J., Ohmoto, M., Matsumoto, I., Dardalhon, V., Cesses, P., Garnier, L., Pouzolles, M., Brulin, B., Bruschi, M., Harcus, Y., Zimmermann, V.S., Taylor,

N., Maizels, R.M. and Jay, P. (2016) 'Intestinal epithelial tuft cells initiate type 2 mucosal immunity to helminth parasites', *Nature*, 529, p. 226.

Gerdes, J., Lemke, H., Baisch, H., Wacker, H.H., Schwab, U. and Stein, H. (1984) 'Cell cycle analysis of a cell proliferation-associated human nuclear antigen defined by the monoclonal antibody Ki-67', *J Immunol*, 133(4), pp. 1710-5.

Geromel, V., Kadhom, N., Cebalos-Picot, I., Ouari, O., Polidori, A., Munnich, A., Rötig, A. and Rustin, P. (2001) 'Superoxide-induced massive apoptosis in cultured skin fibroblasts harboring the neurogenic ataxia retinitis pigmentosa (NARP) mutation in the ATPase-6 gene of the mitochondrial DNA', *Human Molecular Genetics*, 10(11), pp. 1221-1228.

Ghelli, A., Porcelli, A.M., Zanna, C., Martinuzzi, A., Carelli, V. and Rugolo, M. (2008) 'Protection against Oxidant-Induced Apoptosis by Exogenous Glutathione in Leber Hereditary Optic Neuropathy Cybrids', *Investigative Ophthalmology & Visual Science*, 49(2), pp. 671-676.

Gilkerson, R., Bravo, L., Garcia, I., Gaytan, N., Herrera, A., Maldonado, A. and Quintanilla, B. (2013) 'The Mitochondrial Nucleoid: Integrating Mitochondrial DNA into Cellular Homeostasis', *Cold Spring Harbor Perspectives in Biology*, 5(5), p. a011080.

Goodell, M.A., Nguyen, H. and Shroyer, N. (2015) 'Somatic stem cell heterogeneity: diversity in the blood, skin and intestinal stem cell compartments', *Nature Reviews Molecular Cell Biology*, 16, p. 299.

Gorman, G.S., Schaefer, A.M., Ng, Y., Gomez, N., Blakely, E.L., Alston, C.L., Feeney, C., Horvath, R., Yu‐Wai‐Man, P., Chinnery, P.F., Taylor, R.W., Turnbull, D.M. and McFarland, R. (2015) 'Prevalence of nuclear and mitochondrial DNA mutations related to adult mitochondrial disease', *Annals of Neurology*, 77(5), pp. 753-759.

Goto, Y.-i., Nonaka, I. and Horai, S. (1990) 'A mutation in the tRNALeu (UUR) gene associated with the MELAS subgroup of mitochondrial encephalomyopathies'.

Goto, Y.-i., Nonaka, I. and Horai, S. (1991) 'A new mtDNA mutation associated with mitochondrial myopathy, encephalopathy, lactic acidosis and stroke-like episodes (MELAS)', *Biochimica et Biophysica Acta (BBA)-Molecular Basis of Disease*, 1097(3), pp. 238-240.

Grady, J.P., Pickett, S.J., Ng, Y.S., Alston, C.L., Blakely, E.L., Hardy, S.A., Feeney, C.L., Bright, A.A., Schaefer, A.M., Gorman, G.S., McNally, R.J.Q., Taylor, R.W., Turnbull, D.M. and McFarland, R. (2018) 'mtDNA heteroplasmy level and copy number indicate disease burden in m.3243A>G mitochondrial disease', *EMBO Molecular Medicine*, 10(6), p. e8262.

Gray, H. and Wong, T.W. (1992) 'Purification and identification of subunit structure of the human mitochondrial DNA polymerase', *Journal of Biological Chemistry*, 267(9), pp. 5835-41.

Greaves, L.C., Barron, M.J., Plusa, S., Kirkwood, T.B., Mathers, J.C., Taylor, R.W. and Turnbull, D.M. (2010) 'Defects in multiple complexes of the respiratory chain are present in ageing human colonic crypts', *Exp Gerontol*, 45(7-8), pp. 573-9.

Greaves, L.C., Elson, J.L., Nooteboom, M., Grady, J.P., Taylor, G.A., Taylor, R.W., Mathers, J.C., Kirkwood, T.B.L. and Turnbull, D.M. (2012a) 'Comparison of mitochondrial mutation spectra in ageing human colonic epithelium and disease: absence of evidence for purifying selection in somatic mitochondrial DNA point mutations', *PLoS genetics*, 8(11), p. e1003082.

Greaves, L.C., Nooteboom, M., Elson, J.L., Tuppen, H.A.L., Taylor, G.A., Commane, D.M., Arasaradnam, R.P., Khrapko, K., Taylor, R.W. and Kirkwood, T.B.L. (2014) 'Clonal Expansion of Early to Mid-Life Mitochondrial DNA Point Mutations Drives Mitochondrial Dysfunction during Human Ageing', *PLoS genetics*, 10(9), p. e1004620.

Greaves, L.C., Preston, S.L., Tadrous, P.J., Taylor, R.W., Barron, M.J., Oukrif, D., Leedham, S.J., Deheragoda, M., Sasieni, P. and Novelli, M.R. (2006) 'Mitochondrial DNA mutations are established in human colonic stem cells, and mutated clones expand by crypt fission', *Proceedings of the National Academy of sciences of the United States of America*, 103(3), pp. 714-719.

Greaves, L.C., Reeve, A.K., Taylor, R.W. and Turnbull, D.M. (2012b) 'Mitochondrial DNA and disease', *The Journal of pathology*, 226(2), pp. 274-286.

Greber, B.J. and Ban, N. (2016) 'Structure and Function of the Mitochondrial Ribosome', *Annual Review of Biochemistry*, 85(1), pp. 103-132.

Grün, D., Lyubimova, A., Kester, L., Wiebrands, K., Basak, O., Sasaki, N., Clevers, H. and van Oudenaarden, A. (2015) 'Single-cell messenger RNA sequencing reveals rare intestinal cell types', *Nature*, 525, p. 251.

Guerrero-Castillo, S., Baertling, F., Kownatzki, D., Wessels, H.J., Arnold, S., Brandt, U. and Nijtmans, L. (2017) 'The Assembly Pathway of Mitochondrial Respiratory Chain Complex I', *Cell Metabolism*, 25(1), pp. 128-139.

Gustafsson, C.M., Falkenberg, M. and Larsson, N.-G. (2016) 'Maintenance and Expression of Mammalian Mitochondrial DNA', *Annual Review of Biochemistry*, 85(1), pp. 133-160.

Gutierrez‐Gonzalez, L., Deheragoda, M., Elia, G., Leedham, S.J., Shankar, A., Imber, C., Jankowski, J.A., Turnbull, D.M., Novelli, M. and Wright, N.A. (2009) 'Analysis of the clonal architecture of the human small intestinal epithelium establishes a common stem cell for all lineages and reveals a mechanism for the fixation and spread of mutations', *The Journal of pathology*, 217(4), pp. 489-496.

Gyllensten, U., Wharton, D., Josefsson, A. and Wilson, A.C. (1991) 'Paternal inheritance of mitochondrial DNA in mice'.

Hämäläinen, R.H. (2016) 'Mitochondria and mtDNA integrity in stem cell function and differentiation', *Current Opinion in Genetics & Development*, 38, pp. 83-89.

Hämäläinen, R.H., Manninen, T., Koivumäki, H., Kislin, M., Otonkoski, T. and Suomalainen, A. (2013) 'Tissue- and cell-type–specific manifestations of heteroplasmic mtDNA 3243A>G mutation in human induced pluripotent stem cell-derived disease model', *Proceedings of the National Academy of Sciences of the United States of America*, 110(38), pp. E3622-E3630.

Hammans, S.R., Sweeney, M.G., Brockington, M., Lennox, G.G., Lawton, N.F., Kennedy, C.R., Morgan-Hughes, J.A. and Harding, A.E. (1993) 'The mitochondrial DNA transfer RNALysA→ G [8344] mutation and the syndrome of myoclonic epilepsy with ragged red fibres [MERRF]', *Brain*, 116(3), pp. 617-632.

Hansen, O.H., Pedersen, T. and Larsen, J.K. (1976) 'Cell Proliferation Kinetics in Normal Human Gastric Mucosa', *Gastroenterology*, 70(6), pp. 1051-1054.

Harman, D. (1972) 'The Biologic Clock: The Mitochondria?', *Journal of the American Geriatrics Society*, 20(4), pp. 145-147.

Hatefi, Y. (1985) 'The Mitochondrial Electron Transport and Oxidative Phosphorylation System', *Annual Review of Biochemistry*, 54(1), pp. 1015-1069.

Hayashi, J., Ohta, S., Kikuchi, A., Takemitsu, M., Goto, Y. and Nonaka, I. (1991) 'Introduction of disease-related mitochondrial DNA deletions into HeLa cells lacking mitochondrial DNA results in mitochondrial dysfunction', *Proceedings of the National Academy of Sciences of the United States of America*, 88(23), pp. 10614-10618.

Hayashi, T. and Stuchebrukhov, A.A. (2010) 'Electron tunneling in respiratory complex I', *Proceedings of the National Academy of Sciences*, 107(45), pp. 19157-19162.

He, X.C., Zhang, J., Tong, W.-G., Tawfik, O., Ross, J., Scoville, D.H., Tian, Q., Zeng, X., He, X., Wiedemann, L.M., Mishina, Y. and Li, L. (2004) 'BMP signaling inhibits intestinal stem cell self-renewal through suppression of Wnt–β-catenin signaling', *Nature Genetics*, 36, p. 1117.

Hill, J.H., Chen, Z. and Xu, H. (2014) 'Selective propagation of functional mitochondrial DNA during oogenesis restricts the transmission of a deleterious mitochondrial variant', *Nature Genetics*, 46, p. 389.

Hirano, M., Ricci, E., Koenigsberger, M.R., Defendini, R., Pavlakis, S.G., DeVivo, D.C., DiMauro, S. and Rowland, L.P. (1992) 'MELAS: an original case and clinical criteria for diagnosis', *Neuromuscular Disorders*, 2(2), pp. 125-135.

Hofer, A.M., Curci, S., Doble, M.A., Brown, E.M. and Soybel, D.I. (2000) 'Intercellular communication mediated by the extracellular calcium-sensing receptor', *Nature Cell Biology*, 2, p. 392.

Hoffmann, W. (2008) 'Regeneration of the gastric mucosa and its glands from stem cells', *Curr Med Chem*, 15(29), pp. 3133-44.

Holt, I.J., Harding, A.E. and Morgan-Hughes, J.A. (1988) 'Deletions of muscle mitochondrial DNA in patients with mitochondrial myopathies', *Nature*, 331, p. 717.

Holt, I.J., Harding, A.E., Petty, R.K. and Morgan-Hughes, J.A. (1990) 'A new mitochondrial disease associated with mitochondrial DNA heteroplasmy', *American Journal of Human Genetics*, 46(3), pp. 428-433.

Holt, I.J., Lorimer, H.E. and Jacobs, H.T. (2000) 'Coupled leading-and lagging-strand synthesis of mammalian mitochondrial DNA', *Cell*, 100(5), pp. 515-524.

Holt, I.J. and Reyes, A. (2012) 'Human mitochondrial DNA replication', *Cold Spring Harbor perspectives in biology*, 4(12), p. a012971.

Hoppins, S., Lackner, L. and Nunnari, J. (2007) 'The machines that divide and fuse mitochondria', *Annu. Rev. Biochem.*, 76, pp. 751-780.

Hou, Y.-M. (2010) 'CCA Addition to tRNA: Implications for tRNA Quality Control', *IUBMB life*, 62(4), pp. 251-260.

Houshmand, M., Lindberg, C., Moslemi, A.R., Oldfors, A. and Holme, E. (1999) 'A novel heteroplasmic point mutation in the mitochondrial tRNA(Lys) gene in a sporadic case of mitochondrial encephalomyopathy: de novo mutation and no transmission to the offspring', *Hum Mutat*, 13(3), pp. 203-9.

Howell, N., Bindoff, L.A., McCullough, D.A., Kubacka, I., Poulton, J., Mackey, D., Taylor, L. and Turnbull, D.M. (1991) 'Leber hereditary optic neuropathy: identification of the same mitochondrial ND1 mutation in six pedigrees', *American Journal of Human Genetics*, 49(5), pp. 939-950.

Hüttemann, M., Pecina, P., Rainbolt, M., Sanderson, T.H., Kagan, V.E., Samavati, L., Doan, J.W. and Lee, I. (2011) 'The multiple functions of cytochrome c and their regulation in life and death decisions of the mammalian cell: from respiration to apoptosis', *Mitochondrion*, 11(3), pp. 369-381.

Ikezoe, K., Nakagawa, M., Yan, C., Kira, J.-i., Goto, Y.-i. and Nonaka, I. (2002) 'Apoptosis is suspended in muscle of mitochondrial encephalomyopathies', *Acta Neuropathologica*, 103(6), pp. 531-540.

Inoue, K., Nakada, K., Ogura, A., Isobe, K., Goto, Y.-i., Nonaka, I. and Hayashi, J.-I. (2000) 'Generation of mice with mitochondrial dysfunction by introducing mouse mtDNA carrying a deletion into zygotes', *Nature Genetics*, 26, p. 176.

Iwamoto, M., Ahnen, D.J., Franklin, W.A. and Maltzman, T.H. (2000) 'Expression of β-catenin and full-length APC protein in normal and neoplastic colonic tissues', *Carcinogenesis*, 21(11), pp. 1935-1940.

James, A.M., Wei, Y.H., Pang, C.Y. and Murphy, M.P. (1996) 'Altered mitochondrial function in fibroblasts containing MELAS or MERRF mitochondrial DNA mutations', *Biochemical Journal*, 318(Pt 2), pp. 401-407.

James S. Lowe, P.G.A. (2015) *Human histology*. Fourth edition edn. ELSEVIER MOSBY.

Jastroch, M., Divakaruni, A.S., Mookerjee, S., Treberg, J.R. and Brand, M.D. (2010) 'Mitochondrial proton and electron leaks', *Essays in biochemistry*, 47, pp. 53-67.

Jenuth, J.P., Peterson, A.C., Fu, K. and Shoubridge, E.A. (1996) 'Random genetic drift in the female germline explains the rapid segregation of mammalian mitochondrial DNA', *Nature Genetics*, 14(2), pp. 146-151.

Johns, D.R., Neufeld, M.J. and Park, R.D. (1992) 'An ND-6 mitochondrial DNA mutation associated with leber hereditary optic neuropathy', *Biochemical and Biophysical Research Communications*, 187(3), pp. 1551-1557.

Jokinen, R., Marttinen, P., Sandell, H.K., Manninen, T., Teerenhovi, H., Wai, T., Teoli, D., Loredo-Osti, J.C., Shoubridge, E.A. and Battersby, B.J. (2010) 'Gimap3 Regulates Tissue-Specific Mitochondrial DNA Segregation', *PLOS Genetics*, 6(10), p. e1001161.

Jornayvaz, F.R. and Shulman, G.I. (2010) 'Regulation of mitochondrial biogenesis', *Essays in biochemistry*, 47, p. 10.1042/bse0470069.

Jourdain, Alexis A., Koppen, M., Wydro, M., Rodley, Chris D., Lightowlers, Robert N., Chrzanowska-Lightowlers, Zofia M. and Martinou, J.-C. (2013) 'GRSF1 Regulates RNA Processing in Mitochondrial RNA Granules', *Cell Metabolism*, 17(3), pp. 399-410.

Jung, P., Sommer, C., Barriga, Francisco M., Buczacki, Simon J., Hernando-Momblona, X., Sevillano, M., Duran-Frigola, M., Aloy, P., Selbach, M., Winton, Douglas J. and Batlle, E. (2015) 'Isolation of Human Colon Stem Cells Using Surface Expression of PTK7', *Stem Cell Reports*, 5(6), pp. 979-987.

Kamada, S., Kikkawa, U., Tsujimoto, Y. and Hunter, T. (2005) 'Nuclear translocation of caspase-3 is dependent on its proteolytic activation and recognition of a substrate-like protein (s)', *Journal of Biological Chemistry*, 280(2), pp. 857-860.

Karam, S.M. (1999) 'Lineage commitment and maturation of epithelial cells in the gut', *Front Biosci*, 4, pp. D286-98.

Kasahara, A., Ishikawa, K., Yamaoka, M., Ito, M., Watanabe, N., Akimoto, M., Sato, A., Nakada, K., Endo, H., Suda, Y., Aizawa, S. and Hayashi, J.-I. (2006) 'Generation of trans-

mitochondrial mice carrying homoplasmic mtDNAs with a missense mutation in a structural gene using ES cells', *Human Molecular Genetics*, 15(6), pp. 871-881.

Kasamatsu, H. and Vinograd, J. (1974) 'Replication of circular DNA in eukaryotic cells', *Annual review of biochemistry*, 43(1), pp. 695-719.

Katajisto, P., Döhla, J., Chaffer, C., Pentinmikko, N., Marjanovic, N., Iqbal, S., Zoncu, R., Chen, W., Weinberg, R.A. and Sabatini, D.M. (2015) 'Asymmetric apportioning of aged mitochondria between daughter cells is required for stemness', *Science (New York, N.Y.)*, 348(6232), pp. 340-343.

Kauppila, Johanna H.K., Baines, Holly L., Bratic, A., Simard, M.-L., Freyer, C., Mourier, A., Stamp, C., Filograna, R., Larsson, N.-G., Greaves, Laura C. and Stewart, James B. (2016) 'A Phenotype-Driven Approach to Generate Mouse Models with Pathogenic mtDNA Mutations Causing Mitochondrial Disease', *Cell Reports*, 16(11), pp. 2980-2990.

Khrapko, K. and Vijg, J. (2009) 'Mitochondrial DNA mutations and aging: devils in the details?', *Trends in Genetics*, 25(2), pp. 91-98.

Kim, I., Rodriguez-Enriquez, S. and Lemasters, J.J. (2007) 'Selective degradation of mitochondria by mitophagy', *Archives of Biochemistry and Biophysics*, 462(2), pp. 245-253.

Kim, K.-M. and Shibata, D. (2002) 'Methylation reveals a niche: stem cell succession in human colon crypts', *Oncogene*, 21(35), pp. 5441-5449.

King, M.P. and Attardi, G. (1989) 'Human cells lacking mtDNA: repopulation with exogenous mitochondria by complementation', *Science*, 246(4929), pp. 500-3.

Kirichok, Y., Krapivinsky, G. and Clapham, D.E. (2004) 'The mitochondrial calcium uniporter is a highly selective ion channel', *Nature*, 427, p. 360.

Kitada, T., Asakawa, S., Hattori, N., Matsumine, H., Yamamura, Y., Minoshima, S., Yokochi, M., Mizuno, Y. and Shimizu, N. (1998) 'Mutations in the parkin gene cause autosomal recessive juvenile parkinsonism', *Nature*, 392, p. 605.

Koopman, W.J.H., Distelmaier, F., Smeitink, J.A.M. and Willems, P.H.G.M. (2013) 'OXPHOS mutations and neurodegeneration', *The EMBO journal*, 32(1), pp. 9-29.

Koopman, W.J.H., Willems, P.H.G.M. and Smeitink, J.A.M. (2012) 'Monogenic mitochondrial disorders', *New England Journal of Medicine*, 366(12), pp. 1132-1141.

Korhonen, J.A., Gaspari, M. and Falkenberg, M. (2003) 'TWINKLE Has 5′ → 3′ DNA Helicase Activity and Is Specifically Stimulated by Mitochondrial Single-stranded DNA-binding Protein', *Journal of Biological Chemistry*, 278(49), pp. 48627-48632.

Korhonen, J.A., Pham, X.H., Pellegrini, M. and Falkenberg, M. (2004) 'Reconstitution of a minimal mtDNA replisome in vitro', *The EMBO Journal*, 23(12), pp. 2423-2429.

Korinek, V., Barker, N., Moerer, P., van Donselaar, E., Huls, G., Peters, P.J. and Clevers, H. (1998) 'Depletion of epithelial stem-cell compartments in the small intestine of mice lacking Tcf-4', *Nature genetics*, 19(4), pp. 379-383.

Korinek, V., Barker, N., Morin, P.J., van Wichen, D., de Weger, R., Kinzler, K.W., Vogelstein, B. and Clevers, H. (1997) 'Constitutive Transcriptional Activation by a β-Catenin-Tcf Complex in APC−/− Colon Carcinoma', *Science*, 275(5307), pp. 1784-1787.

Kosinski, C., Li, V.S.W., Chan, A.S.Y., Zhang, J., Ho, C., Tsui, W.Y., Chan, T.L., Mifflin, R.C., Powell, D.W., Yuen, S.T., Leung, S.Y. and Chen, X. (2007) 'Gene expression patterns of human colon tops and basal crypts and BMP antagonists as intestinal stem cell niche factors', *Proceedings of the National Academy of Sciences*, 104(39), p. 15418.

Kotton, D.N. and Morrisey, E.E. (2014) 'Lung regeneration: mechanisms, applications and emerging stem cell populations', *Nature medicine*, 20(8), pp. 822-832.

Kouznetsova, I., Kalinski, T., Meyer, F. and Hoffmann, W. (2011) 'Self-renewal of the human gastric epithelium: new insights from expression profiling using laser microdissection', *Molecular BioSystems*, 7(4), pp. 1105-1112.

Kowald, A. and Kirkwood, T.B.L. (2000) 'Accumulation of Defective Mitochondria through Delayed Degradation of Damaged Organelles and Its Possible Role in the Ageing of Post-mitotic and Dividing Cells', *Journal of Theoretical Biology*, 202(2), pp. 145-160.

Kozar, S., Morrissey, E., Nicholson, A.M., van der Heijden, M., Zecchini, H.I., Kemp, R., Tavare, S., Vermeulen, L. and Winton, D.J. (2013) 'Continuous clonal labeling reveals small numbers of functional stem cells in intestinal crypts and adenomas', *Cell Stem Cell*, 13(5), pp. 626-33.

Kraytsberg, Y., Kudryavtseva, E., McKee, A.C., Geula, C., Kowall, N.W. and Khrapko, K. (2006) 'Mitochondrial DNA deletions are abundant and cause functional impairment in aged human substantia nigra neurons', *Nature genetics*, 38(5), pp. 518-520.

Kraytsberg, Y., Simon, D.K., Turnbull, D.M. and Khrapko, K. (2009) 'Do mtDNA deletions drive premature aging in mtDNA mutator mice?', *Aging cell*, 8(4), pp. 502-506.

Krishnan, K.J., Reeve, A.K., Samuels, D.C., Chinnery, P.F., Blackwood, J.K., Taylor, R.W., Wanrooij, S., Spelbrink, J.N., Lightowlers, R.N. and Turnbull, D.M. (2008) 'What causes mitochondrial DNA deletions in human cells?', *Nature genetics*, 40(3), pp. 275-279.

Kuhnert, F., Davis, C.R., Wang, H.-T., Chu, P., Lee, M., Yuan, J., Nusse, R. and Kuo, C.J. (2004) 'Essential requirement for Wnt signaling in proliferation of adult small intestine and colon revealed by adenoviral expression of Dickkopf-1', *Proceedings of the National Academy of Sciences*, 101(1), p. 266.

Kujoth, G.C., Hiona, A., Pugh, T.D., Someya, S., Panzer, K., Wohlgemuth, S.E., Hofer, T., Seo, A.Y., Sullivan, R. and Jobling, W.A. (2005) 'Mitochondrial DNA mutations, oxidative stress, and apoptosis in mammalian aging', *Science*, 309(5733), pp. 481-484.

Larsson, N.-g., Holme, E., Kristiansson, B., Oldfors, A. and Tulinius, M. (1990) 'Progressive increase of the mutated mitochondrial DNA fraction in Kearns-Sayre syndrome', *Pediatric Research*, 28(2), pp. 131-136.

Larsson, N. and Clayton, D.A. (1995) 'Molecular genetic aspects of human mitochondrial disorders', *Annual review of genetics*, 29(1), pp. 151-178.

Larsson, N.G., Tulinius, M.H., Holme, E., Oldfors, A., Andersen, O., Wahlström, J. and Aasly, J. (1992) 'Segregation and manifestations of the mtDNA tRNA (Lys) A--> G (8344) mutation of myoclonus epilepsy and ragged-red fibers (MERRF) syndrome', *American journal of human genetics*, 51(6), p. 1201.

Latil, M., Rocheteau, P., Châtre, L., Sanulli, S., Mémet, S., Ricchetti, M., Tajbakhsh, S. and Chrétien, F. (2012) 'Skeletal muscle stem cells adopt a dormant cell state post mortem and retain regenerative capacity', *Nature communications*, 3, p. 903.

Lee, C.-F., Liu, C.-Y., Chen, S.-M., Sikorska, M., Lin, C.-Y., Chen, T.-L. and Wei, Y.-H. (2006) 'Attenuation of UV-Induced Apoptosis by Coenzyme Q10 in Human Cells Harboring

Large-Scale Deletion of Mitochondrial DNA', *Annals of the New York Academy of Sciences*, 1042(1), pp. 429-438.

Lee, E.R. and Leblond, C.P. (1985a) 'Dynamic histology of the antral epithelium in the mouse stomach: II. Ultrastructure and renewal of isthmal cells', *Am J Anat*, 172(3), pp. 205-24.

Lee, E.R. and Leblond, C.P. (1985b) 'Dynamic histology of the antral epithelium in the mouse stomach: IV. Ultrastructure and renewal of gland cells', *Am J Anat*, 172(3), pp. 241-59.

Lee, H.-C. and Wei, Y.-H. (2005) 'Mitochondrial biogenesis and mitochondrial DNA maintenance of mammalian cells under oxidative stress', *The International Journal of Biochemistry & Cell Biology*, 37(4), pp. 822-834.

Lenaz, G. and Genova, M.L. (2009) 'Structure and Organization of Mitochondrial Respiratory Complexes: A New Understanding of an Old Subject', *Antioxidants & Redox Signaling*, 12(8), pp. 961-1008.

Levy, S.E., Waymire, K.G., Kim, Y.L., MacGregor, G.R. and Wallace, D.C. (1999) 'Transfer of chloramphenicol-resistant mitochondrial DNA into the chimeric mouse', *Transgenic Res*, 8(2), pp. 137-45.

Li, L. and Clevers, H. (2010) 'Coexistence of Quiescent and Active Adult Stem Cells in Mammals', *Science (New York, N.Y.)*, 327(5965), pp. 542-545.

Li, N., Nakauka-Ddamba, A., Tobias, J., Jensen, S.T. and Lengner, C.J. (2016) 'Mouse Label-Retaining Cells Are Molecularly and Functionally Distinct From Reserve Intestinal Stem Cells', *Gastroenterology*, 151(2), pp. 298-310.e7.

Lightowlers, R.N., Taylor, R.W. and Turnbull, D.M. (2015) 'Mutations causing mitochondrial disease: What is new and what challenges remain?', *Science*, 349(6255), pp. 1494-1499.

Lin, C.S., Sharpley, M.S., Fan, W., Waymire, K.G., Sadun, A.A., Carelli, V., Ross-Cisneros, F.N., Baciu, P., Sung, E., McManus, M.J., Pan, B.X., Gil, D.W., MacGregor, G.R. and Wallace, D.C. (2012) 'Mouse mtDNA mutant model of Leber hereditary optic neuropathy', *Proceedings of the National Academy of Sciences*, 109(49), p. 20065.

Lin, M.T. and Beal, M.F. (2006) 'Mitochondrial dysfunction and oxidative stress in neurodegenerative diseases', *Nature*, 443(7113), pp. 787-95.

Liu, C.-Y., Lee, C.-F. and Wei, Y.-H. (2007) 'Quantitative effect of 4977 bp deletion of mitochondrial DNA on the susceptibility of human cells to UV-induced apoptosis', *Mitochondrion*, 7(1), pp. 89-95.

Liu, C.Y., Lee, C.F., Hong, C.H. and Wei, Y.H. (2004) 'Mitochondrial DNA mutation and depletion increase the susceptibility of human cells to apoptosis', *Ann N Y Acad Sci*, 1011, pp. 133-45.

Liu, C.Y., Lee, C.F. and Wei, Y.H. (2009) 'Role of reactive oxygen species-elicited apoptosis in the pathophysiology of mitochondrial and neurodegenerative diseases associated with mitochondrial DNA mutations', *J Formos Med Assoc*, 108(8), pp. 599-611.

Liu, P. and Demple, B. (2010) 'DNA repair in mammalian mitochondria: Much more than we thought?', *Environmental and Molecular Mutagenesis*, 51(5), pp. 417-426.

Liu, P., Qian, L., Sung, J.-S., de Souza-Pinto, N.C., Zheng, L., Bogenhagen, D.F., Bohr, V.A., Wilson, D.M., Shen, B. and Demple, B. (2008) 'Removal of Oxidative DNA Damage via FEN1-Dependent Long-Patch Base Excision Repair in Human Cell Mitochondria', *Molecular and Cellular Biology*, 28(16), pp. 4975-4987.

Liu, V.W.S., Zhang, C., Linnane, A.W. and Nagley, P. (1997) 'Quantitative allele-specific PCR: Demonstration of age-associated accumulation in human tissues of the A→G mutation at nucleotide 3243 in mitochondrial DNA', *Human Mutation*, 9(3), pp. 265-271.

Liu, X., Jakubowski, M. and Hunt, J.L. (2011) 'KRAS Gene Mutation in Colorectal Cancer Is Correlated With Increased Proliferation and Spontaneous Apoptosis', *American Journal of Clinical Pathology*, 135(2), pp. 245-252.

Llopis, J., McCaffery, J.M., Miyawaki, A., Farquhar, M.G. and Tsien, R.Y. (1998) 'Measurement of cytosolic, mitochondrial, and Golgi pH in single living cells with green fluorescent proteins', *Proc Natl Acad Sci U S A*, 95(12), pp. 6803-8.

Longley, M.J., Nguyen, D., Kunkel, T.A. and Copeland, W.C. (2001) 'The Fidelity of Human DNA Polymerase γ with and without Exonucleolytic Proofreading and the p55 Accessory Subunit', *Journal of Biological Chemistry*, 276(42), pp. 38555-38562.

Lopez-Garcia, C., Klein, A.M., Simons, B.D. and Winton, D.J. (2010) 'Intestinal Stem Cell Replacement Follows a Pattern of Neutral Drift', *Science*, 330(6005), p. 822.

Lopez, J. and Tait, S.W.G. (2015) 'Mitochondrial apoptosis: killing cancer using the enemy within', *British Journal Of Cancer*, 112, p. 957.

Losón, O.C., Song, Z., Chen, H. and Chan, D.C. (2013) 'Fis1, Mff, MiD49, and MiD51 mediate Drp1 recruitment in mitochondrial fission', *Molecular Biology of the Cell*, 24(5), pp. 659-667.

Lu, J., Sharma, L.K. and Bai, Y. (2009) 'Implications of mitochondrial DNA mutations and mitochondrial dysfunction in tumorigenesis', *Cell research*, 19(7), pp. 802-815.

Ma, H., Xu, H. and O'Farrell, P.H. (2014) 'Transmission of mitochondrial mutations and action of purifying selection in Drosophila melanogaster', *Nature Genetics*, 46, p. 393.

Mah, A.T., Yan, K.S. and Kuo, C.J. (2016) 'Wnt pathway regulation of intestinal stem cells', *The Journal of Physiology*, 594(17), pp. 4837-4847.

Man, P.Y.W., Griffiths, P.G., Brown, D.T., Howell, N., Turnbull, D.M. and Chinnery, P.F. (2003) 'The epidemiology of Leber hereditary optic neuropathy in the North East of England', *The American Journal of Human Genetics*, 72(2), pp. 333-339.

Marchington, D.R., Barlow, D. and Poulton, J. (1999) 'Transmitochondrial mice carrying resistance to chloramphenicol on mitochondrial DNA: Developing the first mouse model of mitochondrial DNA disease', *Nature Medicine*, 5(8), pp. 957-960.

Margulis, L. (1971) 'The Origin of Plant and Animal Cells: The serial symbiosis view of the origin of higher cells suggests that the customary division of living things into two kingdoms should be reconsidered', *American scientist*, 59(2), pp. 230-235.

Mariotti, C., Savarese, N., Suomalainen, A., Rimoldi, M., Comi, G., Prelle, A., Antozzi, C., Servidei, S., Jarre, L., DiDonato, S. and Zeviani, M. (1995) 'Genotype to phenotype correlations in mitochondrial encephalomyopathies associated with the A3243G mutation of mitochondrial DNA', *J Neurol*, 242(5), pp. 304-12.

Martin Schmeing, T., Huang, K.S., Strobel, S.A. and Steitz, T.A. (2005) 'An induced-fit mechanism to promote peptide bond formation and exclude hydrolysis of peptidyl-tRNA', *Nature*, 438, p. 520.

Martin, W. and Müller, M. (1998) 'The hydrogen hypothesis for the first eukaryote', *Nature*, 392, p. 37.

Matthews, P.M., Hopkin, J., Brown, R.M., Stephenson, J.B., Hilton-Jones, D. and Brown, G.K. (1994) 'Comparison of the relative levels of the 3243 (A--> G) mtDNA mutation in heteroplasmic adult and fetal tissues', *Journal of medical genetics*, 31(1), pp. 41-44.

Mattson, M.P. and Partin, J. (1999) 'Evidence for mitochondrial control of neuronal polarity', *Journal of Neuroscience Research*, 56(1), pp. 8-20.

Mayr, J.A., Haack, T.B., Freisinger, P., Karall, D., Makowski, C., Koch, J., Feichtinger, R.G., Zimmermann, F.A., Rolinski, B., Ahting, U., Meitinger, T., Prokisch, H. and Sperl, W. (2015) 'Spectrum of combined respiratory chain defects', *Journal of Inherited Metabolic Disease*, 38(4), pp. 629-640.

McDonald, S.A.C., Greaves, L.C., Gutierrez–Gonzalez, L., Rodriguez–Justo, M., Deheragoda, M., Leedham, S.J., Taylor, R.W., Lee, C.Y., Preston, S.L. and Lovell, M. (2008) 'Mechanisms of field cancerization in the human stomach: the expansion and spread of mutated gastric stem cells', *Gastroenterology*, 134(2), pp. 500-510.

McFarland, R., Swalwell, H., Blakely, E.L., He, L., Groen, E.J., Turnbull, D.M., Bushby, K.M. and Taylor, R.W. (2008) 'The m.5650G>A mitochondrial tRNAAla mutation is pathogenic and causes a phenotype of pure myopathy', *Neuromuscul Disord*, 18(1), pp. 63-7.

McShane, M.A., Hammans, S.R., Sweeney, M., Holt, I.J., Beattie, T.J., Brett, E.M. and Harding, A.E. (1991) 'Pearson syndrome and mitochondrial encephalomyopathy in a patient with a deletion of mtDNA', *American journal of human genetics*, 48(1), p. 39.

McWilliams, T.G. and Muqit, M.M.K. (2017) 'PINK1 and Parkin: emerging themes in mitochondrial homeostasis', *Current Opinion in Cell Biology*, 45, pp. 83-91.

Medema, J.P. and Vermeulen, L. (2011) 'Microenvironmental regulation of stem cells in intestinal homeostasis and cancer', *Nature*, 474(7351), pp. 318-326.

Meissner, C., Lorenz, H., Weihofen, A., Selkoe, D.J. and Lemberg, M.K. (2011) 'The mitochondrial intramembrane protease PARL cleaves human Pink1 to regulate Pink1 trafficking', *J Neurochem*, 117(5), pp. 856-67.

Mignotte, B., Barat, M. and Mounolou, J.C. (1985) 'Characterization of a mitochondrial protein binding to single-stranded DNA', *Nucleic acids research*, 13(5), pp. 1703-1716.

Mills, J.C. and Shivdasani, R.A. (2011) 'Gastric Epithelial Stem Cells', *Gastroenterology*, 140(2), pp. 412-424.

Mirabella, M., Di Giovanni, S., Silvestri, G., Tonali, P. and Servidei, S. (2000) 'Apoptosis in mitochondrial encephalomyopathies with mitochondrial DNA mutations: a potential pathogenic mechanism', *Brain*, 123(1), pp. 93-104.

Mishra, P. and Chan, D.C. (2014) 'Mitochondrial dynamics and inheritance during cell division, development and disease', *Nat Rev Mol Cell Biol*, 15(10), pp. 634-46.

Mita, S., Schmidt, B., Schon, E.A., DiMauro, S. and Bonilla, E. (1989) 'Detection of" deleted" mitochondrial genomes in cytochrome-c oxidase-deficient muscle fibers of a patient with Kearns-Sayre syndrome', *Proceedings of the National Academy of Sciences*, 86(23), pp. 9509-9513.

Monnot, S., Gigarel, N., Samuels, D.C., Burlet, P., Hesters, L., Frydman, N., Frydman, R., Kerbrat, V., Funalot, B. and Martinovic, J. (2011) 'Segregation of mtDNA throughout human embryofetal development: m. 3243A> G as a model system', *Human mutation*, 32(1), pp. 116-125.

Montgomery, R.K., Carlone, D.L., Richmond, C.A., Farilla, L., Kranendonk, M.E.G., Henderson, D.E., Baffour-Awuah, N.Y., Ambruzs, D.M., Fogli, L.K., Algra, S. and Breault, D.T. (2011) 'Mouse telomerase reverse transcriptase (mTert) expression marks slowly cycling intestinal stem cells', *Proceedings of the National Academy of Sciences*, 108(1), p. 179.

Montoya, J., Gaines, G.L. and Attardi, G. (1983) 'The pattern of transcription of the human mitochondrial rRNA genes reveals two overlapping transcription units', *Cell*, 34(1), pp. 151-159.

Moraes, C.T., DiMauro, S., Zeviani, M., Lombes, A., Shanske, S., Miranda, A.F., Nakase, H., Bonilla, E., Werneck, L.C., Servidei, S., Nonaka, I., Koga, Y., Spiro, A.J., W. Brownell, A.K., Schmidt, B., Schotland, D.L., Zupanc, M., DeVivo, D.C., Schon, E.A. and Rowland, L.P. (1989) 'Mitochondrial DNA Deletions in Progressive External Ophthalmoplegia and Kearns-Sayre Syndrome', *New England Journal of Medicine*, 320(20), pp. 1293-1299.

Moraes, C.T., Ricci, E., Bonilla, E., DiMauro, S. and Schon, E.A. (1992) 'The mitochondrial tRNA(Leu(UUR)) mutation in mitochondrial encephalomyopathy, lactic acidosis, and

strokelike episodes (MELAS): genetic, biochemical, and morphological correlations in skeletal muscle', *American Journal of Human Genetics*, 50(5), pp. 934-949.

Moreno-Lastres, D., Fontanesi, F., García-Consuegra, I., Martín, Miguel A., Arenas, J., Barrientos, A. and Ugalde, C. (2012) 'Mitochondrial Complex I Plays an Essential Role in Human Respirasome Assembly', *Cell Metabolism*, 15(3), pp. 324-335.

Morin, P.J., Sparks, A.B., Korinek, V., Barker, N., Clevers, H., Vogelstein, B. and Kinzler, K.W. (1997) 'Activation of β-Catenin-Tcf Signaling in Colon Cancer by Mutations in β-Catenin or APC', *Science*, 275(5307), pp. 1787-1790.

Morozov, Y.I., Agaronyan, K., Cheung, A.C.M., Anikin, M., Cramer, P. and Temiakov, D. (2014) 'A novel intermediate in transcription initiation by human mitochondrial RNA polymerase', *Nucleic Acids Research*, 42(6), pp. 3884-3893.

Morozov, Y.I., Parshin, A.V., Agaronyan, K., Cheung, Alan C M., Anikin, M., Cramer, P. and Temiakov, D. (2015) 'A model for transcription initiation in human mitochondria', *Nucleic Acids Research*, 43(7), pp. 3726-3735.

Morrison, S.J. and Kimble, J. (2006) 'Asymmetric and symmetric stem-cell divisions in development and cancer', *Nature*, 441(7097), pp. 1068-1074.

Moser, A.R., Luongo, C., Gould, K.A., McNeley, M.K., Shoemaker, A.R. and Dove, W.F. (1995) 'ApcMin: A mouse model for intestinal and mammary tumorigenesis', *European Journal of Cancer*, 31(7), pp. 1061-1064.

Müller-Höcker, J. (1989) 'Cytochrome-c-oxidase deficient cardiomyocytes in the human heart--an age-related phenomenon. A histochemical ultracytochemical study', *The American journal of pathology*, 134(5), p. 1167.

Müller-Höcker, J. (1990) 'Cytochrome c oxidase deficient fibres in the limb muscle and diaphragm of man without muscular disease: an age-related alteration', *Journal of the neurological sciences*, 100(1), pp. 14-21.

Muñoz, J., Stange, D.E., Schepers, A.G., van de Wetering, M., Koo, B.K., Itzkovitz, S., Volckmann, R., Kung, K.S., Koster, J., Radulescu, S., Myant, K., Versteeg, R., Sansom, O.J., van Es, J.H., Barker, N., van Oudenaarden, A., Mohammed, S., Heck, A.J.R. and Clevers, H. (2012) 'The Lgr5 intestinal stem cell signature: robust expression of proposed quiescent '+4' cell markers', *The EMBO Journal*, 31(14), p. 3079.

Münscher, C., Rieger, T., Müller-Höcker, J. and Kadenbach, B. (1993) 'The point mutation of mitochondrial DNA characteristic for MERRF disease is found also in healthy people of different ages', *FEBS Letters*, 317(1-2), pp. 27-30.

Nakada, K., Inoue, K., Ono, T., Isobe, K., Ogura, A., Goto, Y.-I., Nonaka, I. and Hayashi, J.-I. (2001) 'Inter-mitochondrial complementation: Mitochondria-specific system preventing mice from expression of disease phenotypes by mutant mtDNA', *Nature Medicine*, 7, p. 934.

Nakada, K., Sato, A., Sone, H., Kasahara, A., Ikeda, K., Kagawa, Y., Yonekawa, H. and Hayashi, J.-I. (2004) 'Accumulation of pathogenic ΔmtDNA induced deafness but not diabetic phenotypes in mito-mice', *Biochemical and Biophysical Research Communications*, 323(1), pp. 175-184.

Nakada, K., Sato, A., Yoshida, K., Morita, T., Tanaka, H., Inoue, S.-I., Yonekawa, H. and Hayashi, J.-I. (2006) 'Mitochondria-related male infertility', *Proceedings of the National Academy of Sciences*, 103(41), p. 15148.

Nalapareddy, K., Nattamai, K.J., Kumar, R.S., Karns, R., Wikenheiser-Brokamp, K.A., Sampson, L.L., Mahe, M.M., Sundaram, N., Yacyshyn, M.-B., Yacyshyn, B., Helmrath, M.A., Zheng, Y. and Geiger, H. (2017) 'Canonical Wnt Signaling Ameliorates Aging of Intestinal Stem Cells', *Cell Reports*, 18(11), pp. 2608-2621.

Narendra, D., Tanaka, A., Suen, D.-F. and Youle, R.J. (2008) 'Parkin is recruited selectively to impaired mitochondria and promotes their autophagy', *The Journal of Cell Biology*, 183(5), p. 795.

Naviaux, R.K. and Nguyen, K.V. (2004) 'POLG mutations associated with Alpers' syndrome and mitochondrial DNA depletion', *Annals of Neurology*, 55(5), pp. 706-712.

Nefzger C , M., Jardé, T., Rossello F , J., Horvay, K., Knaupp A , S., Powell D , R., Chen, J., Abud H , E. and Polo J , M. (2016) 'A Versatile Strategy for Isolating a Highly Enriched Population of Intestinal Stem Cells', *Stem Cell Reports*, 6(3), pp. 321-9.

Nomura, S., Esumi, H., Job, C. and Tan, S.-S. (1998) 'Lineage and Clonal Development of Gastric Glands', *Developmental Biology*, 204(1), pp. 124-135.

Nooteboom, M., Johnson, R., Taylor, R.W., Wright, N.A., Lightowlers, R.N., Kirkwood, T.B.L., Mathers, J.C., Turnbull, D.M. and Greaves, L.C. (2010) 'Age‐associated

mitochondrial DNA mutations lead to small but significant changes in cell proliferation and apoptosis in human colonic crypts', *Aging cell*, 9(1), pp. 96-99.

Nørby, S., Lestienne, P., Nelson, I., Nielsen, I.M., Schmalbruch, H., Sjö, O. and Warburg, M. (1994) 'Juvenile Kearns-Sayre syndrome initially misdiagnosed as a psychosomatic disorder', *Journal of Medical Genetics*, 31(1), p. 45.

Norddahl, G.L., Pronk, C.J., Wahlestedt, M., Sten, G., Nygren, J.M., Ugale, A., Sigvardsson, M. and Bryder, D. (2011) 'Accumulating mitochondrial DNA mutations drive premature hematopoietic aging phenotypes distinct from physiological stem cell aging', *Cell stem cell*, 8(5), pp. 499-510.

Novelli, M.R., Williamson, J.A., Tomlinson, I.P.M., Elia, G., Hodgson, S.V., Talbot, I.C., Bodmer, W.F. and Wright, N.A. (1996) 'Polyclonal Origin of Colonic Adenomas in an XO/XY Patient with FAP', *Science*, 272(5265), pp. 1187-1190.

Okuno, D., Iino, R. and Noji, H. (2011) 'Rotation and structure of FoF1-ATP synthase', *Journal of biochemistry*, 149(6), pp. 655-664.

Olivo, P.D., Van de Walle, M.J., Laipis, P.J. and Hauswirth, W.W. (1983) 'Nucleotide sequence evidence for rapid genotypic shifts in the bovine mitochondrial DNA D-loop', *Nature*, 306(5941), pp. 400-402.

Olsson, C., Johnsen, E., Nilsson, M., Wilander, E., Syvanen, A.C. and Lagerstrom-Fermer, M. (2001) 'The level of the mitochondrial mutation A3243G decreases upon ageing in epithelial cells from individuals with diabetes and deafness', *Eur J Hum Genet*, 9(12), pp. 917-21.

Orrenius, S., Zhivotovsky, B. and Nicotera, P. (2003) 'Regulation of cell death: the calcium–apoptosis link', *Nature Reviews Molecular Cell Biology*, 4, p. 552.

Palade, G.E. (1952) 'The fine structure of mitochondria', *Anat Rec*, 114(3), pp. 427-51.

Pallotti, F., Chen, X., Bonilla, E. and Schon, E.A. (1996) 'Evidence that specific mtDNA point mutations may not accumulate in skeletal muscle during normal human aging', *American Journal of Human Genetics*, 59(3), pp. 591-602.

Palty, R., Silverman, W.F., Hershfinkel, M., Caporale, T., Sensi, S.L., Parnis, J., Nolte, C., Fishman, D., Shoshan-Barmatz, V., Herrmann, S., Khananshvili, D. and Sekler, I. (2010)

'NCLX is an essential component of mitochondrial Na+/Ca2+ exchange', *Proc Natl Acad Sci U S A*, 107(1), pp. 436-41.

Pappou, E.P. and Ahuja, N. (2010) 'The role of oncogenes in gastrointestinal cancer', *Gastrointestinal cancer research : GCR*, (Suppl 1), pp. S2-S15.

Paradkar, P.N., Zumbrennen, K.B., Paw, B.H., Ward, D.M. and Kaplan, J. (2009) 'Regulation of Mitochondrial Iron Import through Differential Turnover of Mitoferrin 1 and Mitoferrin 2', *Molecular and Cellular Biology*, 29(4), p. 1007.

Park, H.S., Goodlad, R.A. and Wright, N.A. (1995) 'Crypt fission in the small intestine and colon. A mechanism for the emergence of G6PD locus-mutated crypts after treatment with mutagens', *The American Journal of Pathology*, 147(5), pp. 1416-1427.

Patel, S., Rew, D.A., Taylor, I., Potten, C.S., Owen, C. and Roberts, S.A. (1993) 'Study of the proliferation in human gastric mucosa after in vivo bromodeoxyuridine labelling', *Gut*, 34(7), pp. 893-896.

Pearson, H.A., Lobel, J.S., Kocoshis, S.A., Naiman, J.L., Windmiller, J., Lammi, A.T., Hoffman, R. and Marsh, J.C. (1979) 'A new syndrome of refractory sideroblastic anemia with vacuolization of marrow precursors and exocrine pancreatic dysfunction', *J Pediatr*, 95(6), pp. 976-84.

Pellettieri, J. and Alvarado, A.S. (2007) 'Cell Turnover and Adult Tissue Homeostasis: From Humans to Planarians', *Annual Review of Genetics*, 41(1), pp. 83-105.

Perales-Clemente, E., Fernandez-Vizarra, E., Acin-Perez, R., Movilla, N., Bayona-Bafaluy, M.P., Moreno-Loshuertos, R., Perez-Martos, A., Fernandez-Silva, P. and Enriquez, J.A. (2010) 'Five entry points of the mitochondrially encoded subunits in mammalian complex I assembly', *Mol Cell Biol*, 30(12), pp. 3038-47.

Pfaff, E. and Klingenberg, M. (1968) 'Adenine nucleotide translocation of mitochondria. 1. Specificity and control', *Eur J Biochem*, 6(1), pp. 66-79.

Phillips, N.R., Sprouse, M.L. and Roby, R.K. (2014) 'Simultaneous quantification of mitochondrial DNA copy number and deletion ratio: a multiplex real-time PCR assay', *Sci Rep*, 4, p. 3887.

Pinto, M., Pickrell, A.M., Wang, X., Bacman, S.R., Yu, A., Hida, A., Dillon, L.M., Morton, P.D., Malek, T.R., Williams, S.L. and Moraes, C.T. (2016) 'Transient mitochondrial DNA double strand breaks in mice cause accelerated aging phenotypes in a ROS-dependent but p53/p21-independent manner', *Cell Death And Differentiation*, 24, p. 288.

Pohjoismäki, J.L.O., Wanrooij, S., Hyvärinen, A.K., Goffart, S., Holt, I.J., Spelbrink, J.N. and Jacobs, H.T. (2006) 'Alterations to the expression level of mitochondrial transcription factor A, TFAM, modify the mode of mitochondrial DNA replication in cultured human cells', *Nucleic Acids Research*, 34(20), pp. 5815-5828.

Popadin, K., Gunbin, K.V. and Khrapko, K. 'Mitochondrial DNA Mutations and Cancer', *The American Journal of Pathology*, 184(11), pp. 2852-2854.

Potten, C.S., Booth, C. and Pritchard, D. (1997) 'The intestinal epithelial stem cell: the mucosal governor', *International journal of experimental pathology*, 78(4), pp. 219-243.

Pradelli, L.A., Beneteau, M. and Ricci, J.E. (2010) 'Mitochondrial control of caspase-dependent and -independent cell death', *Cell Mol Life Sci*, 67(10), pp. 1589-97.

Puigserver, P. and Spiegelman, B.M. (2003) 'Peroxisome proliferator-activated receptor-gamma coactivator 1 alpha (PGC-1 alpha): transcriptional coactivator and metabolic regulator', *Endocr Rev*, 24(1), pp. 78-90.

Raffaello, A., Mammucari, C., Gherardi, G. and Rizzuto, R. (2016) 'Calcium at the Center of Cell Signaling: Interplay between Endoplasmic Reticulum, Mitochondria, and Lysosomes', *Trends in Biochemical Sciences*, 41(12), pp. 1035-1049.

Rahman, S., Poulton, J., Marchington, D. and Suomalainen, A. (2001) 'Decrease of 3243 A→G mtDNA mutation from blood in MELAS syndrome: a longitudinal study', *The American Journal of Human Genetics*, 68(1), pp. 238-240.

Rajasimha, H.K., Chinnery, P.F. and Samuels, D.C. (2008) 'Selection against pathogenic mtDNA mutations in a stem cell population leads to the loss of the 3243A-->G mutation in blood', *Am J Hum Genet*, 82(2), pp. 333-43.

Rebolledo-Jaramillo, B., Su, M.S.-W., Stoler, N., McElhoe, J.A., Dickins, B., Blankenberg, D., Korneliussen, T.S., Chiaromonte, F., Nielsen, R., Holland, M.M., Paul, I.M., Nekrutenko, A. and Makova, K.D. (2014) 'Maternal age effect and severe germ-line bottleneck in the

inheritance of human mitochondrial DNA', *Proceedings of the National Academy of Sciences*, 111(43), p. 15474.

Reeve, A.K., Krishnan, K.J., Taylor, G., Elson, J.L., Bender, A., Taylor, R.W., Morris, C.M. and Turnbull, D.M. (2009) 'The low abundance of clonally expanded mitochondrial DNA point mutations in aged substantia nigra neurons', *Aging cell*, 8(4), pp. 496-498.

Rich, P.R. (2003) 'The molecular machinery of Keilin's respiratory chain', *Biochemical Society Transactions*, 31(6), pp. 1095-1106.

Richter, C., Park, J.W. and Ames, B.N. (1988) 'Normal oxidative damage to mitochondrial and nuclear DNA is extensive', *Proceedings of the National Academy of Sciences*, 85(17), pp. 6465-6467.

Rizzuto, R., De Stefani, D., Raffaello, A. and Mammucari, C. (2012) 'Mitochondria as sensors and regulators of calcium signalling', *Nature Reviews Molecular Cell Biology*, 13, p. 566.

Rocha, M.C., Grady, J.P., Grünewald, A., Vincent, A., Dobson, P.F., Taylor, R.W., Turnbull, D.M. and Rygiel, K.A. (2015) 'A novel immunofluorescent assay to investigate oxidative phosphorylation deficiency in mitochondrial myopathy: understanding mechanisms and improving diagnosis', *Scientific Reports*, 5, p. 15037.

Rodríguez-Colman, M.J., Schewe, M., Meerlo, M., Stigter, E., Gerrits, J., Pras-Raves, M., Sacchetti, A., Hornsveld, M., Oost, K.C., Snippert, H.J., Verhoeven-Duif, N., Fodde, R. and Burgering, B.M.T. (2017) 'Interplay between metabolic identities in the intestinal crypt supports stem cell function', *Nature*, 543, p. 424.

Ronaghi, M., Uhlén, M. and Nyrén, P. (1998) 'A Sequencing Method Based on Real-Time Pyrophosphate', *Science*, 281(5375), p. 363.

Rosing, H.S., Hopkins, L.C., Wallace, D.C., Epstein, C.M. and Weidenheim, K. (1985) 'Maternally inherited mitochondrial myopathy and myoclonic epilepsy', *Annals of Neurology*, 17(3), pp. 228-237.

Ross, J.M., Stewart, J.B., Hagström, E., Brené, S., Mourier, A., Coppotelli, G., Freyer, C., Lagouge, M., Hoffer, B.J., Olson, L. and Larsson, N.-G. (2013) 'Germline mitochondrial DNA mutations aggravate ageing and can impair brain development', *Nature*, 501, p. 412.

Roth, S.M., Martel, G.F., Ivey, F.M., Lemmer, J.T., Metter, E.J., Hurley, B.F. and Rogers, M.A. (2000) 'Skeletal muscle satellite cell populations in healthy young and older men and women', *The Anatomical Record*, 260(4), pp. 351-358.

Rotig, A., Colonna, M., Bonnefont, J.P., Blanche, S., Fischer, A., Saudubray, J.M. and Munnich, A. (1989) 'MITOCHONDRIAL DNA DELETION IN PEARSON'S MARROW/PANCREAS SYNDROME', *The Lancet*, 333(8643), pp. 902-903.

Saeki, K., Suzuki, H., Tsuneoka, M., Maeda, M., Iwamoto, R., Hasuwa, H., Shida, S., Takahashi, T., Sakaguchi, M. and Endo, T. (2000) 'Identification of mammalian TOM22 as a subunit of the preprotein translocase of the mitochondrial outer membrane', *Journal of Biological Chemistry*, 275(41), pp. 31996-32002.

Salazar-Roa, M. and Malumbres, M. (2017) 'Fueling the Cell Division Cycle', *Trends in Cell Biology*, 27(1), pp. 69-81.

Sangiorgi, E. and Capecchi, M.R. (2008a) 'Bmi1 is expressed in vivo in intestinal stem cells', *Nature Genetics*, 40, p. 915.

Sangiorgi, E. and Capecchi, M.R. (2008b) 'Bmi1 is expressed in vivo in intestinal stem cells', *Nature genetics*, 40(7), pp. 915-920.

Sasaki, N., Sachs, N., Wiebrands, K., Ellenbroek, S.I.J., Fumagalli, A., Lyubimova, A., Begthel, H., van den Born, M., van Es, J.H., Karthaus, W.R., Li, V.S.W., López-Iglesias, C., Peters, P.J., van Rheenen, J., van Oudenaarden, A. and Clevers, H. (2016) 'Reg4+ deep crypt secretory cells function as epithelial niche for Lgr5+ stem cells in colon', *Proceedings of the National Academy of Sciences of the United States of America*, 113(37), pp. E5399-E5407.

Sato, T., van Es, J.H., Snippert, H.J., Stange, D.E., Vries, R.G., van den Born, M., Barker, N., Shroyer, N.F., van de Wetering, M. and Clevers, H. (2010) 'Paneth cells constitute the niche for Lgr5 stem cells in intestinal crypts', *Nature*, 469, p. 415.

Sato, T., Vries, R.G., Snippert, H.J., van de Wetering, M., Barker, N., Stange, D.E., van Es, J.H., Abo, A., Kujala, P., Peters, P.J. and Clevers, H. (2009) 'Single Lgr5 stem cells build crypt– villus structures in vitro without a mesenchymal niche', *Nature*, 459, p. 262.

Scarpulla, R.C. (2011) 'Metabolic control of mitochondrial biogenesis through the PGC-1 family regulatory network', *Biochimica et Biophysica Acta (BBA) - Molecular Cell Research*, 1813(7), pp. 1269-1278.

Scarpulla, R.C., Vega, R.B. and Kelly, D.P. (2012) 'Transcriptional integration of mitochondrial biogenesis', *Trends in Endocrinology & Metabolism*, 23(9), pp. 459-466.

Schaefer, A.M., Taylor, R.W., Turnbull, D.M. and Chinnery, P.F. (2004) 'The epidemiology of mitochondrial disorders—past, present and future', *Biochimica et Biophysica Acta (BBA) - Bioenergetics*, 1659(2), pp. 115-120.

Schäfer, E., Seelert, H., Reifschneider, N.H., Krause, F., Dencher, N.A. and Vonck, J. (2006) 'Architecture of Active Mammalian Respiratory Chain Supercomplexes', *Journal of Biological Chemistry*, 281(22), pp. 15370-15375.

Schägger, H. and Pfeiffer, K. (2000) 'Supercomplexes in the respiratory chains of yeast and mammalian mitochondria', *The EMBO Journal*, 19(8), p. 1777.

Schoeler, S., Szibor, R., Gellerich, F.N., Wartmann, T., Mawrin, C., Dietzmann, K. and Kirches, E. (2005) 'Mitochondrial DNA deletions sensitize cells to apoptosis at low heteroplasmy levels', *Biochemical and Biophysical Research Communications*, 332(1), pp. 43-49.

Scholzen, T. and Gerdes, J. (2000) 'The Ki-67 protein: From the known and the unknown', *Journal of Cellular Physiology*, 182(3), pp. 311-322.

Schon, E.A., DiMauro, S. and Hirano, M. (2012) 'Human mitochondrial DNA: roles of inherited and somatic mutations', *Nature Reviews Genetics*, 13(12), pp. 878-890.

Schon, E.A., Rizzuto, R., Moraes, C.T., Nakase, H., Zeviani, M. and DiMauro, S. (1989) 'A direct repeat is a hotspot for large-scale deletion of human mitochondrial DNA', *Science*, 244(4902), pp. 346-349.

Schon, E.A., Santra, S., Pallotti, F. and Girvin, M.E. (2001) 'Pathogenesis of primary defects in mitochondrial ATP synthesis', *Seminars in Cell & Developmental Biology*, 12(6), pp. 441-448.

Schuijers, J., van der Flier, Laurens G., van Es, J. and Clevers, H. (2014) 'Robust Cre-Mediated Recombination in Small Intestinal Stem Cells Utilizing the Olfm4 Locus', *Stem Cell Reports*, 3(2), pp. 234-241.

Schultz, B.E. and Chan, S.I. (2001) 'Structures and Proton-Pumping Strategies of Mitochondrial Respiratory Enzymes', *Annual Review of Biophysics and Biomolecular Structure*, 30(1), pp. 23-65.

Sciacco, M., Bonilla, E., Schon, E.A., DiMauro, S. and Moraes, C.T. (1994) 'Distribution of wild-type and common deletion forms of mtDNA in normal and respiration-deficient muscle fibers from patients with mitochondrial myopathy', *Human Molecular Genetics*, 3(1), pp. 13-19.

Sciacco, M., Fagiolari, G., Lamperti, C., Messina, S., Bazzi, P., Napoli, L., Chiveri, L., Prelle, A., Comi, G.P., Bresolin, N., Scarlato, G. and Moggio, M. (2001) 'Lack of apoptosis in mitochondrial encephalomyopathies', *Neurology*, 56(8), p. 1070.

Sena, Laura A. and Chandel, Navdeep S. (2012) 'Physiological Roles of Mitochondrial Reactive Oxygen Species', *Molecular Cell*, 48(2), pp. 158-167.

Seo, A.Y., Joseph, A.-M., Dutta, D., Hwang, J.C.Y., Aris, J.P. and Leeuwenburgh, C. (2010) 'New insights into the role of mitochondria in aging: mitochondrial dynamics and more', *Journal of cell science*, 123(15), pp. 2533-2542.

Shadel, G.S. and Clayton, D.A. (1997) 'Mitochondrial DNA maintenance in vertebrates', *Annu Rev Biochem*, 66, pp. 409-35.

Shi, R.Y., Zhu, S.H., Li, V., Gibson, S.B., Xu, X.S. and Kong, J.M. (2014) 'BNIP3 interacting with LC3 triggers excessive mitophagy in delayed neuronal death in stroke', *CNS Neurosci Ther*, 20(12), pp. 1045-55.

Shimizu, A., Mito, T., Hashizume, O., Yonekawa, H., Ishikawa, K., Nakada, K. and Hayashi, J.-I. (2015) 'G7731A mutation in mouse mitochondrial tRNALys regulates late-onset disorders in transmitochondrial mice', *Biochemical and Biophysical Research Communications*, 459(1), pp. 66-70.

Shimizu, A., Mito, T., Hayashi, C., Ogasawara, E., Koba, R., Negishi, I., Takenaga, K., Nakada, K. and Hayashi, J.-I. (2014) 'Transmitochondrial mice as models for primary prevention of diseases caused by mutation in the tRNA(Lys) gene', *Proceedings of the National Academy of Sciences of the United States of America*, 111(8), pp. 3104-3109.

Shin, M.G., Kajigaya, S., McCoy, J.P., Levin, B.C. and Young, N.S. (2004a) 'Marked mitochondrial DNA sequence heterogeneity in single CD34+ cell clones from normal adult bone marrow', *Blood*, 103(2), pp. 553-561.

Shin, M.G., Kajigaya, S., Tarnowka, M., McCoy, J.P., Levin, B.C. and Young, N.S. (2004b) 'Mitochondrial DNA sequence heterogeneity in circulating normal human CD34 cells and granulocytes', *Blood*, 103(12), pp. 4466-4477.

Shoffner, J.M., Lott, M.T., Lezza, A.M.S., Seibel, P., Ballinger, S.W. and Wallace, D.C. (1990) 'Myoclonic epilepsy and ragged-red fiber disease (MERRF) is associated with a mitochondrial DNA tRNA Lys mutation', *Cell*, 61(6), pp. 931-937.

Shokolenko, I., Venediktova, N., Bochkareva, A., Wilson, G.L. and Alexeyev, M.F. (2009) 'Oxidative stress induces degradation of mitochondrial DNA', *Nucleic Acids Research*, 37(8), pp. 2539-2548.

Shoshan-Barmatz, V., De Pinto, V., Zweckstetter, M., Raviv, Z., Keinan, N. and Arbel, N. (2010) 'VDAC, a multi-functional mitochondrial protein regulating cell life and death', *Molecular aspects of medicine*, 31(3), pp. 227-285.

Shoubridge, E.A., Karpati, G. and Hastings, K.E.M. (1990) 'Deletion mutants are functionally dominant over wild-type mitochondrial genomes in skeletal muscle fiber segments in mitochondrial disease', *Cell*, 62(1), pp. 43-49.

Shoubridge, E.A. and Wai, T. (2007) 'Mitochondrial DNA and the Mammalian Oocyte', in *Current Topics in Developmental Biology*. Academic Press, pp. 87-111.

Sligh, J.E., Levy, S.E., Waymire, K.G., Allard, P., Dillehay, D.L., Nusinowitz, S., Heckenlively, J.R., MacGregor, G.R. and Wallace, D.C. (2000) 'Maternal germ-line transmission of mutant mtDNAs from embryonic stem cell-derived chimeric mice', *Proceedings of the National Academy of Sciences*, 97(26), p. 14461.

Smeitink, J., van den Heuvel, L. and DiMauro, S. (2001) 'The genetics and pathology of oxidative phosphorylation', *Nature Reviews Genetics*, 2(5), pp. 342-352.

Smirnova, E., Griparic, L., Shurland, D.-L. and van der Bliek, A.M. (2001) 'Dynamin-related Protein Drp1 Is Required for Mitochondrial Division in Mammalian Cells', *Molecular Biology of the Cell*, 12(8), pp. 2245-2256.

Smits, P., Smeitink, J. and van den Heuvel, L. (2010) 'Mitochondrial Translation and Beyond: Processes Implicated in Combined Oxidative Phosphorylation Deficiencies', *Journal of Biomedicine and Biotechnology*, 2010, p. 24.

Snippert, H.J., Schepers, A.G., van Es, J.H., Simons, B.D. and Clevers, H. (2014) 'Biased competition between Lgr5 intestinal stem cells driven by oncogenic mutation induces clonal expansion', *EMBO reports*, 15(1), p. 62.

Snippert, H.J., van der Flier, L.G., Sato, T., van Es, J.H., van den Born, M., Kroon-Veenboer, C., Barker, N., Klein, A.M., van Rheenen, J., Simons, B.D. and Clevers, H. (2010) 'Intestinal Crypt Homeostasis Results from Neutral Competition between Symmetrically Dividing Lgr5 Stem Cells', *Cell*, 143(1), pp. 134-144.

Soleimanpour-Lichaei, H.R., Kühl, I., Gaisne, M., Passos, J.F., Wydro, M., Rorbach, J., Temperley, R., Bonnefoy, N., Tate, W., Lightowlers, R. and Chrzanowska-Lightowlers, Z. (2007) 'mtRF1a Is a Human Mitochondrial Translation Release Factor Decoding the Major Termination Codons UAA and UAG', *Molecular Cell*, 27(5), pp. 745-757.

Spelbrink, J.N., Li, F.-Y., Tiranti, V., Nikali, K., Yuan, Q.-P., Tariq, M., Wanrooij, S., Garrido, N., Comi, G., Morandi, L., Santoro, L., Toscano, A., Fabrizi, G.-M., Somer, H., Croxen, R., Beeson, D., Poulton, J., Suomalainen, A., Jacobs, H.T., Zeviani, M. and Larsson, C. (2001) 'Human mitochondrial DNA deletions associated with mutations in the gene encoding Twinkle, a phage T7 gene 4-like protein localized in mitochondria', *Nature Genetics*, 28, p. 223.

Spradling, A., Drummond-Barbosa, D. and Kai, T. (2001) 'Stem cells find their niche', *Nature*, 414(6859), pp. 98-104.

Squier, C.A. and Kremer, M.J. (2001) 'Biology of oral mucosa and esophagus', *J Natl Cancer Inst Monogr*, (29), pp. 7-15.

Srinivasula, S.M., Hegde, R., Saleh, A., Datta, P., Shiozaki, E., Chai, J., Lee, R.-A., Robbins, P.D., Fernandes-Alnemri, T., Shi, Y. and Alnemri, E.S. (2001) 'A conserved XIAP-interaction motif in caspase-9 and Smac/DIABLO regulates caspase activity and apoptosis', *Nature*, 410, p. 112.

Stamp, C. (2016) 'Determining the impact of mitochondrial dysfunction on stem cell dynamics and proliferation within the colon'.

Stamp, C., Zupanic, A., Sachdeva, A., Stoll, E.A., Shanley, D.P., Mathers, J.C., Kirkwood, T.B.L., Heer, R., Simons, B.D., Turnbull, D.M. and Greaves, L.C. (2018) 'Predominant Asymmetrical Stem Cell Fate Outcome Limits the Rate of Niche Succession in Human Colonic Crypts', *EBioMedicine*, 31, pp. 166-173.

Stange, Daniel E., Koo, B.-K., Huch, M., Sibbel, G., Basak, O., Lyubimova, A., Kujala, P., Bartfeld, S., Koster, J., Geahlen, Jessica H., Peters, Peter J., van Es, Johan H., van de Wetering, M., Mills, Jason C. and Clevers, H. (2013) 'Differentiated Troy+ Chief Cells Act as Reserve Stem Cells to Generate All Lineages of the Stomach Epithelium', *Cell*, 155(2), pp. 357-368.

Stehling, O. and Lill, R. (2013) 'The Role of Mitochondria in Cellular Iron–Sulfur Protein Biogenesis: Mechanisms, Connected Processes, and Diseases', *Cold Spring Harbor Perspectives in Biology*, 5(8), p. a011312.

Stewart, J.B. and Chinnery, P.F. (2015) 'The dynamics of mitochondrial DNA heteroplasmy: implications for human health and disease', *Nature Reviews Genetics*, 16, p. 530.

Stewart, J.B., Freyer, C., Elson, J.L., Wredenberg, A., Cansu, Z., Trifunovic, A. and Larsson, N.-G. (2008) 'Strong purifying selection in transmission of mammalian mitochondrial DNA', *PLoS biology*, 6(1), p. e10.

Stewart, J.B. and Larsson, N.-G. (2014) 'Keeping mtDNA in Shape between Generations', *PLoS genetics*, 10(10), p. e1004670.

Stierum, R.H., Dianov, G.L. and Bohr, V.A. (1999) 'Single-nucleotide patch base excision repair of uracil in DNA by mitochondrial protein extracts', *Nucleic Acids Research*, 27(18), pp. 3712-3719.

Stzepourginski, I., Nigro, G., Jacob, J.-M., Dulauroy, S., Sansonetti, P.J., Eberl, G. and Peduto, L. (2017) 'CD34⁺ mesenchymal cells are a major component of the intestinal stem cells niche at homeostasis and after injury', *Proceedings of the National Academy of Sciences*, 114(4), p. E506.

Su, T., Turnbull, D. and Greaves, L. (2018) 'Roles of Mitochondrial DNA Mutations in Stem Cell Ageing', *Genes*, 9(4), p. 182.

Suzuki, T., Nagao, A. and Suzuki, T. (2011) 'Human Mitochondrial tRNAs: Biogenesis, Function, Structural Aspects, and Diseases', *Annual Review of Genetics*, 45(1), pp. 299-329.

t Hart, L.M., Jansen, J.J., Lemkes, H.H., de Knijff, P. and Maassen, J.A. (1996) 'Heteroplasmy levels of a mitochondrial gene mutation associated with diabetes mellitus decrease in leucocyte DNA upon aging', *Hum Mutat*, 7(3), pp. 193-7.

Taanman, J.-W. (1999) 'The mitochondrial genome: structure, transcription, translation and replication', *Biochimica et Biophysica Acta (BBA)-Bioenergetics*, 1410(2), pp. 103-123.

Taanman, J.W., Bodnar, A.G., Cooper, J.M., Morris, A.A.M., Clayton, P.T., Leonard, J.V. and Schapira, A.H.V. (1997) 'Molecular Mechanisms in Mitochondrial DNA Depletion Syndrome', *Human Molecular Genetics*, 6(6), pp. 935-942.

Tait, S.W.G. and Green, D.R. (2010) 'Mitochondria and cell death: outer membrane permeabilization and beyond', *Nature Reviews Molecular Cell Biology*, 11, p. 621.

Takahashi, K. and Yamanaka, S. (2006) 'Induction of pluripotent stem cells from mouse embryonic and adult fibroblast cultures by defined factors', *cell*, 126(4), pp. 663-676.

Takeda, N., Jain, R., LeBoeuf, M.R., Wang, Q., Lu, M.M. and Epstein, J.A. (2011) 'Interconversion Between Intestinal Stem Cell Populations in Distinct Niches', *Science*, 334(6061), p. 1420.

Tan, D.Q. and Suda, T. (2017) 'Reactive oxygen species and mitochondrial homeostasis as regulators of stem cell fate and function', *Antioxidants & redox signaling*.

Tang, G., Rios, P.G., Kuo, S.-H., Akman, H.O., Rosoklija, G., Tanji, K., Dwork, A., Schon, E.A., DiMauro, S. and Goldman, J. (2013) 'Mitochondrial abnormalities in temporal lobe of autistic brain', *Neurobiology of disease*, 54, pp. 349-361.

Tao, S., Tang, D., Morita, Y., Sperka, T., Omrani, O., Lechel, A., Sakk, V., Kraus, J., Kestler, H.A., Kühl, M. and Rudolph, K.L. (2015) 'Wnt activity and basal niche position sensitize intestinal stem and progenitor cells to DNA damage', *The EMBO Journal*, 34(5), p. 624.

Tarasov, A.I., Griffiths, E.J. and Rutter, G.A. (2012) 'Regulation of ATP production by mitochondrial Ca(2+)', *Cell Calcium*, 52(1), pp. 28-35.

Taylor, R.W., Barron, M.J., Borthwick, G.M., Gospel, A., Chinnery, P.F., Samuels, D.C., Taylor, G.A., Plusa, S.M., Needham, S.J. and Greaves, L.C. (2003) 'Mitochondrial DNA mutations in human colonic crypt stem cells', *Journal of Clinical Investigation*, 112(9), p. 1351.

Taylor, R.W. and Turnbull, D.M. (2005) 'MITOCHONDRIAL DNA MUTATIONS IN HUMAN DISEASE', *Nature reviews. Genetics*, 6(5), pp. 389-402.

Taylor, R.W. and Turnbull, D.M. (2007) 'Mitochondrial DNA Transcription: Regulating the Power Supply', *Cell*, 130(2), pp. 211-213.

Teir, H. and Rasanen, T. (1961) 'A study of mitotic rate in renewal zones of nondiseased portions of gastric mucosa in cases of peptic ulcer and gastric cancer, with observations on differentiation and so-called "intestinalization" of gastric mucosa', *J Natl Cancer Inst*, 27, pp. 949-71.

Temperley, R., Richter, R., Dennerlein, S., Lightowlers, R.N. and Chrzanowska-Lightowlers, Z.M. (2010) 'Hungry Codons Promote Frameshifting in Human Mitochondrial Ribosomes', *Science*, 327(5963), p. 301.

Tetteh, Paul W., Basak, O., Farin, Henner F., Wiebrands, K., Kretzschmar, K., Begthel, H., van den Born, M., Korving, J., de Sauvage, F., van Es, Johan H., van Oudenaarden, A. and Clevers, H. (2016) 'Replacement of Lost Lgr5-Positive Stem Cells through Plasticity of Their Enterocyte-Lineage Daughters', *Cell Stem Cell*, 18(2), pp. 203-213.

The Cancer Genome Atlas, N., Muzny, D.M., Bainbridge, M.N., Chang, K., Dinh, H.H., Drummond, J.A., Fowler, G., Kovar, C.L., Lewis, L.R., Morgan, M.B., Newsham, I.F., Reid, J.G., Santibanez, J., Shinbrot, E., Trevino, L.R., Wu, Y.-Q., Wang, M., Gunaratne, P., Donehower, L.A., Creighton, C.J., Wheeler, D.A., Gibbs, R.A., Lawrence, M.S., Voet, D., Jing, R., Cibulskis, K., Sivachenko, A., Stojanov, P., McKenna, A., Lander, E.S., Gabriel, S., Getz, G., Ding, L., Fulton, R.S., Koboldt, D.C., Wylie, T., Walker, J., Dooling, D.J., Fulton, L., Delehaunty, K.D., Fronick, C.C., Demeter, R., Mardis, E.R., Wilson, R.K., Chu, A., Chun, H.-J.E., Mungall, A.J., Pleasance, E., Gordon Robertson, A., Stoll, D., Balasundaram, M., Birol, I., Butterfield, Y.S.N., Chuah, E., Coope, R.J.N., Dhalla, N., Guin, R., Hirst, C., Hirst, M., Holt, R.A., Lee, D., Li, H.I., Mayo, M., Moore, R.A., Schein, J.E., Slobodan, J.R., Tam, A., Thiessen, N., Varhol, R., Zeng, T., Zhao, Y., Jones, S.J.M., Marra, M.A., Bass, A.J., Ramos, A.H., Saksena, G., Cherniack, A.D., Schumacher, S.E., Tabak, B., Carter, S.L., Pho, N.H., Nguyen, H., Onofrio, R.C., Crenshaw, A., Ardlie, K., Beroukhim, R., Winckler, W., Getz, G., Meyerson, M., Protopopov, A., Zhang, J., Hadjipanayis, A., Lee, E., Xi, R., Yang, L., Ren, X., Zhang, H., Sathiamoorthy, N., Shukla, S., Chen, P.-C., et al. (2012) 'Comprehensive molecular characterization of human colon and rectal cancer', *Nature*, 487, p. 330.

Thompson, M., Fleming, K.A., Evans, D.J., Fundele, R., Surani, M.A. and Wright, N.A. (1990) 'Gastric endocrine cells share a clonal origin with other gut cell lineages', *Development*, 110(2), pp. 477-481.

Tian, H., Biehs, B., Warming, S., Leong, K.G., Rangell, L., Klein, O.D. and de Sauvage, F.J. (2011) 'A reserve stem cell population in small intestine renders Lgr5-positive cells dispensable', *Nature*, 478, p. 255.

Tiranti, V., Chariot, P., Carella, F., Toscano, A., Soliveri, P., Girlanda, P., Carrara, F., Fratta, G.M., Reid, F.M., Mariotti, C. and Zeviani, M. (1995) 'Maternally inherited hearing loss, ataxia and myoclonus associated with a novel point mutation in mitochondrial tRNASer(UCN) gene', *Hum Mol Genet*, 4(8), pp. 1421-7.

Treuting, P.M. and Dintzis, S.M. (2011) *Comparative Anatomy and Histology: A Mouse and Human Atlas (Expert Consult)*. Elsevier Science.

Trifunovic, A., Hansson, A., Wredenberg, A., Rovio, A.T., Dufour, E., Khvorostov, I., Spelbrink, J.N., Wibom, R., Jacobs, H.T. and Larsson, N.G. (2005) 'Somatic mtDNA mutations cause aging phenotypes without affecting reactive oxygen species production', *Proc Natl Acad Sci U S A*, 102(50), pp. 17993-8.

Trifunovic, A., Wredenberg, A., Falkenberg, M., Spelbrink, J.N., Rovio, A.T., Bruder, C.E., Bohlooly-y, M., Gidlöf, S., Oldfors, A. and Wibom, R. (2004) 'Premature ageing in mice expressing defective mitochondrial DNA polymerase', *Nature*, 429(6990), pp. 417-423.

Truscott, K.N., Kovermann, P., Geissler, A., Merlin, A., Meijer, M., Driessen, A.J.M., Rassow, J., Pfanner, N. and Wagner, R. (2001) 'A presequence- and voltage-sensitive channel of the mitochondrial preprotein translocase formed by Tim23', *Nature Structural Biology*, 8, p. 1074.

Tuppen, H.A.L., Blakely, E.L., Turnbull, D.M. and Taylor, R.W. (2010) 'Mitochondrial DNA mutations and human disease', *Biochimica et Biophysica Acta (BBA) - Bioenergetics*, 1797(2), pp. 113-128.

Tyynismaa, H., Mjosund, K.P., Wanrooij, S., Lappalainen, I., Ylikallio, E., Jalanko, A., Spelbrink, J.N., Paetau, A. and Suomalainen, A. (2005) 'Mutant mitochondrial helicase Twinkle causes multiple mtDNA deletions and a late-onset mitochondrial disease in mice',

Proceedings of the National Academy of Sciences of the United States of America, 102(49), pp. 17687-17692.

Umaki, Y., Mitsui, T., Endo, I., Akaike, M. and Matsumoto, T. (2002) 'Apoptosis-related changes in skeletal muscles of patients with mitochondrial diseases', *Acta Neuropathologica*, 103(2), pp. 163-170.

Upholt, W.B. and Dawid, I.B. (1977) 'Mapping of mitochondrial DNA of individual sheep and goats: Rapid evolution in the D loop region', *Cell*, 11(3), pp. 571-583.

Valenta, T., Degirmenci, B., Moor, A.E., Herr, P., Zimmerli, D., Moor, M.B., Hausmann, G., Cantù, C., Aguet, M. and Basler, K. (2016) 'Wnt Ligands Secreted by Subepithelial Mesenchymal Cells Are Essential for the Survival of Intestinal Stem Cells and Gut Homeostasis', *Cell Reports*, 15(5), pp. 911-918.

Valente, E.M., Abou-Sleiman, P.M., Caputo, V., Muqit, M.M.K., Harvey, K., Gispert, S., Ali, Z., Del Turco, D., Bentivoglio, A.R., Healy, D.G., Albanese, A., Nussbaum, R., González-Maldonado, R., Deller, T., Salvi, S., Cortelli, P., Gilks, W.P., Latchman, D.S., Harvey, R.J., Dallapiccola, B., Auburger, G. and Wood, N.W. (2004) 'Hereditary Early-Onset Parkinson's Disease Caused by Mutations in PINK1', *Science*, 304(5674), pp. 1158-1160.

Valko, M., Leibfritz, D., Moncol, J., Cronin, M.T.D., Mazur, M. and Telser, J. (2007) 'Free radicals and antioxidants in normal physiological functions and human disease', *The International Journal of Biochemistry & Cell Biology*, 39(1), pp. 44-84.

van den Ouweland, J.M.W., Lemkes, H.H.P.J., Ruitenbeek, W., Sandkuijl, L.A., de Vijlder, M.F., Struyvenberg, P.A.A., van de Kamp, J.J.P. and Maassen, J.A. (1992) 'Mutation in mitochondrial tRNALeu(UUR) gene in a large pedigree with maternally transmitted type II diabetes mellitus and deafness', *Nature Genetics*, 1, p. 368.

van der Bliek, A.M., Shen, Q. and Kawajiri, S. (2013) 'Mechanisms of Mitochondrial Fission and Fusion', *Cold Spring Harbor Perspectives in Biology*, 5(6).

Van der Flier, L.G., Sabates–Bellver, J., Oving, I., Haegebarth, A., De Palo, M., Anti, M., Van Gijn, M.E., Suijkerbuijk, S., Van de Wetering, M., Marra, G. and Clevers, H. (2007) 'The Intestinal Wnt/TCF Signature', *Gastroenterology*, 132(2), pp. 628-632.

van der Flier, L.G., van Gijn, M.E., Hatzis, P., Kujala, P., Haegebarth, A., Stange, D.E., Begthel, H., van den Born, M., Guryev, V., Oving, I., van Es, J.H., Barker, N., Peters, P.J.,

van de Wetering, M. and Clevers, H. (2009) 'Transcription Factor Achaete Scute-Like 2 Controls Intestinal Stem Cell Fate', *Cell*, 136(5), pp. 903-912.

van Es, J.H., Haegebarth, A., Kujala, P., Itzkovitz, S., Koo, B.-K., Boj, S.F., Korving, J., van den Born, M., van Oudenaarden, A., Robine, S. and Clevers, H. (2012a) 'A Critical Role for the Wnt Effector Tcf4 in Adult Intestinal Homeostatic Self-Renewal', *Molecular and Cellular Biology*, 32(10), p. 1918.

van Es, J.H., Sato, T., van de Wetering, M., Lyubimova, A., Yee Nee, A.N., Gregorieff, A., Sasaki, N., Zeinstra, L., van den Born, M., Korving, J., Martens, A.C.M., Barker, N., van Oudenaarden, A. and Clevers, H. (2012b) 'Dll1+ secretory progenitor cells revert to stem cells upon crypt damage', *Nature Cell Biology*, 14, p. 1099.

Vincent, A.E., Rosa, H.S., Pabis, K., Lawless, C., Chen, C., Grünewald, A., Rygiel, K.A., Rocha, M.C., Reeve, A.K., Falkous, G., Perissi, V., White, K., Davey, T., Petrof, B.J., Sayer, A.A., Cooper, C., Deehan, D., Taylor, R.W., Turnbull, D.M. and Picard, M. (2018) 'Subcellular origin of mitochondrial DNA deletions in human skeletal muscle', *Annals of Neurology*, 0(0).

Virbasius, J.V. and Scarpulla, R.C. (1994) 'Activation of the human mitochondrial transcription factor A gene by nuclear respiratory factors: a potential regulatory link between nuclear and mitochondrial gene expression in organelle biogenesis', *Proceedings of the National Academy of Sciences of the United States of America*, 91(4), pp. 1309-1313.

Vogel, F., Bornhövd, C., Neupert, W. and Reichert, A.S. (2006) 'Dynamic subcompartmentalization of the mitochondrial inner membrane', *The Journal of Cell Biology*, 175(2), p. 237.

von Moltke, J., Ji, M., Liang, H.-E. and Locksley, R.M. (2015) 'Tuft-cell-derived IL-25 regulates an intestinal ILC2–epithelial response circuit', *Nature*, 529, p. 221.

Wallace, D.C. (1989) 'Mitochondrial DNA mutations and neuromuscular disease', *Trends in Genetics*, 5, pp. 9-13.

Wallace, D.C. (1992) 'Mitochondrial genetics: a paradigm for aging and degenerative diseases?', *Science*, 256(5057), pp. 628-632.

Wallace, D.C. (1999) 'Mitochondrial Diseases in Man and Mouse', *Science*, 283(5407), p. 1482.

Wallace, D.C., Singh, G., Lott, M.T., Hodge, J.A., Schurr, T.G., Lezza, A.M., Elsas, L.J. and Nikoskelainen, E.K. (1988) 'Mitochondrial DNA mutation associated with Leber's hereditary optic neuropathy', *Science*, 242(4884), pp. 1427-1430.

Wang, C. and Youle, R.J. (2009) 'The role of mitochondria in apoptosis', *Annual review of genetics*, 43, pp. 95-118.

Wang, F., Scoville, D., He, X.C., Mahe, M.M., Box, A., Perry, J.M., Smith, N.R., Lei, N.Y., Davies, P.S., Fuller, M.K., Haug, J.S., McClain, M., Gracz, A.D., Ding, S., Stelzner, M., Dunn, J.C., Magness, S.T., Wong, M.H., Martin, M.G., Helmrath, M. and Li, L. (2013a) 'Isolation and characterization of intestinal stem cells based on surface marker combinations and colony-formation assay', *Gastroenterology*, 145(2), pp. 383-95.e1-21.

Wang, G.J., Nutter, L.M. and Thayer, S.A. (1997) 'Insensitivity of cultured rat cortical neurons to mitochondrial DNA synthesis inhibitors: Evidence for a slow turnover of mitochondrial DNA', *Biochemical Pharmacology*, 54(1), pp. 181-187.

Wang, J. and Pantopoulos, K. (2011) 'Regulation of cellular iron metabolism', *Biochemical Journal*, 434(3), p. 365.

Wang, T., Sha, H., Ji, D., Zhang, H.L., Chen, D., Cao, Y. and Zhu, J. (2014) 'Polar body genome transfer for preventing the transmission of inherited mitochondrial diseases', *Cell*, 157(7), pp. 1591-1604.

Wang, X., Pickrell, A.M., Rossi, S.G., Pinto, M., Dillon, L.M., Hida, A., Rotundo, R.L. and Moraes, C.T. (2013b) 'Transient systemic mtDNA damage leads to muscle wasting by reducing the satellite cell pool', *Human Molecular Genetics*, 22(19), pp. 3976-3986.

Wang, Y. and Bogenhagen, D.F. (2006) 'Human mitochondrial DNA nucleoids are linked to protein folding machinery and metabolic enzymes at the mitochondrial inner membrane', *J Biol Chem*, 281(35), pp. 25791-802.

Warrell, D.A., Benz, E.J., Cox, T.M. and Firth, J.D. (2003) *Oxford textbook of medicine*. Oxford University Press, USA.

Watanabe, T., Dewey, M.J. and Mintz, B. (1978) 'Teratocarcinoma cells as vehicles for introducing specific mutant mitochondrial genes into mice', *Proceedings of the National Academy of Sciences*, 75(10), p. 5113.

White, S.L., Shanske, S., McGill, J.J., Mountain, H., Geraghty, M.T., DiMauro, S., Dahl, H.H. and Thorburn, D.R. (1999) 'Mitochondrial DNA mutations at nucleotide 8993 show a lack of tissue- or age-related variation', *J Inherit Metab Dis*, 22(8), pp. 899-914.

Whittaker, R.G., Blackwood, J.K., Alston, C.L., Blakely, E.L., Elson, J.L., McFarland, R., Chinnery, P.F., Turnbull, D.M. and Taylor, R.W. (2009) 'Urine heteroplasmy is the best predictor of clinical outcome in the m. 3243A> G mtDNA mutation', *Neurology*, 72(6), pp. 568-569.

Wiedemann, N. and Pfanner, N. (2017) 'Mitochondrial Machineries for Protein Import and Assembly', *Annual Review of Biochemistry*, 86(1), pp. 685-714.

Winge, D.R. (2012) 'Sealing the Mitochondrial Respirasome', *Molecular and Cellular Biology*, 32(14), p. 2647.

Winton, D.J., Blount, M.A. and Ponder, B.A.J. (1988) 'A clonal marker induced by mutation in mouse intestinal epithelium', *Nature*, 333, p. 463.

Wong, V.W.Y., Stange, D.E., Page, M.E., Buczacki, S., Wabik, A., Itami, S., van de Wetering, M., Poulsom, R., Wright, N.A., Trotter, M.W.B., Watt, F.M., Winton, D.J., Clevers, H. and Jensen, K.B. (2012) 'Lrig1 controls intestinal stem-cell homeostasis by negative regulation of ErbB signalling', *Nature Cell Biology*, 14, p. 401.

Wu, J. and Izpisua Belmonte, J.C. (2016) 'Stem Cells: A Renaissance in Human Biology Research', *Cell*, 165(7), pp. 1572-1585.

Wu, Z., Puigserver, P., Andersson, U., Zhang, C., Adelmant, G., Mootha, V., Troy, A., Cinti, S., Lowell, B., Scarpulla, R.C. and Spiegelman, B.M. (1999) 'Mechanisms Controlling Mitochondrial Biogenesis and Respiration through the Thermogenic Coactivator PGC-1', *Cell*, 98(1), pp. 115-124.

Xochitl, P.-M., Soledad, F., Yolanda, C.-V., Sanna, M., Faviola, T.-C. and Miguel, S.-V. (2008) 'Protein Synthesis and Assembly in Mitochondrial Disorders', *Current Topics in Medicinal Chemistry*, 8(15), pp. 1335-1350.

Xu, X., Duan, S., Yi, F., Ocampo, A., Liu, G.-H. and Izpisua Belmonte, Juan C. (2013) 'Mitochondrial Regulation in Pluripotent Stem Cells', *Cell Metabolism*, 18(3), pp. 325-332.

Yakubovskaya, E., Chen, Z., Carrodeguas, J.A., Kisker, C. and Bogenhagen, D.F. (2006) 'Functional Human Mitochondrial DNA Polymerase γ Forms a Heterotrimer', *Journal of Biological Chemistry*, 281(1), pp. 374-382.

Yamamoto, H., Itoh, N., Kawano, S., Yatsukawa, Y.-i., Momose, T., Makio, T., Matsunaga, M., Yokota, M., Esaki, M., Shodai, T., Kohda, D., Aiken Hobbs, A.E., Jensen, R.E. and Endo, T. (2011) 'Dual role of the receptor Tom20 in specificity and efficiency of protein import into mitochondria', *Proceedings of the National Academy of Sciences*, 108(1), p. 91.

Yamano, K., Yatsukawa, Y.-i., Esaki, M., Hobbs, A.E.A., Jensen, R.E. and Endo, T. (2008) 'Tom20 and Tom22 share the common signal recognition pathway in mitochondrial protein import', *Journal of Biological Chemistry*, 283(7), pp. 3799-3807.

Yan, K.S., Chia, L.A., Li, X., Ootani, A., Su, J., Lee, J.Y., Su, N., Luo, Y., Heilshorn, S.C., Amieva, M.R., Sangiorgi, E., Capecchi, M.R. and Kuo, C.J. (2012) 'The intestinal stem cell markers Bmi1 and Lgr5 identify two functionally distinct populations', *Proc Natl Acad Sci U S A*, 109(2), pp. 466-71.

Yan, K.S., Gevaert, O., Zheng, G.X.Y., Anchang, B., Probert, C.S., Larkin, K.A., Davies, P.S., Cheng, Z.-f., Kaddis, J.S., Han, A., Roelf, K., Calderon, R.I., Cynn, E., Hu, X., Mandleywala, K., Wilhelmy, J., Grimes, S.M., Corney, D.C., Boutet, S.C., Terry, J.M., Belgrader, P., Ziraldo, S.B., Mikkelsen, T.S., Wang, F., von Furstenberg, R.J., Smith, N.R., Chandrakesan, P., May, R., Chrissy, M.A.S., Jain, R., Cartwright, C.A., Niland, J.C., Hong, Y.-K., Carrington, J., Breault, D.T., Epstein, J., Houchen, C.W., Lynch, J.P., Martin, M.G., Plevritis, S.K., Curtis, C., Ji, H.P., Li, L., Henning, S.J., Wong, M.H. and Kuo, C.J. (2017) 'Intestinal Enteroendocrine Lineage Cells Possess Homeostatic and Injury-Inducible Stem Cell Activity', *Cell Stem Cell*, 21(1), pp. 78-90.e6.

Yano, M., Hoogenraad, N., Terada, K. and Mori, M. (2000) 'Identification and Functional Analysis of Human Tom22 for Protein Import into Mitochondria', *Molecular and Cellular Biology*, 20(19), pp. 7205-7213.

Yasukawa, T., Suzuki, T., Ishii, N., Ueda, T., Ohta, S. and Watanabe, K. (2000a) 'Defect in modification at the anticodon wobble nucleotide of mitochondrial tRNALys with the MERRF encephalomyopathy pathogenic mutation', *FEBS Letters*, 467(2-3), pp. 175-178.

Yasukawa, T., Suzuki, T., Suzuki, T., Ueda, T., Ohta, S. and Watanabe, K. (2000b) 'Modification Defect at Anticodon Wobble Nucleotide of Mitochondrial tRNAsLeu(UUR)

with Pathogenic Mutations of Mitochondrial Myopathy, Encephalopathy, Lactic Acidosis, and Stroke-like Episodes', *Journal of Biological Chemistry*, 275(6), pp. 4251-4257.

Yokota, M., Shitara, H., Hashizume, O., Ishikawa, K., Nakada, K., Ishii, R., Taya, C., Takenaga, K., Yonekawa, H. and Hayashi, J.-I. (2010) 'Generation of trans-mitochondrial mito-mice by the introduction of a pathogenic G13997A mtDNA from highly metastatic lung carcinoma cells', *FEBS Letters*, 584(18), pp. 3943-3948.

Yoneda, M., Miyatake, T. and Attardi, G. (1995) 'Heteroplasmic mitochondrial tRNALys mutation and its complementation in MERRF patient‐derived mitochondrial transformants', *Muscle & nerve*, 18(S14), pp. S95-S101.

Youle, R.J. and Narendra, D.P. (2011) 'Mechanisms of mitophagy', *Nature reviews Molecular cell biology*, 12(1), pp. 9-14.

Youle, R.J. and Van Der Bliek, A.M. (2012) 'Mitochondrial fission, fusion, and stress', *Science*, 337(6098), pp. 1062-1065.

Yousefi, M., Li, L. and Lengner, C.J. (2017) 'Hierarchy and Plasticity in the Intestinal Stem Cell Compartment', *Trends in cell biology*, 27(10), pp. 753-764.

Yousefi, M., Li, N., Nakauka-Ddamba, A., Wang, S., Davidow, K., Schoenberger, J., Yu, Z., Jensen, S.T., Kharas, M.G. and Lengner, C.J. (2016) 'Msi RNA-binding proteins control reserve intestinal stem cell quiescence', *The Journal of Cell Biology*, 215(3), p. 401.

Zeviani, M., Moraes, C.T., DiMauro, S., Nakase, H., Bonilla, E., Schon, E.A. and Rowland, L.P. (1988) 'Deletions of mitochondrial DNA in Kearns-Sayre syndrome', *Neurology*, 38(9), pp. 1339-46.

Zhang, C.F., Linnane, A.W. and Nagley, P. (1993) 'Occurrence of a Particular Base Substitution (3243 A to G) in Mitochondrial DNA of Tissues of Ageing Humans', *Biochemical and Biophysical Research Communications*, 195(2), pp. 1104-1110.

Zhang, H., Burr, Stephen P. and Chinnery, Patrick F. (2018) 'The mitochondrial DNA genetic bottleneck: inheritance and beyond', *Essays In Biochemistry*, 62(3), pp. 225-234.

Zheng, W., Khrapko, K., Coller, H.A., Thilly, W.G. and Copeland, W.C. (2006) 'Origins of human mitochondrial point mutations as DNA polymerase γ-mediated errors', *Mutation Research/Fundamental and Molecular Mechanisms of Mutagenesis*, 599(1), pp. 11-20.

Zhou, Q. and Melton, D.A. (2018) 'Pancreas regeneration', *Nature*, 557(7705), pp. 351-358.

Zhu, J., Wang, K.Z.Q. and Chu, C.T. (2013) 'After the banquet', *Autophagy*, 9(11), pp. 1663-1676.

Zinovkina, L.A. (2018) 'Mechanisms of Mitochondrial DNA Repair in Mammals', *Biochemistry (Moscow)*, 83(3), pp. 233-249.